INSTABILITIES OF SLENDER TAPERED TUBULAR BEAMS INDUCED BY INTERNAL AND EXTERNAL AXIAL FLOW

by

Michel Hannoyer
Department of Mechanical Engineering
McGill University

Under the supervision of Dr. M.P. Paidoussis

Submitted to the Faculty of Graduate Studies
and Research of McGill University,
in partial fulfilment of the
requirements for the degree of
Doctor of Philosophy

McGill University January 1977.

ABSTRACT

This thesis examines the dynamics and stability of slender tubular beams conveying fluid and simultaneously subjected to axial external flow.

In deriving the equation of small motions, inviscid hydrodynamic forces are obtained by slender-body theory, modified to account for the boundary-layer thickness of the external flow; internal dissiptation and gravity effects are also taken into account. The equation of motions is sufficiently general to deal with nonuniform - but smoothly varying and axisymmetric - internal and/or external shapes of the tubular beam. Solutions are obtained by means of a method similar to Galerkin's, with the eigenfunctions approximated by Fourier series. Calculations are presented for tubular beams of conical shape subjected to either internal or external flow and for cylindrical tubular beams subjected to both flows simultaneously.

It is shown that for sufficiently high flow velocities, either internal or external, such beams are subject to divergence and/or flutter. Tubular beams conveying a conically convergent flow are found to be less stable than uniform pipes; in the case of conical beams in external flow, tapering has a stabilizing effect which mainly depends upon the boundary-layer thickness relative to the diameter.

For clamped-clamped cylindrical tubular beams the effect of the two flows (internal and external) on stability is additive, so that if either flow is just below the corresponding critical value for instability, an increase in the other flow precipitates instability. This is not always the case for cantilevered systems; if the system is just below the threshold of instability due to either flow, instability may be *eliminated* if the other flow is increased.

Experiments conducted with moulded rubber tubular beams in a vertical water tunnel corroborate the theoretically predicted behaviour.

SOMMAIRE

Cette thèse traite de la dynamique et de la stabilité de poutres tubulaires soumises a l'effet d'un écoulement interne et d'un écoulement externe parallèle à leur axe.

La mise en équation pour des petits déplacements s'effectue à partir d'écoulements potentiels qui, dans le cas du fluide externe, tiennent compte de la couche limite; l'effet de la gravité et des forces de dissipation interne ont été prises en consideration dans le modèle mathématique. L'équation est assez générale pour qu'on puisse traiter de poutres tubulaires non cylindriques - mais néanmoins axisymmétriques et sans discontinuités de section. La méthode de resolution s'inspire de celle de Galerkin, et la recherche des fonctions propres s'effectue à l'aide de séries de Fourier. Les resultats sont offerts d'une part dans le cas d'élements de forme conique soumis à un écoulement unique (interne ou externe) et d'autre part dans le cas de tubes cylindriques soumis à des écoulements simultanés.

Pour des vitesses d'écoulement interne ou externe suffisamment élevées, on trouve que de tels éléments risquent à la fois le flambage et le flottement. De plus, on s'aperçoit qu'une poutre creuse ayant un boyau conique convergent est moins stable qu'avec un boyau cylindrique. Par contre, dans le cas d'un écoulement externe et d'éléments en forme de tronc de cone, la stabilité dépend plus de l'épaisseur relative de la couche limite par rapport au diamètre que de l'angle du cône. Pour ce qui est des tubes cylindriques soumis à des écoulements simultanés, on s'aperçoit que dans le cas d'éléments encastrés aux deux extrémités, l'effet des deux écoulements est additif; à savoir qu'au seuil d'une instabilité on peut déclancher cette dernière en augmentant indifféremment, ou bien la vitesse du fluide interne, ou celle du fluide externe. Tel n'est par toujours le cas pour des éléments encastrés à une extrémité et libres à l'autre: certaines instabilités peuvent être évitées si au lieu d'augmenter la vitesse du fluide externe au delà de certaines limites, on augmente plutôt celle du fluide interne ou vice versa.

Les prédictions concernant les écoulements critiques ont été confirmées expérimentalement dans une soufflerie (à eau) munie d'une section d'essais verticale où des éléments tubulaires coulés dans du caoutchou étaient suspendus.

ACKNOWLEDGEMENTS

The author wishes to express his deep gratitude to his research director, Professor M.P. Paidoussis, for the valuable guidance and continued encouragement which he has offered throughout the course of this work.

The financial support of this research by the National Research Council of Canada and Defense Research Board of Canada is gratefully acknowledged.

The author also thanks the staff of the Department of Mechanical Engineering for their patience and assistance, his colleagues in the Elastohydrodynamics group for fruitful discussions, and finally Mrs. R. Gray for the excellent job of typing a difficult manuscript.

TABLE OF CONTENTS

NOMENCLATURE

Symbol	Definition	Page
	Roman Symbols -	
A	cross-sectional area of tubular beam alone = $\frac{\pi}{4}(D_e^2-D_i^2)$	19
A_e	overall cross-sectional area of tubular beam = $\frac{\pi}{4}D_e^2$	28
A_e^*	overall cross-sectional area with b.l. displacement thickness	34
A_i	internal cross-sectional area of tubular beam = $\frac{\pi}{4}D_i^2$	23
$[A]$	matrix of differential equation of motion	69
B	buoyancy force	29
c	longitudinal wave propagation velocity in tube	78
C_{fe}	base drag coefficient associated with external flow	50
C_{fi}	base drag coefficient associated with internal flow	50
C_{fn}	normal external friction coefficient	32
C_{ft}	tangential external friction coefficient	32
C_{fx}	coupled-flow base drag coefficient	50
c_n, c_t	dimensionless friction coefficients	60
c_p	axisymmetric pressure coefficient	30
c_v	viscous friction coefficient	60
D_b	afterbody base drag	30
D_e	outside diameter of tubular beam	32
D_i	internal diameter of tubular beam	64
E	Young's modulus	20
E^*	complex elastic modulus	20
F_b	drag force exerted on the tapered end piece	48
F_{en}	normal force due to external fluid, per unit length	19
F_{et}	tangential force due to external fluid, per unit length	19

Symbol	Definition	Page
F_{in}	normal force due to internal fluid, per unit length	19
F_{it}	tangential force due to internal fluid, per unit length	19
F_x, F_y	axial and transverse external fluid forces per unit length	30
f_r	variable coefficients of the equation of motion	67
g_r	constant coefficients of the boundary conditions	67
g	acceleration due to gravity	19
I	area moment of inertia	20
k	Kelvin-Voigt damping constant	20
L	length of beam	46
M	moment along the beam	20
M_e	moment induced by external fluid	20
M_i	moment induced by internal fluid	10
$\vec{n}$	normal unit vector pointing outwards	29
p_e	external pressure	29
p_{eh}	hydrostatic pressure in external fluid	30
p_i	internal pressure	26
Q	normal shear in the beam	19
q_{en}	external normal friction per unit length of beam	33
q_{et}	external tangential friction per unit length of beam	33
r	radial coordinate	28
s_e	dimensionless cross-sectional area for the end piece	60
S_e	equivalent cross-sectional area of a conical end piece	58
t	time	19
T	tension in beam	19
T_o	external tension	51
T_l	generalized tension	46

Symbol	Definition	Page
u_e	dimensionless external flow velocity	60
u_e^*	dimensionless velocity corrected for the boundary layer	60
U_e^*	velocity of the undisturbed external flow	27
U_e	reduced external flow velocity	37
U_i	average internal flow velocity	22
U_v	fictitious velocity due to viscous friction effects	33
v_i	dimensionless internal discharge velocity	60
V	absolute velocity of a particle of internal fluid	23
x	axial coordinate	18
x_o	approximate length of the support	64
y	transverse coordinate	18
z	coordinate normal to the plane of motion	41

- Greek Symbols -

α	taper coefficient due to external taper and boundary layer	64
α_e	taper coefficient due to external taper angle	64
α_i	taper coefficient due to internal taper angle	64
α_e'	coefficient for tension related to external friction	53
α_i'	coefficient for tension related to internal velocity	53
β_e	external taper angle (rad.)	63
β_i	internal taper angle (rad.)	22
δ	ratio of internal to external diameters at $\xi=0$	60
δ_1	boundary layer displacement thickness	64
δ_2	momentum boundary layer thickness	37
γ	dimensionless gravity parameter specific to the material	60
γ_e	external density parameter	60

Symbol	Definition	Page
γ_i	internal density parameter	60
γ_n	Fourier coefficients	68
Γ	dimensionless gravity parameter	60
ϵ	length ratio of tubular beam = $L/D_e(0)$	60
ϵ_o	length ratio of support	64
η	dimensionless transverse displacement	60
θ	dimensionless tension	60
μ	hysteretic damping coefficient	66
μ_e	dynamic viscosity of external flow	32
ν	dimensionless viscoelastic damping coefficient	60
ξ	dimensionless axial coordinate	60
Π	dimensionless external tension at $\xi=1$	60
ρ	density of tube	19
ρ_e	density of external fluid	28
ρ_i	density of internal fluid	24
σ	boundary-layer coefficient	64
σ_e	dimensionless external cross-sectional area ratio	60
σ_i	dimensionless internal area ratio	60
τ	dimensionless time	60
χ	ratio of end-piece length to diameter at $\xi=0$	60
χ_e	ratio of end-piece length to diameter at $\xi=1$	60
Ψ	complex displacement function	62
ω	dimensionless frequency	62
Ω	angular velocity	23

Symbol	- *Script and other symbols* -	page
$\mathcal{D}_e$	convective derivative for external flow	39
$\mathcal{D}_e^*$	convective derivative for external flow with boundary layer	39
$\mathcal{D}_i$	convective derivative for internal flow	39
ℓ	length of tapered end-piece	47
L	hydrodynamic lift per unit length	28
M_e	virtual mass of the beam	27

Note: other quantities are defined in the text.

- Equation numbering scheme -

Section	Equations	pages
§2.1	(1.1) - (1.3)	19,20
§2.2	(2.1) - (2.3)	24,26
§2.3	(3.1) - (3.11)	28-38
§2.4	(4.1) - (4.3)	42,44
§2.5	(5.1) - (5.14)	45,59
§2.6	(6.1) - (6.8)	61-66
§3.1	(7.1), (7.2)	67,69
§3.2	(8.1)	70
§4.2	(9.1)	78
§5.2	(10.1) - (10.5)	88-97
§5.3	(11.1) - (11.4)	114-117

1. INTRODUCTION

1.1 PRELIMINARY REMARKS

Over the past century dynamicists have been confronted with vibration and stability problems in such things as travelling chains, bands of band-saws, conveyor and power-transmission belts and textile fibres: namely, problems involving an essentially one-dimensional elastic continuum, associated with continuous transport of mass. More recently, problems involving fluid transport were added to the list; such as pipes conveying fluid (e.g., pipe-lines and hydroelectric power-plant conduits) and cylindrical components subjected to an external flow parallel to their axis (e.g., tubes in certain types of heat exchangers, and fuel rods in some types of nuclear reactors).

The study of the dynamics of such systems leads to basically similar linearized equations of motion, namely to partial differential equations of second order with respect to time, and of second or fourth order with respect to the spatial coordinate, depending on whether the one-dimensional elastic continuum is modelled as a string or a beam, and subject to two or four boundary conditions, respectively. Apart from the familiar terms due to tension and stiffness, the inertial loading associated with axial mass transport is typically of the following form:

$$- M\left(\frac{\partial^2 y}{\partial t^2} + 2U \frac{\partial^2 y}{\partial x \partial t} + U^2 \frac{\partial^2 y}{\partial x^2}\right) ,$$

where M is the mass transported per unit length with a velocity U, and y is the lateral displacement of the structure involved; in the case of external flows, M is the so-called "virtual" mass of the fluid per unit length. The three terms within brackets in the above expression may be identified, respectively, as (i) the transverse acceleration, (ii) the Coriolis acceleration associated with the axial velocity U and angular velocity $\partial\theta/\partial t$, where $\theta \equiv \partial y/\partial x$ and (iii) the centripetal acceleration associated with the axial velocity and the curvature of the structure.

This inertial loading is found to be responsible for the peculiar behaviour of such systems. Thus, if the system is otherwise conservative, the presence of Coriolis forces renders it *gyroscopic*† conservative, which clearly changes its character in a basic manner. Also, the last term of the equation is seen to be of the same form as a compressive loading, and obviously centrifugal and compressive forces have similar effects on the dynamics of such one-dimensional structures; if, however, the system has a free downstream* end, this term should best be viewed as due to a follower force of magnitude MU^2, rendering the system non-conservative (*circulatory*†) - in the same sense as that of a column subjected to a tangential (follower) compressive load. Although the implications of the form of the inertial loading exerted by the transported mass were not realized immediately, they are useful to us in classifying the type of problems considered here within the wider framework of dynamical systems. Furthermore, the dynamical behaviour of these systems then becomes easier to understand.

---

†According to Ziegler's classification of dynamical systems, [84].

*downstream, in the sense of the direction of mass transport.

The main feature of the dynamical behaviour of these systems is that at sufficiently high transport velocities, the structure may be subject to divergence (buckling) or to flutter (oscillatory instability) in its first and higher flexural modes. For a given structure the magnitude of the velocity to induce instability (the so-called "critical" mass-transport velocity), as well as the type of instability obtained, depend to a large extent on the boundary conditions involved.

In undertaking a dynamical analysis of such systems, one normally seeks to determine (i) the lowest critical mass transport velocities above which instability occurs, and (ii) the relationship between the characteristic frequencies (eigen-frequencies) and transport velocity. The former is the main goal in stability analysis, while the latter is essential if one is interested in the free vibration characteristics and in the response of the structure to a prescribed excitation field.

Because of the subject of this thesis, our attention will henceforth be focused on problems involving fluid mass transport in its general form, i.e. either "internal" flow as in a pipe, or "external" flow parallel to the axis as in a cylinder in axial flow. In the historical review that follows it will be seen that the problem of a pipe conveying fluid has been studied quite extensively, whereas that of cylindrical bodies immersed in axial flow has received considerably less attention. One important reason for this is that the instabilities associated with internal flow have been observed a long time ago (e.g., "snaking" of a fire-hose), while those associated with external flow have only been

discovered less than twenty years ago. Another reason is the relative ease of both theoretical and experimental study of pipes conveying fluid. Thus, in that case, the hydrodynamics of the problem are reduced to a trivial level, as the fluid may be adequately modelled as an infinitely flexible travelling string; also, such factors as frictional and base drag forces, which must be considered in the case of external flow and which require empirical approximations, do not arise in the case of internal flow.

The foregoing discussion might lead the reader to think that the main, if not the sole, motivation for studying these phenomena has been primarily utilitarian, in the sense of aiming to solve practical engineering problems. Although, practical problems do exist, as in heat exchangers, nuclear reactors and piping applications, it is true to say that their solution can be accomplished by common-sense or empirical means, requiring fairly simple understanding of the phenomena involved. The main impetus for much of the work done in this field stems rather from scientific curiosity, in seeking to understand a set of intriguing physical phenomena or in studying mathematically interesting problems as part of the wider class of problems mentioned at the beginning of this discussion. A case in point is the study of cantilevered pipes conveying fluid - clearly a geometry of limited practical importance. If one recognizes, however, that this problem is closely related to that of a column subjected to a follower tangential load (Beck's problem), one can see why the study of such problems transcends the practical problem-solving engineering dimension and is rather a convenient vehicle for the study of a wider class of dynamical systems of fundamental importance in applied mechanics.

1.2 LITERATURE REVIEW

1.2.1 Dynamics of pipes conveying fluid

A series of experiments by Aitken [1], reported in 1876, on travelling chains and flexible hoses conveying fluid, which illustrated the balance between motion-induced tensile and centrifugal forces, is perhaps among the earliest work pertinent to the study of dynamics of structures subject to parallel flow.

The self-excited oscillations of a pipe conveying water were apparently first recognized by M. Brillouin in 1885, but his work remained unpublished. Bourrières, one of Brillouin's students, was the first to undertake a serious study of this problem. In a remarkable paper [2], published in 1939, Bourrières examined the nature of the oscillatory instability of cantilevered pipes conveying fluid, both theoretically and experimentally. This paper remained unknown to later workers in the field until rediscovered by Paidoussis in 1972. Bourrières was unable, however, to obtain analytically the critical flow velocity for the onset of oscillatory instability.

Interest in the subject was reactivated in 1950, to study the vibrations of the Trans-Arabian pipeline, by Ashley and Haviland [3]; unfortunately, the equations of motion obtained were incorrect, as were the main conclusions reached therein. The correct equations were derived by Feodos'ev [4], Housner [5] and Niordson [6], who studied theoretically the case of a simply-supported pipe and found that for sufficiently high flow velocities the pipe may buckle.

The case of cantilevered pipes conveying fluid was examined by Long [7], but his method of solution was applicable only to relatively small flow velocities, so that he could not find the oscillatory instabilities observed by Brillouin and Bourrières.

Handelman [8], Heinrich [9], Bolotin [10], Hu and Tsoon [11] and Movchan [12] studied various aspects of the problem of a tube conveying fluid with both ends supported, and made important contributions mainly in the mathematical analysis of the problem. Heinrich [9], however, introduced a correction associated with internal pressurization of the tube which may become significant for high pressures. Finally, the experiments of Dodds and Runyan [13] showed excellent agreement with theory with regard to flow-induced divergence.

In all the above studies, excepting Bourrières "lost" work, the only form of instability involved was buckling (divergence). It was not until 1963 that Gregory and Paidoussis [14] rediscovered theoretically and experimentally the oscillatory instabilities (flutter) of cantilevered pipes conveying fluid. However, it must be said that Benjamin [15], in dealing with the dynamics of articulated pipes (i.e. rigid pipe segments, flexibly connected), had examined a similar phenomenon, and had predicted analytically the existence of oscillatory instability of cantilevered pipes conveying fluid; moreover, he perceived that the problem was independent of fluid friction. Both effects were later confirmed by Gregory and Paidoussis's work. Gregory and Paidoussis were able to obtain the critical flow velocity for the onset of oscillatory

instability and compared it with their own experimental values. Agreement was quite good.

Later on, Paidoussis extended the theory and performed experiments with vertical pipes, where gravity is operative [16]. Paidoussis and Deksnis also studied articulated vertical pipes [17], and specifically the transition from a discrete to a continuously flexible system, showing the inadequacy of two-degree-of-freedom approximations of continuous non-conservative systems. Chen [18] studied the stability of a pipe with the upstream end clamped and the downstream end constrained by a linear spring. Chen also studied the dynamics of curved pipes conveying fluid [19], [20], as well as pipes multiply supported, at regular intevals [21].

Herrmann [22] and Herrmann and Nemat-Nasser [23] showed the connection between the problem of a cantilever conveying fluid and the more general problem of a cantilever subjected to an end follower load. Subsequently, Wiley and Furkert [24] considered a fluid jet attached to a beam within the span; they found that either buckling or oscillatory instabilities, or both, may occur, depending on the boundary conditions.

Paidoussis and Denise [26] studied the dynamics of very thin pipes (shells) conveying fluid, both theoretically and experimentally. In addition to the classical flexural beam modes, they predicted and observed instabilities in the circumferential shell modes. Similar theoretical results were obtained independently by Weaver and Unny [17] and extended by Weaver and Myklatun [28].

In the case of fairly short shells supported at both ends, shell-mode divergence was found to occur first, with increasing flow velocity, and was closely followed by flutter - in the theory. In the experiments shell flutter only could be observed.

Paidoussis and Issid [29] re-examined the stability of pipes conveying fluid supported at both ends and found for the first time that, in this case also, if the flow velocity was increased beyond the point of onset of divergence, flutter could be precipitated. This matter of a conservative, albeit gyroscopic, system being subject to flutter was examined further [30].

In an attempt to improve the theory, especially for short tubes, Paidoussis and Laithier [31] used the Timoshenko beam theory to describe the dynamics of the pipe. They found that for short cantilevered tubes this theory agrees with experiments quite well, although for longer tubes, surprisingly, agreement in terms of the critical flow velocities is better when employing the Euler-Bernoulli theory. Moreover, buckling of very short heavy cantilevered pipes was predicted by theory for the first time, but not substantiated experimentally as yet.

Increasing interest has been developing recently in the nonlinear analysis of stability of pipes conveying fluid. Thurman and Mote [32] presented such an analysis for simply-supported pipes; the importance of nonlinear terms resulting from the extension of the pipes was found to increase with flow velocity, thus restricting the range of applicability of linear theory. Nevertheless, the predicted behaviour of the system was essentially as given by linear theory. Liu and Mote [33] conducted some careful experiments

in which they measured the frequency as a function of flow velocity, and found that for pipes supported at both ends they did not obtain the zero-frequency condition which characterizes divergence (buckling) - contrary to Dodds and Runyan's earlier observations. It is of interest that this is contrary, not only to linear theory, but also to Thurman and Mote's nonlinear theory, and the matter remains unresolved. More recently, Holmes [34] studied the qualitative effect of third-order nonlinear terms, which arise when axial displacements are not neglected, by means of ordinary nonlinear analysis and also by centre-manifold theory.

In all the studies above, the flow velocity was taken to be steady. Recently, Chen [35], albeit utilizing an incorrect equation of motion, and later Paidoussis and Issid [29] and Ginsberg [36] examined the stability of pipes conveying fluid with a flow velocity which has a small time-dependent harmonic component superposed on a steady flow velocity. They found that parametric resonances (instabilities) are possible for both cantilevered pipes and pipes supported at both ends. This theoretical work was extended by Paidoussis and Sundararajan [37], who found that combination resonances are also possible. The existence of both ordinary parametric and combination resonances was confirmed experimentally by Paidoussis and Issid [38].

The above is not meant to be an exhaustive literature review. The interested reader is referred to Paidoussis and Issid's paper [29] or to Chen's recent review [39].

1.2.2 Dynamics of cylindrical structures immersed in external axial flow

A common instability of structures subject to external flow is panel flutter. Since Lord Rayleigh, and subsequently Lamb [40], first discussed the problem of a flapping flag, considerable attention has been devoted to the flutter of sails, wings and panels, as evidenced by extensive literature reviews, e.g. [41], [42], [43], [44]. However, this subject is of limited usefulness to the study of the dynamics of bodies of revolution in axial flow, the flow conditions being quite different in the two cases. Similarly, the topic of thin structures (shells) subjected to flutter in parallel flow will not be discussed here.

Investigating the stability of (rigid) airships, Munk [45] calculated the aerodynamic forces exerted on their hulls. He showed that the fluid inertial loading may be expressed in terms of a virtual fluid mass which may be calculated from inviscid, ideal flow theory around ellipsoids of revolution; for slender bodies of circular cross-section, this mass is approximately equal to that of the displaced fluid. This result was later extended by Lighthill [46] to slender flexible bodies moving in fluid, in connection with his studies of aquatic animal propulsion. Incidentally, this work illustrated the similarity in fluid inertial loading on cylindrical beams moving in fluid to that experienced by a pipe conveying fluid.

Taking advantage of this similarity, Hawthorne [47] investigated the large-scale lateral motions ("snaking") of slender towed rubber oil tanks, called "Dracones", which were deleterious

to efficient towing. By a simplified analysis, he demonstrated that buckling was possible at sufficiently high towing speeds. Later, Paidoussis [48] showed theoretically and experimentally that rigid-body oscillations and flexural oscillatory instabilities are also possible, provided that the tow-rope is sufficiently long and the tail streamlined.

Starting *circa* the late 1950's a parallel body of literature had begun forming, in connection with the dynamics of nuclear fuel elements, normally arranged in bundles, in axial flow - which by now has become quite voluminous, as may be seen in a recent literature review [49]. Most of the early work on the subject did not perceive the observed small-amplitude vibrations of fuel elements as a true fluidelastic phenomenon; i.e. the coupled fluid-elastic forces were not considered, and the problem was simply viewed as one of response of the fuel elements to unspecified flow perturbations or to the boundary-layer pressure field, which were taken to be uncoupled to the motions of the cylindrical fuel elements.

The first systematic study of the dynamics of a cylinder immersed in axial flow was conducted by Paidoussis both theoretically and experimentally [50]. It was shown that flow damped free oscillations and reduced the natural frequencies of oscillation at small flow velocities; however, at sufficiently high flow velocities, cylindrical beams could buckle and, at yet higher flows, flutter. It was found, however, that for practical engineering structures, and nuclear reactors in particular, these instabilities

occur at extremely high flow velocities, due to the relatively high rigidity of the structures, and so are unlikely to be encountered in practice [51].

Nevertheless, the above study enabled researchers to study the problem in its proper perspective, and considerable progress was made in the study of the so-called "sub-critical" vibrations of reactor internals observed in practice - "sub-critical" denoting the fact that they occur below the critical values for onset of hydroelastic instabilities - by Paidoussis [52] and Chen and Wambsganss [53]. Moreover, at the moment there are four empirical or semi-empirical expressions for predicting the amplitude of these vibrations: Reavis' [54], Gorman's [55] mainly for two-phase flows, Paidoussis' [52], and Y.N. Chen's [56]. Chen and Wambsganss [53] also have means for obtaining these amplitudes, but their work is limited to very "quiet" flow systems, where the pressure near-field arising in the boundary layer is dominant. Further information may be obtained from critical reviews of this area of work [49], [57], [58], [59].

In all the above studies, even when considering bundles of very closely spaced cylinders, it was assumed that motions of one cylinder did not influence those of adjacent ones, i.e. the possibility of fluid coupling in the motions of cylinders was ignored. An attempt to take into account this effect, by considering the increase in the virtual mass due to confinement (by other cylinders and the flow channel), was made by Paidoussis [60]. In two remarkable recent papers, Chen [61], [62] calculated the virtual mass of arrays of cylinders in stationary liquid, and paved the way to taking fluid coupling fully into account. Some further work on the

subject was done by Chung and Chen [63]. It should be mentioned that most of this work is directed mainly towards the study of dynamics of arrays of cylinders in cross flow.

Finally, Curioni and Cesari [64] were probably the only researchers to date to deal with the case of a system subjected both to internal and external flow. In their short article, they consider buckling of horizontal pipes subjected to both flows, under various conditions.

1.2.3 General comments

The short literature review of the previous section will have given the reader, it is hoped, a fair impression of the remarkable developments that have taken place in the area of dynamics of "one-dimensional" structures subject to axial (internal or external) flow, during the past twenty years.

Several matters may be commented upon. Firstly, that unlike the proliferation of theoretical studies, experimental investigations are rather few. Thus, even in the case of pipes conveying fluid where experimentation is relatively simple, experimental work was only conducted by Dodds and Runyan [13], Paidoussis and co-workers [14], [16], [26], [38], Williams and Naguleswaran [25] and Liu and Mote [33]. A more acute state of affairs exists in the case of external flow, if one excludes the very considerable *ad hoc* work done on the response, rather than basic dynamics, of specific designs of nuclear fuel elements.

Another tendency in research in this field is the following. After the basic character of the dynamical behaviour of such systems was understood, researchers have generally looked in two distinct directions: (i) into more esoteric aspects of the problem, and (ii) into more applied features. The former sometimes yielded valuable and unexpected results (e.g., the discovery of flutter of "conservative" gyroscopic systems, shell-type instabilities with internal incompressible flow), but inevitably has led to a series of publications reporting on results which could have been foreseen *a priori*, at least qualitatively; although this is inevitable in terms of conducting research, perhaps the contribution of this latter series of papers is of doubtful value. The latter direction of research, into more practical problems, is of unquestionable value, provided of course that it addresses itself to real, as opposed to academically conceived, practical problems.

The topic of this thesis is a mixture of (i) and (ii) above. One of the original aims of this research was to extend the theory for the dynamics of flexible cylindrical bodies in axial flow to the case of conical bodies and test the theory experimentally. Although this would appear a straightforward extension of existing theory, some rather unexpected results showed the need for a much more careful and rewarding study of certain aspects of the theory - as will become apparent in the thesis. Another, more practical aim of this research was to fill a gap in existing knowledge by studying the dynamics of tubular slender bodies subjected simultaneously

to both internal and external flow, as would be the case in some heat exchangers (or in certain regions of some heat exchangers), the legitimate question having been asked of whether the effects of the two flows on stability are simply linearly superposable. The only previous study on the aspect of the problem, that of Gurioni and Cesari [64] is very limited in scope (e.g., surprisingly, only buckling instabilities are considered) and is not supported by experiments.

1.3 SCOPE

This thesis develops a general approach for the study of the instabilities of slender tubular beams, not necessarily of uniform cross-section, subjected to internal and external flows simultaneously. The tubular beams are assumed sufficiently thick and slender to be represented as Euler-Bernoulli beams; in addition, the effect of gravity (in the case of vertical systems) and material damping have been taken into consideration.

The equation of free vibrations is derived by classical vectorial mechanics and linearized for small coplanar motions. The internal and external flows are presumed to be independent one from the other along the full length of the beams, yet, coupling between the two flow velocities will appear in the equation through the base drag (in the case of a free downstream end). The forces exerted by the two flows are calculated separately; in the case of the external flow, the lift, calculated by use of slender body theory, will be corrected to account for the boundary layer.

Once the equation of motion and its boundary conditions have been obtained and rendered dimensionless, periodic solutions will be investigated. The method of solution is similar to Galerkin's, with eigenfunctions approximated by appropriate Fourier series.

The mathematical model thus obtained will be used (i) to compare the stability of quasi-cylindrical (in practice, only conical) structures to that of similar cylindrical structures, in cases where one of the two flows is at rest, and (ii) to investigate the superposability of the effects of simultaneous flows on the stability of cylindrical structures. Because of the linearity

of the model, the criterion for stability is the sign of the imaginary parts of the eigenfrequencies: instability is predicted for flow velocities which allow for at least one eigenfrequency with a negative imaginary part; the onset of buckling is characterized by a zero eigenfrequency and that of flutter by a purely real eigenfrequency different from zero.

In parallel to the theoretical work, experiments conducted in a vertical water-tunnel especially designed to provide the two (coaxial) flows will be reported. The dynamic behaviour of moulded rubber slender beams (solid or tubular), clamped at both ends or cantilevered (clamped upstream, free downstream) will be discussed for increasing internal and external flow velocities.

The prime purpose of the experiments is to check the theoretical predictions of instabilities in terms of critical flow velocities. In addition, however, because the physical parameters affecting stability (e.g. length, density, friction, damping, etc.) are too numerous to calculate stability diagrams for all possible combinations, the available experimental data will provide a framework for the theoretical calculations. Incidentally, the experiments provide additional information which, although of secondary importance to us here, is nevertheless useful: e.g. qualitative information on nonlinear effects and sub-critical vibrations, on the critical frequencies of oscillations and the associated modal shapes.

2. DERIVATION OF THE EQUATIONS OF MOTION

2.1 DYNAMIC EQUATIONS OF THE TUBE

Consider a tubular beam whose axis of symmetry, when vertically in its undeformed equilibrium state, coincides with both the direction of the undisturbed external flow and with the vertical x-axis pointing downwards; moreover, the inner and outer cross sections of the tube are concentric, but need not be uniform with respect to x. Because both internal and external surfaces of the tubular beam may have different taper angles, it will be convenient to express all forces along two directions only; namely, the tangential direction, i.e. that of the centerline, and the lateral direction, i.e. that of the normal to the centerline in the x-y plane in which motion is assumed to occur.

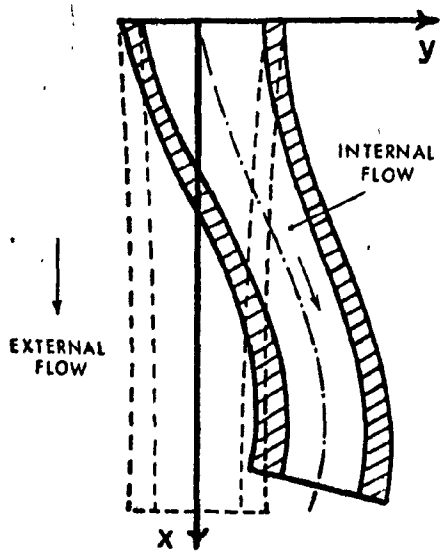

Furthermore, the x-direction will be referred to as 'axial', or vertical, and the y-direction as 'transverse', or horizontal, to distinguish them from the tangential and lateral directions defined above.

As briefly mentioned in the previous paragraph, we assume planar motion of the tube: no torsion, nor rotation around the x-axis will be considered because it is assumed that the eigenfrequencies of the torsional modes are well above those of

the flexural modes, and accordingly are subject to much greater damping; moreover, and by the same assumption, negligible coupling between flexural and torsional modes is expected.

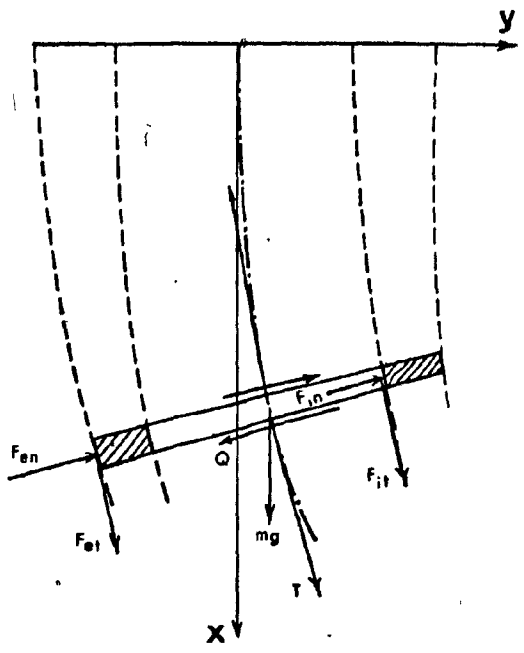

We shall first seek to derive the differential equations governing small motions of the tubular beam, in terms of the forces to which it is subjected, i.e. gravity force, tension T, shear force Q, and fluid forces F_{in}, F_{it}, F_{en}, F_{et} accounting for the normal and tangential forces per unit length exerted on the beam by the internal and external fluid, respectively. The functional form of these forces will be given later.

We restrict the analysis to small displacements and small slopes and assume that the effects of transverse-shear deformation is negligible; thus, first order balance of forces in the x- and y-directions yields the following two equations:

$$0 = \frac{\partial T}{\partial x} + F_{it} + F_{et} - (F_{in} + F_{en})\frac{\partial y}{\partial x} + \frac{\partial}{\partial x}(Q\frac{\partial y}{\partial x}) + \rho A g, \quad (1.1)$$

$$\rho A\frac{\partial^2 y}{\partial t^2} = \frac{\partial Q}{\partial x} + F_{in} + F_{en} + (F_{it} + F_{et})\frac{\partial y}{\partial x} + \frac{\partial}{\partial x}(T\frac{\partial y}{\partial x}), \quad (1.2)$$

where we assumed that the axial acceleration (stretching), in

the first equation, is negligible; ρ is the density of the material, and A the cross-sectional area of the tubular beam.

A third equation is derived from the moments; upon neglecting rotatory inertia (*vide* Appendix I), we obtain

$$0 = \frac{\partial M_e}{\partial x} + \frac{\partial M_i}{\partial x} + \frac{\partial M}{\partial x} + Q \ ,$$

where M_e and M_i are the moments induced by external and internal fluids respectively; and we write the flexural moment, M, in terms of the complex Young's modulus, E*, and the moment of inertia, I, as follows:

$$M = E^* I \frac{\partial^2 y}{\partial x^2} \ .$$

We shall normally use a viscoelastic Kelvin-Voigt model to represent the internal damping of the material. Thus, we set

$$M = EI\left(1 + k\frac{\partial}{\partial t}\right)\frac{\partial^2 y}{\partial x^2} \ ;$$

however, we shall later consider k to depend upon the frequency of motion in order to take into account hysteretical damping characterestics (*vide* Appendix K).

The third equation now yields

$$Q = -\frac{\partial}{\partial x}\left[EI\left(1 + k\frac{\partial}{\partial t}\right)\frac{\partial^2 y}{\partial x^2}\right] - \frac{\partial M_i}{\partial x} - \frac{\partial M_e}{\partial x} \qquad (1.3)$$

Clearly, the shear Q may be eliminated from the other equations by use of eq.(1.3), and T can be calculated by integrating eq.(1.1); hence, eq.(1.2) becomes the equation of motion. In the next four chapters we shall complete the derivation of the equation of motion by calculating

a) the components of the internal fluid forces F_{in} and F_{it},

b) the components of the external fluid forces F_{en} and F_{et},

c) the internal and external moments M_i and M_e (in order to obtain Q),

d) the axial and transverse boundary conditions (in order to obtain T, and the boundary conditions governing y).

2.2 DYNAMIC EQUATIONS OF THE INTERNAL, FLOW

We shall assume the following approximations to hold in any cross-section:

a) the axial velocity profile is uniform,

b) there is no significant secondary cross-flow, i.e. kinematically the fluid moves laterally as a flexible solid of zero rigidity (except for the taper effects).

Such approximations are reasonable whenever the boundary layer is turbulent and fully developed, and if small curvatures of the flow trajectories are being considered. In fig.a we illustrate the convergent velocity profile for a spherical cross-section of fluid in a conical conduit, inclined with respect to the x-axis and stationary. The velocity is (quasi) uniform in a cross-section, i.e. the value of U_i is constant. Terms of second order with respect to the taper angle β_i are negligible, and therefore we may neglect the axial curvature and consider a flat cross-section, as illustrated in fig.b. It will be found convenient to define the non-inertial axes OX,OY,OZ attached to the cross-section of the tubular beam.

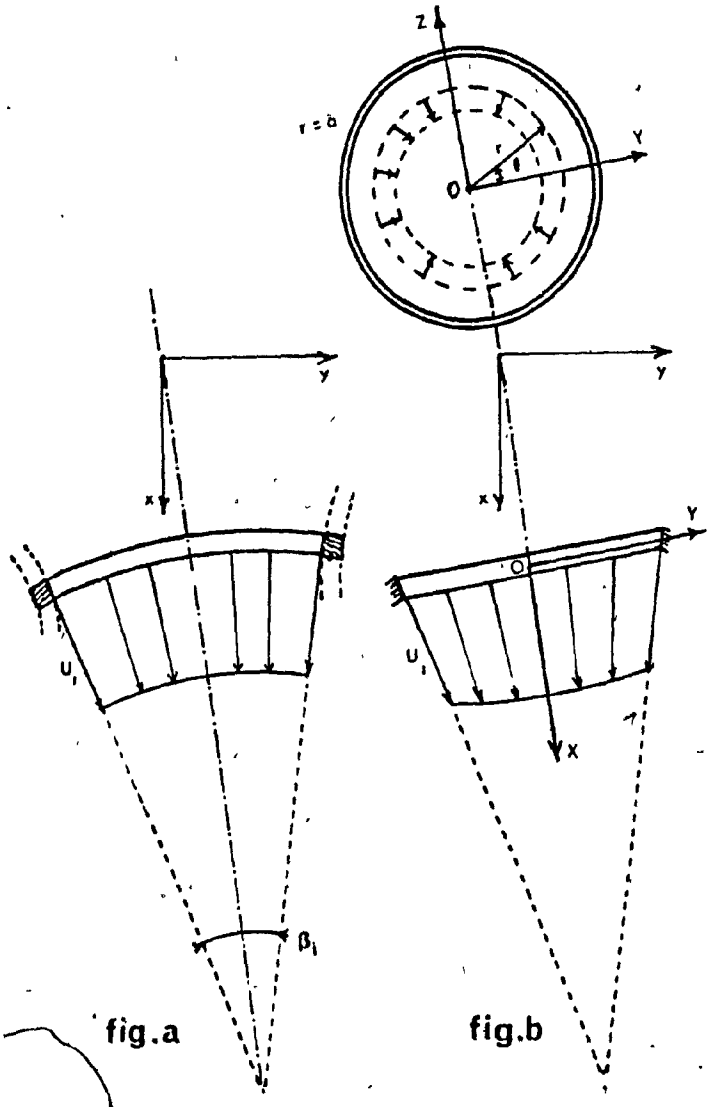

fig.a fig.b

When the tubular beam suffers lateral motions, we shall neglect secondary-flow effects. Hence, the absolute velocity of the fluid, $\vec{V}_i$, is the sum of the relative velocity $\vec{U}_i$ and the velocity of point O on the centerline, which has the value $\partial y/\partial t$.

We need not account for axial motion of the beam because the axial displacement, which is equal to the integral of $\frac{1}{2}[\partial y/\partial x]^2$, is small to the second order.

However, we must consider the effect of rotation of a cross-section of the tubular beam around the Z-axis. Let the angular velocity be $\Omega=\partial^2 y/\partial x \partial t$. For small angular motions the displacement of the tube is tangential and parallel to the main direction of the flow; therefore, apart from additional shear at the wall and in the boundary layer (assumed negligibly thin), the fluid will slip and the rotation will have little effect on the absolute velocity distribution; in fact, the streamlines relative to the beam are constant and therefore, at a distance Y from the Z-axis, the flow velocity relative to the tubular beam is expressed as follows:

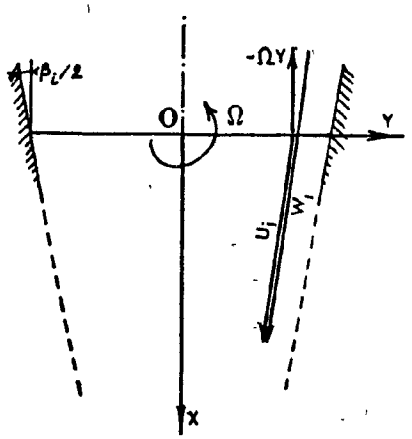

$$\vec{W}_i = \vec{U}_i\left(1 + \frac{\Omega Y}{U_i}\right),$$

where, upon neglecting second order terms with respect to β_i, ΩY is the additional velocity component, along the flow trajectory due to rotation.

The rate of change of the flow momentum, inside the control volume Δw of an element of the tube of length dx, may be expressed in terms of the convective derivative of the absolute

velocity V_i, and the density, ρ_i, as follows:

$$\frac{d}{dt}\int_{\Delta w}\rho_i\vec{V}_i\,d(\Delta w) = \int_{\Delta w}\rho_i\{\frac{\partial\vec{V}_i}{\partial t} + (\vec{V}_i\cdot\vec{\nabla})\vec{V}_i\}d(\Delta w).$$

Alternatively, we may evaluate the rate of change of the flow momentum relative to the non-inertial control volume attached to the tubular beam, and then add the apparent body forces as follows:

$$\int_{\Delta s}\rho_i\vec{W}_i[\vec{W}_i\cdot d(\Delta\vec{s})] + \frac{\partial}{\partial t}\int_{\Delta w}\rho_i\vec{W}_i d(\Delta w) + \int_{\Delta w}(\frac{d^2\vec{O}}{dt^2}+2\vec{\Omega}\times\vec{W}_i+\vec{\Omega}\times\vec{\Omega}\times\vec{r}+\frac{d\vec{\Omega}}{dt}\times\vec{r})\rho_i d(\Delta w). \tag{2.1}$$

The second alternative is more attractive; thus, the first integral represents the net flux of momentum across the non-inertial control volume boundaries; since no momentum flux crosses the wall, the net flux is merely the difference between the fluxes across the two flat faces of the control volume, which may be written as follows:

$$\frac{\partial}{\partial x}\{\int_{A_i}\rho_i\vec{W}_i(\vec{W}_i\cdot\vec{dA}_i)\}dx\ ,$$

A_i being the cross-sectional area. Now, upon considering elementary areas on each face bounded by the same streamlines, we obtain

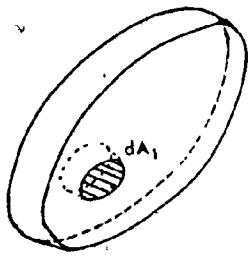

$$\rho_i dx\int_{A_i}\frac{\partial}{\partial x}(\vec{W}_i)W_i dA_i\ ,$$

where continuity has been invoked for each stream-tube. The second integral of (2.1) represents the rate of increase of momentum within the volume; the size of the control volume

remains constant, hence,

$$\frac{\partial}{\partial t}\int_{\Delta w}\rho_i \vec{W}_i dw = \rho_i dx \int_{A_i}\frac{\partial \vec{W}_i}{\partial t}\, dw \ ;$$

however, the value of $\vec{W}_i$ at a point fixed with respect to the control volume changes in time because of the rotation of the control volume, and we have

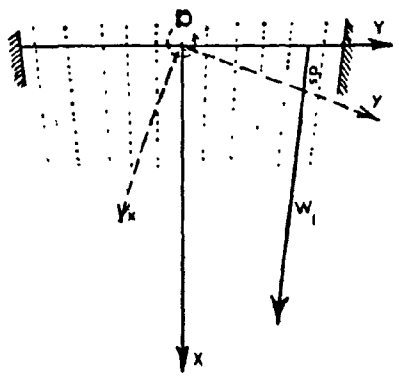

$$\frac{\partial \vec{W}_i}{\partial t} = \frac{\partial \vec{W}_i}{\partial s}\frac{\partial s}{\partial t} \sim \frac{\partial \vec{W}_i}{\partial x}\times(-Y\Omega) \ .$$

Hence, the two integrals of (2.1) relative to the non-inertial control volume yield

$$\rho_i dx \int_{A_i}\frac{\partial \vec{W}_i}{\partial x}(W_i - Y\Omega)dA_i = \rho_i dx \int_{A_i}\frac{\partial \vec{W}_i}{\partial x}U_i dA_i$$

$$= \rho_i U_i dx \int_{A_i}\frac{\partial \vec{W}_i}{\partial x}dA_i \ ,$$

which, upon neglecting second order terms, yields

$$\rho_i A_i U_i \frac{\partial \vec{V}}{\partial x}dx \ ,$$

where $\vec{V}$ is the value of $\vec{W}_i$ and $\vec{U}_i$ at the center line. Finally, the last integral of (2.1), which relates to the acceleration of the origin of the moving frame of reference and the Coriolis, centrifugal and tangential accelerations, yields

$$\int_{\Delta w} [\frac{\partial^2 \vec{y}}{\partial t^2} + 2\vec{\Omega}\times\vec{U}_i(1+\frac{\Omega Y}{U_i}) + \vec{\Omega}\times\vec{\Omega}\times\vec{r} + \frac{d\vec{\Omega}}{dt}\times\vec{r}]\rho_i d(\Delta w) \sim \int_{\Delta w} (\frac{\partial^2 \vec{y}}{\partial t^2} + 2\vec{\Omega}\times\vec{U}_i)\rho_i d(\Delta w)$$

$$\sim \rho_i A_i (\frac{\partial^2 \vec{y}}{\partial t^2} + 2U_i \frac{\partial^2 \vec{y}}{\partial x \partial t}) dx .$$

In summary, the rate of change of momentum per unit length is,

$$\rho_i A_i [\frac{\partial^2 \vec{y}}{\partial t^2} + 2U_i \frac{\partial^2 \vec{y}}{\partial x \partial t} + U_i \frac{\partial \vec{V}}{\partial x}] ,$$

which yields two components,

a) in the x-direction $\rho_i A_i U_i \frac{\partial U_i}{\partial x}$;

b) in the y-direction $\rho_i A_i [\frac{\partial^2 y}{\partial t^2} + 2U_i \frac{\partial^2 y}{\partial x \partial t} + U_i \frac{\partial}{\partial x}(U_i \frac{\partial y}{\partial x})]$. (2.2)

This rate of change of momentum balances the external forces on the fluid element; hence, we obtain

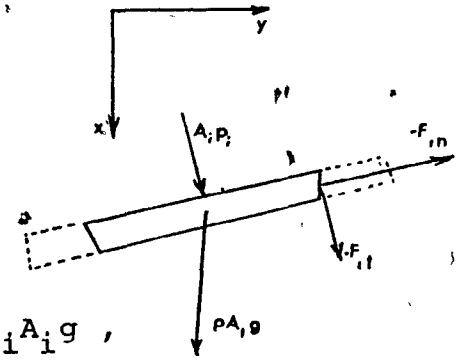

$$\rho_i A_i U_i \frac{\partial U_i}{\partial x} = - \frac{\partial}{\partial x}(A_i p_i) - F_{it} + F_{in} \frac{\partial y}{\partial x} + \rho_i A_i g ,$$

$$\rho_i A_i (\frac{\partial}{\partial t} + U_i \frac{\partial}{\partial x})^2 y = \frac{\partial}{\partial x}(A_i p_i \frac{\partial y}{\partial x}) - F_{it} \frac{\partial y}{\partial x} - F_{in} ,$$

where $p_i(x)$ is the average pressure along the median line. Then, as required for eq. (1.1) and (1.2), we write

$$F_{it} - F_{in} \frac{\partial y}{\partial x} = - \frac{\partial}{\partial x}(A_i p_i) - \rho_i A_i U_i \frac{\partial U_i}{\partial x} + \rho_i A_i g ,$$

$$F_{in} + F_{it} \frac{\partial y}{\partial x} = - \frac{\partial}{\partial x}(A_i p_i \frac{\partial y}{\partial x}) - \rho_i A_i (\frac{\partial}{\partial t} + U_i \frac{\partial}{\partial x})^2 y . \qquad (2.3)$$

2.3 DYNAMICS OF THE EXTERNAL FLOW

2.3.1 General Derivation

It is unfortunately impossible to proceed with the formulation of forces due to the external flow exactly in the same manner as for the internal flow. For instance, for an unconfined external flow*, we will have a constant total-pressure head in the main, large-scale flow and a boundary layer; friction at the wall of the tubular beam* can no longer be related to the pressure drop in the large-scale flow but to the boundary layer. Another difference with the previous case arises as we now take into account the secondary (cross) flow, since the axial velocity does not coincide, not even approximately, with the axis of the beam; the lateral resultant velocity between the beam and the undisturbed axial flow, is $v_e \simeq \frac{\partial y}{\partial t} + U_e \frac{\partial y}{\partial x}$, as illustrated in the diagram.

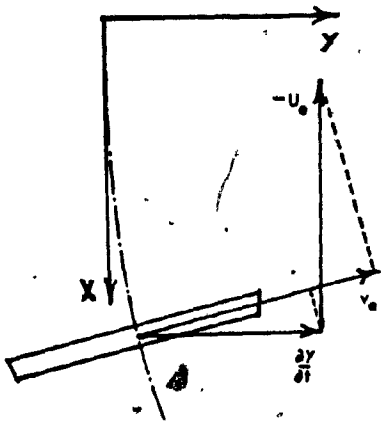

Consequently, it is impracticable to derive dynamic equations from a control volume as in the case of internal flow; instead, we shall directly evaluate all forces entering the calculation of F_{en}, F_{et}.

According to slender body theory, the lateral flow generated by motions of the beam may adequately be represented, near the beam, by a two-dimensional potential flow; such a flow has a momentum $M_e v_e$ per unit length, where the virtual mass M_e

---

* To be referred to simply as "the beam" for short, in this section.

will be approximately equal to $\rho_e A_e$, the value corresponding to an infinitely long circular cylinder; ρ_e is the density of the external fluid, and A_e the full cross-sectional area of the beam. The corresponding change of flow momentum in the tangential direction is zero for an infinite cylinder and may be neglected for very elongated yet non-cylindrical beams, such as those under consideration, provided that the wavelength of motion remains large in comparison to the diameter. Hence, we need only consider the rate of change of momentum of the lateral flow which exerts an opposite force on the beam; this force, calculated per unit length, will be referred to as the lift, L;

$$L = -\left(\frac{\partial}{\partial t} + U_e \frac{\partial}{\partial x}\right)\{M_e v_e\} = -\left(\frac{\partial}{\partial t} + U_e \frac{\partial}{\partial x}\right)\{\rho_e A_e \left(\frac{\partial y}{\partial t} + U_e \frac{\partial y}{\partial x}\right)\}. \quad (3.1)$$

We now consider shear at the surface of the beam; let q_{et} and q_{en} be the tangential and normal frictional forces exerted per unit length; in the absence of any other pressure effects, we may write

$$F_{en} = -\left(\frac{\partial}{\partial t} + U_e \frac{\partial}{\partial x}\right)\{\rho_e A_e \left(\frac{\partial y}{\partial t} + U_e \frac{\partial y}{\partial x}\right)\} + q_{en}$$

$$F_{et} = q_{et};$$

then, adding F_x and F_y, the steady pressure forces per unit length of beam in the x- and y-directions, the fluid forces in the two directions as required for eq.(1.1) and (1.2) are given by

$$F_{et} - F_{en}\frac{\partial y}{\partial x} = q_{et} - q_{en}\frac{\partial y}{\partial x} + F_x ,$$

$$F_{en} + F_{et}\frac{\partial y}{\partial x} = -\left[\frac{\partial}{\partial t} + U_e\frac{\partial}{\partial x}\right]\left[\rho_e A_e\left(\frac{\partial y}{\partial t} + U_e\frac{\partial y}{\partial x}\right)\right] + q_{en} \qquad (3.2)$$

$$+ q_{et}\frac{\partial y}{\partial x} + F_y .$$

The pressure components F_x and F_y will now be calculated.

2.3.2 Pressure and gravity effects

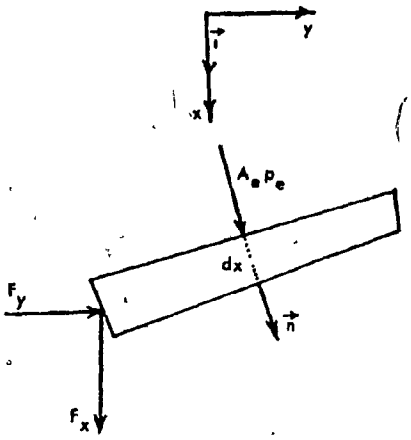

If we consider an element dx of beam immersed in fluid on all sides, the buoyancy force acting on it is simply the integral of the pressure forces acting on the total surface Δs of the element, i.e.

$$\Delta\vec{B} = \int_{\Delta s} -p_e\vec{n}\, ds = \int_{\Delta w}\vec{\nabla}p_e\, dw = -\frac{\partial p_e}{\partial x}\Delta w\,\vec{i} ,$$

where Δw is the volume of the element, i.e. $A_e dx$, and $\vec{i}$ a unit vector in the x- direction, (provided there is only an axial pressure gradient). Clearly, if we now subtract from the buoyancy force the pressure forces acting on the top and bottom flat faces, we shall obtain the resultant of the pressure forces acting on the outer surface; the force acting on each face is $A_e p_e$, and is applied at the center, hence

$$\vec{F}\,dx = \Delta\vec{B} - [(-A_e p_e \vec{n})_{x+dx} + (A_e p_e \vec{n})_x] = \Delta\vec{B} + \frac{\partial}{\partial x}[A_e p_e \vec{n}]dx \ ;$$

$\vec{n}$ is the unit normal pointing towards $x>0$.

Hence, the two components of $\vec{F}$ are simply

$$F_x = -\frac{\partial p_e}{\partial x} A_e + \frac{\partial}{\partial x}[A_e p_e] \text{ or } p_e \frac{\partial A_e}{\partial x}$$

and $$F_y = \frac{\partial}{\partial x}[A_e p_e \frac{\partial y}{\partial x}] \ .$$

Now, p_e may be written as follows:

$$p_e(x) = p_{eh}(x) + \frac{1}{2}\rho_e U_e^2 \, c_p(x) \ , \qquad (3.3)$$

where $p_{eh}(x)$ is the pressure in the uniform vertical flow far from the beam, and c_p is a corrective pressure coefficient to take into account the effects of taper, boundary layer and motion of the beam; c_p is normally small, and we will choose p_{eh} sufficiently large in order to have

$$p_{eh} >> \frac{1}{2}\rho_e U_e^2 \, c_p$$

and then $p_e \sim p_{eh}$ and $F_x \sim p_{eh} \frac{\partial A_e}{\partial x}$; we may also write

$$F_x \sim \frac{\partial}{\partial x}(A_e p_{eh}) - A_e \frac{\partial p_{eh}}{\partial x} = \frac{\partial}{\partial x}(A_e p_{eh}) - \rho_e A_e g \ .$$

If we now expand F_y, we obtain

$$F_y = \frac{\partial p_e}{\partial x}\left(A_e \frac{\partial y}{\partial x}\right) + p_e \frac{\partial}{\partial x}\left(A_e \frac{\partial y}{\partial x}\right) \ .$$

Even though $p_e \sim p_{eh}$, we may not set a priori

$$\frac{\partial p_{eh}}{\partial x} \sim \frac{\partial p_e}{\partial x} ;$$

however, the derivative of c_p with respect to x is small compared with q_{et} and may therefore be neglected in eq.(3.2) as shown in Appendix F. Hence, provided that the beam tapers slowly we may set

$$p_e = p_{eh}$$

and rewrite eq.(3.2) as follows:

$$F_{et} - F_{en}\frac{\partial y}{\partial x} = q_{et} - q_{en}\frac{\partial y}{\partial x} - \rho_e g A_e + \frac{\partial}{\partial x}(A_e p_e),$$

$$F_{en} + F_{et}\frac{\partial y}{\partial x} = -\left(\frac{\partial}{\partial t} + U_e\frac{\partial}{\partial x}\right)\left\{\rho_e A_e\left(\frac{\partial y}{\partial t} + U_e\frac{\partial y}{\partial x}\right)\right\} \qquad (3.4)$$

$$+ q_{en} + q_{et}\frac{\partial y}{\partial x} + \frac{\partial}{\partial x}\left[A_e p_e \frac{\partial y}{\partial x}\right].$$

2.3.3 External Frictional Forces

We shall assume the boundary layer to be turbulent over the whole length of the beam; transition from laminar to turbulent layer will be assumed to take place some short distance from the leading edge, prior to the beam itself, on the upstream support. This assumption will not be too restrictive since our major concern in this study is not directed at sub-critical vibrations, which might involve sub-critical Reynolds numbers, but at instabilities which will generally require Reynolds numbers of the order of 10^6.

For long cylinders, inclined in a turbulent flow Taylor [65] established the following expressions for the normal and tangential forces per unit length

$$F_n = \frac{1}{2}\rho_e D_e U_e^2 [C_{dp} \sin^2 i + C_f \sin i] ,$$

$$F_t = \frac{1}{2}\rho_e D_e U_e^2 C_f \cos i , \qquad (3:5)$$

where D_e is the diameter of the beam, C_{dp} and C_f are coefficients associated with form and skin-friction drag for a cylinder in cross-flow, and i is the angle of attack; upon generalizing to a beam which incurs very small transverse motions we have

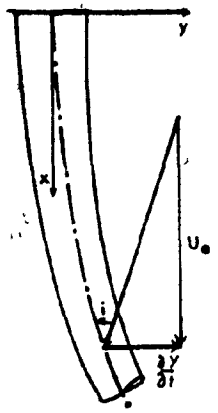

$$i = \frac{\partial y}{\partial x} + \tan^{-1}[\frac{1}{U_e}\frac{\partial y}{\partial t}] \sim \frac{\partial y}{\partial x} + \frac{1}{U_e}\frac{\partial y}{\partial t} . \qquad (3.6)$$

The formulae in eq.(3.5) have been subsequently transformed by Paidoussis [57] to yield, for small motions,

$$F_n = \frac{C_{fn}}{2}\rho_e D_e U_e [\frac{\partial y}{\partial t} + U_e \frac{\partial y}{\partial x}] + \frac{\mu_e}{2} C_D \frac{\partial y}{\partial t} ,$$

$$F_t = \frac{C_{ft}}{2}\rho_e D_e U_e^2 ,$$

where, apart from the dynamic viscosity μ_e, C_D is an empirical coefficient depending upon Reynolds and Strouhal numbers, which has been introduced to account for viscous damping at the lower

flow velocities; moreover, as suggested by Taylor [65], we have $C_{fn} \sim C_{ft}$.

It will now be convenient to introduce the following parameter, which has the dimensions of a velocity

$$U_v = \frac{\mu_e C_D}{\rho_e D_e} ,$$

and rewrite the previous formulae as follows:

$$F_n = \frac{1}{2}\rho_e D_e [C_{fn} U_e (\frac{\partial y}{\partial t} + U_e \frac{\partial y}{\partial x}) + U_v \frac{\partial y}{\partial t}] ,$$

$$F_t = \frac{1}{2} C_{ft} \rho_e D_e U_e^2 .$$

We shall further assume that these formulae hold for slender tapered beams with very small taper angles (e.g. less than 1 deg.) - in order to remain well below critical angles for which flow separation would occur. Hence, we shall write the local friction forces (per unit length), as

$$q_{en}(x) = -\frac{1}{2}\rho_e D_e(x) [U_e C_{fn} (\frac{\partial y}{\partial t} + U_e \frac{\partial y}{\partial x}) + U_v \frac{\partial y}{\partial t}] ,$$

$$q_{et}(x) = \frac{1}{2}\rho_e D_e(x) U_e^2 C_{ft} . \qquad (3.7)$$

As previously mentioned, since we shall devote little attention to flows in the subcritical range of Reynolds numbers, we shall usually assume that $U_v << U_e C_{fn}$ and set $U_v = 0$. The value of C_{ft} (and C_{fn}) will be derived from boundary layer calculations at zero incidence (in Appendix G).

2.3.4 Boundary Layer Effects

In previous work [57],[66] the effect of the boundary layer was considered merely by taking into account the friction terms, as represented by eq.(3.7). The lift exerted on the beam was calculated by slender body theory, neglecting the boundary layer displacement thickness with respect to the diameter of the beam. However, such an assumption may become less applicable as we move from uniform to tapered beams, especially as we approach fully conical shapes. Indeed, the observed stability of such beams cannot be explained by the theory developed up to now, as will be discussed more fully in Chapter 5.

In order to take into account the effect of the axial boundary layer on the lateral motions, we first consider the body formed by the beam surrounded by the displacement thickness, δ_1; the cross-sectional area is now A_e^*, instead of A_e, and the lift derived from eq.(3.1), yields

$$L = -\left(\frac{\partial}{\partial t} + U_e \frac{\partial}{\partial x}\right)\left\{\rho_e A_e^* \left(\frac{\partial y}{\partial t} + U_e \frac{\partial y}{\partial x}\right)\right\}. \qquad (3.8)$$

Unfortunately, this result assumes that the fluid within the displacement thickness remains at the wall even for the lateral motion of the beam; in particular, it implies that there is a displacement thickness in the cross-flow which is identical to that in the axial flow! In fact, we are dealing here with a three-dimensional rather than a two-

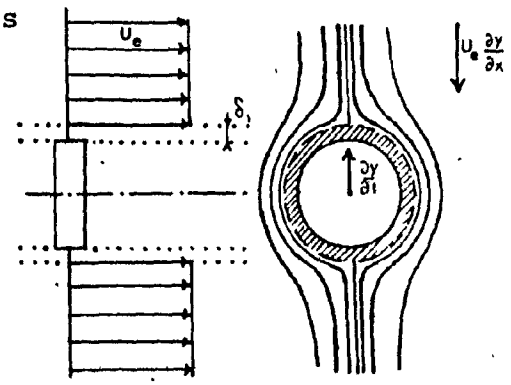

dimensional problem, and the cross-flow displacement thickness is likely to be negligible, because (a) the cross-flow velocities are of first order with respect to $\frac{\partial y}{\partial t}$ and $U_e \frac{\partial y}{\partial x}$, thus yielding Reynolds numbers small enough to avoid separation, and (b) the shear in the lateral flow is low due to the high level of turbulence induced by the axial boundary layer. Now, if there is no boundary layer due to the lateral motion of the beam, the quantity of fluid displaced and the lift derived in eq.(3.8), have been overestimated. Making this assumption, the momentum of the fluid supposedly displaced by the axial boundary layer, moving at a velocity, $\frac{\partial y}{\partial t}$, is approximately equal to that of the fluid within the displacement thickness; its rate of change is

$$(\frac{\partial}{\partial t} + U_e \frac{\partial}{\partial x})\{\rho_e (A_e^* - A_e)\frac{\partial y}{\partial t}\} ;$$

and, the resulting lift, which is the opposite, must be subtracted from eq.(3.8); the following expression is now obtained:

$$L = - (\frac{\partial}{\partial t} + U_e \frac{\partial}{\partial x})\{\rho_e (A_e \frac{\partial y}{\partial t} + A_e^* U_e \frac{\partial y}{\partial x})\} . \qquad (3.9)$$

This expression can be interpreted simply upon considering the cross-flow to be the superposition of two potential flows; one results from the motion of the beam alone, i.e. of cross-sectional

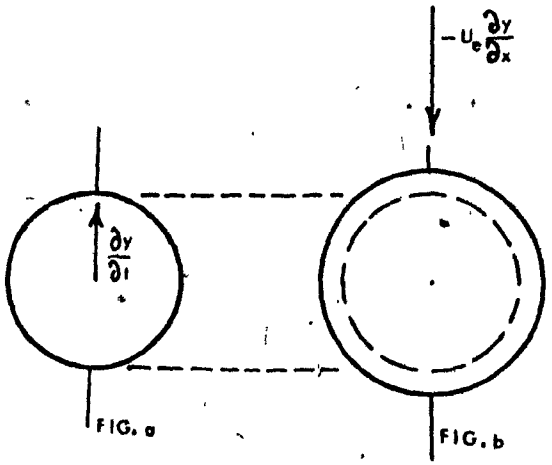

area A_e, moving at velocity $\frac{\partial y}{\partial t}$ (as shown on fig.a); the other one results from the motion of the fluid, flowing at an average velocity $-U_e \frac{\partial y}{\partial x}$, past the contour formed by the beam and the axial boundary layer thickness, i.e. of cross-sectional area A_e^* (fig.b); eq.(3.9) states that the lift exerted on the beam is simply the sum of the lifts exerted by the two flows. Such a result is generally false, but we expect eq.(3.9) to give useful approximations, when the trajectories of the both flows are close, i.e. for small boundary layer, or when one flow prevails over the other.

Let us now examine another assumption concerning the axial boundary layer implied in this sub-section. The derivation of eq.(3.8) and, subsequently (3.9) assumes that, with respect to the cross-flow, the relative velocity of the beam and the beam augmented by δ_1 are the same, i.e. $\frac{\partial y}{\partial t} + U_e \frac{\partial y}{\partial x}$; in other words, the boundary layer is fixed with respect to the beam and consequently axisymmetric, as for a beam in a co-axial flow. In fact, as the boundary layer increases, it becomes less sensitive to the motion of the beam which, in turn, becomes insulated from the axial flow. We may then imagine that the beam moves within its boundary layer as if the axial velocity were reduced in that region. In order to represent this insulation effect, we shall reduce the lift calculated in eq.(3.9) by multiplying U_e with a corrective factor. This factor should be close to unity when the boundary layer thickness is negligible with respect to the local diameter, and close to zero when it is very large. The ratio A_e/A_e^* appears to be a good and convenient

measure of this effect; the reduced velocity, U_e^*, which we now consider, is such that

$$A_e^* U_e^* = A_e U_e \ .$$

Finally, eq.(3.9) yields

$$L = - \left(\frac{\partial}{\partial t} + U_e^* \frac{\partial}{\partial x}\right) \left[\rho_e A_e \left(\frac{\partial y}{\partial t} + U_e \frac{\partial y}{\partial x}\right)\right] . \qquad (3.10)$$

The validity of eq.(3.10) can be checked in two cases. First, for a cylinder translating laterally and parallel to the axis of the flow, the lift reduces to the following term:

$$- \rho_e A_e \frac{\partial^2 y}{\partial t^2} \ ,$$

which illustrates adequately that the virtual mass of the cross-flow is independent of the boundary layer. Second, for a stationary bent cylinder, the lift reduces to the following term:

$$- \rho_e A_e U_e U_e^* \frac{\partial^2 y}{\partial x^2} \text{ or } - \rho_e \frac{A_e^2}{A_e^*} U_e^2 \frac{\partial^2 y}{\partial x^2} \ ,$$

which depends on the boundary layer and diminishes as the displacement thickness increases. In the above, the choice of the displacement thickness, δ_1, rather than the momentum thickness, δ_2, is disputable; however, for a turbulent flow, the two values are not drastically different: experimentally, the shape factor is close to 1.4 for a flat plate, whereas the familiar n=7 power law predicts $\delta_1/\delta_2 = 1+2/n \sim 1.3$.

The two equations of (3.4) are now rewritten as follows:

$$F_{et} - F_{en}\frac{\partial y}{\partial x} = q_{et} - q_{en}\frac{\partial y}{\partial x} - \rho_e g A_e + \frac{\partial}{\partial x}(A_e p$$

$$F_{en} + F_{et}\frac{\partial y}{\partial x} = q_{en} + q_{et}\frac{\partial y}{\partial x} + \frac{\partial}{\partial x}(A_e p_e \frac{\partial y}{\partial x}) \qquad (3.11)$$

$$-(\frac{\partial}{\partial t} + U_e^* \frac{\partial}{\partial x})[\rho_e A_e (\frac{\partial y}{\partial t} + U_e \frac{\partial y}{\partial x})] \ ,$$

in order to substitute F_{en} and F_{et} from eq.(1.1) and eq.(1.2).

2.4 MOMENTS INDUCED BY EXTERNAL AND INTERNAL FLOWS

2.4.1 Notation

Before proceeding to calculate the moments induced by the flows we shall introduce specific operators to denote convective derivatives. We shall define the operator $\mathcal{D}$ such that

$$\mathcal{D}(\ldots) = \left(\frac{\partial}{\partial t} + U\frac{\partial}{\partial x}\right)(\ldots) \quad .$$

Hence,

a) for the external fluid,

$$\mathcal{D}_e = \left(\frac{\partial}{\partial t} + U_e \frac{\partial}{\partial x}\right) \quad \text{and} \quad \mathcal{D}_e^* = \left(\frac{\partial}{\partial t} + U_e^* \frac{\partial}{\partial x}\right).$$

and $$\mathcal{D}_e^2 = \left(\frac{\partial}{\partial t} + U_e \frac{\partial}{\partial x}\right)^2 = \left(\frac{\partial^2}{\partial t^2} + 2U_e \frac{\partial^2}{\partial x \partial t} + U_e^2 \frac{\partial^2}{\partial x^2}\right) \quad ;$$

b) for the internal fluid,

$$\mathcal{D}_i = \left(\frac{\partial}{\partial t} + U_i \frac{\partial}{\partial x}\right)$$

and because U_i is function of x we will have, for instance,

$$\mathcal{D}_i^2 = \left(\frac{\partial}{\partial t} + U_i \frac{\partial}{\partial x}\right)^2 = \left(\frac{\partial^2}{\partial t^2} + 2U_i \frac{\partial^2}{\partial x \partial t} + U_i^2 \frac{\partial^2}{\partial x^2} + U_i \frac{\partial U_i}{\partial x} \frac{\partial}{\partial x}\right) .$$

2.4.2 Evaluation of the Moments

Let Σ represent the external or internal wall of an element dx of the tubular beam: in the case of external flow the pressure acts on the outside of Σ, whereas for the internal flow it acts on the inside.

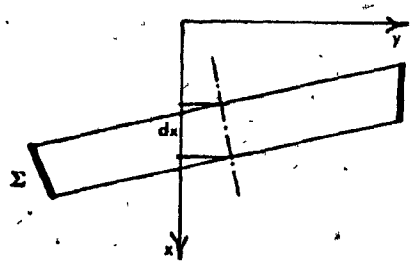

We may express the pressure at a given flow velocity as

$$p(x,\theta,t) = p_o(x) + p_1(x,\theta,t);$$

where p_o is the component of pressure independent of lateral displacement, hydrostatic in the case of external flow, and quasi-hydrostatic in the case of internal flow (because taper angles and frictional losses are small); p_1 is the perturbation component, which is function of the motion and the position of the beam, and symmetrically distributed with respect to the plane of motion (symmetric with respect to the polar angle θ).

Let us first eliminate the moment due to p_o. By use of the rationale employed in §2.3.2, we imagine the element immersed in fluid on all sides; the total moment exerted on this element being null, the moment exerted on Σ is equal and opposite to that exerted on the two flat faces; this moment, calculated in O, yields $\frac{1}{2} A p_o (\partial^2 y/\partial x^2) dx^2$; this is negligible because of the factor dx^2. Therefore, any moment results from p_1 only. Let Q be any point on Σ, the moment calculated about O, on the center-line, is

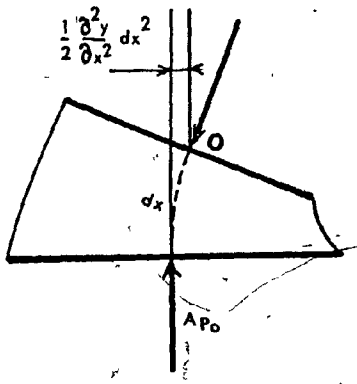

$$d\vec{M} = \int_{\Sigma} -p_1 \vec{n} \times \vec{OQ}\, d\sigma \quad ;$$

$\vec{n}$ is the normal unit vector pointing out of the wall. Since p_1 is of first order with respect to y (or its derivatives) and since no higher order terms are required in eq.(1.3), we may consider an element, undeformed and centered on the x-axis.

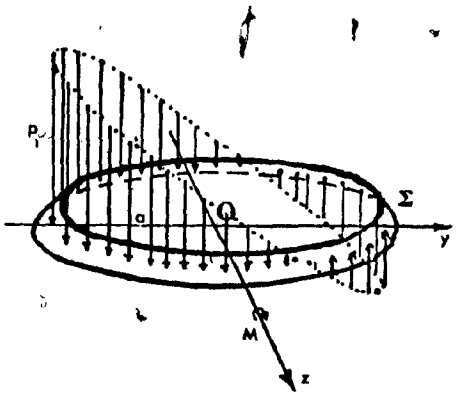

The only finite cylindrical coordinate of $O\vec{Q}$ is radial, horizontal and equal to a, the local radius of Σ; hence, only the axial components of the pressure forces will contribute to dM; moreover, Σ and p_1 being symmetric with respect to the x-y plane, the resultant will be in the z direction as illustrated on the diagram. Let $\vec{i},\vec{j},\vec{k}$ be unit vectors in the x,y,z directions; then,

$$d\vec{M} = \int_\Sigma (-\vec{p}_1\vec{n}\times O\vec{Q}).\vec{k}\, d\sigma$$

$$= -\int_\Sigma (O\vec{Q}\times\vec{k}).p_1\vec{n}\, d\sigma = -\int_\Sigma (O\vec{Q}.\vec{j})(\vec{j}\times\vec{k}).p_1\vec{n}\, d\sigma$$

$$= -\int_\Sigma (O\vec{Q}.\vec{j})(\vec{n}.\vec{i})\, p_1 d\sigma .$$

Let us now compare dM with the transverse lift, $L\,dx$, exerted on Σ; we have

$$L\,dx = \int_\Sigma -p_1\vec{n}.\vec{j}\, d\sigma \quad ;$$

upon introducing the unit radial vector $\vec{r}$, such that $O\vec{Q} = a\vec{r}$ we obtain

$$\vec{n}.\vec{j} = (n_r\vec{r}+n_x\vec{i}).\vec{j} = (\vec{n}.\vec{r}).\ (\frac{O\vec{Q}}{a}.\vec{j}).$$

Since $\vec{n}.\vec{i}$ and $\vec{n}.\vec{r}$ represent the cosine and the sine of the taper angle, which is constant around the element, then

$$dM = a\,\frac{\vec{n}.\vec{i}}{\vec{n}.\vec{r}}\,L\,dx = a\frac{da}{dx}\,L\,dx \quad ;$$

hence

$$\frac{dM}{dx} = a\frac{da}{dx}\,L = \frac{1}{2\pi}\frac{dA}{dx}\,L \tag{4.1}$$

with $A = \pi a^2$.

We now consider the external and internal cases separately; using the convective notation we rewrite the two last terms in eq.(1.3):

a) for an external flow, by use of eq.(3.9), we get

$$-\frac{\partial M_e}{\partial x} = \frac{-1}{2\pi}\frac{\partial A_e}{\partial x}\,L = \frac{\rho_e}{2\pi}\frac{\partial A_e}{\partial x}\,\mathcal{D}_e^*[A_e\mathcal{D}_e(y)] \ ,$$

b) for an internal flow, by use of eq.(2.2), we get

$$-\frac{\partial M_i}{\partial x} = \frac{-1}{2\pi}\frac{\partial A_i}{\partial x}\,L = \frac{\rho_i A_i}{2\pi}\frac{\partial A_i}{\partial x}\,\mathcal{D}_i^2(y) \ .$$

In order to calculate $\frac{\partial Q}{\partial x}$ in eq.(1.2), we need to differentiate eq.(1.3); the last two terms yield

$$-\frac{\partial^2 M_e}{\partial x^2} - \frac{\partial^2 M_i}{\partial x^2} = \frac{\partial}{\partial x}\{\frac{\rho_e}{2\pi}\frac{\partial A_e}{\partial x}\,\mathcal{D}_e^*[A_e\mathcal{D}_e(y)] + \frac{\rho_i}{2\pi}\frac{\partial A_i}{\partial x}\,A_i\mathcal{D}_i^2(y)\} \ . \tag{4.2}$$

The first expression in brackets of the right-hand side expands as follows:

$$-\frac{\partial M_e}{\partial x} = \frac{\rho_e A_e}{2\pi}\frac{\partial A_e}{\partial x}\left[\frac{\partial^2 y}{\partial t^2} + (U_e + U_e^*)\frac{\partial^2 y}{\partial x \partial t} + U_e U_e^* \frac{\partial^2 y}{\partial x^2}\right]$$

$$+ \frac{\rho_e}{2\pi}\left(\frac{\partial A_e}{\partial x}\right)^2 U_e^*\left[\frac{\partial y}{\partial t} + U_e \frac{\partial y}{\partial x}\right] .$$

In the final equation of motion we shall only retain the terms which are of zero and first order with respect to the taper angles; thus, A_i or A_e will be taken to be of order zero, $\partial A_i/\partial x$, $\partial A_e/\partial x$ and $\partial U_i/\partial x$ will be of first order; furthermore, $U_e^* - U_e$ will also be considered to be of similar order. Hence, we write

$$-\frac{\partial^2 M_i}{\partial x^2} - \frac{\partial^2 M_e}{\partial x^2} = \rho_i \frac{A_i}{2\pi}\frac{\partial A_i}{\partial x}\frac{\partial}{\partial x}[\mathcal{V}_i^2(y)] + \rho_e \frac{A_e}{2\pi}\frac{\partial A_e}{\partial x}\frac{\partial}{\partial x}[\mathcal{V}_e^2(y)] ,$$

and, in $\mathcal{V}_i^2(y)$, we may consider U_i to be constant.

In fact, provided that internal and external flow velocities remain small compared to some fraction of the natural wave propagation celerity in the material, and upon satisfying assumptions such as large slenderness ratio and low critical modes, it will be shown, in the final equation of motion, that any term resulting from the convergent (or divergent) fluid induced moments is small. This will become more obvious when we assume particular solutions for $y(x,t)$.

For the present time we shall rewrite eq.(1.3) as follows:

$$\frac{\partial Q}{\partial x} = -(1+k\,\frac{\partial}{\partial t})\{\frac{\partial^2}{\partial x^2}(EI\,\frac{\partial^2 y}{\partial x^2})\} + \rho_i\,\frac{A_i}{2\pi}\,\frac{\partial A_i}{\partial x}\,\frac{\partial}{\partial x}[\mathcal{D}_i^2(y)]$$

$$+ \rho_e\,\frac{A_e}{2\pi}\,\frac{\partial A_e}{\partial x}\,\frac{\partial}{\partial x}[\mathcal{D}_e^2(y)]\ . \qquad (4.3)$$

2.5 DERIVATION OF THE EQUATIONS OF SMALL MOTIONS

2.5.1 Equation of small motions

By use of eq.(2.3) and (3.4) we now rewrite eq.(1.1) as follows:

$$\frac{\partial T}{\partial x} - \frac{\partial}{\partial x}[A_i p_i] - \rho_i A_i U_i \frac{\partial U_i}{\partial x} + \rho_i A_i g + \frac{\partial}{\partial x}[A_e p_e]$$

$$+ q_{et} - q_{en} \frac{\partial y}{\partial x} - \rho_e A_e g + \frac{\partial}{\partial x}(Q \frac{\partial y}{\partial x}) + \rho A g = 0 .$$

The shear Q and the normal friction q_{en} are of first order of magnitude with respect to y; hence $\frac{\partial}{\partial x}(Q \frac{\partial y}{\partial x})$ and $q_{en} \frac{\partial y}{\partial x}$ are of second order and can be neglected. Because the internal discharge $A_i U_i = (AU)_i$ is constant with respect to x, we rewrite the previous equation in the following manner:

$$\frac{\partial}{\partial x}[T + A_e p_e - A_i p_i - \rho_i (AU)_i U_i] = (\rho_e A_e - \rho_i A_i - \rho A) g - q_{et} \qquad (5.1)$$

Similarly, by use of eq.(2.3), (3.11) and (4.3) we rewrite eq.(1.2) as follows:

$$\rho A \frac{\partial^2 y}{\partial t^2} = -(1 + k\frac{\partial}{\partial t})\{\frac{\partial^2}{\partial x^2}(EI \frac{\partial^2 y}{\partial x^2})\}$$

$$+ \frac{\rho_i A_i}{2\pi} \frac{\partial A_i}{\partial x} \frac{\partial}{\partial x}[\mathcal{D}_i^2(y)] + \frac{\rho_e A_e}{2\pi} \frac{\partial A_e}{\partial x} \frac{\partial}{\partial x}[\mathcal{D}_e^2(y)]$$

$$- \frac{\partial}{\partial x}(A_i p_i \frac{\partial y}{\partial x}) - \rho_i A_i \mathcal{D}_i^2(y)$$

$$+ \frac{\partial}{\partial x}(A_e p_e \frac{\partial y}{\partial x}) - \rho_e \mathcal{D}_e^*[A_e \mathcal{D}_e(y)] + q_{en} + q_{et} \frac{\partial y}{\partial x}$$

$$+ \frac{\partial}{\partial x}(T \frac{\partial y}{\partial x}) ,$$

which, by use of eq.(5.1) may be transformed to

$$\rho A\frac{\partial^2 y}{\partial t^2} = -(1+k\frac{\partial}{\partial t})\{\frac{\partial^2}{\partial x^2}(EI\frac{\partial^2 y}{\partial x^2})\}$$
$$+ \frac{\rho_i A_i}{2\pi}\frac{\partial A_i}{\partial x}\frac{\partial}{\partial x}[\mathcal{V}_i^2(y)] + \frac{\rho_e A_e}{2\pi}\frac{\partial A_e}{\partial x}\frac{\partial}{\partial x}[\mathcal{V}_e^2(y)]$$
$$- \rho_i A_i[\mathcal{V}_i^2 - U_i\frac{\partial U_i}{\partial x}\frac{\partial}{\partial x}](y) - \rho_e \mathcal{V}_e^*[A_e \mathcal{V}_e(y)] \qquad (5.2)$$
$$+ (\rho_e A_e - \rho_i A_i - \rho A)g\frac{\partial y}{\partial x} + (T + A_e p_e - A_i p_i)\frac{\partial^2 y}{\partial x^2} + q_{en}.$$

$T + A_e p_e - A_i p_i$ is the last unknown expression in eq.(5.2); let us set

$$T_1 = T + A_e p_e - A_i p_i .$$

Once we obtain T_1 by integrating eq.(5.1), the equations of motion will be reduced to one single differential equation of fourth order with respect to x and second with respect to t.

The integration of eq.(5.1) between x and L yields:

$$T_1(x) = T_1(L) + \rho_i (AU)_i [U_i]_L^x + \int_L^x [(\rho_e A_e - \rho_i A_i - \rho A)g - q_{et}]dx . \qquad (5.3)$$

The differential equation of motion will be fully formulated once we find $T_1(L)$ from the axial boundary conditions; we will then analyse the transverse conditions at x=0 and x=L in order to obtain the boundary conditions governing y.

2.5.2 Axial boundary conditions

In order to evaluate the expression $T_1(L) \equiv [T+A_e p_e - A_i p_i]_L$ in eq. (5.3), we define the geometric characteristics of the downstream end of the tubes.

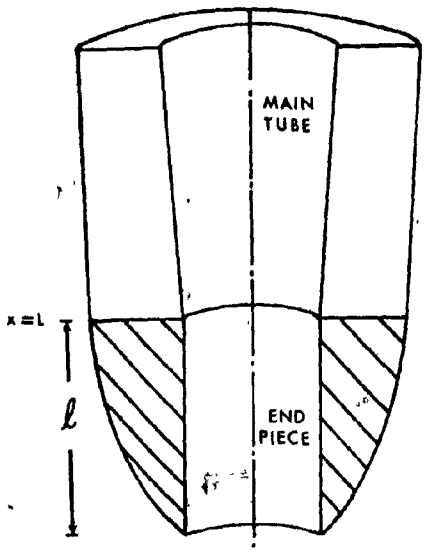

At x=L, a small rigid end piece of length ℓ is added to the main tube, as illustrated in the figure; on the outside it is generally streamlined, and cylindrical inside. We shall distinguish two cases, i.e. whether the end piece is supported or not, and more precisely whether it is free to move axially or not.

A] free or sliding end

Let us consider the system composed of the end piece and of the internal fluid within; the axial accelerations are negligible, hence, the rate of change of tangential momentum of the system is null.

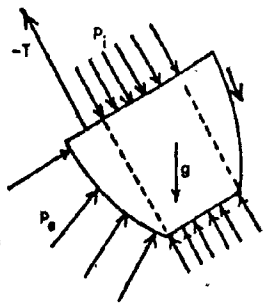

The following forces yield tangential components which must hence balance:

(a) the tension in the main tube (at x=L), $-T(L)$

(b) the gravity force, $\int_L^{L+\ell} (\rho A + \rho_i A_i) g dx$

(c) the pressure forces acting on the two internal cross-sections, $-[A_i p_i]_L^{L+\ell}$

(d) the pressure force acting on the external surface, $F_e = \int_L^{L+\ell} p_e(x) \frac{\partial A_e}{\partial x} dx$

(e) the frictional force on the external surface will be neglected in comparison with F_e.

We thus obtain the following equation:

$$- T(L) - [A_i p_i]_L^{L+\ell} + F_e + \int_L^{L+\ell} (\rho A + \rho_i A_i) g dx = 0,$$

or

$$[T - A_i p_i]_L = F_e - [A_i p_i]_{L+\ell} + \int_L^{L+\ell} (\rho A + \rho_i A_i) g dx \,. \tag{5.4}$$

In order to evaluate F_e, of (d) above, we set, as in eq.(3.3)

$$p_e = p_{eh}(x) + \tfrac{1}{2}\rho_e U_e^2 c_p(x) \,,$$

where p_{eh} is hydrostatically distributed and c_p accounts for the taper and flow separation over the end piece; furthermore c_p depends to some extent upon the jet characteristics of the internal flow exiting at $x=L+\ell$, but we need not take into consideration first order terms due to the motion.

Hence,

$$F_e = \int_L^{L+\ell} \frac{\partial A_e}{\partial x} p_{eh} dx + \int_L^{L+\ell} \tfrac{1}{2}\rho_e U_e^2 c_p \frac{\partial A_e}{\partial x} dx$$

$$= [A_e p_{eh}]_L^{L+\ell} - \int_L^{L+\ell} A_e \rho_e g \, dx + F_b \,,$$

where F_b represents the drag exerted on the end piece. Since we previously assumed $p_{eh} = p_e$ up to $x=L$ and, because the thickness

of the tube is null at the very end, i.e. $A_i(L+\ell) = A_e(L+\ell)$, we may rewrite eq.(5.4) as follows:

$$[T+A_e p_e - A_i p_i]_L = [A_e(p_{eh}-p_i)]_{L+\ell} + F_b + \int_L^{L+\ell} (\rho A + \rho_i A_i - \rho_e A_e) g dx \quad (5.5)$$

Let us illustrate the significance of this equation when $\ell=0$, i.e. when the end of the main tube is blunt, as illustrated on the right.

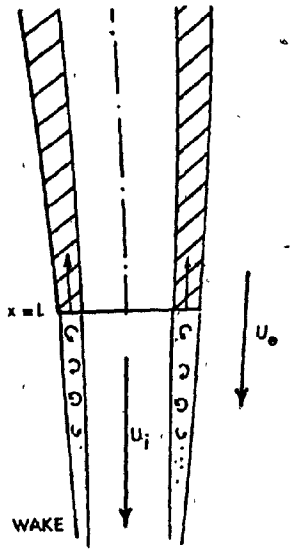

For such a configuration, flow separation will occur at the edges of the external and internal surfaces, and if we assume as a first approximation that the pressure at the base is uniform and equal to that prevailing in the main external flow, we write $p_e=p_{eh}$, or $c_p=0$; and therefore, $F_b=0$ and $[p_{eh}]_L=[p_i]_L$; hence, the previous equation reduces to

$$[T+A_e p_e - A_i p_i]_L = 0 \quad \text{or} \quad T = -\{[A_e-A_i]p_{eh}\}_L$$

which, as could be expected, merely states that the tension at x=L is the compression due to the pressure acting upon the base of the tube.

However, if the end piece is not blunt, or if the pressure at the base is different from that in the main flow at x=L, there is a drag effect; from eq.(5.5) we see that the

drag force consists of the drag exerted on the end piece of the beam, F_b, and that of the internal flow, $[A_e(p_{eh}-p_i)]_{L+\ell}$; we shall express it as follows:

$$D_b = [A_e(p_{eh}-p_i)]_{L+\ell} + \int_L^{L+\ell} \frac{1}{2}\rho_e c_p U_e^2 \frac{\partial A_e}{\partial x} dx \ .$$

Upon considering eq.(5.2), we recall that the term $T+A_e p_e - A_i p_i$ is multiplied by $\partial^2 y/\partial x^2$; hence we need evaluate $[T+A_e p_e - A_i p_i]_L$, and consequently D_b, only with zero order terms with respect to y; therefore, we proceed as if the end piece were at zero incidence. As shown in Appendix H a quadratic fit was selected to represent the base drag measured behind cylindrical tubes; we thus set

$$D_b = \frac{1}{2}C_{fe}\rho_e(A_e U_e^2)_L + \frac{1}{2}C_{fi}\rho_i(A_i U_i^2)_L + \frac{1}{2}C_{fx}(\rho_e\rho_i A_e A_i U_e^2 U_i^2)^{\frac{1}{2}}_L \ . \quad (5.6)$$

We found semi-empirical expressions for C_{fe}, C_{fi} and C_{fx} which will be representative of base drag effects behind cylindrical and smoothly tapered tubular beams.

We finally obtain $T_1(L)$ as required in eq.(5.3),

$$T_1(L) = [T+A_e p_e - A_i p_i]_L$$

$$= \int_L^{L+\ell} [(\rho-\rho_e)A_e + (\rho_i-\rho)A_i] g dx$$

$$+ \frac{1}{2}[\rho_e A_e U_e^2 C_{fe} + \rho_i A_i U_i^2 C_{fi} + (\rho_e\rho_i A_e A_i)^{\frac{1}{2}} U_e U_i C_{fx}]_L \ . \quad (5.7)$$

B] Supported ends:

At zero flow velocities the tension, T^*, which acts at x=L on the tubular beam is the sum of the hydrostatic pressure force applied at the base and possibly an external tension labelled T_o; we thus write

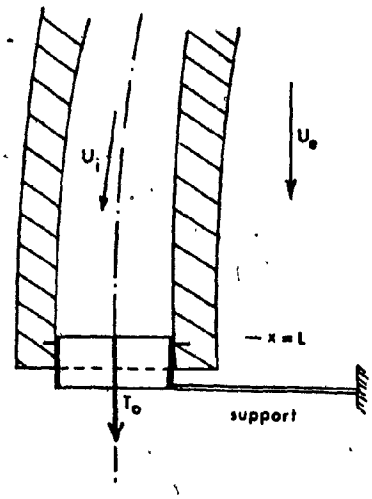

$$T^* = -(A_e - A_i)p_e^* + T_o \ ;$$

(note:in this subsection the superscripted asterisk will characterize the zero flow condition). We assume that the external and internal fluids are almost in contact at the end of the tubular beam, as illustrated on the diagram; hence $[p_e]_L^* \sim [p_i]_L^*$, and

$$T_1^*(L) = [T + A_e p_e - A_i p_i]_{x=L}^* = T_o \ .$$

From eq.(5.3), with no flow, we thus obtain

$$T_1^*(x) = T_1^*(L) + \int_L^x (\rho_e A_e - \rho_i A_i - \rho A) g dx \ .$$

Departing from this reference case of zero flow velocities which defined T_o, we now set

$$T = T^* + T'$$
$$p_e = p_e^* + p_e'$$
$$p_i = p_i^* + p_i' \ .$$

By use of the previous equations, eq.(5.3) reduces to

$$[T' + A_e p_e' - A_i p_i']_x = [T' + A_e p_e' - A_i p_i']_L + \rho_i (AU)_i [U_i]_L^x - \int_L^x q_{et} dx \ ,$$

or

$$T'(x) = T'(L) + [A_e p_e' - A_i p_i' - \rho_i A U_i^2]_x^L + \int_x^L q_{et} dx ,$$

and we shall approximate this tension distribution with that corresponding to an axial stress distribution

$$\sigma_{xx} = \frac{T'(x)}{A(x)}$$

where we recall that $A(x) = A_e(x) - A_i(x)$.

Let us now consider the effect of p_i' and p_e'. Because of the small taper angles considered and of the small pressure gradients in the x-direction we shall make use of the stress distribution which applies to a cylindrical tube subjected to constant internal and external pressure [67]; this stress distribution yields

$$\sigma_{rr} + \sigma_{\theta\theta} = 2\frac{p_i' A_i - p_e' A_e}{A_e - A_i} .$$

We superpose the two distributions and we obtain the following axial strain distribution in terms of Poisson's ratio, μ_p:

$$\epsilon_x = \frac{\sigma_{xx} - \mu_p(\sigma_{rr}+\sigma_{\theta\theta})}{E} = \frac{T'(x) - 2\mu_p[p_i' A_i - p_e' A_e]_x}{E[A_e - A_i]_x}$$

hence,

$$E\epsilon_x = \frac{[T' + A_e p_e' - A_i p_i']_L - (1-2\mu_p)(A_e p_e' - A_i p_i')_x - \rho_i [A_i U_i^2]_x^L + \int_x^L q_{et} dx}{[A_e - A_i]_x}$$

If we now take Poisson's ratio $\mu_p \sim \frac{1}{2}$, as for rubber materials, we note that the local pressure terms disappear from the previous equation. It is not surprising that the internal fluid friction does not appear in the expression above, because the internal fluid friction and the internal pressure drop due to friction, have opposite effects on elongation; this does not hold for external friction.

The condition of non-sliding end support requires $\int_o^L \varepsilon_x dx = 0$; hence we may write

$$[T' + A_e p_e' - A_i p_i']_L \int_o^L \frac{dx}{A_e - A_i} = \rho_i (AU)_i \int_o^L \frac{U_i(L) - U_i(x)}{[A_e - A_i]_x} dx - \int_o^L \frac{\int_x^L q_{et} dx}{[A_e - A_i]_x} dx$$

or

$$[T' + A_e p_e' - A_i p_i']_L = \rho_i (AU)_i \, U_i(L) \alpha_i' - \tfrac{1}{2} q_{et}(x=0) L \, \alpha_e' ; \qquad (5.8)$$

for quasi-uniform beams $\alpha_i' \sim 0$ and $\alpha_e' \sim 1$, and other values of α_i' and α_e' have been calculated in Appendix D for conical tubular beams. We now write

$$T_1(L) = T_1^*(L) + [T' + A_e p_e' - A_i p_i']_L$$

$$= T_o + \rho_i (AU)_i \alpha_i' U_i(L) - \tfrac{1}{2} \alpha_e' q_{et}(0) L,$$

and finally, by use of eq. (3.7),

$$T_1(L) = T_o + \rho_i \alpha_i' (A_i U_i^2)_L - \rho_e \alpha_e' \frac{C_{ft}}{4} D_e(0) L U_e^2 . \qquad (5.9)$$

C] General case

The similarity between eq.(5.9) and eq.(5.7) suggests that in both cases we set

$$T_1(L) = T_o + \frac{1}{2}[\rho_e A_e U_e^2 C_{fe} + \rho_i A_i U_i^2 C_{fi} + (\rho_e \rho_i A_e A_i)^{\frac{1}{2}} U_e U_i C_{fx}]_L \quad (5.10)$$

(a) For a free end we shall set

$$T_o = \int_L^{L+\ell} [(\rho - \rho_e)A_e + (\rho_i - \rho)A_i] g dx$$

because in this case, the only external tension to be considered is the immersed weight of the end piece; in addition, the base drag coefficients calculated in Appendix H are

$$C_{fe} = \frac{1.35}{9+(2\ell/D)^3}$$

$$C_{fi} = \frac{0.02}{1.25+(2\ell/D)^{\frac{1}{2}}}$$

$$C_{fx} = 0.05\ \frac{0.2+2\ell/D}{0.1+2\ell/D}, \quad \text{with } D=D_e(L).$$

(b) For a supported end, T_o represents the external tension applied at x=L, and

$$C_{fe} = -\frac{L}{2}\alpha_e' C_{ft} \frac{D_e(0)}{A_e(L)}$$

$$C_{ft} = 2\ \alpha_i'$$

$$C_{fx} = 0$$

2.5.3 Transverse Boundary Conditions

i) Conditions at x=0. The beam will usually be clamped, hence the displacement and the slope are both zero, i.e.

$$y(0) = y'(0) = 0.$$

Should it be pinned we shall assume no displacement and no moment; hence

$$y(0) = y''(0) = 0.$$

ii) Conditions at x=L. The same conditions as above will also apply to clamped or pinned cases. Let us now devote our attention to the case of a free end.

We shall assume that due to the small size of the end piece the moment at x=L is negligible; thus $y''(L) = 0$.

The second condition will be found in the balance of the external and inertia lateral forces exerted on the end piece; hence, we consider

a - the gravity and buoyancy lateral resultant,

$$-\int_L^{L+\ell} (\rho A+\rho_i A_i-\rho_e A_e) g \frac{\partial y}{\partial x} dx;$$

b - the internal hydrodynamic force,

$$-\int_L^{L+\ell} \rho_i A_i \mathcal{D}_i^2(y) dx;$$

c - the external hydrodynamic force which we express as

$$-f \int_L^{L+\ell} \rho_e \mathcal{D}_e^* [A_e \mathcal{D}_e(y)] dx ;$$

where we kept the same expression as for the slender portion of the beam, but compounded by a factor f to account for the rapid change of cross section and slenderness, as reported by Paidoussis [50], and further elaborated in appendix J. In practice, f=0 will be used for a bluntly ended tubular beam, and f will approach 1 for smooth, streamlined end pieces; because we introduced the corrective factor f, U_e^* will now be assumed constant over the end piece and equal to the value at x=L.

d - shear reaction

$$-Q(L) = \frac{\partial}{\partial x}\left(EI\,\frac{\partial^2 y}{\partial x^2}\right) = EI\left(\frac{\partial^3 y}{\partial x^3}\right)_L$$

e - friction will be neglected in comparison with the hydrodynamic force.

The balance of lateral forces yields

$$\int_L^{L+\ell} \rho A\,\frac{\partial^2 y}{\partial t^2}\,dx = \tag{5.11}$$

$$\int_L^{L+\ell} \{[(\rho_e-\rho)A_e+(\rho+\rho_i)A_i]g-\rho_i A_i \mathcal{D}_i^2(y)-\rho_e f \mathcal{D}_e^*[A_e \mathcal{D}_e(y)]\}dx-Q(L)$$

Let us now integrate the hydrodynamic terms over the end piece, namely

$$\int_L^{L+\ell} \rho_i A_i \left(\frac{\partial}{\partial t}+U_i\,\frac{\partial}{\partial x}\right)^2 y\,dx \qquad \text{for internal flow,}$$

and $$\int_L^{L+\ell} f\rho_e \left(\frac{\partial}{\partial t}+U_e^*\,\frac{\partial}{\partial x}\right)\left[A_e\left(\frac{\partial y}{\partial t}+U_e\,\frac{\partial y}{\partial x}\right)\right]dx \qquad \text{for external flow.}$$

In evaluating the first integral we recall that we have assumed a rigid end piece with a cylindrical duct for the internal flow; then, for $0<\zeta<\ell$, we have

$$[y]_{L+\zeta} = [y]_L + [\frac{\partial y}{\partial x}]_L \zeta \ ;$$

hence,

$$\int_L^{L+\ell} A_i (\frac{\partial}{\partial t} + U_i \frac{\partial}{\partial x})^2 y \, dx = \frac{\partial}{\partial t} \int_L^{L+\ell} A_i (\frac{\partial y}{\partial t} + U_i \frac{\partial y}{\partial x}) dx + A_i U_i [\frac{\partial y}{\partial t} + U_i \frac{\partial y}{\partial x}]_L^{L+\ell}$$

$$= A_i \frac{\partial}{\partial t}\{\ell \frac{\partial y}{\partial t} + \frac{1}{2}\ell^2 \frac{\partial^2 y}{\partial x \partial t} + U_i \ell \frac{\partial y}{\partial x}\}_L + A_i U_i \ell [\frac{\partial^2 y}{\partial x \partial t}]_L$$

$$\sim A_i \ell [\frac{\partial^2 y}{\partial t^2} + 2U_i \frac{\partial^2 y}{\partial x \partial t}]_L .$$

With respect to the second integral (external flow) we write

$$\int_L^{L+\ell} (\frac{\partial}{\partial t} + U_e^* \frac{\partial}{\partial x}) [A_e (\frac{\partial y}{\partial t} + U_e \frac{\partial y}{\partial x})] dx$$

$$= \int_L^{L+\ell} \frac{\partial}{\partial t} [A_e (\frac{\partial y}{\partial t} + U_e \frac{\partial y}{\partial x})] dx + U_e^* [A_e (\frac{\partial y}{\partial t} + U_e \frac{\partial y}{\partial x})]_L^{L+\ell}$$

$$= \int_L^{L+\ell} \{A_e \frac{\partial^2}{\partial t^2} [(y)_L + (\frac{\partial y}{\partial x})_L (x-L)] + U_e [\frac{\partial^2 y}{\partial x \partial t}]_L\} dx$$

$$+ U_e^* \{[A_e \frac{\partial y}{\partial x}]_L^{L+\ell} + [A_e]_L^{L+\ell} U_e (\frac{\partial y}{\partial x})_L\}$$

$$\sim [\frac{\partial^2 y}{\partial t^2} + U_e \frac{\partial^2 y}{\partial x \partial t}]_L \int_L^{L+\ell} A_e dx$$

$$+ U_e^* \{[A_e]_L^{L+\ell} [\frac{\partial y}{\partial t}]_L + \ell [A_e]_{L+\ell} \frac{\partial^2 y}{\partial x \partial t} + U_e [A_e]_L^{L+\ell} [\frac{\partial y}{\partial x}]_L\} \ ;$$

in this last expression we neglected the terms of order ℓ^2 and we have also used the fact that the slope of the end piece is constant, i.e. $(\frac{\partial y}{\partial x})_{L+\ell} = (\frac{\partial y}{\partial x})_L$.

From eq.(5.11) we may now rewrite the balance of lateral forces up to first order terms with respect to ℓ, and in ascending order with respect to axial derivatives, as follows:

$$[\frac{\partial^2 y}{\partial t^2}]_L \{\rho_i A_i \ell + \int_L^{L+\ell} [\rho(A_e - A_i) + f\rho_e A_e]dx\} + [\frac{\partial y}{\partial t}]_L f\rho_e U_e^* [A_e]_L^{L+\ell}$$

$$+ [\frac{\partial^2 y}{\partial x \partial t}]_L \{2\rho_i A_i U_i \ell + f\rho_e U_e \int_L^{L+\ell} A_e dx + f\rho_e U_e^* \ell [A_e]_{L+\ell}\} \qquad (5.12)$$

$$+ [\frac{\partial y}{\partial x}]_L \{f\rho_e U_e U_e^* [A_e]_L^{L+\ell} - \int_L^{L+\ell} [(\rho_e - \rho)A_e + (\rho - \rho_i)A_i]gdx\}$$

$$= [EI(1+k\frac{\partial}{\partial t}) \cdot \frac{\partial^3 y}{\partial x^3}]_L \quad .$$

In order to integrate the overall cross sectional area A_e over the end piece, we will assume that the end piece can be adequately represented by a conical element of cross section $(A_e)_L$ at x=L and $(A_i)_L$ at $x=L+\ell$. Then, we introduce S_e such that

$$S_e \ell = \int_L^{L+\ell} A_e dx$$

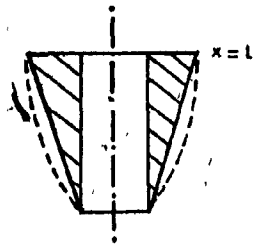

hence,

$$S_e = \frac{1}{3} \frac{(A_e)_L^{\frac{3}{2}} - (A_i)_L^{\frac{3}{2}}}{(A_e)_L^{\frac{1}{2}} - (A_i)_L^{\frac{1}{2}}} \quad .$$

We now write eq.(5.12) as follows:

$$[(\rho+f\rho_e)S_e + (\rho_i-\rho)(A_i)_L].\ell[\frac{\partial^2 y}{\partial t^2}]_L - f\rho_e(A_e-A_i)_L U_e^*[\frac{\partial y}{\partial t}]_L$$

$$+ \{f\rho_e[(A_i)_L U_e^* + S_e U_e] + 2\rho_i A_i U_i\}.\ell[\frac{\partial^2 y}{\partial x \partial t}]_L - [EI(1+k\frac{\partial}{\partial t})\frac{\partial^3 y}{\partial x^3}]_L \qquad (5.13)$$

$$-\{f\rho_e(A_e-A_i)_L U_e U_e^* + [(\rho_e-\rho)S_e + (\rho-\rho_i)(A_i)_L]g\ell\}[\frac{\partial y}{\partial x}]_L = 0 .$$

2.5.4 Summary

The mathematical model for the dynamics of the system has now been fully formulated. For the benefit of the reader, the final equation, abstracted from the previous sections (subject to boundary conditions given in §2.5.3) is given below.

$$\rho A \frac{\partial^2 y}{\partial t^2} =$$

$$- (1+k\frac{\partial}{\partial t})\{\frac{\partial^2}{\partial x^2}(EI\frac{\partial^2 y}{\partial x^2})\}$$

$$+ \frac{\rho_i A_i}{2\pi}\frac{\partial A_i}{\partial x}\frac{\partial}{\partial x}\{\frac{\partial^2 y}{\partial t^2} + 2U_i\frac{\partial^2 y}{\partial x \partial t} + U_i^2\frac{\partial^2 y}{\partial x^2}\}$$

$$+ \frac{\rho_e A_e}{2\pi}\frac{\partial A_e}{\partial x}\frac{\partial}{\partial x}\{\frac{\partial^2 y}{\partial t^2} + 2U_e\frac{\partial^2 y}{\partial x \partial t} + U_e^2\frac{\partial^2 y}{\partial x^2}\}$$

$$- \rho_i A_i\{\frac{\partial^2 y}{\partial t^2} + 2U_i\frac{\partial^2 y}{\partial x \partial t} + U_i^2\frac{\partial^2 y}{\partial x^2}\} \qquad (5.14)$$

$$- \rho_e\{A_e\frac{\partial^2 y}{\partial t^2} + A_e(U_e+U_e^*)\frac{\partial^2 y}{\partial x \partial t} + A_e U_e U_e^*\frac{\partial^2 y}{\partial x^2} + U_e\frac{\partial A_e}{\partial x}(\frac{\partial y}{\partial t} + U_e\frac{\partial y}{\partial x})\}$$

$$+ \{T_1(L) + \rho_i A_i U_i[U_i - U_i(L)] + \int_L^x [(\rho_e-\rho)gA_e + (\rho-\rho_i)gA_i - q_{et}]dx\}\frac{\partial^2 y}{\partial x^2}$$

$$- \frac{1}{2}\rho_e D_e[U_e C_{fn}(\frac{\partial y}{\partial t} + U_e\frac{\partial y}{\partial x}) + U_v\frac{\partial y}{\partial t}] + (\rho_e A_e - \rho_i A_i - \rho A)g\frac{\partial y}{\partial x} .$$

2.6 DIMENSIONLESS EQUATIONS

2.6.1 General Slender Bodies

The detailed rendering of the equation of motion and of the boundary conditions dimensionless is carried out in Appendix A. Here we give an abbreviated account.

We define the following dimensionless quantities:

$$\xi = x/L \qquad \eta = y/L$$

$$\sigma_e = A_e(\xi)/A_e(0) \qquad \sigma_i = A_i(\xi)/A_i(0)$$

$$\tau = [EI/(\rho A+\rho_e A_e+\rho_i A_i)]^{\frac{1}{2}}_{\xi=0} t/L^2 \qquad \nu = [EI/(\rho A+\rho_e A_e+\rho_i A_i)]^{\frac{1}{2}}_{\xi=0} k/L^2$$

$$u_e = [\rho_e A_e/EI]^{\frac{1}{2}}_{\xi=0} LU_e \qquad u_e^* = u_e[A_e/A_e^*]_\xi \qquad v_i = [\rho_i A_i/EI]^{\frac{1}{2}}_{\xi=0} LU_i(0)$$

$$\delta^2 = [A_i/A_e]_{\xi=0} \qquad \varepsilon = L/[D_e]_{\xi=0} \qquad \gamma = \frac{\rho}{E} 16g[D_e]_{\xi=0}$$

$$\gamma_e = 1 \pm \rho_e/\rho \qquad \gamma_i = (\rho_i/\rho - 1)\delta^2 \qquad \Gamma = [\rho A_e/EI]_{\xi=0} gL^3$$

$$c_n = 2C_{fn}/\pi \qquad c_t = 2C_{ft}/\pi \qquad c_v = 2[\rho_e A_e/EI]^{\frac{1}{2}}_{\xi=0} U_v L \ ;$$

and for the end conditions at $\xi=1$,

$$\Pi = T_o L^2/EI(0),$$

$$\Theta = T_1(L)L^2/EI(0) = \Pi + \tfrac{1}{2}C_{fe}\sigma_e(1)u_e^2 + \tfrac{1}{2}C_{fi}\frac{v_i^2}{\sigma_i(1)} + \tfrac{1}{2}C_{fx}\left[\frac{\sigma_e(1)}{\sigma_i(1)}\right]^{\frac{1}{2}} u_e v_i$$

$$\chi = \ell/L \qquad \text{and} \qquad \chi_e = \ell/D_e(L),$$

$$s_e = \frac{1}{3}\frac{\sigma_e(1)^{\frac{3}{2}} - \delta^3\,\sigma_i(1)^{\frac{3}{2}}}{\sigma_e(1)^{\frac{1}{2}} - \delta\,\sigma_i(1)^{\frac{1}{2}}} = \tfrac{1}{3}[\sigma_e(1) + \delta^2\sigma_i(1) + \delta\sigma_e(1)^{\frac{1}{2}}\sigma_i(1)^{\frac{1}{2}}] \ .$$

Incidentally, the parameters defined above are independent except for three, namely s_e, χ_e and γ.

Substituting these into the equation of motion, i.e. eq.(5.14), we obtain

$$(1+\nu\frac{\partial}{\partial\tau})\frac{\partial^2}{\partial\xi^2}\{\frac{\sigma_e^2-\delta^4\sigma_i^2}{1-\delta^4}\frac{\partial^2\eta}{\partial\xi^2}\} - \{\frac{\delta^2 v_i^2}{8\varepsilon^2\sigma_i}\frac{d\sigma_i}{d\xi} + \frac{\sigma_e u_e^2}{8\varepsilon^2}\frac{d\sigma_e}{d\xi}\}\frac{\partial^3\eta}{\partial\xi^3}$$

$$+ \{u_e u_e^*\sigma_e + \frac{v_i^2}{\sigma_i(1)} - \Theta\int_\xi^1 \{\Gamma[(2-\gamma_e)\sigma_e+\gamma_i\sigma_i] + \varepsilon c_t u_e^2\sigma_e^{\frac{1}{2}}\}d\xi\}\frac{\partial^2\eta}{\partial\xi^2}$$

$$- \{[\frac{\delta^2+\gamma_i}{\gamma_e+\gamma_i}]^{\frac{1}{2}}\frac{\delta^2 v_i}{4\varepsilon^2}\frac{d\sigma_i}{d\xi} + [\frac{\gamma_e-1}{\gamma_e+\gamma_i}]^{\frac{1}{2}}\frac{u_e\sigma_e}{4\varepsilon^2}\frac{d\sigma_e}{d\xi}\}\frac{\partial^3\eta}{\partial\xi^2\partial\tau}$$

$$+ \{\Gamma[(2-\gamma_e)\sigma_e + \gamma_i\sigma_i] + \frac{d\sigma_e}{d\xi}u_e^*u_e + \varepsilon\sigma_e^{\frac{1}{2}}c_n u_e^2\}\frac{\partial\eta}{\partial\xi}$$

$$+ \{2[\frac{\delta^2+\gamma_i}{\gamma_e+\gamma_i}]^{\frac{1}{2}}v_i + [\frac{\gamma_e-1}{\gamma_e+\gamma_i}]^{\frac{1}{2}}\sigma_e(u_e+u_e^*)\}\frac{\partial^2\eta}{\partial\xi\partial\tau} \qquad (6.1)$$

$$- \{\frac{\delta^2+\gamma_i}{\gamma_e+\gamma_i}\frac{\delta^2\sigma_i}{8\varepsilon^2}\frac{d\sigma_i}{d\xi} + \frac{\gamma_e-1}{\gamma_e+\gamma_i}\frac{\sigma_e}{8\varepsilon^2}\frac{d\sigma_e}{d\xi}\}\frac{\partial^3\eta}{\partial\xi\partial\tau^2}$$

$$+ \{[\frac{\gamma_e-1}{\gamma_e+\gamma_i}]^{\frac{1}{2}}[\varepsilon\sigma_e^{\frac{1}{2}}(c_n u_e+c_v') + u_e^*\frac{d\sigma_e}{d\xi}]\}\frac{\partial\eta}{\partial\tau} + \frac{\gamma_e\sigma_e+\gamma_i\sigma_i}{\gamma_e+\gamma_i}\frac{\partial^2\eta}{\partial\tau^2} = 0,$$

and for a free end, at $\xi=1$, eq.(5.13) yields

$$\frac{\sigma_e^2-\delta^4\sigma_i^2}{1-\delta^4}(1+\nu\frac{\partial}{\partial\tau})[\frac{\partial^3\eta}{\partial\xi^3}] - \chi\{f[u_e s_e+\delta^2\sigma_i u_e^*](\frac{\gamma_e-1}{\gamma_e+\gamma_i})^{\frac{1}{2}} + 2v_i(\frac{\delta^2+\gamma_i}{\gamma_e+\gamma_i})^{\frac{1}{2}}\}[\frac{\partial^2\eta}{\partial\xi\partial\tau}]$$

$$+ \{fu_e u_e^*[\sigma_e-\delta^2\sigma_i] + \Gamma[(\gamma_e-2)s_e-\gamma_i\sigma_i]\chi\}[\frac{\partial\eta}{\partial\xi}]$$

$$+ fu_e^*(\frac{\gamma_e-1}{\gamma_e+\gamma_i})^{\frac{1}{2}}(\sigma_e-\delta^2\sigma_i)[\frac{\partial\eta}{\partial\tau}] - \chi\frac{[1+f(\gamma_e-1)]s_e+\gamma_i\sigma_i}{\gamma_e+\gamma_i}[\frac{\partial^2\eta}{\partial\tau^2}] = 0.$$

We next separate the variables by looking for a complex solution of the following form

$$\eta(\xi,\tau) = \psi(\xi)e^{i\omega\tau}.$$

Let us recall that both real and purely imaginary parts represent the same solution, within a scale factor and a phase shift, and upon setting $\omega=\omega_r+i\omega_i$ and $\psi=\psi_1+i\psi_2$, the real part of the solution reads

$$\mathrm{Re}\{\eta(\xi,\tau)\} = \psi_1(\xi)e^{-\omega_i\tau}\cos\omega_r\tau - \psi_2(\xi)e^{-\omega_i\tau}\sin\omega_r\tau \quad . \tag{6.2}$$

Using the complex notation equation (6.1) becomes

$$\begin{aligned}
&(1+i\omega\nu)\frac{d^2}{d\xi^2}\{\frac{\sigma_e^2-\delta^4\sigma_i^2}{1-\delta^4}\frac{d^2\psi}{d\xi^2}\} - \{\frac{\delta^2 v_i^2}{8\varepsilon^2\sigma_i}\frac{d\sigma_i}{d\xi} + \frac{\sigma_e u_e^2}{8\varepsilon^2}\frac{d\sigma_e}{d\xi}\}\frac{d^3\psi}{d\xi^3} \\
&+ \{u_e u_e^* \sigma_e + \frac{v_i^2}{\sigma_i(1)} - \theta - \int_\xi^1 [\Gamma(2-\gamma_e)\sigma_e+\gamma_i\sigma_i)+\varepsilon c_t\sigma_e^{\frac{1}{2}}u_e^2]d\xi \\
&\quad - i\omega[(\frac{\gamma_e-1}{\gamma_e+\gamma_i})^{\frac{1}{2}}\frac{\sigma_e}{4\varepsilon^2}\frac{d\sigma_e}{d\xi}u_e + (\frac{\delta^2+\gamma_i}{\gamma_e+\gamma_i})^{\frac{1}{2}}\frac{\delta^2}{4\varepsilon^2}\frac{d\sigma_i}{d\xi}v_i]\}\frac{d^2\psi}{d\xi^2} \\
&+\{\Gamma[(2-\gamma_e)\sigma_e + \gamma_i\sigma_i] + [\varepsilon c_n u_e\sigma_e^{\frac{1}{2}} + \frac{d\sigma_e}{d\xi}u_e^*]u_e \\
&\quad + i\omega[(\frac{\gamma_e-1}{\gamma_e+\gamma_i})^{\frac{1}{2}}(u_e+u_e^*)\sigma_e + 2\{\frac{\delta^2+\gamma_i}{\gamma_e+\gamma_i})^{\frac{1}{2}}v_i] \\
&\quad + \omega^2[\frac{\gamma_e-1}{\gamma_e+\gamma_i}\frac{\sigma_e}{8\varepsilon^2}\frac{d\sigma_e}{d\xi} + \frac{\delta^2+\gamma_i}{\gamma_e+\gamma_i}\frac{\delta^2\sigma_i}{8\varepsilon^2}\frac{d\sigma_i}{d\xi}]\}\frac{d\psi}{d\xi} \\
&+ \{i\omega[\frac{\gamma_e-1}{\gamma_e+\gamma_i}]^{\frac{1}{2}}[\varepsilon\sigma_e^{\frac{1}{2}}(c_n u_e+c_v) + \frac{d\sigma_e}{d\xi}u_e^*] - \omega^2\frac{\gamma_e\sigma_e+\gamma_i\sigma_i}{\gamma_e+\gamma_i}\}\psi = 0 \ ,
\end{aligned} \tag{6.3}$$

and the various boundary conditions yield

a) for a clamped end: $\Psi = \frac{\partial \Psi}{\partial \xi} = 0$,

b) for a pinned end: $\Psi = \frac{\partial^2 \Psi}{\partial \xi^2} = 0$,

c) for a free downstream end: $\frac{\partial^2 \Psi}{\partial \xi^2} = 0$, and

$$(1+i\omega\nu)\frac{\sigma_e^2-\delta^4\sigma_i^2}{1-\delta^4}\frac{\partial^3\Psi}{\partial\xi^3}$$

$$+\{f[\sigma_e-\delta^2\sigma_i]u_e^*u_e-\chi\Gamma[(2-\gamma_e)s_e+\gamma_i\sigma_i] \qquad (6.4)$$

$$-i\omega\chi[f(s_eu_e+\delta^2\sigma_iu_e^*)(\frac{\gamma_e-1}{\gamma_e+\gamma_i})^{\frac{1}{2}}+2v_i(\frac{\delta^2+\gamma_i}{\gamma_e+\gamma_i})^{\frac{1}{2}}]\}\frac{\partial\Psi}{\partial\xi}$$

$$+\{i\omega fu_e^*[\sigma_e-\delta^2\sigma_i](\frac{\gamma_e-1}{\gamma_e+\gamma_i})^{\frac{1}{2}}+\omega^2\chi\frac{[1+f(\gamma_e-1)]s_e+\gamma_i\sigma_i}{\gamma_e+\gamma_i}\}\Psi = 0.$$

As suggested in §2.4.2 and further elaborated upon in Appendix I, if we assume that u_i and u_e are smaller than ε, the second term of eq.(6.3), i.e.

$$\{\frac{\delta^2v_i^2}{8\varepsilon^2\sigma_i}\frac{d\sigma_i}{d\xi}+\frac{\sigma_eu_e^2}{8\varepsilon^2}\frac{d\sigma_e}{d\xi}\}\frac{d^3\Psi}{d\xi^3}$$

is negligible vis-à-vis the first term of the equation, and will be dropped.

2.6.2 Conical Tubular Beams

From here on we shall deal with constant taper angles β_e and β_i, over the whole length of the tubular beam, i.e. both inside and outside diameters vary linearly with the axial coordinate.

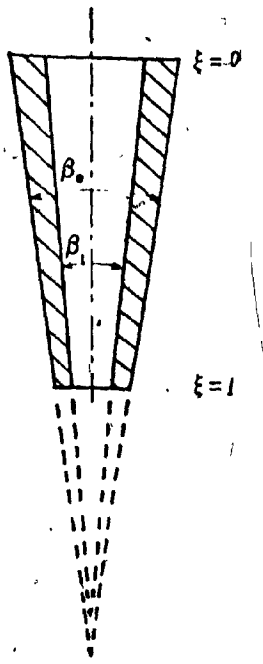

We set

$$D_e = D_e(0)[1+\alpha_e\xi],\quad D_i = D_i(0)[1+\alpha_i\xi];$$

hence

$$\sigma_e = (1+\alpha_e\xi)^2,\quad \sigma_i = (1+\alpha_i\xi)^2,$$

and (6.5)

$$\beta_e = \tan^{-1}\frac{D_e(1)-D_e(0)}{L} \sim \frac{\alpha_e}{\varepsilon}$$

$$\beta_i = \tan^{-1}\frac{D_i(1)-D_i(0)}{L} \sim \frac{\delta\alpha_i}{\varepsilon}\ .$$

It is noted that α_e and α_i may be varied independently as the apexes of the cones, illustrated above, need not coincide (as would be the case if $\alpha_e=\alpha_i$).

Let us evaluate $u_e^*(\xi)$; in §2.3.4 we defined A_e^* as the overall cross section of the beam plus the displacement thickness, i.e. $\delta_1(x) = 0.325(x_0+x)c_t$ (as derived in Appendix G); hence,

$$u_e^* = \frac{A_e}{A_e^*}u_e = \left\{\frac{1+\alpha_e\xi}{1+\alpha_e\xi+0.65[x_o/D_e(0)+\varepsilon\xi]c_t}\right\}^2 u_e$$

and upon setting $\sigma = 1+0.65\varepsilon_o c_t$ with $\varepsilon_o = x_o/D_e(0)$, we obtain

$$\frac{u_e^*}{u_e} = \frac{1}{\sigma^2}\left\{\frac{1+\alpha_e\xi}{1+(\alpha_e+0.65\varepsilon c_t)\xi/\sigma}\right\}^2 = \frac{1}{\sigma^2}\left\{1-\left[\frac{\alpha_e+0.65\varepsilon c_t}{\sigma}-\alpha_e\right]\xi + \ldots\right\}^2$$

which will be linearized as

$$\frac{u_e^*}{u_e} = \left[\frac{1-\alpha\xi}{\sigma}\right]^2,\quad \text{with}\quad \alpha = \frac{0.65c_t(\varepsilon-\alpha_e\varepsilon_o)}{\sigma}\ .$$

We may now write eq.(6.3) as follows:

$$(1+i\omega\nu)\frac{d^2}{d\xi^2}\{\frac{(1+\alpha_e\xi)^4-\delta^4(1+\alpha_i\xi)^4}{1-\delta^4}\frac{d^2\psi}{d\xi^2}\}$$

$$+\{(\frac{1-\alpha\xi}{\sigma})^2(1+\alpha_e\xi)^2u_e^2+(\frac{v_i}{1+\alpha_i})^2-\Theta$$

$$-\int_\xi^1[\Gamma(2-\gamma_e)(1+\alpha_e\xi)^2+\Gamma\gamma_i(1+\alpha_i\xi)^2+\varepsilon c_t(1+\alpha_e\xi)u_e^2]d\xi$$

$$-i\omega[(\frac{\delta^2+\gamma_i}{\gamma_e+\gamma_i})^{\frac{1}{2}}\frac{\delta^2\alpha_i}{2\varepsilon^2}(1+\alpha_i\xi)v_i+(\frac{\gamma_e-1}{\gamma_e+\gamma_i})^{\frac{1}{2}}\frac{\alpha_e}{2\varepsilon^2}(1+\alpha_e\xi)^3u_e]\}\frac{d^2\psi}{d\xi^2}$$

$$+\{\Gamma(2-\gamma_e)(1+\alpha_e\xi)^2+\Gamma\gamma_i(1+\alpha_i\xi)^2+u_e^2[\varepsilon c_n+2\alpha_e(\frac{1-\alpha\xi}{\sigma})^2](1+\alpha_e\xi) \qquad (6.6)$$

$$+i\omega[2(\frac{\delta^2+\gamma_i}{\gamma_e+\gamma_i})^{\frac{1}{2}}v_i+(\frac{\gamma_e-1}{\gamma_e+\gamma_i})^{\frac{1}{2}}[1+(\frac{1-\alpha\xi}{\sigma})^2]u_e(1+\alpha_e\xi)^2]$$

$$+\omega^2[\frac{\delta^2+\gamma_i}{\gamma_e+\gamma_i}\frac{\delta^2\alpha_i}{4\varepsilon^2}(1+\alpha_i\xi)^3+\frac{\gamma_e-1}{\gamma_e+\gamma_i}\frac{\alpha_e}{4\varepsilon^2}(1+\alpha_e\xi)^3]\}\frac{d\psi}{d\xi}$$

$$+\{i\omega(\frac{\gamma_e-1}{\gamma_e+\gamma_i})^{\frac{1}{2}}[\varepsilon(c_nu_e+c_v)+2u_e\alpha_e(\frac{1-\alpha\xi}{\sigma})^2](1+\alpha_e\xi)$$

$$-\omega^2\frac{\gamma_e(1+\alpha_e\xi)^2+\gamma_i(1+\alpha_i\xi)^2}{\gamma_e+\gamma_i}\}\psi=0$$

and, by use of eq. (6.4), the boundary conditions for a cantilever yield $\psi(0)=\psi'(0)=0$; and, at $\xi=1$, $\frac{d^2\psi}{d\xi^2}=0$ and

$$(1+i\omega\nu)\frac{(1+\alpha_e)^4-\delta^4(1+\alpha_i)^4}{1-\delta^4}\frac{d^3\psi}{d\xi^3}+$$

$$\{f[(1+\alpha_e)^2-\delta^2(1+\alpha_i)^2](\frac{1-\alpha}{\sigma})^2u_e^2-\chi\Gamma[(2-\gamma_e)s_e+\gamma_i(1+\alpha_i)^2] \qquad (6.7)$$

$$-i\omega\chi[f(s_e+\delta^2(1+\alpha_i)^2(\frac{1-\alpha}{\sigma})^2)(\frac{\gamma_e-1}{\gamma_e+\gamma_i})^{\frac{1}{2}}u_e+2(\frac{\delta^2+\gamma_i}{\gamma_e+\gamma_i})^{\frac{1}{2}}v_i]\}\frac{d\psi}{d\xi}+$$

$$\{i\omega fu_e(\frac{1-\alpha}{\sigma})^2[(1+\alpha_e)^2-\delta^2(1+\alpha_i)^2](\frac{\gamma_e-1}{\gamma_e+\gamma_i})^{\frac{1}{2}}+\omega^2\chi\frac{[1+f\gamma_e-f]s_e+\gamma_i(1+\alpha_i)^2}{\gamma_e+\gamma_i}\}\psi=0.$$

We now assume that we deal either with quasicylindrical elements or slender bodies, in which case we may neglect any moments due to the convergent flow (see Appendix I); furthermore, since we shall mainly be concerned with flow velocities at the onset of instability usually well above 1, we shall neglect c_v compared to $c_n u_e$.

We also account for a modified viscoelastic damping which exhibits hysteretical behaviour at the higher frequencies (Appendix K) by multiplying the constant viscoelastic coefficient ν by the following function of frequency

$$\mu(\mu+\nu|\omega|)^{-1},$$

where μ is the hysteretical damping coefficient when $\omega\to\infty$. We may finally write the differential equation of motion as follows:

$$\begin{aligned}
&\left(1+\frac{i\omega\mu\nu}{\mu+\nu|\omega|}\right)\frac{d^2}{d\xi^2}\left\{\frac{(1+\alpha_e\xi)^4-\delta^4(1+\alpha_i\xi)^4}{1-\delta^4}\frac{d^2\psi}{d\xi^2}\right\}\\
&+\left\{\left(\frac{1-\alpha\xi}{\sigma}\right)^2(1+\alpha_e\xi)^2u_e^2+\left(\frac{v_i}{1+\alpha_i}\right)^2-\Pi\right.\\
&\quad-\frac{1}{2}(1+\alpha_e)^2C_{fe}u_e^2-\frac{1}{2}\frac{C_{fi}v_i^2}{(1+\alpha_i)^2}-\frac{1}{2}\frac{1+\alpha_e}{1+\alpha_i}C_{fx}u_ev_i\\
&\quad\left.-\int_\xi^1\left[\Gamma(2-\gamma_e)(1+\alpha_e\xi)^2+\Gamma\gamma_i(1+\alpha_i\xi)^2+\varepsilon c_t(1+\alpha_e\xi)u_e^2\right]d\xi\right\}\frac{d^2\psi}{d\xi^2} \qquad (6.8)\\
&+\left\{\Gamma\left[(2-\gamma_e)(1+\alpha_e\xi)^2+\gamma_i(1+\alpha_i\xi)^2\right]+\left[\varepsilon c_n+2\alpha_e\left(\frac{1-\alpha\xi}{\sigma}\right)^2\right](1+\alpha_e\xi)u_e^2\right.\\
&\quad+i\omega\left[2\left(\frac{\delta^2+\gamma_i}{\gamma_e+\gamma_i}\right)^{\frac{1}{2}}v_i+\left(\frac{\gamma_e-1}{\gamma_e+\gamma_i}\right)^{\frac{1}{2}}\left[1+\left(\frac{1-\alpha\xi}{\sigma}\right)^2\right]u_e(1+\alpha_e\xi)^2\right]\left.\right\}\frac{d\psi}{d\xi}\\
&+\left\{i\omega\left(\frac{\gamma_e-1}{\gamma_e+\gamma_i}\right)^{\frac{1}{2}}\left[\varepsilon c_n+2\alpha_e\left(\frac{1-\alpha\xi}{\sigma}\right)^2\right](1+\alpha_e\xi)u_e-\omega^2\frac{\gamma_e(1+\alpha_e\xi)^2+\gamma_i(1+\alpha_i\xi)^2}{\gamma_e+\gamma_i}\right\}\psi=0.
\end{aligned}$$

3. NUMERICAL ANALYSIS AND METHOD OF SOLUTION

3.1 CHARACTERISTIC MATRIC EQUATION

We now stand with an eigenvalue problem described by a fourth-order linear ordinary differential equation with four boundary conditions, which takes the following form:

$$\sum_{r=0}^{4} f_r(\xi,\omega)\,\frac{d^r\psi}{d\xi^r} = 0\,, \qquad (7.1)$$

and

$$\sum_{r=0}^{3} g_r^j(\omega)\left[\frac{d^r\psi}{d\xi^r}\right]_{\xi=\xi_j} = 0\,, \quad \text{with } j = 1,2,3,4 \text{ and } \xi_1=\xi_2=0,\ \xi_3=\xi_4=1\,.$$

The functions f_r and the coefficients g_r^j depend on the characteristics of the beam and the internal and external flows; they are derived from eqs. (6.7) and (6.8) and have been summarized in Appendix C.

In this chapter we present a brief discussion of the method of solution, which is presented in detail in Appendix B. The general solution of (7.1) is a linear combination of an infinite set of independent eigenfunctions, $\psi_0, \psi_1, \ldots \psi_n \ldots$ corresponding to an equal set of distinct eigenfrequencies, $\omega_0, \omega_1, \ldots \omega_n \ldots$ respectively. This eigenvalue problem is seldom self-adjoint, and classical tools such as Galerkin or normal-mode methods are not easily applicable because one normally uses as comparison functions the eigenfunctions of a simpler problem in the same domain which are difficult to find; however, one may conveniently use Fourier series, which offer numerous advantages of calculations and require relatively few terms for synthesizing the modal shapes.

The periodicity of the series must be greater than one in order to satisfy, at $\xi=0$ and $\xi=1$, distinct boundary conditions and to allow for the continuity of Ψ and its derivatives; for convenience a periodicity of two is chosen and we set

$$\Psi(\xi) = \sum_{-\infty}^{+\infty} a_n \frac{e^{in\pi\xi}}{\sqrt{2}} = \sum_{0}^{\infty} \{\gamma_{2n-1} \sin n\pi\xi + \gamma_{2n} \cos n\pi\xi\}$$

The coefficients γ are complex, and the real and imaginary parts of Ψ, which are usually independent, represent the two modal shapes (within an amplification factor) at time $\tau=0$ and $\tau=\pi/(2\omega)$, as can be seen from eq. (6.2). We may now rewrite the original system of equations as follows:

$$D(\xi,\omega) = \sum_{r=0}^{4} f_r(\xi,\omega) \frac{d^r}{d\xi^r}[\gamma_{2n-1} \sin n\pi\xi + \gamma_{2n} \cos n\pi\xi] = 0,$$

and $$\sum_{r=0}^{3} g_r^j(\omega) \{\frac{d^r}{d\xi^r} \sum_{n=0}^{\infty} [\gamma_{2n-1} \sin n\pi\xi + \gamma_{2n} \cos n\pi\xi]\}_{\xi=\xi_j} = 0.$$

In order to satisfy the differential equation, independently of ξ, we equate to zero the following integrals which represent the Fourier coefficients of $D(\xi,\omega)$,

$$\int_0^1 D(\xi,\omega) \sin p\pi\xi d\xi = 0,$$

$$\int_0^1 D(\xi,\omega) \cos p\pi\xi d\xi = 0;$$

when p varies from zero to infinity such conditions are equivalent to satisfying the differential equation for $0<\xi<1$.

Each equation yields a linear homogeneous relation between the γ's; the four boundary conditions are linear and homogeneous too. Hence, all the equations may be summarized in the following matrix equation:

$$[A(i\omega)][\Gamma] = [0] \quad , \qquad (7.2) \ ,$$

where the first four rows of matrix [A] are occupied by the boundary conditions and the following by the conditions derived from the differential equation for increasing values of p. $[\Gamma]$ is the infinite column vector of the γ's.

The next step is to look for singular matrices [A] in terms of ω, so as to obtain other than trivial solutions for $[\Gamma]$; for this purpose we equate to zero the determinant of square truncated submatrices of [A], which result from truncating the Fourier series (the order of the matrix being equal to the number of terms in the series). The eigenvalues of ω converge rapidly with the size of the submatrices, although higher orders are required for higher eigenvalues; in general, less than fifteen terms in the Fourier series are required to obtain the first eigenfrequencies with good accuracy; for instance, as indicated on p.26 of Appendix B, ten terms yield the five lowest natural frequencies of a classical cylindrical cantilevered beam within one percent error; however, if flowing fluid or conical cantilevers are being considered, the number of terms must be increased.

3.2 SYMMETRY OF EIGENFREQUENCIES

The only complex terms in eq.(6.8) arise from differentiation with respect to time, thus introducing the factor $i\omega$; this, as will be shown below, results in symmetry of the eigenfrequencies around the imaginary axis. However, before this is proven, let us mention that such symmetry would not have occurred had we introduced hysteretic damping in the form of a term, $EI(1+i\mu)$ rather than viscoelastic damping in the form $EI(1+k\frac{\partial}{\partial t})$.

Since the general term of matrix [A] is a polynomial of $i\omega$ with real coefficients, the conjugate of [A] will simply be

$$[\bar{A}(i\omega)] = [A(\overline{i\omega})],$$

where $\overline{i\omega}$ is the conjugate of $i\omega$.

Let $\omega_n = a_n + ib_n$ be a complex root of the characteristic equation; if ω_n is not a multiple (repeated) root we can calculate the corresponding solution vector $[\Gamma_n]$ from eq.(7.2). Let $\tilde{\omega}_n = -a_n + ib_n$. Now, if eq.(7.2) is satisfied, so is its conjugate; hence we also have

$$[A(i\omega_n)][\Gamma_n] = [\bar{A}(i\omega_n)][\bar{\Gamma}_n] = [A(i\tilde{\omega}_n)][\bar{\Gamma}_n] = 0, \qquad (8.1)$$

which simply implies that $\tilde{\omega}_n$ is also a root of the characteristic equation, and it is associated with $[\bar{\Gamma}_n]$, conjugate of $[\Gamma_n]$. Incidentally, the solution given by eq.(6.2) is the same whether ω takes the value ω_n or $\tilde{\omega}_n$. Thus, we have proven the statement made in the first paragraph.

Therefore, as illustrated on the diagram in the next page, we only need to represent the loci of ω in quadrants I and IV of an Argand diagram, the loci in the other two quadrants being mirror images of those in I and IV.

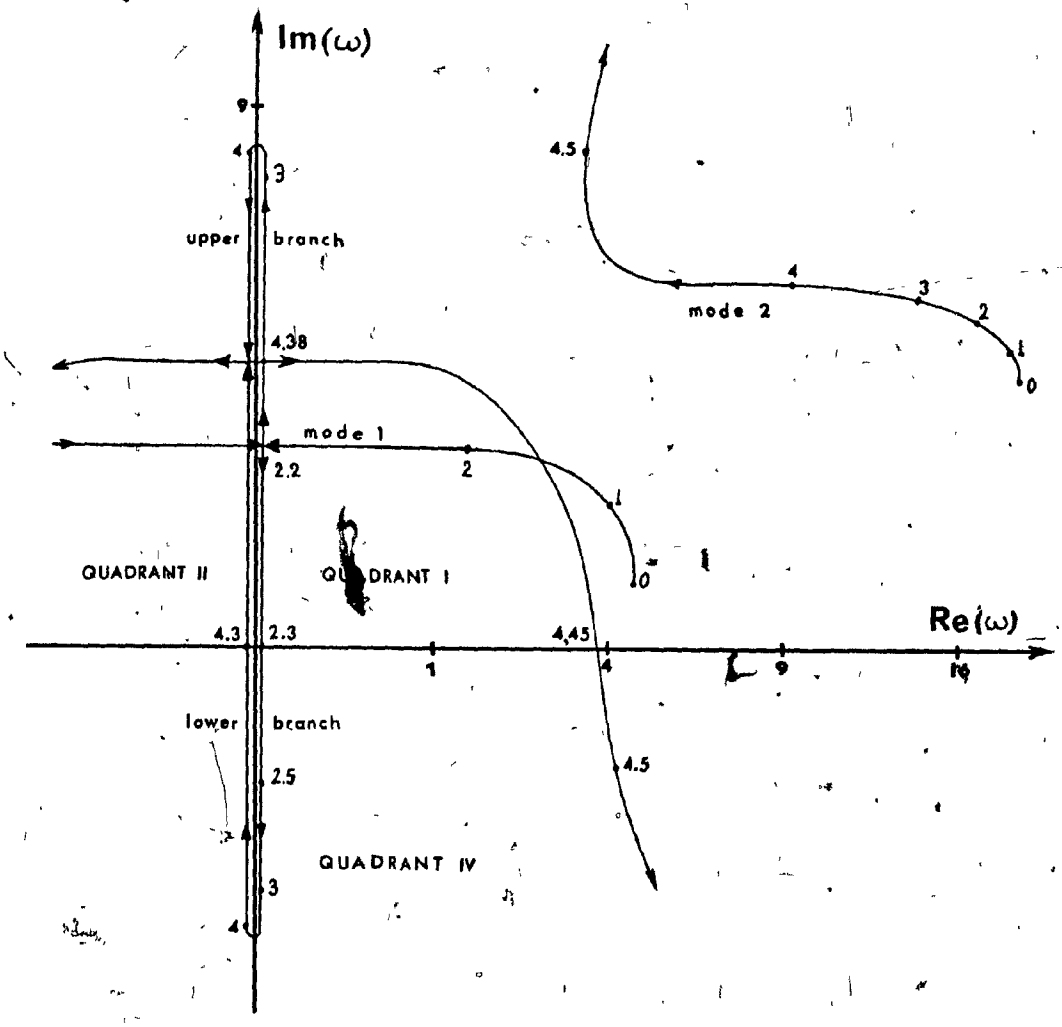

However, special attention must be paid to the two distinct branches on the Im(ω)-axis which arise from the "collision" of symmetric loci, as illustrated above. In this case, which is typical of viscoelastic cantilevered beams in external flow (ν=.01, δ=0, α_e=-.5), the two symmetric first modes collide on the imaginary axis (at velocity u_e=2.2); this results in two branches on the Im(ω)-axis, one going down and the other up. Eventually, the lower branch having become negative (buckling at u_e=2.3), doubles back, while the upper one begins to diminish. These two branches then collide (u_e=4.38) and depart from the axis in opposite directions.

3.3 COMPUTER CALCULATION PROCEDURES

Computations and programming accounted for a large share of this work; here, we shall outline the general process and some of the tools which were developed. The major computer programs are given in Appendix L.

First, a standard case corresponding to one of the experimental cases is selected and the following independent parameters are read in:

$$\alpha_e,\ \alpha_i,\ \delta,\ c_n,\ c_t,\ \varepsilon,\ \varepsilon_o$$
$$\gamma_e,\ \gamma_i,\ \gamma,\ \nu,\ \mu,\ \Pi,\ \chi_e$$
$$u_e,\ v_i$$

Then, mainly two different classes of operations are performed and usually in the following sequence:

A) The complex frequencies for increasing flow velocities, i.e. either u_e or v_i, depending upon the case, are calculated with all other parameters fixed; the values are plotted, real versus imaginary part, as illustrated on the previous page. The initial steps at zero flow velocities are estimated by use of the perturbation method (Appendix E); moreover, since the perturbation solution predicts hydrodynamic damping of the system over a range of velocities which increases with the mode number our investigations were restricted to the three lowest modes.

B) Then, if the previous frequency loci intersect the real axis (e.g. at u_e=2.3, 4.3, 4.45 on the figure of the previous page), the critical velocties corresponding to purely real frequencies are calculated. Now, some of the other relevant parameters listed above are varied step by step, usually one at a time, and

the corresponding critical velocities are calculated; neutral stability contours are thereby obtained.

A small library of general double-precision complex subprograms was developed, each of which has a specific function, as summarized below:

a) Root prediction. A predictor subprogram constitutes the core of class (A) operations. Apart from extrapolating to give estimated values of frequencies from the previous last three steps, it increases or reduces velocity steps according to the 'regularity' of the frequency loci; it also overcomes discontinuities such as might arise from coalescence on the imaginary axis of opposite branches.

b) Critical velocity calculation. A subprogram iterates both on velocities and frequencies to find a critical velocity corresponding to $Im(\omega)=0$; this subprogram stores the characteristics of the frequency locus (slope and partial derivatives) in order to facilitate prediction of the next critical velocity at the next step, when the variable parameter is varied incrementally (as described in class (B) operations).

c) Singular velocity calculation. A subprogram iterates both on velocities and frequencies to investigate singular points corresponding to a double root of the frequency. These points are encountered when two modes collide at the same velocity such as two symmetric branches reaching the imaginary axis. (If the singular eigenfrequency lies on the imaginary axis with a negative sign, the corresponding critical velocity indicates a transition from buckling to flutter.)

d) Matrix filling. The matrix of eq.(7.2) is filled for input values of the frequency and the variable parameters. The other parameters and the CC, CS, SS coefficients of Appendix C (recalculated for each new value of α_e, α_i and α) are transmitted through 'common' blocks. The determinant of the matrix is calculated by a standard pivoting method.

e) Secant method application. Standard secant and Lagrange methods were improved to detect slow convergence or divergence of complex frequencies. The number of iterations required to find the root with a given accuracy is stored and eventually used in the calling subroutine as an indicator to vary the step size of the parameter being varied.

f) Modal shape calculation. A subroutine solves eq.(7.2) at given flow velocities, in terms of the coefficients of the Fourier series; the eigenfunction obtained thereby is normalized and then plotted (real part, imaginary part and absolute value as functions of x) in order to illustrate the modal shape at different times. This subroutine calls a modified version of an IBM subprogram to solve simultaneous equations with complex coefficients with double precision.

4. EXPERIMENTS

4.1 APPARATUS

In parallel to the theoretical work, experiments were conducted in a specially constructed, vertical water tunnel. In this tunnel, the water runs through an approximately 15 m (50 ft) long closed loop, most of which consists of 0.2 m stainless-steel piping (8 in. I.D.), as illustrated in Fig. 1.

A variable belt drive, 50 H.P. motor propels a single stage centrifugal pump which delivers up to 0.25 m^3/s (60 gal/s). Downstream from the pump, two Venturi nozzles connected to a mercury manometer measure the flow discharge. One Venturi, on the main (8 in.) pipe is used for discharges above 0.06 m^3/s whereas the second, on a smaller (4 in.) branch-line is used for flows below this value. The distribution of discharge through the two branches is controlled by two pinch valves, one after each Venturi, and, in practice, either one or the other is closed.

At the top of the rig a 3.5 m (12 ft.) long heat exchanger is used whenever necessary; in addition, the filling of the tunnel is done through this exchanger which is connected directly to the pump by a vertical 5 cm (2 in.) I.D. pipe thus producing more than the minimum pressure head required at the intake of the pump to avoid cavitation.

Having passed the exchanger, the flow reaches the last elbow before the test-section; in order to prevent the formation of major vortices and large-scale secondary flow, a bundle of thin stiff plastic tubes, approximately 3 cm in diameter and packed one against

the other, was inserted in the elbow around the bend; further down, the flow passes a series of straightening vanes and grids. The test section consists of a 0.75 m vertical plastic tube, of 0.2 m I.D. and 0.02 m wall-thickness; it is transparent and has a 0.12 m door similar to a port-hole, machined to match exactly the internal contour of the test section; the upper part of the section is telescopic, sliding on two horizontal rubber O-rings, so that the fragile plastic tube can be easily inserted, aligned and tightened top and bottom to the stainless-steel piping without danger; thick rubber gaskets provide additional flexibility for the alignment.

Ahead of the pump, a 1 m heavy rubber tube (valve liner) is intended to absorb major vibrations arising from the flow, especially at velocities of the order of 3 m/s and above. Finally, just before re-entering the pump, the flow goes into a short diffuser.

Obviously, other necessary devices were added to the tunnel, such as pressure gauges, thermometers, water filters, more grids, and a deaerator which pumps the water from the top of the loop, drains the air away and links back with the pump. Moreover, the velocity profile in the test section was checked to be reasonably flat in the neighbourhood of the center-line and axisymmetric; yet the value of the local velocity, read from Pitot tubes, is approximately fifteen percent above the average for the whole cross-section as obtained from the Venturi readings.

The internal flow is supplied independently of the external flow by a long pipe of 5 cm diameter; an orifice plate

is located in this branch with fifty and thirty diameters of straight pipe upstream and downstream, respectively; the diameter then reduces to 1.3 cm (half-inch) as the pipe enters the rig, one meter above the test-section; the pipe runs along the axis of the water-tunnel down to the test-section, where it fits into the support of the tubular beams.

4.2 FLEXIBLE TUBULAR TUBES

The tubular beams were cast, in special moulds, from liquid silicon rubbers which harden with the aid of a catalyst; the specific gravity and characteristic velocity of propagation of a longitudinal wave in the four types of material which were tested are tabulated below.

type	sp. gr.	c (m/s)
A	1.14	40
B	1.38	61
D	1.50	55
E	1.12	41

(9.1)

Following early experiments, the last type, i.e. 'Silastic' E, was usually preferred to the others, because its elastic and internal damping characteristics appeared to be more reliable and consistent; this material exhibits little plasticity but rather, as defined in Appendix K, hysteritic viscoelasticity.

The liquid rubber, free from air bubbles, is injected from below in the mould, up to a cylindrical metal piece, labelled clamp adaptor in Figure 2; this piece, inserted in the axis of the mould becomes solidly attached to the beam after the curing time has elapsed, and provides a means to pull the beam from the mould and then to clamp it to the support in the test-section with best alignment. The support consists of a thick tube supported by four horizontal aerofoil struts; its outside diameter is the same as that of the clamp adaptor, which in turn is the same as the upper extremity of the beams, i.e. 2.5 cm (1 in.); the pipe

conveying the internal flow fits into the top and the clamp adaptor into the bottom, both fits being water-tight by the use of O-rings.

In the experiments where cylindrical tubular cantilevers were tested in external flow but with no internal flow, several end pieces, with shapes ranging from blunt to well streamlined, were fitted at the downstream free end of the beam, as illustrated in Fig.2; their density is close to that of the beam. If the cantilever is not cylindrical, or if internal flow is being considered, it was found more convenient to grind the extremity of the beam itself to the desired shape rather than to adapt end pieces to such beams; although the end is no longer rigid, as assumed in the transverse boundary conditions, in fact the curvature obtained thereby is extremely small since the moment is negligible over the end.

In the experiments conducted with cylindrical tubular beams supported at both ends, the downstream support consists of a thin vertical tube supported by a horizontal aerofoil strut; the tubular beam fits over this tube and it is loose enough to let the beam slide axially. Although the beam is supported over nearly 2 cm, the clamped-sliding boundary condition thus obtained is not ideal; however, the errors suffered thereby are expected to be equivalent to some underestimation of the length by a few percent.

4.3 EXPERIMENTAL PROCEDURE

The experimental data was collected from a set of experiments performed on several beams which differed either in the rubber material used, to which parameters γ, γ_e, γ_i, and k are related, or in the geometry of the external and internal moulds, which sets β_e, β_i and the parameter δ.

Each experiment consists of a series of tests conducted with the same beam, but progressively truncated shorter; starting from a length of 50 cm ($\varepsilon \sim 20$), which corresponds to the maximum distance available in the test-section, the length was reduced by five centimeters at each step, down to 25 cm, which corresponds to $\varepsilon \sim 10$, and beyond which the slender-body assumptions are probably violated; in fact, for $\varepsilon \sim 10$ the flow velocities required to render such short beams unstable exceed the possibilities of our apparatus.

In the tests conducted with internal flow only, or with supports at both ends, the downstream end was blunt; the stability of such beams is almost independent of the external shape at this extremity because the effect of the base drag, if any, and of the immersed weight of the end piece is small. However, for cantilevered beams subjected to external flow, up to four downstream end configurations were investigated, ranging from a smoothly tapered, well-streamlined shape ($\chi_e \sim 1.5$) to a blunt end ($\chi_e = 0$).

In summary, among the independent dimensionless parameters previously defined, all but three, i.e. c_n, c_t and ε_o, were investigated experimentally (α_e and α_i being derived from β_e, β_i, δ and ε). A typical experiment, conducted with a cantilevered tubular beam will now be described.

Once the beam is cast, it is pulled from its mould with great care (so as not to tear it) and its free end is machined down to the proper length and to a smooth taper ($\chi_e \sim 1$), as illustrated in Fig.2 (bottom left). Then, the beam is hung in the water tunnel from its support, the door of the test-section is closed and the water valves are opened. When the rig is filled to the top, the pump is switched on at low speed for a few minutes while the air from the main loop (external flow), internal flow piping, flowmeters and manometers is drained and the water deaerated. The procedure to be described below applies to experiments with both internal and external flow.

The pump is switched off and the internal flow velocity is gradually increased until the beam eventually departs from its stable position at rest along the x-axis; the instabilities usually gain rapidly in amplitude; hence, the flow velocity is set back below the level of instability and increased again until it is felt that the threshold of stability has been established. The critical flow velocity and, if applicable, the corresponding frequency, as well as the approximate modal shape are then recorded; the frequencies are generally small enough for them to be measured visually with a stop watch; yet a stroboscope was used to 'freeze' the modal shapes. Once the relevant data has been recorded, the internal flow is set back to zero. Now the external flow is increased in small steps; at each step the internal flow is turned on and increased, repeating the procedure described before. Usually the limit on internal flow was set by the danger of failure of the beam due to very large deflections. The test ends when the external flow velocity is approximately 6 m/s, which corresponds to the maximum

attainable with the existing pump.

The rig is then emptied, the beam removed from the test-section and the tapered end chopped off (hence, $\chi_e=0$). The complex Young's modulus is then calculated for this specific beam from its free lateral oscillations as reported in Appendix K. The beam is clamped back in the test-section and the test is repeated. Once both tests are completed, the length of the beam is reduced by roughly three centimeters, the end is streamlined and the previous operations are repeated, until the length becomes too small for meaningful experiments.

4.4 GENERAL OBSERVATIONS

As a result of observations based upon different tubular beams and different support conditions, two classes of instabilities were found, namely buckling and transverse flutter. Such phenomena have been described with accuracy by Paidoussis [16,50] and we now give an abbreviated account of their occurrence and of their main features.

4.4.1 Buckling

If the beam is supported at both ends, buckling is the first instability to develop as the flow velocity, either internal or external, is increased. However, if the beam is supported at one end only, buckling cannot be obtained by the sole action of the internal flow, nor is it observed with external flow when the end is bluntly shaped.

The critical flow velocities delimiting the buckling zone are always difficult to pinpoint because, contrary to what the linear theory predicts, the beam does not buckle all of a sudden when the critical velocity is reached. In fact, the beam tends towards a slightly buckled shape, similar to a first beam-mode, before the "critical" flow velocity is reached; as the flow is increased further, the deflection away from the x-axis increases continuously, then reaches a maximum which does not exceed one or two diameters and finally diminishes. Had the position of the beam been stationary, it might have been possible to determine the "real" critical flow velocity from a plot of the displacement vs the velocities by extrapolation; unfortunately the plane in which buckling takes place often rotates slowly; moreover, the beam continuously responds to random

perturbations in the flow, thus generating erratic motion. For tapered beams, subcritical vibrations resulting from those perturbations in the flow are amplified as they propagate along the beam (because of the diminishing cross-section and flexural rigidity) to the extent that they eventually offset the deflections arising from buckling (and, for that matter, flutter). In fact buckling could not be isolated (nor flutter) with certainty for almost conical beams ($-0.7>\alpha_e>-1.$) because the level of turbulence in the apparatus was too high; for quasi-cylindrical beams we selected the criteria for buckling to be a minimum deflection from the position of rest by approximately half a diameter.

In establishing the upper limit of buckling, another difficulty is met because the next instability (second mode flutter) often overlaps the buckling zone; in this range of velocities, the modal shapes and the amplitude of the two neighbouring instabilities are very close and they can only be distinguished by their frequency, i.e. one oscillates (flutter) and the other does not (buckling); yet, the frequency of flutter is sometimes very low whereas the buckled beam may oscillate due to flow separation and vortices at the free end.

4.4.2 Flutter

Flutter generally supersedes buckling at higher flow velocities and the modal shape of the oscillation is close to a second mode, except for cantilevers conveying internal flow which do not buckle at all and may flutter in the first mode.

As the velocity increases, higher-mode flutter is encountered and the beam never regains complete stability between

successive instabilities. The transition between two kinds of flutter occurs abruptly; travelling waves shake the beam until the new modal shape has established itself.

Although the modal shapes do not have nodes exactly fixed with respect to the x-axis, some portions of the beam experience smaller displacements than others and the number of these regions usually increases by one as the instability switches from one flutter mode to the next; moreover, such regions are stationary, so that no single travelling wave can be observed. However, the beam does not oscillate in phase, and the phase shift between the two ends of the beam can be significant, although it never appears to keep the same sign over the whole length of the beam; in other words, the motion of the beam is the superposition of a sinusoidal oscillation and small waves (of not necessarily the same amplitude) travelling at different speeds and in opposite directions.

In the case of beams supported at both ends, the available external flow in the water tunnel did not allow for flutter to be observed without internal flow; however, at the maximum external flow velocity, a small internal flow precipitated flutter. As opposed to the case of a cantilevered beam, where flutter develops with a specific frequency, in this case the transition from buckling to flutter is a continuous process, as described below; moreover, no diminution of the amplitude of the buckled beam is observed. Flutter starts in the form of a travelling wave of roughly four diameters in transverse amplitude and with a half-wavelength (from one node to the next) close to half the length of the beam, which propagates very slowly downstream; further increase in the flow velocity causes the motion to become brisker, the frequency of the

oscillations to increase and the travelling wave to be more difficult to observe; the oscillations then look more or less like those of a second beam-mode.

Flutter due to the external flow, irrespective of support conditions, usually involves amplitudes and deflections much smaller than for the internal flow; rather than the ever-growing amplitudes predicted by linear theory, small limit cycles are obtained, thus implying important non-linear forces. However, in the case of internal flow, oscillations may develop until the tubular beam hits the wall of the test-section; therefore, the flow had to be reduced quickly to stop flutter and avoid ruining the beam. It seems that non-linearity affects the experiments in external flow more than those in internal flow, presumably because flow separation may occur along the beam and flow velocities are smaller away from the x-axis. Consequently, it is preferable to investigate the influence of internal flow on an instability caused by the external flow, rather than vice versa; in addition, the stabilizing or destabilizing effect of internal flow on the amplitude of a small limit cycle can be easily assessed.

Finally, it is generally observed that, below the critical flow velocity, the beams are stable in the small, but unstable in the large; for example, another manifestation of non-linear behaviour is that flutter persists below the critical velocity for a small range of flow velocities; similarly, a higher-mode flutter persists below the velocity where, by increasing the flow, it had first superseded the previous lower-mode flutter.

5. COMPARISON BETWEEN EXPERIMENTAL AND THEORETICAL RESULTS

Rather than presenting the theoretical and experimental results separately, and then comparing them in another part of the Thesis, it was decided to present the two together, wherever both are available, and compare theory to experiment directly. Two important reasons for this are that (a) there are many different, albeit related types of systems considered (e.g. with internal flow, with external flow, conical or cylindrical, etc.), (b) the physical parameters affecting stability are too numerous to be able to calculate stability criteria for all possible combinations, and hence the available experimental data provides a framework for the theoretical calculations.

5.1 CASES OF ZERO EXTERNAL FLOW

In this section we will consider cases where only the internal fluid possesses an axial velocity, whereas the only significant motion of the external surrounding fluid is the cross-flow due to lateral motion of the tubular beam. Thus, the flow along the beam resulting from the mixing of the jet of internal fluid with the external fluid at rest will be neglected. The tests involved only vertical cantilevers clamped upstream and hanging either in air or in water, but the internal fluid was always water. In all cases the thickness ratio was at least equal to 0.5 along the tube, to prevent shell type instabilities and swelling. Finally, the free end was always blunt ($\chi=\Pi=0$).

According to the geometry of the internal duct and that of the external surface, we may classify the beams tested into the following three classes:

a) cylindrical tubes; both external and internal cross-sections are uniform.

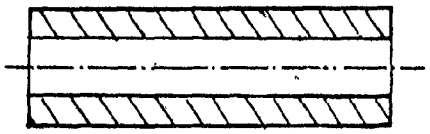

b) cylindrical-conical tubes; the external cross-section is uniform, and the internal conduit constitutes a truncated cone.

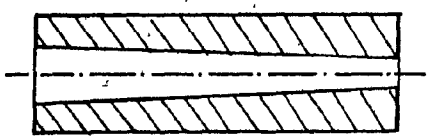

c) conical tubes; both external and internal surfaces are truncated cones.

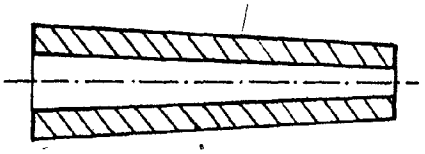

The fourth possibility, i.e. a conical beam with a cylindrical duct was not investigated because of experimental difficulties; for instance, an initial upstream thickness ratio of 2:1 led to a fragile downstream end, whereas a larger upstream ratio would have required critical flow velocities beyond the capabilities of the experimental apparatus.

5.1.1 Cylindrical tubes

In the case of cylindrical tubes, i.e. $\alpha_e=\alpha_i=0$, eq. (6.8) reduces to

$$\{1+\frac{i\omega\nu\mu}{\mu+\nu|\omega|}\}\frac{d^4\psi}{d\xi^4} + \{v_i^2(1-\tfrac{1}{2}C_{fi}) - \Gamma(2-\gamma_e+\gamma_i)(1-\xi)\}\frac{d^2\psi}{d\xi^2}$$

$$+ \{\Gamma(2-\gamma_e+\gamma_i) + 2i\omega(\frac{\delta^{2+\gamma_i}}{\gamma_e+\gamma_i})^{\frac{1}{2}} v_i\}\frac{d\psi}{d\xi} - \omega^2\psi \doteq 0 \ , \qquad (10.1)$$

and, for a free downstream end, the boundary condition of eq. (6.7) simply reduces to $(d^3\Psi/d\xi^3)_{\xi=1} = 0$ for a blunt end, i.e. for $\chi=0$.

Apart from the additions allowing for an external fluid other than air, and for both viscoelastic and hysteretical damping, the equation above is basically identical to those previously derived by M.P. Paidoussis. This case has been treated extensively by numerous authors with good predictions of flutter, and we shall only focus on the effect of the external surrounding fluid. In Fig.3 are plotted frequency loci for a cantilever in air and in water. The coordinates have been scaled to represent the square roots of the real and imaginary parts of the eigenfrequency ω_i; this repesentation has been adopted for such diagrams because it yields almost equidistant spacing between the modes at small flow velocities (e.g. for the cylindrical tubular beams presently considered, the interval between consecutive modes is approximately equal to π). In this example, since we did not account for internal damping of the material, the modes start on the real axis at zero flow velocity. Great similarity is observed between the frequency loci, for example in terms of the intersection of the first mode with the imaginary axis (damped motion without oscillations) and flutter in the second mode. However, the surrounding fluid, whether air or water, has a significant influence on both velocities and frequencies; e.g. the critical dimensionless flow velocities for flutter are 8.5 and 5 with frequencies of 25 and 14 in air and water, respectively. This can be mainly attributed to the different gravity effects introduced by the term $\Gamma(2-\gamma_e+\gamma_i)$ in eq. (10.1). If Γ, which is a measure of gravity versus flexural forces specific to the tube, is not negligible, the eigenfrequencies of the

same tube at the same flow velocities will differ in the two cases, since the values of $2-\gamma_e+\gamma_i$ are close to 1 if the surrounding fluid is air and closer to 0 if it is water. Apart from the gravity effects, the inertia effects introduced independently by the parameters γ_e, γ_i and δ differ in the two cases; for instance, as shown in Appendix E, the imaginary parts of the frequencies are approximately equal to $2v_i[(\delta^2+\gamma_i)/(\gamma_e+\gamma_i)]^{\frac{1}{2}}$ for small-flow velocities, thus resulting in higher hydrodynamic damping when the surrounding fluid is air rather than water.

5.1.2 Cylindrical-conical tubes

Theoretical results.

For this case $\alpha_e=0$ and equation (6.8) yields

$$(1+\frac{i\omega\mu\nu}{\mu+\nu|\omega|})\frac{d^2}{d\xi^2}\{\frac{1-\delta^4(1+\alpha_i\xi)^4}{1-\delta^4}\frac{d^2\psi}{d\xi^2}\} + \{[\frac{v_i}{1+\alpha_i}]^2(1-\frac{1}{2}C_{fi})$$

$$-\Gamma[(2-\gamma_e+\gamma_i)(1-\xi) + \gamma_i\alpha_i(1-\xi^2) + \gamma_i\frac{\alpha_i^2}{3}(1-\xi^3)]\}\frac{d^2\psi}{d\xi^2} \qquad (10.2)$$

$$+ \{\Gamma[2-\gamma_e+\gamma_i(1+\alpha_i\xi)^2] + 2i\omega[\frac{\delta^2+\gamma_i}{\gamma_e+\gamma_i}]^{\frac{1}{2}}v_i\}\frac{d\psi}{d\xi} - \omega^2\frac{\gamma_e+\gamma_i(1+\alpha_i\xi)^2}{\gamma_e+\gamma_i}\psi = 0.$$

The frequency loci for a cantilever in air or water are shown in Fig.4. Great similarity, both in the general shapes and critical characteristics is now observed for the two sets of loci; moreover, these pairs of loci are very close to those of a cylindrical tube in water (Fig.3), except for the values of the velocity. This arises because the value of γ_i, i.e. $(1-\frac{\rho}{\rho_i})\delta^2$, is usually small compared to γ_e when we take $\delta<\frac{1}{2}$ and $\rho<1.5\rho_i$, and δ^4 is small compared

to 1; hence the main difference between eq.(10.1) and eq.(10.2) is the division of the velocity v_i by $(1+\alpha_i)$ in the factor associated with the second derivative of Ψ. Indeed, at high flow velocities we may expect the frequency loci to be similar, except for a velocity ratio between 1 and $1+\alpha_i$ depending on whether ω is large or small; the ratio will be close to $1+\alpha_i$ if ω is small since the only other significant term involving v_i is multiplied by $i\omega$. For instance, in Figs. 3 and 4 respectively, the frequencies at velocities in a ratio of .5 such as $v_i=10$ and $v_i=5$, are close, since $1+\alpha_i=0.5$; similarly, when the frequency loci intersect the real axis, the critical velocities in water are $v_i\sim5$ and $v_i\sim2.25$ respectively, yielding a ratio of .45 which is close to the value of $1+\alpha_i$.

Comparison with experiments

Our prime concern is the determination of critical flow velocities at the onset of instability; in practice this was done by increasing the flow velocity until small regular oscillations were observed; then it was a matter of time before they began increasing in amplitude so as to yield large deflections; consequently, the critical frequencies were measured rapidly while the displacements were still small in order to avoid large non-linear effects.

The results for a single beam truncated to different lengths are presented in Figs. 5 and 6, for the beam in water and in air, respectively; the experiments were not conducted below a length ratio $\varepsilon=L/D=10$ because the actual critical velocities and frequencies, as opposed to their dimensionless counterparts, increase rapidly and exceeded the capabilities of the apparatus; besides, beam theory becomes inaccurate for beams of small slenderness. As

indicated on the abscissa of the figures we only investigate length ratios corresponding to values of the taper ratio, α_i, varying from around -0.3 to -0.6; the lower range i.e. from -0.3 to 0.0 is of little interest, as the beam approaches the cylindrical shape. The upper range in the vicinity of -1.0 would clearly be more interesting, as we expect the beam to become unstable at very low flow velocities; however, stretching of the tubes and swelling at the upstream extremity become important in such cases, and eventually failure of the material may occur.

In all cases, frequencies and critical velocities are very precise, and easier to pinpoint than for a similar cylindrical tube; in both Figs. 5 and 6, the effect of a tapered internal conduit can be appreciated in terms of the good agreement between the critical velocities obtained experimentally and those predicted by theory. On the other hand, the frequencies are off by as much as 30%, which is not too surprising as internal damping has not been taken into account in these particular figures.

If the buoyancy and gravity forces balance, i.e. $\gamma_e=2$ and $\gamma_i=0$, eqs. (10.1) and (10.2) become independent of Γ. Now, for a cylindrical tube and in the absence of damping ($\nu=0$), Γ is the only parameter depending upon ε; hence, as observed in Fig.5, the critical velocity is almost independent of ε if the surrounding fluid is water, whereas it increases significantly with ε if in air (Fig.6). This is not the case for a conical duct, as predicted earlier: the figures show that the critical velocity decreases with larger values of $-\alpha_i$; moreover, the effect of gravity, which increases as ε^3, appears to be small, as illustrated in Fig.7, where

the difference between the two critical velocities may be seen not to vary significantly with ε. Finally, for both the cylindrical and the cylindrical-conical tubes we observe that the critical velocities are higher in air than in water.

Fig. 7 illustrates the influence of damping in the case of the cylindrical-conical beam. We observe that, irrespective of whether the beam is immersed in water or hanging in air, the critical velocity is only increased by roughly 5% if we take into account viscohysteretic damping (dotted lines); yet agreement with the experiments is not significantly different. However, the critical frequencies, especially in water, are indeed more significantly reduced and the discrepancy with the experiments is now always less than 20%.

5.1.3 Conical Tubes

Theoretical results

We now consider the general case of a conical external surface and a conical internal duct. The differential equation (6.8) may be simplified due to $u_e=0$, yielding

$$(1 + \frac{i\omega\mu\nu}{\mu+\nu|\omega|})\frac{d^2}{d\xi^2}\{\frac{(1+\alpha_e\xi)^4 - \delta^4(1+\alpha_i\xi)^4}{1-\delta^4}\frac{d^2\psi}{d\xi^2}\} +$$

$$+ \{\frac{v_i^2}{(1+\alpha_i)^2}(1 - \frac{1}{2}C_{fi}) - \Gamma[(2-\gamma_e+\gamma_i)(1-\xi) \qquad (10.3)$$

$$+ ((2-\gamma_e)\alpha_e+\gamma_i\alpha_i)(1-\xi^2) + \frac{1}{3}((2-\gamma_e)\alpha_e+\gamma_i\alpha_i)(1-\xi^3)]\}\frac{d^2\psi}{d\xi^2}$$

$$+ \{\Gamma[(2-\gamma_e)(1+\alpha_e\xi)^2 + \gamma_i(1+\alpha_i\xi)^2] + 2i\omega[\frac{\delta^2+\gamma_i}{\gamma_e+\gamma_i}]^{\frac{1}{2}}v_i\}\frac{d\psi}{d\xi}$$

$$- \omega^2\frac{\gamma_e(1+\alpha_e\xi)^2+\gamma_i(1+\alpha_i\xi)^2}{\gamma_e+\gamma_i}\psi = 0.$$

In Fig.8 are plotted the frequency loci for such a tube, hanging either in air or in water; because internal damping has been taken into account, the natural frequencies at zero flow velocity are complex and the mode loci no longer start on the real axis. At first, the external fluid would appear to have a critical effect on the dynamics of the system when we compare the two diagrams. For instance, the mode which becomes unstable first is mode 1 in water and mode 2 in air; however, closer examination indicates that the two cases are quite similar if, independently of what happens at velocities in the vicinity of 0.75 and above, we consider that the loci of mode 1 and mode 2 have interchanged roles. Such mode interchange is commonly encountered in elastohydrodynamics and usually has little influence on the critical characteristics.

If we compare these loci to those obtained in Fig.4 for a cylindrical-conical tube, the major difference is obviously that here both mode 1 and mode 2 become unstable; furthermore, if we extrapolate the diagrams in Figs. 5 and 6 for $\alpha_i=-.7$, we obtain for a cylindrical-conical tube critical velocities which in each case are higher than those of a similar conical tube.

Experimental results

In Fig.9 we compare experimental and theoretical critical velocities and frequencies with the beam truncated to progressively shorter lengths; hence, the values of α_e and α_i in the abscissa are proportional to the length ratio ε. The theoretical calculations take into account the viscohysteretical characteristics of the material, with either air or water as the external fluid. We observe

that the critical velocity drops even more rapidly with ε than in the case of cylindrical-conical tubes, due to the weakening of the tube as the external cross-section tapers off.

Comparison between experimental and theoretical results appears generally good, provided that ε remains above 10. As ε approaches 20, a sudden increase of the frequency occurs when the external fluid is air. This is typical of the influence of gravity terms, i.e. terms involving Γ; Γ is proportional to ε^3 and the frequency locus would exhibit several other "jumps" if calculations had been pursued to larger values of ε. Such jumps have been observed by Paidoussis [16] for cylindrical tubes hanging in air (γ_e=1) for values of Γ up to 100; in Fig.6 we may observe one around ε=19, corresponding to Γ~15, and in Fig.9 the corresponding value in air is Γ~11; however, in comparing these two values we must realize that the coefficients of Γ are not identical in eq.(10.3) and (10.1). If the external fluid is water such jumps only occur for higher values of ε, due to the effect of buoyancy.

5.2 CASES OF NO INTERNAL FLOW

In this sub-chapter we shall consider external flow only, and mostly for full beams rather than tubular beams. Moreover, we shall restrict our investigations to vertical cantilevered beams clamped at their upstream (upper) extremity. The beams are terminated at their free end with bullet-shaped rigid end pieces.

Two major classes of beams will be considered, the first comprises cylindrical beams with a uniform circular cross-section ($\alpha_e=0$), and the second consists of beams, referred to as conical, which have the shape of a convergent truncated cone ($-1<\alpha_e<0$).

5.2.1 Cylindrical beams

Upon setting $\alpha_e=\alpha_i=v_i=0$ and $\Pi\sim\frac{\chi}{3}(2-\gamma_e)$ (for the immersed weight of an approximately conical end piece), eq.(6.8) yields

$$\{1+\frac{i\omega\mu\nu}{\mu+\nu|\omega|}\}\frac{d^4\Psi}{d\xi^4}$$

$$+\{(\frac{1-\alpha\xi}{\sigma})^2u_e^2-\frac{1}{2}C_{fe}u_e^2-\frac{\chi}{3}(2-\gamma_e)-[\Gamma(2-\gamma_e+\gamma_i)+\varepsilon c_t u_e^2](1-\xi)\}\frac{d^2\Psi}{d\xi^2}$$

$$+\{\Gamma(2-\gamma_e+\gamma_i)+\varepsilon c_n u_e^2+i\omega(\frac{\gamma_e-1}{\gamma_e+\gamma_i})^{\frac{1}{2}}[1+(\frac{1-\alpha\xi}{\sigma})^2]u_e\}\frac{d\Psi}{d\xi} \qquad (10.4)$$

$$+\{i\omega(\frac{\gamma_e-1}{\gamma_e+\gamma_i})^{\frac{1}{2}}\varepsilon c_n u_e-\omega^2\}\Psi=0.$$

Excepting a few cases, γ_i will be null because no internal duct is present in the beam. The end piece will always be full (not hollow) and rigid, and the boundary condition related to shear at the free end obtained from eq.(6.7) is

$$\{1 + \frac{i\omega\mu\nu}{\mu+\nu|\omega|}\}\frac{d^3\Psi}{d\xi^3}$$

$$+ \{f(\frac{1-\alpha}{\sigma})^2 u_e^2 - \frac{\chi}{3}[\Gamma(2-\gamma_e) + i\omega(\frac{\gamma_e-1}{\gamma_e})^{\frac{1}{2}} fu_e]\}\frac{d\Psi}{d\xi} \qquad (10.5)$$

$$+ \{i\omega(\frac{1-\alpha}{\sigma})^2 (\frac{\gamma_e-1}{\gamma_e})^{\frac{1}{2}} fu_e + \omega^2 \frac{\chi}{3} \frac{1+f(\gamma_e-1)}{\gamma_e}\}\Psi = 0.$$

These equations are basically identical to those derived by Paidoussis [57], apart from the modified expression for damping and new factors premultiplying the velocity to account for the boundary layer. In addition, eq.(10.1) for the internal flow and eq.(10.4) for the external flow are almost identical, except for the addition of three terms related to friction and for the substitution of the internal velocity, v_i, by the external velocity, u_e, or by $u_e(\frac{1-\alpha\xi}{\sigma})$; therefore, we may expect parameters such as Γ, γ_e, μ and ν which appear identically in the two equations to have similar stabilizing or destabilizing effects; however, this similarity may be altered by the boundary conditions which are not the same for internal and external flows if the beams are not supported at both ends - unless the free end is blunt; in the latter case the boundary condition expressed by eq.(10.5) for external flow reduces to $d^3\Psi/d\xi^3=0$ (since χ and, consequently, f vanish), which is then identical to that for internal flow.

5.2.1.1 Gravity

a) Influence of Γ and γ_e on stability.

In §5.1 the values of Γ were found to have a significant effect on the critical internal flow velocities mainly for tubes hanging in air. However, we are now dealing with a surrounding

fluid which is water, and the coefficient of Γ in eq.(10.4) will be small since $\gamma_i \sim 0$ and $\gamma_e \sim 2$ for materials with a specific gravity close to 1. The influence of Γ on the critical velocities for buckling and flutter, which was investigated using the values of γ_e for two commonly used materials, i.e. type B and type E silicon rubber, may be observed in Fig.10. The critical velocities increase with increasing γ and Γ (more flexible beams) and decreasing values of γ_e (heavier beams). Material of type B is heavier than material of type E but it is stiffer; as a result, the regions of instability (buckling) spanning the two critical flow velocities for beams of the same length, shown (for $\varepsilon=20$) between the two arrows, are almost identical; this result is corroborated fairly well by the experimental data.

b) Influence of μ and ν.

Obviously internal damping of a viscous type has no influence on the limits of buckling ($\omega=0$). In the case of flutter, the effect of μ and ν on the critical velocities and frequencies yields similar results to the case of internal flow: as damping increases, the critical velocity at the onset of flutter remains almost unchanged whereas the corresponding frequency of oscillations diminishes rapidly.

This effect is illustrated in Fig.12; in one case the internal damping characteristics of one of the materials used in experiments has been used (rubber type E, $\mu=0.08$, $\nu=0.015$) in the calculations of the eigenfrequencies, whereas in the second case no damping was assumed. The lowest critical velocity which gives flutter varies by less than one percent because of material damping, while the corresponding frequency drops from 6.7 to 4.6; in fact,

for heavy dimensionless damping, such as would apply to very short beams (the value of ν being inversely proportional to ε^2), the critical frequency was found to drop to zero, and flutter gave way to buckling at $u_e=5.6$ - which is the value obtained, independently of internal damping for $\omega=0$. Thus, this critical velocity appears to be almost unaffected even by heavy damping. However, the next critical velocity, which is obtained along the third mode at $u_e=9.15$ with no damping, disappears with damping because the third mode is seen to remain stable. Due to damping, the second and third modes have interchanged roles in the vicinity of $u_e=9$: the second mode which regained stability at $u_e=9.2$ with no damping, remains unstable with damping - although a minimum degree of instability is found to occur in the neighbourhood of $9<u_e<9.5$, close to the critical velocities $u_e=9.15$, $u_e=9.2$. This region corresponds to the transition from second mode to third mode flutter and is difficult to pinpoint experimentally; however, the experiments indicate that it is definitely larger than the short overlap obtained without damping. From a theoretical point of view, it is more convenient to assume no damping and compute two critical velocities, i.e. the points where flutter ends in the second mode and where it starts in the third mode, rather than to consider damping and compute the velocity which corresponds to a minimum negative imaginary part of ω.

c) Influence of ε.

In eq.(10.4) ε is encountered several times, either explicitly in the terms related to friction forces, such as εc_n and εc_t, or implicitly in the calculation of α (which also involves εc_t) and of Γ. The overall effect of ε on the critical velocities for

buckling and flutter has been calculated and compared to the experimental results in Fig.11. The theoretical trend which predicts that the critical velocities should increase slowly with the length appears to be corroborated by the experiments; moreover, the two types of material used for the beams yield similar experimental results within the range of experimental uncertainty.

In summary, from the previous paragraphs we realize that the type of material used in the experiments has little effect on the dimensionless critical velocities, and we may thus compare in the same figure several results obtained with different materials; moreover, from a practical point of view, we may select for each experiment the material which is the most suitable, e.g. in terms of strength or reliability - although in most cases the most important criterion used was low flexural rigidity which enabled us to investigate a larger range of dimensionless flow velocities for the same experimentally available range of dimensional flow velocities.

5.2.1.2 Friction and boundary layer effects.

a) influence of c_n and c_t on the critical velocities.

As eq.(10.4) stands, it would be difficult to evaluate the effects due to skin friction and those due to thickness of the boundary layer separately, because both depend on the same parameter, c_t. For this reason, we resort to the following artifice: since the value of c_n and c_t are equal, we shall replace c_t by c_n when c_t applies to friction, i.e. when it appears in eq.(10.4); then, we shall use c_t exclusively for the calculation of the boundary layer parameters α and σ; in this way, c_n and c_t may be varied

independently. The results are presented in Fig.13. It is seen that the influence of skin friction alone (c_t=0, c_n variable) is smaller than that of the boundary layer thickness alone (c_n=0, c_t variable); and if both are combined (c_n=c_t), the critical velocities for buckling and flutter increase sharply with increasing values of c_n and c_t, especially for the latter. By assuming a smooth beam surface and an average Reynolds number around 2×10^6, a skin friction coefficient $c_t = 8 \times 10^{-3}$ was derived in Appendix G; agreement between experimental and theoretical points corresponding to this value appears to be optimum if the boundary layer is taken into account (dark circle data points); in addition we notice that boundary layer thickness is responsible for approximately a 15% increase in the critical velocities, as illustrated by the brackets in the figure. In the same figure are plotted the critical velocity zones measured by Paidoussis [50] in an experiment where a fine cotton thread was wrapped helically around the beam; the total skin friction coefficient, commonly labelled c_f, has been estimated from standard tables* by assuming a rough regime and an equivalent sand roughness ratio, based on the diameter of the thread, equal to 2×10^3 (indeed, for such a roughness the regime is no longer hydraulically smooth for Reynolds numbers above 10^5); the value thus obtained is $c_f = 7 \times 10^{-3}$. We may not simply use the values $c_n = c_t = 2c_f$ (as derived in Appendix G) to plot this data in Fig.13, because the values of ε do not match: ε=20 for the figure and ε=25 for the tests conducted by Paidoussis. However, as previously noticed, the characteristic parameter for friction and boundary layer effects is εc_t

---

* Schlichting *op. cit.* figure 21.6.

rather than c_t; using his new abscissa, the data could thus be plotted in Fig.13 for $\varepsilon c_t=0.35$. The agreement between experimental and theoretical data is striking. In fact the critical velocities should be adjusted downwards to account for the fact that Paidoussis considered horizontal beams ($\Gamma=0$), whereas we considered vertical beams; however, gravity only accounts for a small amount in the critical velocities, as observed in Fig.10.

b) influence of the boundary layer thickness alone.

Fig.14 shows the three lowest modes of a vertical cantilever preceded by a short coaxial cylindrical support of the same diameter. In one case the boundary layer has been taken into account (with $c_t=8 \times 10^{-3}$ yielding $\alpha=0.1$, $\sigma=1.05$), and in the other case it has not been (with $c_t=0$ yielding $\alpha=0$, $\sigma=1$). It is seen that the two sets of modes are close. Considering pairs of points, one from each set, corresponding to the shortest distance between the two loci; we then note the following:

i) the velocities along the loci which take account of the boundary layer are larger than their counterparts on the other loci;

ii) when positive, i.e. in the case of damped motions, the imaginary parts of the eigenfrequencies are generally larger for the loci which account for the boundary layer, as illustrated by the pairs of points corresponding to the velocities (2, 1.75), (5, 4.5) and (8, 7) in modes 1, 2 and 3 respectively.

In summary, addition of the boundary layer thickness in the theory appears to be equivalent to a reduction of the flow velocity combined with a stabilizing effect.

Unfortunately, the influence of the boundary layer alone could not be assessed experimentally. An attempt was made at boundary layer suction using hollow tubes inserted in small diameter holes drilled in approximately one hundred locations. However, the quantity of fluid which could be removed was too small to obtain a significant reduction of boundary layer thickness (see Appendix G); moreover it was suspected that the small internal counter flow created thereby produced some hydrodynamic damping which probably offset most of the destabilizing effect which might have arisen from suction. Another attempt was made where, rather than trying to reduce boundary layer effects, it was thought that it might be easier to attempt to increase them, e.g. by choosing longer axial supports or by using smaller diameters for the beams (in order to increase the ratio of the boundary layer thickness to the diameter); however, the existing apparatus and equipment was not suited for the fairly major modifications necessitated thereby.

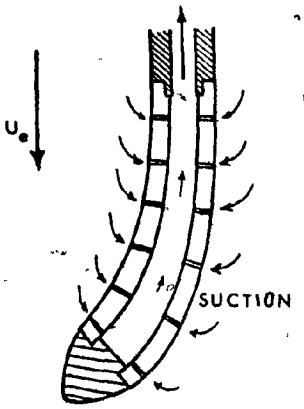

5.2.1.3 Effect of the shape of the tapered end.

This effect is the most critical for stability of cantilevered beams. In Fig.15 are shown the critical velocities for buckling and flutter which were obtained experimentally for two types of cylindrical beams (made of different silicone rubbers); with at least three different end pieces, i.e. χ_e=1.5, 1.0, 0.5; those obtained by Paidoussis [50] for horizontal beams have been

added in the same figure. The experimental data is now compared to the theoretical boundaries of the zones of buckling, and first and second flutter, which were computed (i) with the boundary layer assumptions (full lines) and (ii) without (dotted lines). In agreement with previous work, the beams were found to be stable at any flow velocity if the end piece is almost blunt (no instability up to $u_e \sim 10$ for $\chi_e < 0.5$); if the end piece is more tapered than a hemisphere ($\chi_e > 0.5$) the beams are found to be stable at low flow velocities, then to buckle around $u_e = 3$; as the flow is further increased, flutter is observed, first around $u_e = 6$ with oscillations of a second mode type, then around $u_e = 9$ with oscillations similar to a third mode. The beams usually regain complete stability between buckling and the first flutter, although in some cases there is some overlapping between them which sometimes makes it difficult to decide when one ends and the other begins; in these latter cases the symbol used in Fig.15 to pinpoint the end of the lower instability has been plotted just above the symbol for the start of the higher one. Transition from first to second flutter was found to be accompanied by a marked diminuition of amplitude, without an interval of stability between them.

The consistency among the experimental results and the agreement with the theoretical critical velocities are generally poor for $\chi_e < 1.5$; this is not too surprising because the value of the parameter f in eq.(10.5) has been established for a potential flow over the tapered end with no consideration for flow separation, and also because the experimental critical velocities are difficult to pinpoint, especially for buckling. Nevertheless, the theoretical

predictions are generally better when boundary layer effects are taken into account (c_t=0.008) in the calculations. This may not be clearcut, considering that the results obtained by Paidoussis for flutter fall below the full lines, and closer to the dotted line (c_t=0) for χ_e>1.0. However, this may be due to several factors:

a) our theoretical critical velocities are overestimated with respect to his data because the ratio of the diameter of his test-section to that of the beams was only 4; consequently, a significantly larger virtual mass of the beam should be introduced in the equations of motion by multiplying the terms representing the lift with a factor greater than 1, thus reducing the flow velocities required to reach the critical conditions, and thereby the gap with the experimental data;

b) another similar reason is that we accounted for gravity whereas it was inoperative in his experiments (Γ=0); however, the small de-stabilizing effect not accounted for is balanced by the fact that his beams were slightly longer than ours (ε~23.5 as opposed to 20), thus resulting in relatively more friction and a stabilizing effect (as can be observed in Fig.13 for larger values of εc_t);

c) Paidoussis assumed a flat velocity profile in the test-section and thus measured the average velocity rather than the velocity in the neighbourhood of the beam; for comparison purposes, in our tests the critical velocities would be underestimated by 15% with such an assumption.

For these reasons we may conclude that taking into account the boundary layer improves prediction of the instability thresholds.

5.2.2 Conical beams

Although relatively short, this section accounts for most of the time spent on both theoretical and experimental work. For one thing, the computations required approximately 17 terms in the Fourier series for convergence of the first critical eigenfrequencies when the shape of the conical beam approaches that of a full cone, namely $\alpha_e<-0.8$, as opposed to 10 terms for uniform beams. Also, unforeseen theoretical problems arose when the observed stability of almost conical beams could not be explained with the sole use of potential flow and slender body theories; this is the reason why the new assumptions of §2.3.4 concerning the effect of the boundary layer were developed.

As far as the experiments are concerned, many difficulties arose because we chose to test quasi-conical, i.e. $\alpha_e<-0.5$, rather than quasi-cylindrical beams; as mentioned in §4.4.1, such beams are very sensitive to turbulence-induced subcritical vibrations; as a result, erratic oscillations, up to two diameters in amplitude at the free end, made it difficult to pinpoint the thresholds of instabilities, and even to distinguish between the types of instability.

5.2.2.1 Eigenfrequencies and modal shapes

The complex frequencies of the three lowest modes of a tapered beam having the shape of a full cone truncated in half ($\alpha_e=-0.5$) have been plotted in Fig.16 for dimensionless flow velocities up to 10; the loci are not significantly different from those obtained in Fig.12 for a cylindrical beam of the same length; in both cases mode 1 reaches the Im(ω)- axis, buckling follows and then

stability is regained just as the system loses stability in mode 2 by flutter; similarly, stability is regained in mode 2 and lost in mode 3 by flutter; subsequently, mode 2 reaches the Im(ω)-axis and the system buckles.

For the six critical velocities obtained in Fig.16, the modal shapes of the conical beam have been computed and they are presented in Fig.17. The top three diagrams show buckling and the others flutter; in the latter case the two positions of the beam, obtained from the real and imaginary parts of the standardized solution (derived in Appendix B, section 4), illustrate the (undamped) oscillations at two moments in time, out of phase by a quarter of a period. The diagrams indicate that distinct modes may result in similar modal shapes around the same flow velocities; for instance, the modal shapes of modes 1 and 2 at u_e=4.6 and 4.8, (respectively, upper limit of buckling and lower limit of flutter), have similar features; this similarity may be easier to observe by looking at the (shaded) areas, i.e. those swept by the beam during flutter, and those between deflected position and position at rest in the case of buckling.

5.2.2.2 Influence of ε

a) for constant values of α_e

At a given taper ratio, larger values of ε result in higher theoretical critical velocities; as in the case of cylindrical beams, several factors have stabilizing effects with increasing lengths; gravity is one, and, around α_e=-0.5 and ε=17, it accounts

for approximately a five-percent increase in the threshold for buckling (corresponding to beams cast in material E), but less for higher instabilities; the remaining factors, i.e. friction and boundary layer, are more important and, under similar conditions, yield a fifteen percent increase, independently of the kind of instability.

In Fig.18 both theoretical and experimental critical velocities have been plotted for α_e=-0.5 and -0.6; in addition, the data obtained for α_e=0, in Fig.11, has been reproduced for comparison purposes. For each value of α_e two solid lines indicate the theoretical lower limits of buckling and flutter, respectively, whereas the dotted line indicates the upper limit of buckling. The experimental points have been obtained with beams cast with different materials and different moulds (which, of course, give different taper angles in the diagram). The scatter of the experimental points is such that the influence of ε predicted by the theory cannot be positively verified. Moreover, the short region of stability predicted theoretically between buckling and flutter, and indicated by brackets in the figure, could not be observed any more clearly for conical than for cylindrical beams. The kind of agreement obtained in Fig.18 between theoretical and experimental results, and the poor consistency among the experimental data is typical of all the experiments conducted with conical beams. One can only say that the variations in the theoretical critical velocities are relatively small over the experimental range of lengths, as compared to the experimental uncertainties.

b) for constant taper angles.

In Fig.19, the theoretical and experimental critical velocities and frequencies obtained with a conical beam truncated progressively shorter, have been presented; the taper angle of the cone is β_e=0.035 rad, its (full) length ratio is ε=27.5, and the relation thereby obtained between α_e and ε is ε=-27.5 α_e. Up to the maximum (dimensionless) experimental flow velocity the first four modes have been computed and investigated for instabilities. Buckling is obtained in mode 1, then flutter for each of the other modes, with very little overlap between instabilities; additional buckling was predicted to occur simultaneously with the flutter of the odd numbered modes; for instance, buckling (in mode 3) is superimposed on flutter in mode 3. This sequence of instabilities was observed experimentally and the modal shapes observed are very similar to those plotted in Fig.17. As far as frequencies are concerned, the experimental and theoretical results are presented in the right-hand-side diagram of Fig.19; the arrows match those in the left-hand-side diagram and, therefore, the experimental points which have been measured at the lower end of the instability regions should be compared with the portion of the contour aiming rightwards. Generally speaking, both critical velocities and frequencies are underestimated by the theory and the quantitative agreement deteriorates further as the truncation ratio, $-\alpha_e$, increases towards unity (full cone).

As previously mentioned, for very tapered beams the critical velocities and modal shapes are difficult to assess and the frequencies are too irregular to be counted, as indicated in Fig.19 by short vertical dotted lines. Such difficulties are even

more serious for the third instability region where buckling and flutter occur simultaneously and combine in fast, erratic motions.

5.2.2.3 Influence of α_e

We now investigate the effect of α_e on the critical velocities assuming the lengths of the beams constant. The theoretical results have been calculated for ε=17 and plotted in Fig.20; the unstable regions obtained coincide with those of Fig.19 for α_e=-0.63 (which yields ε=17 in Fig.19) but otherwise do not differ significantly; in addition, it is recalled from Fig.18 that the variations of the theoretical critical velocities within the experimental range of length ratios are less than ten percent with respect to the value for ε=17. Because of the above, we plotted in Fig.20 all the experimental data which was obtained for $11<\varepsilon<21$, rather than only the few points corresponding exactly (ε=17) to the theoretical curves. However, in order to notice any possible effect of length, two types of symbols have been used for the experimental data points: for a specific material the symbol is black (full) if the taper angle is relatively small, i.e. $\beta_e<0.03$, and hollow (open) for $\beta_e>0.035$; hence, conical beams in the former category are at least twenty percent longer than the others, for the same value of α_e. For clarity, only the points for the experimental lower limit of each instability zone have been plotted in the figure; as a matter of fact, the upper limit is generally concealed by the next instability.

The conclusions to be derived from Fig.20 are similar to those of Fig.19. It may be added that the four lowest regions of

instability are quite distinct, yet, the quantitative agreement with the theory is generally poor; besides, no marked difference between the longer and shorter beams is to be noticed. Nevertheless, the patterns of the experimental instability zones do correspond to the theoretical ones.

5.2.2.4 Influence of the boundary layer

In the case of a cylindrical beam, with $\varepsilon=20$, the boundary layer thickness was found to be responsible for a fifteen percent increase of the theoretical critical velocities. For conical beams of the same length, the effect of the boundary layer is expected to increase for larger taper angles, because its thickness is correspondingly larger relative to the diameter for beams with larger taper angles; as a result, the reduction in lift exerted on such beams would be more important. This is illustrated in Fig.21 where the same instability regions are plotted, computed either with or without the boundary layer. The dotted lines illustrate the case of no boundary layer ($c_t=0$) and the regions which have been calculated are the three lowest buckling areas and the first flutter (the buckling zones are as convenient as the flutter zones for assessing the boundary layer effect but several times cheaper to compute). In addition we reproduced the experimental data of Fig.20. The shaded areas indicate the sequence of theoretical velocity ranges for buckling and flutter around $\alpha_e=-0.25$ and -0.5, respectively, and the direction of shading differentiates between the two sets of theoretical curves, i.e. with or without boundary layer.

It is clear that, if the boundary layer is neglected, theory predicts that almost fully conical beams may become unstable;

this is contrary to our observations and agrees with theory when boundary-layer effects are included. Moreover, by accounting for the boundary layer, higher critical velocities are predicted; since the experimental velocities are generally above the theoretical ones, the introduction of boundary layer effects has thus improved the prediction of instability thresholds. As a matter of fact, this improvement is more significant for conical than for quasi-cylindrical beams.

5.2.2.5 Influence of the tapered end

Most of the theoretical results derived in the previous sections were obtained with χ_e=1.5, (f=0.9), i.e. for an elongated tapered end (the value of f approaches unity for χ_e>2). However, in Figs. 19 and 20, the results for χ_e=0.75 (f~0.7) have been drawn in dotted lines; it is seen in these figures that the critical velocity zones corresponding to χ_e=0.75 are included within the zones calculated for χ_e=1.5; this is supported by the experimental results. However, with respect to the critical frequencies, there is little evidence among the experimental data in Fig.19 that beams provided with a shorter end piece do flutter at higher frequencies, as suggested by the theoretical results.

In Fig.22 the effect of the shape of the tapered end has been investigated on the boundaries of buckling for several taper ratios; the theoretical buckling zone shrinks rapidly as α_e decreases, and disappears for α_e<-0.75; besides, the smallest value of χ_e which yields buckling is almost independent of α_e in the interval $0>\alpha_e>-0.6$ and approximately equal to χ_e=0.5. For illustration purposes, the experimental data has been gathered from tests conducted

with half cones (α_e=-0.5) of equal length (ε=13.75); the shapes of the three tapered ends to be tested were actually more round than the theoretical conical elements, drawn in the bottom of Fig. 22, and used to calculate the parameter f. Given the fact that the present theory underestimates critical flow velocities, agreement between experimental and theoretical data with respect to the stabilizing effect of shorter ends appears to be reasonably good.

Similar comparisons were attempted for more conical beams, especially around the value α_e=-0.65, because no buckling could be observed further along, i.e. for α_e=-0.7, even for well streamlined end pieces; unfortunately the experimental data was inaccurate and generally too far above the theoretical predictions to yield a meaningful comparison.

5.3 CASES OF SIMULTANEOUS INTERNAL AND EXTERNAL FLOWS

In this sub-chapter we shall consider tubular beams subject to both internal and external axial flows, the velocity of each flow being independent of the other. Although the theory allows for different fluids for the two flows, the experiments were conducted with one fluid only, namely water. In addition, only cylindrical tubular beams are considered here; the beams are vertical and can be either cantilevered; i.e. clamped-free, or clamped at both ends; in the latter case the downstream end is free to slide axially during the tests, and no external tension is applied. The downstream end is usually blunt, except for cantilevered tubular beams, in which case as illustrated in Fig.2, hollow (tubular) tapered ends will be considered.

The differential equation of motion obtained from eq.(6.8) may be written in the form

$$\{1 + \frac{i\omega\mu\nu}{\mu+\nu|\omega|}\} \frac{d^4\Psi}{d\xi^4}$$

$$+ \{(\frac{1-\alpha\xi}{\sigma})^2 u_e^2 + v_i^2 - \tfrac{1}{2}C_{fe}u_e^2 - \tfrac{1}{2}C_{fi}v_i^2 - \tfrac{1}{2}C_{fx}u_e v_i - \chi\Gamma[2-\gamma_e)s_e+\gamma_i]$$

$$- [\Gamma(2-\gamma_e+\gamma_i) + \varepsilon c_t u_e^2](1-\xi)\} \frac{d^2\Psi}{d\xi^2} \qquad (11.1)$$

$$+ \{\Gamma(2-\gamma_e+\gamma_i) + \varepsilon c_n u_e^2 + i\omega[2(\frac{\delta^2+\gamma_i}{\gamma_e+\gamma_i})^{\frac{1}{2}} v_i + [1 + (\frac{1-\alpha\xi}{\sigma})^2](\frac{\gamma_e-1}{\gamma_e+\gamma_i})^{\frac{1}{2}} u_e]\} \frac{d\Psi}{d\xi}$$

$$+ \{i\omega(\frac{\gamma_e-1}{\gamma_e+\gamma_i})^{\frac{1}{2}} \varepsilon c_n u_e - \omega^2\}\Psi = 0,$$

and, in the case of cantilevered beams, the boundary conditions at $\xi=1$ are

$$\frac{d^2\psi}{d\xi^2} = 0$$

and

$$\{1 + \frac{i\omega\mu\nu}{\mu+\nu|\omega|}\} \frac{d^3\psi}{d\xi^3}$$

$$+ \{f(1-\delta^2)(\frac{1-\alpha}{\sigma})^2 u_e^2 - \chi\Gamma[(2-\gamma_e)s_e+\gamma_i]$$

$$- i\omega\chi[2(\frac{\delta^2+\gamma_i}{\gamma_e+\gamma_i})^{\frac{1}{2}} v_i + f(\frac{\gamma_e-1}{\gamma_e+\gamma_i})^{\frac{1}{2}} (s_e+\delta^2(\frac{1-\alpha}{\sigma})^2)u_e]\} \frac{d\psi}{d\xi} \qquad (11.2)$$

$$+ \{i\omega f(\frac{\gamma_e-1}{\gamma_e+\gamma_i})^{\frac{1}{2}} (1-\delta^2)(\frac{1-\alpha}{\sigma})^2 u_e + \omega^2\chi \frac{(1+f\gamma_e-f)s_e+\gamma_i}{\gamma_e+\gamma_i}\} = 0 ,$$

where $s_e = \frac{1+\delta+\delta^2}{3}$ and $f = \frac{4\varepsilon^2\chi^2}{4\varepsilon^2\chi^2+(1-\delta)^2}$.

5.3.1 Theoretical results

We shall now proceed to investigate eq.(11.1) from a simplified theoretical point of view. For this purpose, we shall make a few assumptions based on the theoretical and experimental results obtained in the previous sections which will simplify the expression of the differential equation; however, some of these assumptions will be abandoned later on, in order to obtain a proper comparison with the experimental results.

First, the external and internal fluids will be assumed identical, i.e. $\gamma_i = -\delta^2[2-\gamma_e]$; then, the gravity effect will be assumed negligible compared to the hydrodynamic forces, as would

be the case for very stiff or horizontal beams ($\Gamma<<1$), or beams with density close to that of the fluid ($\gamma_e \sim 2$); the skin friction forces will also be assumed relatively small ($\varepsilon c_n<<1$) as would be the case for rather short beams and large Reynolds numbers; moreover, assuming short supports, the boundary layer thickness will be neglected ($\varepsilon_o c_t$, $\varepsilon c_t<<1$). Finally, for the sake of clarity, it will be convenient to neglect the base drag terms and internal damping.

Eq. (11.1) has now been reduced to the following very simple form

$$\frac{d^4\psi}{d\xi^4} + (u_e^2+v_i^2)\frac{d^2\psi}{d\xi^2} + 2i\omega\left(\frac{\gamma_e-1}{\gamma_e+\gamma_i}\right)^{\frac{1}{2}}(\delta v_i+u_e)\frac{d\psi}{d\xi} - \omega^2\psi = 0. \quad (11.3)$$

Incidentally, judging from the values of the parameters neglected, this equation is not an unreasonable approximation within the framework of the experimental data; in fact, the largest discrepancy probably arises from omitting the boundary layer which accounts for approximately fifteen percent of the magnitude of the critical velocities (as for $\varepsilon=2\varepsilon_o=20$ and $\varepsilon c_t=0.16$).

5.3.1.1 Equivalent single flow

It appears that eq.(11.3) is very similar to the equation of a beam subject to a single flow; in fact, if

$$u_e^2 + v_i^2 = (u_e+\delta v_i)^2,$$

which occurs for

$$\frac{u_e}{v_i} = \frac{1-\delta^2}{2\delta},$$

the equation is that of the beam subject solely to an external flow of velocity $u_e + \delta v_i$; similarly, if

$$u_e^2 + v_i^2 = (v_i + \frac{u_e}{\delta})^2, \quad \text{i.e. for} \quad \frac{u_e}{v_i} = -\frac{2\delta}{1-\delta^2}$$

then, the equation is equivalent to that obtained with an internal flow alone, of velocity $v_i + u_e/\delta$; in this latter case it ought to be noted that the internal and external flows are in opposite directions.

When the beams are supported at both ends, or when the downstream end is free and blunt, the boundary conditions are independent of the flows. For a free tapered end, when neglecting gravity and boundary layer, and assuming identical internal and external fluids, the following boundary condition is obtained from eq.(11.2):

$$\frac{d^3\psi}{d\xi^3} + \{f(1-\delta^2)u_e^2 - i\omega\chi(\frac{\gamma_e-1}{\gamma_e-\gamma_i})^{\frac{1}{2}}[f(s_e+\delta^2)u_e+2\delta v_i]\}\frac{d\psi}{d\xi}$$
$$+ \{i\omega f(\frac{\gamma_e-1}{\gamma_e+\gamma_i})^{\frac{1}{2}}(1-\delta^2)u_e + \omega^2\chi\frac{(1-f\gamma_e-f)s_e-\gamma_i}{\gamma_e+\gamma_i}\}\psi = 0 . \qquad (11.4)$$

Generally, neither of the two single flows previously calculated would yield such a condition; nevertheless, provided that δv_i is small compared to u_e, the boundary condition obtained with the single external flow of velocity

$$V = u_e + \delta v_i,$$

will be close*, and better than with a single internal flow (i.e.

* In eq.(11.4) set $v_i = 0$ and replace u_e by V.

$u_e=0$ and $v_i=V$). Consequently, whenever possible, attempts will be made to compare the case of simultaneous flows to that of a single external flow.

5.3.1.2 Equivalent flow conditions

We now consider the general case; let

$$U^2 = u_e^2 + v_i^2$$

$$V = u_e + \delta v_i, \qquad \text{and } U \neq V.$$

U and V are the characteristic parameters of the flow velocities in eq.(11.3); provided that the boundary conditions are independent of the flow velocities (or if they depend on U and V only), for any combination of velocities (u_e,v_i), there exists another, (u_e',v_i'), which yields the same characteristic parameters for the same equation of motion.

Those velocities are such that

$$u_e^2 + v_i^2 = u_e'^2 + v_i'^2 ,$$

$$u_e + v_i = u_e' + \delta v_i' ;$$

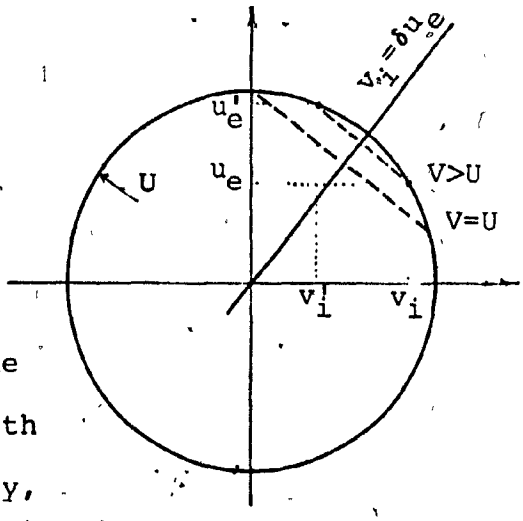

hence, as illustrated in the diagram, the point (u_e',v_i') is symmetric to (u_e,v_i) with respect to the line $v_i= u_e$. Incidentally, if V<U negative internal flow velocities are obtained, which are perfectly permissible solutions.

Let us now consider small increases of the flow velocities in eq.(11.3); the incremental changes of the characteristic terms are

$$2U\,dU = 2u_e du_e + 2v_i dv_i \ ,$$

$$dV = du_e + \delta dv_i \ .$$

It is possible to have dU=dV=0 if

$$du_e = -\delta dv_i \quad \text{and} \quad v_i = u_e \ .$$

This illustrates the fact that, for specific flow conditions, the effect resulting from increasing one flow may be exactly counteracted by decreasing the other.

It should now be clear to the reader that the stability of tubular beams subject to both internal and external flow is not directly obtainable from stability considerations of the beam subject to each flow separately. Generally, it is foreseen that the effect of the combination of the two flows will be similar to that of an external flow with a velocity greater than that of each single flow, but less than their sum.

5.3.1.3 Buckling

From eq.(11.3) the critical flow velocities for buckling may be calculated easily; upon setting $\omega=0$, the equation reduces to the following expression

$$\frac{d^4\psi}{d\xi^4} + U^2 \frac{d^2\psi}{d\xi^2} = 0 \ , \qquad \text{with} \qquad U^2 = u_e^2 + v_i^2 \ ,$$

which describes the well-known Euler buckling problem for a beam subject to an axial compressive load U^2. The general solution of this differential equation is

$$\Psi = a + b\xi + c \cos U\xi + d \sin U\xi$$

where U and the constants a,b,c,d depend upon the boundary conditions. Now

a) For clamped-clamped beams we have $\Psi(0)=\Psi'(0)=\Psi(1)=\Psi'(1)=0$ and non-trivial values of a,b,c,d require that

$$U(2 \cos U + U \sin U - 2) = 0.$$

The root U=0 is irrelevant and the following critical values are obtained

$$U = 2\pi,\ 8.9868,\ 4\pi,\ 15.4505,\ 6\pi,\ 21.8082,\ 8\pi,\ \ldots$$

which yield the circular critical boundaries with respect to u_e and v_i illustrated in the right-hand side of Fig.23; every second root being approximately equal to $(2k+1)\pi-4/(2k+1)\pi$, the consecutive boundaries become equivalent as k increases.

Incidentally, should one of the extremities be pinned instead of clamped the necessary condition becomes, tan U-U=0, which allows for the following roots: U=4.49, 7.73, 10.9, 14.1,... $(2k+1)\frac{\pi}{2}$.

b) For cantilevered beams we have $\Psi(0)=\Psi'(0)=\Psi''(1)=0$, and the fourth condition, obtained from eq.(11.4) is

$$\Psi'''(1) + f(1-\delta^2)u_e^2\Psi'(1) = 0\ ;$$

The condition for compatibility is now the following:

$$\frac{U^2}{u_e^2} = (1-\cos U) f(1-\delta^2) \ .$$

Since the left-hand side is greater than unity (except if $v_i=0$), and since $0<1-\cos U<2$, no critical velocities can be obtained if

$$f(1-\delta^2) < \frac{1}{2} \ ;$$

alternatively, values of $(v_i/u_e)^2$ such that

$$(\frac{v_i}{u_e})^2 < 2f(1-\delta^2) - 1$$

yield two roots of U in each 2π interval, as illustrated below; the largest interval between the two roots is obtained for $v_i=0$ and the maximum ratio between v_i and u_e is obtained for $U=(2k+1)\pi$ i.e. for

$$u_e^2 = \frac{(2k+1)^2\pi^2}{2f(1-\delta^2)} \ , \ v_i^2 = [2f(1-\delta^2)-1] \ u_e^2$$

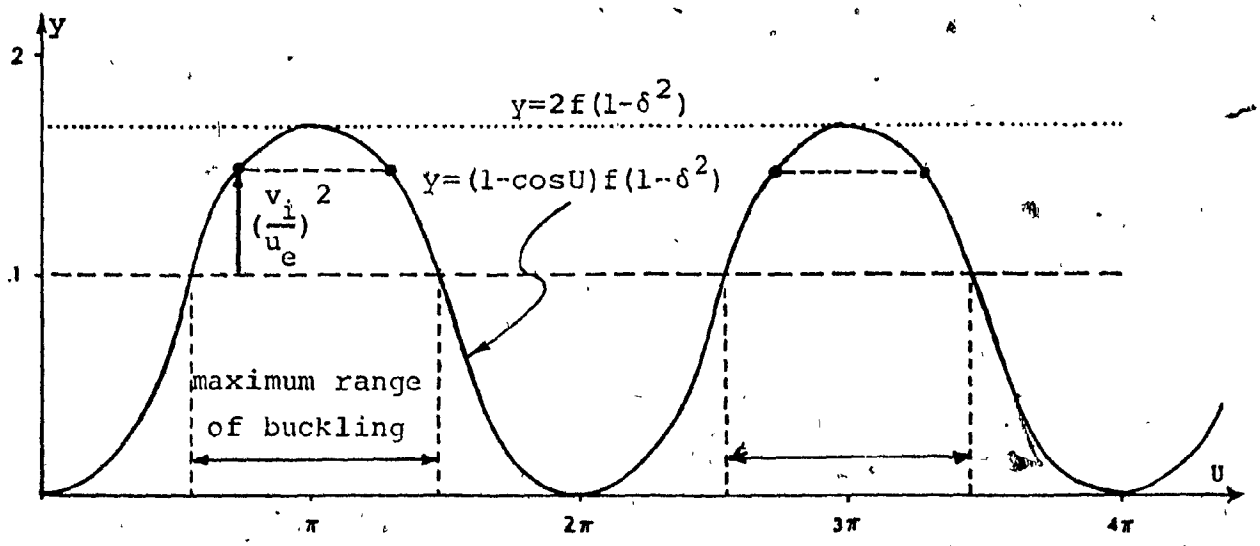

The boundaries of the three lowest regions of buckling have been drawn in Fig.23; the regions are symmetrically distributed around a circular center line located at $U=(2k+1)\pi$. Four values of the term $f(1-\delta^2)$ have been investigated; the largest possible buckling regions are obtained when $f(1-\delta^2)\to 1$, whereas they shrink to points $[v_i=0,\ u_e=(2k+1)\pi, k=0,1,\ldots]$ for $f(1-\delta^2)=0.5$.

Before proceeding to the experimental results let us recall that knowledge of the limits of buckling, as in Fig.23, is of limited use because one cannot always tell *a priori* which side of the limit corresponds to an unstable region, e.g., the two diagrams below illustrate cases where $\omega=0$ for $U=2$ and $U=3$, and where buckling is obtained for $2<U<3$, yet, in fig.a buckling stops when $U>3$ whereas it does not in fig.b.

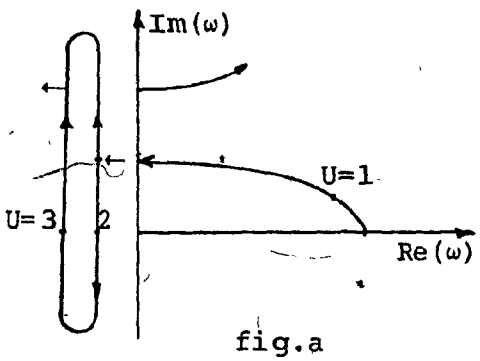

fig.a

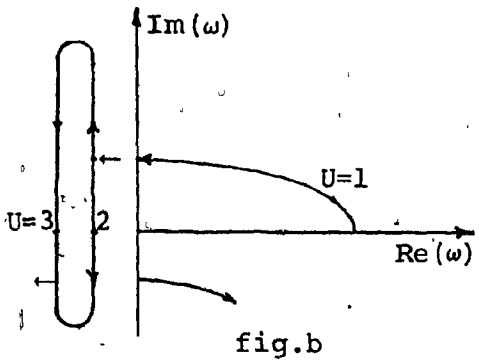

fig.b

Nevertheless, this section has provided a quick insight into the periodicity of the buckling instability with respect to the absolute velocity $U=(u_e^2+v_i^2)^{\frac{1}{2}}$. In addition, it provides a simple check of the stability regions computed by Curioni and Cesari [64] with additional information on the unstable areas, especially in the case of cantilevered beams where the authors apparently missed the importance of the shape of the free end.

5.3.1.4 Flutter

Clearly the limits of flutter could be obtained in a similar manner; one first needs to solve the fourth-order characteristic polynomial of eq.(11.3) for a general solution of the form

$$\Psi(\xi) = \sum_{n=1}^{n=4} a_n e^{\lambda_n \xi};$$

then, in order to satisfy the boundary conditions, a general relation between ω, u_e and v_i and parameters such as $f, \chi, \gamma, \gamma_e$, and γ_i will be obtained. The threshold of instability by flutter is obtained either when ω is purely real or when a frequency locus leaves the negative Im(ω)-axis, as shown on the previous page in fig.b; hence, the equation governing the critical velocities is obtained either by equating the imaginary part of ω to zero or by looking for double purely imaginary (negative) roots in ω. Unfortunately, in contrast to the case of buckling, the analytical relation between u_e and v_i is intractable by hand; therefore, it is not worth devoting much more attention to this, since in the next section the theoretical limits of flutter (and buckling) will be computed from eq.(11.1) directly.

However, we shall take this opportunity to show frequency diagrams in the case of clamped-clamped beams. The loci plotted in Fig.24 have been computed from eq.(11.3) for either internal or external flow; they are presented in quadrant IV (see §3.2) because all quadrants are symmetric in this case; in addition to the symmetry with respect to the Im(ω)-axis, symmetry around the origin

arises because the differential equation and the boundary conditions remain identical if the direction of the flow and the sign of ω are reversed simultaneously. Except for coupled-mode flutter, the frequencies are either real or purely imaginary; for the sake of clarity the loci that actually lie on the axes have been drawn slightly off the axes but parallel to them. It is noticed that in one case the beam regains stability after first-mode buckling, before the onset of flutter ($v_i=0$, $8.99<u_e<9.3$), whereas it does not in the other case; such behaviour is not specific to the type of flow, i.e. whether internal or external, but depends only upon the values of γ_e, γ_i and δ.

5.3.2 Comparison between experimental and theoretical results

5.3.2.1 Clamped-clamped tubular beams.

Two beams of equal length were cast with different rubbers. For the stiffer beam (rubber type B), the maximum available flow velocity in the apparatus only allowed for the first instability to be observed, namely buckling; with the other beam (rubber type E), flutter could be reached for a range of combinations of internal and external flow velocities close to their respective maxima.

In Fig.25 experimental and theoretical critical velocities have been plotted. The theoretical boundaries of instability are close to those obtained in Fig.23 where several effects had not been accounted for; as a matter of fact, the effects of the density and stiffness of the material of the beams on stability were found

to remain very small provided that the eigenfrequencies remain small. As observed from the figure, experimental and theoretical results are approximately twenty-five percent apart; moreover, the narrow region of stability predicted above buckling, provided that $u_e>3$ (upper left part of the figure) could hardly be noticed in the experiments; instead, close to the upper limit of buckling, an almost standing wave which resembled a natural second mode replaced the first-mode-like buckling; it appeared to move downwards and gain speed as the internal flow was further increased, and finally disappeared as flutter developed. To some extent such a behaviour was not expected along this portion of the contour, but rather along the portion out of reach of our tests, which corresponds to small external flows ($u_e>3$) and very large internal flows; in this latter case, the two unstable regions are adjacent but do not overlap; as can be seen from the lower diagram of Fig. 24 in a similar case, the transition from buckling to flutter is a continuous process which involves combined modes on the $\mathrm{Im}(\omega)$-axis.

The discrepancy between experimental and theoretical results is probably due to several reasons. It is unlikely to be due to the few theoretical approximations made in accounting for the forces exerted on the beams, as the discrepancies resulting thereby are likely to be small, good agreement having generally been obtained for other cylindrical beams, especially for cantilevers conveying flow. It thus appears that the most significant errors likely arise from the physical boundary conditions; indeed, at the downstream extremity of the beams the contact with the support was loose enough to let the beam slide axially but not

enough to constitute a perfect (lateral) clamp; therefore, the conditions of a partially pinned and partially clamped support prevailed. In addition, large deflections of the beam rendered the end condition closer to a pinned one, because the beam almost slipped off its support, the element in contact becoming too small. As a matter of interest it was found that the experimental data lies in between the theoretical results obtained for clamped-clamped and clamped-pinned boundary conditions: as from §5.3.1.3.a, the lowest critical velocity in the latter case is approximately thirty percent lower (4.49 as opposed to 6.28). However, the buckling region is larger than expected, and flutter does not occur below the theoretical predictions for clamped-clamped beams. Such a result is all the more surprising when one considers that the actual length of the beam between - supports increased by roughly five percent because of the deflections involved; thus one would expect the critical velocities to decrease by approximately the same amount. On the other hand, since the beam never regained stability once buckling first developed, the important non-linear effects introduced by large deflections may possibly have extended the buckling region.

5.3.3.2 Cantilevered tubular beams

All the tubular beams tested in this section had the same overall length ($\varepsilon+\chi_e=20$); some had a blunt base ($\chi_e=0$) while the others were smoothly tapered ($\chi_e=1$). As in the previous section, two materials were used for the beams (rubber type B or E). The experimental and theoretical combinations of critical velocities have been plotted in Figs. 26 and 27.

In Fig.26, beams with blunt bases are considered. Stability prevails for small internal flow velocities, irrespectively of the external flow. Although the theory predicts that the densities and stiffnesses of the two materials should not have a large influence on the critical velocities, a significant difference is observed in the experimental data. However, it is believed that the discrepancy between the results for the two beams could be reduced significantly by accounting for internal damping, because the net effect of damping is relatively more important for the stiffer beam (silicon rubber type B) due to its higher real frequencies of flutter. Nevertheless, the general agreement between both predicted and experimental velocities and frequencies is fairly good.

As opposed to the case of clamped-clamped beams, it should be noticed that the roles of the internal and external flows are quite asymmetric: along the critical boundary a small increase of internal flow will always precipitate flutter whereas an increase of the external flow velocity will either stabilize the beam when $u_e<3$, or have little effect when $u_e>3$. Comparison between Figs. 25 and 26 illustrates the critical effect of the boundary conditions on stability: it may seem paradoxical that the same differential equation combined with two sets of boundary conditions which are different yet independent of the flow velocities (for blunt bases in both cases) result in such dissimilar boundaries of stability. However, one must realize that forces specific to the external flow, such as tangential friction forces and base drag (which is almost

independent of the internal flow), act differently when the beam is clamped-clamped or clamped-free; in the first case they yield steady axial tension, whereas in the second case they act as follower forces.

In Fig.27 the boundaries of stability for tubular beams with tapered ends have been plotted. A destabilizing effect of the external flow is now obtained theoretically and experimentally. For small internal flow velocities, as the external flow is increased, the beam first buckles, then regains stability for a small range of velocities before fluttering; subsequently, buckling is super-imposed on flutter at regular intervals and flutter may switch to higher modes. It is of interest to note that the two buckling regions obtained in Fig.27 are similar to those predicted in Fig. 23 for a value of $f(1-\delta^2)$ approximately equal to 0.7 ($\delta=0.5, f=\frac{16}{17}$).

As previously observed, the characteristics of the beams cast with different materials cause the experimental data to diverge at high frequencies of oscillations; for buckling and flutter with slow oscillations, the experimental results obtained with the two beams may be considered to be reasonably close, considering that the tapered shapes of the ends of the two beams could not be ground exactly identical.

Lastly, let us observe two interesting features of Fig. 27. First, the external and internal flows have almost symmetric effects on flutter in the sense that the unstable areas (except for buckling) are almost symmetric with respect to the diagonal $u_e=v_i$. Finally, it is the first time that we encounter stability when combining internal and external flows which, on their own

(i.e. at the same individual flow velocities), would destabilize the beam; e.g. flutter which occurs at $v_i=5$ for $u_e=0$ can be postponed until $v_i=8$ with a small external flow around $u_e=3$ and similarly we may reach $u_e=9$ with $v_i=4$, whereas buckling first develops around $u_e=2$ when $v_i=0$. It is of interest to recall that the maximum values of the flow velocities (internal or external) at which a beam clamped at both extremities could be stable were smaller than those found here for cantilevers and approximately equal to $v_i=6$ and $u_e=8$, as indicated in Fig.25 - contrary to intuitive expectation.

6. CONCLUSIONS

6.1 GENERAL CONCLUSIONS

A mathematical model was developed in this thesis to account for the dynamics of slender tubular beams of not necessarily uniform cross-section, subjected simultaneously to internal and external axial flow - the two flows being independent of each other and the fluids involved incompressible.

The derivation of the linearized equations of motion is perhaps the most careful done to date, and the equations obtained are the most general currently available. Thus, most of the assumptions usually made without proof have been carefully tested, and a number of effects not usually taken into account have been incorporated for the first time. Perhaps the most important of these is associated with the boundary layer of the external flow.

It is recalled that one of the original aims of the work described in this thesis was, what was hoped to be, the straightforward extension of the theory for uniform cylindrical beams in axial flow to slender conical beams; it was found that the predictions obtained from such a theory were in complete disagreement with experimental observations. This eventually led to the realization that the source of the problem was the complete neglect of boundary-layer effects, which are more significant for conical beams, than for cylindrical ones, as the boundary-layers are thicker in relation to the beam diameter. In due course some corrections were introduced to the lift as predicted by slender-body theory, to take

boundary-layer effects into account approximately. In essence, the following procedure was adopted, applicable to all cases where the boundary-layer displacement thickness is not negligibly small (as compared to the local diameter). In a first step, the single potential cross-flow which arises in the straightforward application of slender-body theory to the problem at hand is replaced by two superimposed potential flows: one due to lateral motion of the beam alone, and the other representing the flow about an inclined body of cross-sectional area augmented by the displacement thickness. In the second step, instead of the actual mean flow velocity, a reduced flow velocity (related to the relative boundary-layer thickness) is introduced to account for the insulating effect on the beam from the mean flow exerted by the boundary layer. The results of these corrections have been fairly successful, as discussed in the main text of the thesis, and reiterated a little later here.

Among other effects taken into account are those of gravity (in the case of vertical systems) and of internal dissipation in the material of the beam, and the incorporation of a base drag which may be determined rather than guessed. However, the main point is that the theoretical model derived here can deal with tubular beams of non-uniform internal shape and/or external shape - although they must be axisymmetric and changes in the cross-sectional area cannot be abrupt - and at the same time deal with simultaneous internal and external flow.

A new method of solution was developed. It is a matrix

method, which may be viewed as an extension of the Galerkin method. The comparison functions involve Fourier series. One advantage of the method is that one need not determine new comparison functions when the boundary conditions are changed, because the same kind of Fourier series is used irrespectively. The method was tested in solving dynamical problems of a fairly general type and was found to be very powerful - and economical - not only in determining the low modes of the system, but also the higher modes of fairly complex systems without loss of efficiency. Some useful work has also been done with the aid of the perturbation method for determing the eigenvalues of the problem when the flow velocities are small; these eigenvalues may then be used as initial values for the calculation of the free vibration characteristics (eigenvalues and eigenfunctions) with increasing flow. Incidentally, for the first time, these calculations show conclusively what was heretofore taken as intuitively evident, i.e. that the stability of the system may be assessed by determining the characteristics of only the lower few modes of the system.

The validity of the theoretical model was tested by experiments in a water tunnel. Specifically the model was tested for three distinct classes of systems. The first class involved cantilevered beams of conical or cylindrical external shape and a conical internal conduit, conveying fluid. The second class involved externally conical cantilevered beams in axial (external) flow. The third class involved cantilevered and clamped-clamped cylindrical tubular beams subjected to internal and external flow simultaneously.

Internal flow cases

In the case of the first class of systems, involving a convergent internal conduit, it was found that they behave very much like similar beams with a uniform (cylindrical) internal conduit. Thus, the only type of instability encountered (for cantilevered systems) is flutter. It was found that the critical flow velocity depends on the flexural rigidity of the sytem and the flow velocity at the free end, rather than on the actual shape of the conical conduit. Consequently, if the flexural rigidity does not depend significantly on the internal diameter (i.e. for relatively thick tubes with a cylindrical external form), it is possible to assess stability by assuming that the tubular beam is essentially internally uniform, with a diameter equal to the diameter at the free end. Thus, for externally cylindrical beams with a conical conduit, quick estimates of the lowest critical flow velocity may be obtained in this way, since the case of cylindrical pipes has been extensively treated. Incidentally, the same conclusions should hold for tubular beams supported at both ends; in fact, buckling being the lowest type of instability in such cases, the estimates of the critical velocities would probably be even more accurate than for cantilevered beams, since the similarity of the equations of motion for conical and cylindrical internal conduits becomes closer when time derivations are eliminated ($\omega=0$).

Experiments conducted on several tubular beams with conical internal conduits, conveying fluid and hanging in air or

in water corroborated the theoretical predictions. Clearly, therefore, the theoretical assumptions made in formulating the dynamical effect of the internal flow are reasonable (e.g., that the influence of the internal non-uniform flow velocity distribution on the dynamics of the system is of secondary importance). Indeed, agreement between theory and experiment in the critical flow velocity is within 5%, which must be judged most satisfactory.

External flow cases

As was mentioned at the beginning of this section, it was found necessary to introduce a number of modifications to the theory - relating to the boundary layer - before the theoretically predicted behaviour began to resemble the observed behaviour. When boundary-layer effects are taken into account - even when considering uniform cylinders - the critical flow velocities become higher. As a rule of thumb, it may be said that the relative increase of the lowest critical flow velocity is close to the average ratio of the boundary-layer displacement thickness to the radius along the beam. However, if this ratio becomes too large, as in the case of almost fully conical (rather than truncated conical) beams, it is possible that no critical flow velocity may be found - as the system becomes unconditionally stable.

The above statement anticipates some further comments pertinent to the stability of conical cantilevered beams in axial flow. Contrary to intuitive expectation, a conical beam of diameter D at its supported end first loses stability by buckling at a *higher* flow velocity than a cylindrical beam of diameter D, the

same length and similar free-end shape, despite the fact that the conical beam is more flexible. Moreover, for nearly complete cones (as opposed to truncated cones with an ogival free end) the system does not lose stability at all. Without boundary-layer considerations this last result would have appeared very curious indeed, since a full conical shape, in terms of slender body theory, represents a more streamlined form than just a tapered "end" - which accordingly should be least stable. Now in terms of the higher-mode instabilities - again excepting nearly fully conical beams, which are unconditionally stable - a first region of flutter supersedes buckling at flow velocities which are almost independent of the taper ratio; higher mode flutter occurs at higher flow velocities, but not as high as for cylindrical beams. Thus the net effect is to compress the instabilities into a smaller flow velocity range, as compared to cylindrical beams.

Among the parameters which most critically affect stability is the shape of the free downstream end. Linearly tapering beams ranging from cylinders (α_e=0) to half cones (α_e=-0.5) only buckle if the downstream end is no blunter than a hemisphere; elongated end shapes of increasing fineness are required for more tapered beams to buckle, until the taper ratio reaches a critical value ($\alpha_e \approx -0.75$), beyond which, even with a very streamlined end shape, the beam cannot become unstable.

The main dynamical characteristics of conical beams in axial flow predicted by theory were corroborated by the experiments, qualitatively at least. The critical flow velocities

are still found to be generally higher than predicted, although this gap has already been significantly reduced by introducing the boundary layer corrections. It should be mentioned that the experimental data exhibits a certain lack of consistency; it is believed that this is due partly to undetected imperfections in the beams and partly, and perhaps most importantly, because the free ends were not ground to identical standard shapes.

A noteworthy observation, from the practical point of view, is that, although nearly-conical cantilevered beams experience neither buckling nor oscillatory instabilities, they are very susceptible to so-called sub-critical vibrations, i.e. vibrations induced by turbulence and other departures from ideal flow conditions at flow velocities below the critical. In fact, the severity of such vibrations all but eliminates the benefit of stability of conical beams, from the practical point of view.

Simultaneous external and internal flow

The stability characteristics of tubular beams supported at both ends are relatively straightforward. Increasing either the internal or external flow velocity, or both, the system eventually loses stability by divergence (buckling); its subsequent behaviour with increasing flows involves a succession of flutter and buckling instabilities. In the case of cantilevered tubular beams, the behaviour of the system is much more complex, depending on the absolute values of internal and external dimensionless flow velocities and on the shape of the downstream end. Cantilevered beams with a blunt free end can only lose stability by flutter in

a process dominated by the internal flow; if the free end is streamlined, however, a complex sequence of buckling and flutter instabilities may occur. Surprisingly, when comparing the results for clamped-clamped and clamped-free beams, it was found that clamped-clamped beams subjected to buckling can be stabilized for specific combinations of the two flows if the downstream end is set free.

The theoretically predicted behaviour was supported by experiments, and agreement between theory and experiment was found to be reasonably good.

It was shown that the state of a system with both internal and external flows present cannot generally be inferred from knowledge of its state when subjected separately to the internal and external flow. However, in a few simple cases the stability of the system can be inferred exactly from that of a similar beam subjected to an equivalent single internal or external flow, while in many cases, a single, almost equivalent external flow will provide useful approximations of the lowest critical flow velocities.

Of course, in terms of practical application of this work, a designer is probably not interested in the intricacies of the succession of instabilities to which the system may be subjected, but rather to the critical conditions associated with the first instability encountered with increasing internal or external flow velocities. With this is mind, a simplified analysis relating exclusively to buckling was conducted, and it was shown

to provide approximate "universal" stability criteria for the first buckling instability. These criteria (the lowest curves of Fig. 23) are applicable to tubular beams with clamped ends, and to cantilevered beams where the internal flow velocity is not excessively high ($u_i<3$). These diagrams actually apply even to counterflow situations, i.e. where the internal and external flows are in opposite directions.

6.2 SUGGESTIONS FOR FUTURE WORK

There are many possible directions in which the work presented in this thesis could be extended. Thus, one could utilize the Timoshenko, rather than the Euler-Bernoulli, beam theory. However, as in most hydroelastic and aeroelastic phenomena, the main theoretical difficulties arise in modelling adequately the fluid mechanics rather than the solid mechanics, side of the theory; hence, the greatest improvements and/or generalizations of the theory are associated with the fluid mechanics of the problem. Possible useful extensions to the theory would involve the consideration of compressible and two-phase flows; perhaps less useful, but theoretically important is the case of pulsating flow. However, two areas may be singled out as requiring more urgent attention and where even moderate progress is likely to yield most interesting results.

The first area concerns the dynamical effect of the boundary layer. More experiments should be undertaken where boundary-layer thickness at various regimes would be varied systematically; such experiments could be performed on cylindrical beams of various sizes (lengths and diameters) and with variable support (forebody) sizes, investigating also the effect of the laminar and turbulent regimes. The fluctuations of the boundary layer for specific motions of beams should also be taken into account.

The second area deals with nonlinear effects. Clearly, nonlinear effects appear to be more important in the case of external flows as evidenced by the small limit cycles observed

experimentally. Experiments with simultaneous flows may provide a useful tool for distinguishing nonlinear effects specifically related to the beam itself from those associated with the two flows. Also, this is an area where much useful theoretical work could be done. It is noted that the current linear theories - including the one presented in this thesis - strictly speaking collapse once the point of instability has been reached. The question of post-critical behaviour is important. For instance, if linear theory predicts that an instability ceases at a specific flow velocity, in reality the instability may persist to higher flows, because the system for that range of flow is stable in-the-small but unstable in-the-large.

REFERENCES

1. Aitken, J., 1878, "An account of some experiments on rigidity produced by centrifugal force". *Philosophical Magazine*, Series V, Vol.5, p.81-105.

2. Bourrières, F-J., 1939, "Sur un phénomène d'oscillation auto-entretenue en mécanique des fluides réels". *Publications Scientifiques et Techniques du Ministère de l'Air*, No.147.

3. Ashley, H., and Haviland, G., 1950, "Bending vibrations of a pipeline containing flowing fluid". *Journal of Applied Mechanics, Transactions of the ASME*, Vol.17, p.229-232.

4. Feodos'ev, V.P., 1951, "Vibrations and stability of a pipe when liquid flows through it". *Inzhenernyi Sbornik*, Vol.10, p.169-170.

5. Housner, G.W., 1952, "Bending vibrations of a pipeline containing flowing fluid". *Journal of Applied Mechanics*, Vol.19, p.205-208.

6. Niordson, F.I., 1953, "Vibrations of a cylindrical tube containing flowing fluid". *Kungliga Tekniska Högskolans Handlingar*, No.73.

7. Long, R.H., 1955, "Experimental and theoretical study of transverse vibrations of a tube containing flowing fluid". *Journal of Applied Mechanics*, Vol.22, p.65-68.

8. Handelman, G.H., 1955, "A note on the transverse vibration of a tube containing flowing fluid". *Quarterly of Applied Mathematics*, Vol.13, p.326-330.

9. Heinrich, G., 1956, "Vibrations of tubes with flow". *Zeitschrift für Angewandte Mathematik und Mechanik*, Vol.36, p.417-427.

10. Bolotin, V.V., 1956, "End deformations of flexible pipelines". *Trudy Moskovskogo Energeticheskogo Instituta*, No.19, p.272-291.

11. Hu, H.H., and Tsoon, W.S., 1957, "On the flexural vibrations of pipeline containing flowing fluid". *Proceedings of Theoretical and Applied Mechanics* (India), p.203-216.

12. Movchan, A.A., 1965, "On the problem of stability of a pipe with fluid flowing through it". *Journal of Applied Mathematics and Mechanics*, Vol.29, p.760-762.

13. Dodds, H.L. Jr. and Runyan, H.L., 1965, "Effect of high velocity fluid flow on the bending vibrations and static divergence of a simply supported pipe". *NASA Technical Note D.2870*.

14. Gregory, R.W. and Paidoussis, M.P., 1966; "Unstable oscillation of tubular cantilevers conveying fluid - Part I: theory; Part II: experiments". *Proceedings of the Royal Society (London)*, Vol.293(A), p.512-527 and p.528-542.

15. Benjamin, T.B., 1961, "Dynamics of a system of articulated pipes conveying fluid - Part I: theory; Part II: experiments". *Proceedings of the Royal Society (London)*", Vol.261(A), p.457-486 and p.487-499.

16. Paidoussis, M.P., 1970, "Dynamics of tubular cantilevers conveying fluid". *Journal of Mechanical Engineering Science*, Vol.12, p.85-103.

17. Paidoussis, M.P. and Deksnis, E.B., 1970, "Articulated model of cantilevers conveying fluid: the study of a paradox". *Journal of Mechanical Engineering Science*, Vol.12, p.288-300.

18. Chen, S.-S., 1971, "Flow induced instability of an elastic tube". *ASME Vibration Conference*, ASME Paper 71-vibr-39, Toronto, Canada.

19. Chen, S.-S., 1972, "Flow-Induced in-plane instabilities of curved pipes". *Nuclear Engineering and Design*, Vol.23, p.29-38.

20. Chen, S.-S., 1973, "Out-of-plane Vibration and Stability of curved tubes conveying fluid". *Journal of Applied Mechanics, Transactions of ASME*, Vol.40, p.362-368.

21. Chen, S.-S., 1972, "Vibrations of continuous pipes conveying fluid". *Proceedings of the International Symposium on flow-induced structural vibrations*, paper G1, Karlsruhe, Germany.

22. Herrmann, G., 1967, "Stability of Equilibrium of elastic systems subjected to non-conservative forces". *Applied Mechanics Reviews*, Vol.20, p.103-108.

23. Herrmann, G., and Nemat-Nasser, S., 1967, "Instability modes of cantilevered bars induced by fluid flow through attached pipes". *International Journal of Solids and Structures*, Vol.3, p.39-52.

24. Wiley, J.C., and Furkert, R.E., 1972, "Beams subjected to follower force within the span". *Journal of the Engineering Mechanics Division, Proceedings of the ASCE*, Vol.98, p.1353-1364.

25. Naguleswaran, S., and Williams, C.J.H., 1968, "Lateral vibration of a pipe conveying a fluid". *Journal of Mechanical Engineering Science*, Vol.10, p.228-238.

26. Paidoussis, M.P., and Denise, J.-P., 1972, "Flutter of thin cylindrical shells conveying fluid". *Journal of Sound and Vibration*, Vol.20, p.9-26.

27. Weaver, D.S. and Unny, T.E., 1973, "Dynamic stability of fluid-conveying pipes". *Journal of Applied Mechanics*, Vol.40, p.48-52.

28. Weaver, D.S. and Myklatun, B., 1973, "On the stability of thin pipes with an internal flow". *Journal of Sound and Vibration*, Vol.31, p.399-410.

29. Paidoussis, M.P. and Issid, N.T., 1974, "Dynamic stability of pipes conveying fluid". *Journal of Sound and Vibration*, Vol.33, p.267-294.

30. Paidoussis, M.P., 1975, "Flutter of conservative systems of pipes conveying incompressible fluid". *Journal of Mechanical Engineering Science*, Vol.17, p.19-25.

31. Paidoussis, M.P. and Laithier, B.E., 1976, "Dynamics of Timoshenko beams conveying fluid". *Journal of Mechanical Engineering Science*", Vol.18, p.210-220.

32. Thurman, A.L., and Mote, C.D. Jr., 1969, "Non-linear oscillation of a cylinder containing flowing fluid". *ASME Journal of Engineering for Industry*, Vol.91, p.1147-1155.

33. Liu, H., and Mote, C.D., 1974, "Dynamic response of pipes transporting fluids". *ASME Journal of Engineering for Industry*, Vol.96, p.591-596.

34. Holmes, P.J., 1976, "Bifurcations to divergence and flutter in flow induced oscillations of pipes". *Report, Institute of Sound and Vibration Research, University of Southampton.*

35. Chen, S.-S., 1971, "Dynamic stability of fluid-conveying pipes". *Journal of the Engineering Mechanics Division, Proceedings of the ASCE*, Vol. 97, p.1469-1485.

36. Ginsberg, J.H., 1973, "The dynamic stability of a pipe conveying a pulsatile flow". *International Journal of Engineering Science*, Vol.11, p.1013-1024.

37. Paidoussis, M.P., and Sundararajan, C., 1975, "Parametric and combination resonances of a pipe conveying pulsating fluid". *Journal of Applied Mechanics*, Vol.42, *Transactions of the ASME*, Vol.97, Series E, p.780-784.

38. Paidoussis, M.P. and Issid, N.T., 1976, "Experiments on parametric resonance of pipes containing pulsatile flow". *Journal of Applied Mechanics*, Vol.98, p.198-202.

39. Chen, S.-S., 1974, "Parallel flow-induced vibrations and instabilities of cylindrical structures". *Shock and Vibration Digest*, Vol.16, No.10, p.1-11.

40. Lamb, H., 1879, *Hydrodynamics*, Sixth edition (1932), Dover Publications, New York, p.374.

41. Bisplinghoff, R.L., Ashley, H. and Halfman, R.L., 1955, *Aeroelasticity*, Addison-Wesley Publications, Reading, Massachusetts.

42. Bisplinghoff, R.L., 1969, "Aerodynamic flutter". *AIAA Selected Reprint Series*, Vol.V (Ed. I.E. Garrick), published by AIAA, New York.

43. Dowell, E.H., 1970, "Panel flutter: a review of the aeroelastic stability of plates and shells". *AIAA Journal*, Vol.8, p.385-399.

44. Kornecki,A., 1971, "Travelling wave type flutter of flat panels in inviscid flow; Part 1: Infinite panels; Part 2: Panels of finite length". *Technion-Israel Institute of Technology*, Haifa, Israel, publications Nos.132 and 133 (Agricultural Engineering Faculty).

45. Munk, M.M., 1924, "The aerodynamic force on airship hulls". *NACA Report* No. 184.

46. Lighthill, M.J., 1960 "Note on the swimming of slender fish". *Journal of Fluid Mechanics*, Vol.9, p.305-317.

47. Hawthorne, W.R., 1961, "The early development of the Dracone flexible barge". *Proceedings of the Institution of Mechanical Engineers*, Vol.175, p.52-83.

48. Paidoussis, M.P., 1968, "Stability of towed, totally submerged flexible cylinders", *Journal of Fluid Mechanics*, Vol.34, p.273-297.

49. Paidoussis, M.P., 1973, "Vibrations of cylindrical structures induced by axial flow". *Aéro-Hydro-Elasticité*, published by Eyrolles, Paris, p.197-278.

50. Paidoussis, M.P., 1966, "Dynamics of flexible slender cylinders in axial flow. Part I: theory; Part II; experiments". *Journal of Fluid Mechanics*, Vol.26, p.717-736 and p.737-751.

51. Paidoussis, M.P., 1966, "Vibration of cylinders with supported ends, induced by axial flow". *Proceedings Institution of Mechanical Engineers*, Vol.180, p.268-278.

52. Paidoussis, M.P., 1969, "An experimental study of the vibration of flexible cylinders induced by nominally axial flow". *Nuclear Science and Engineering*, Vol.35, p.127-138.

53. Chen, S.-S and Wambsganss, M.W., 1972, "Parallel-flow induced vibrations of fuel rods". *Nuclear Engineering Design*, Vol. 18, p.253-278.

54. Reavis, J.R., 1969, "Vibration correlation for maximum fuel-element displacement in parallel turbulent flow". *Nuclear Science and Engineering*, Vol.38, p.63-69.

55. Gorman, D., 1971, "An analytical and experimental investigation of cylindrical reactor fuel elements in two-phase parallel flow". *Nuclear Science and Engineering*, Vol.44, p.277-290.

56. Chen, Y.N., 1970, "Flow-induced vibrations in tube bundle heat exchangers with cross and parallel flow. Part 1: parallel flow". *Proceedings of Flow-Induced Vibrations in Heat Exchangers*, ASME, New York, Dec.1970, p.57-66.

57. Paidoussis, M.P., 1974, "The dynamical behaviour of cylindrical structures in axial flow". *Annals of Nuclear Science and Engineering*, Vol.1, p.83-106, Pergamon Press.

58. Chen, S.-S., 1970, "Vibration of a class of nonconservative systems with time-dependent boundary conditions". *Shock and Vibrations Bulletin*, Vol.41, p.141-150.

59. Seiveright, G.R., 1975, "State of the art report on vibration and fretting wear". *Westinghouse Canada Report* CWAPD-282, Hamilton, Ontario.

60. Paidoussis, M.P., 1973, "Dynamics of cylindrical structures subjected to axial flow". *Journal of Sound and Vibration*, Vol.29, p.365-385.

61. Chen, S.-S., 1975, "Vibrations of a group of circular cylindrical structures in a liquid". *Transactions, 3rd International Conference on Structural Mechanics in Reactor Technology*, Vol.1. Paper D2/7; London, U.K.

62. Chen, S.-S., 1975, "Vibrations of a row of circular cylinders in a liquid", *ASME Journal of Engineering for Industry*, Vol.9, p.1212-1218.

63. Chung, H., and Chen, S.-S., 1976, "Vibration of a group of circular cylinders in a confined fluid". *Argonne National Laboratory Report* ANL-CT-76-25.

64. Cesari, F., and Curioni, S., 1971, "Buckling instability in tubes subject to internal and external axial fluid flow". *Proceedings of the 41st conference on dimensioning and strength calculations*, Budapest, 1971, published by Akad Kiado.

65. Taylor, G.I., 1952, "Analysis of the swimming of long and narrow animals". *Proceedings of the Royal Society (London)*, Vol.214(A), p.158-182.

66. Hannoyer, M.J., 1971, *Elastohydrodynamic instabilities of flexible truncated cones in axial flow*, Master's thesis, McGill University, Montreal.

67. Sechler, E.E., 1952, *Elasticity in Engineering*, Dover Publications, New York.

68. Hamming, R.W., 1952, *Numerical Methods for Scientists and Engineers*, McGraw Hill, p.249-264.

69. Hannoyer, M.J., 1972, "A solution to linear differential equations in the field of dynamics of continuous systems". *MERL Report 72-5*, McGill University, Montreal.

70. Bishop, R.E. and Johnson, D.C., 1960, *The Mechanics of Vibration*, Cambridge University Press, p.382-387.

71. Wrinch, D., 1922, "On lateral vibrations of bars of conical type". *Proceedings of the Royal Society (London)*, Vol.101(A), p.493.

72. Housner, G.W. and Keightley, W.O., 1962, "Vibrations of linearly tapered cantilever beams". *Journal of the Engineering Mechanics Division, Proceedings of the ASCE*, Vol. 88, p.95.

73. Sears, W.R., 1960, *Small Perturbation Theory*, Princeton Aeronautical Paperbacks, Princeton University Press.

74. Schlichting, H., 1968, *Boundary Layer Theory*, 6th ed.,Chapt.XXI, McGraw Hill, New York.

75. Hoerner, S.F., 1957, *Fluid Dynamic Drag*, published by author, Washington.

76. Rosinger, H.E., and Ritchie, I.G., 1974, "A critical assessment of the cantilever beam method for the determination of dynamic Young's modulus", *Journal of Testing and Evaluation*, Vol.2, p.131-138.

77. Upson, R.H. and Klikoff, W.A., 1931, "Application of practical hydrodynamics to airship design". *NACA Report* 405.

78. Kelly, H.R., 1954, "Estimation of normal force, drag, and pitching moment coefficients for blunt-based bodies of revolution at large angle of attack". *Journal of Aeronautical Sciences*, p.549-565.

79. Nakayama, A., Patel, V.C. and Damian, R., 1974, "Measurements in the thick axisymmetric turbulent boundary layer near the tail of a body of revolution". *Journal of Fluid Mechanics*, Vol.63, p.345-367.

80. Nakayama, A., Patel, V.C. and Landweber, L., 1976, "Flow interaction near the tail of a body of revolution. Part 1: flow exterior to boundary layer and wake; Part 2: Iterative solution for flow within and exterior to boundary layer and wake". *Journal of Fluids Engineering*, ASME publications Nos.76-FE-M and 76-FE-N.

81. Myring, D.F., 1972, "The profile drag of bodies of revolution in subsonic flow". *Royal Aircraft Establishment Technical Report* No. 72234.

82. Paidoussis, M.P. and Yu, B.K., 1976, "Elastohydrodynamics of towed slender bodies: the effect of nose and tail shapes on stability". *Journal of Hydronautics*, Vol.10, p.127-134.

83. Snowdon, J.C., 1968, *Vibration and Shock in Damped Mechanical Systems*, published by Wiley & Sons, New York.

84. Ziegler, H., 1967, *Principles of Structural Stability*, published by Blaisdell, Waltham, Massachusetts.

FIGURES

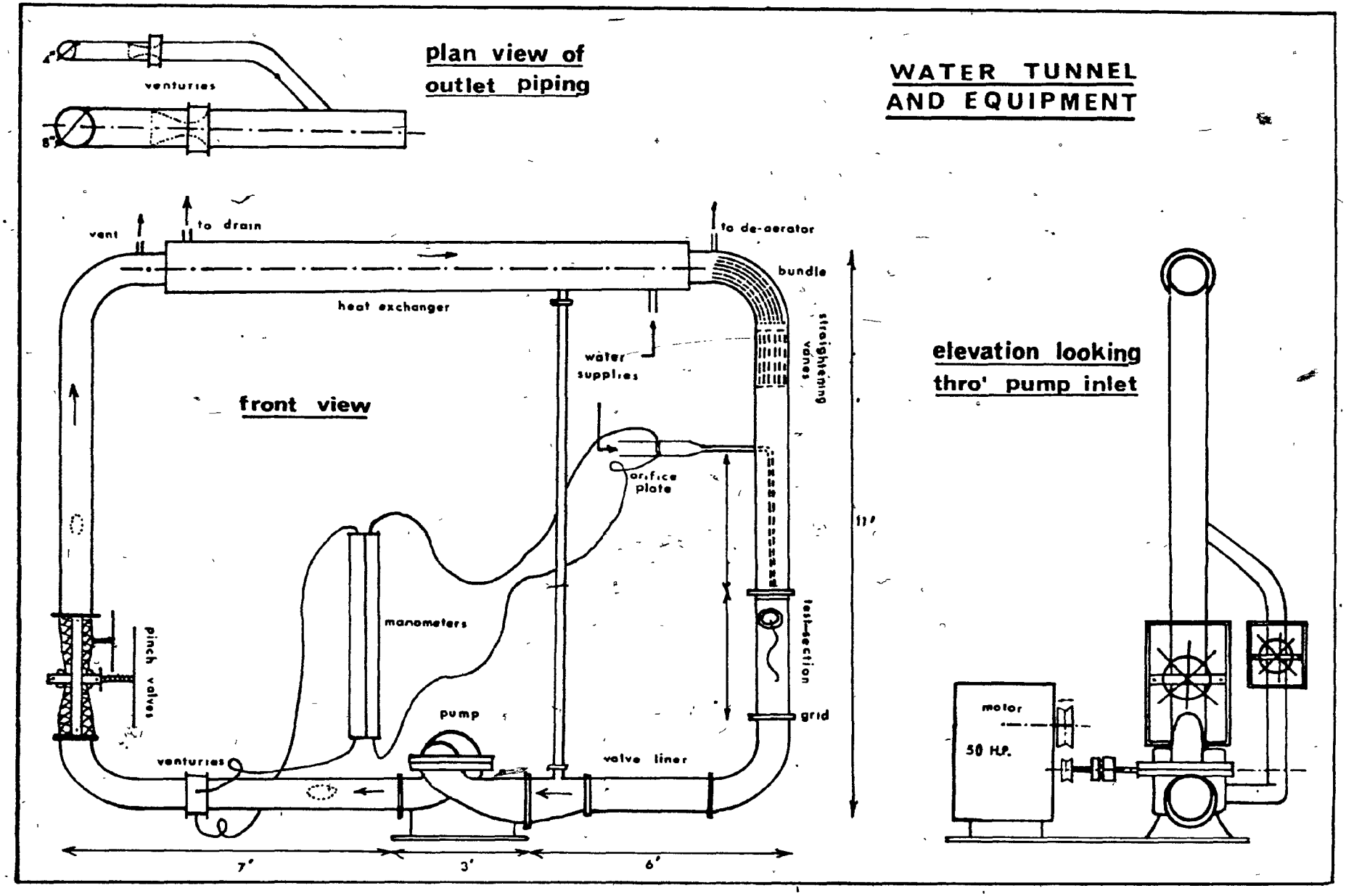

Fig.1 Diagrammatic view of the water-tunnel.

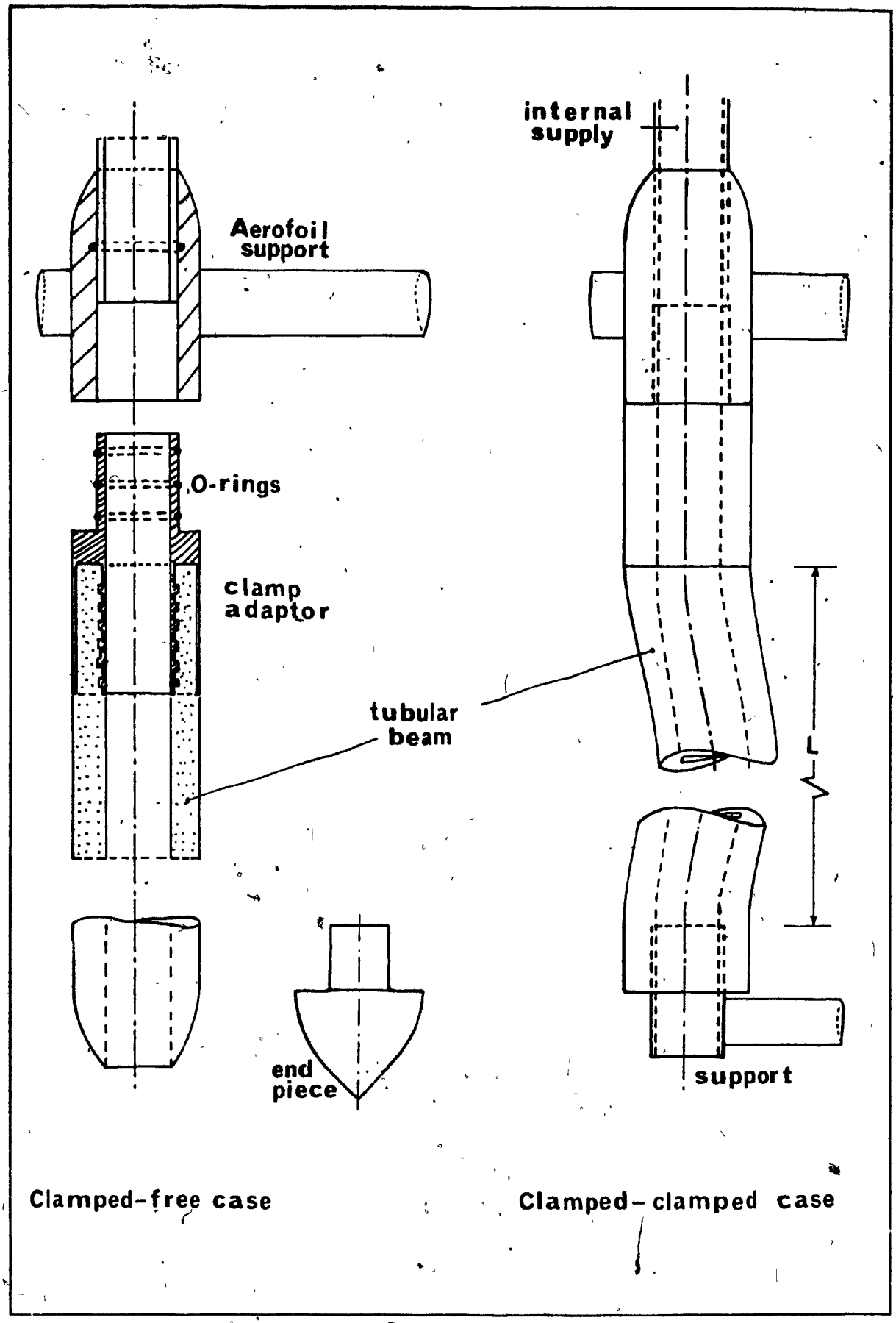

Fig.2 The tubular beams and supports used in the experiments.

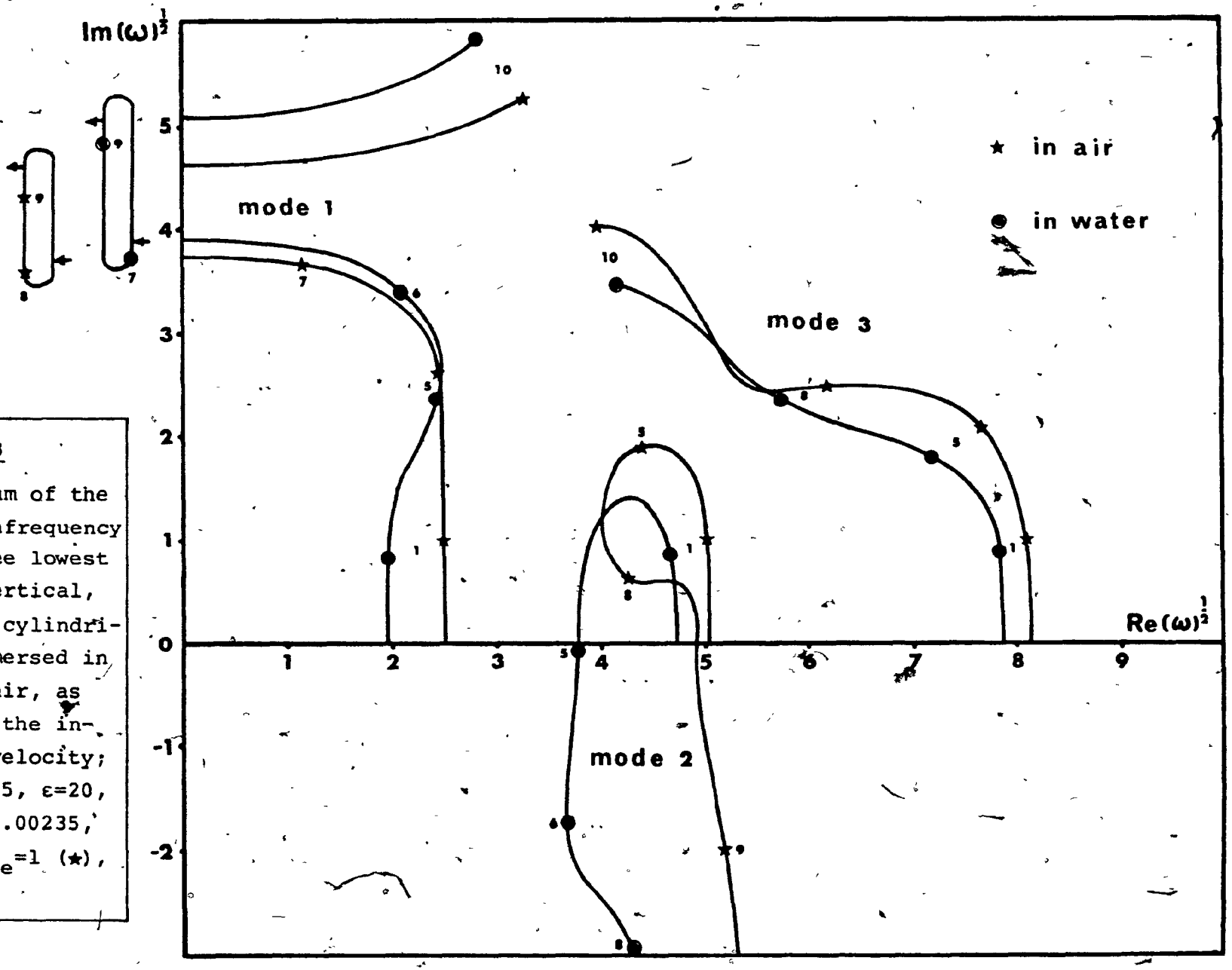

Fig. 3

Argand diagram of the complex eigenfrequency ω of the three lowest modes of a vertical, cantilevered cylindrical tube, immersed in water or in air, as functions of the internal flow velocity; $\alpha_e=\alpha_i=0$, $\delta=0.5$, $\varepsilon=20$, $\gamma_i=-0.03$, $\gamma=0.00235$, $\gamma_e=0.9$ (●), $\gamma_e=1$ (★), $\chi_e=\mu=\nu=0$.

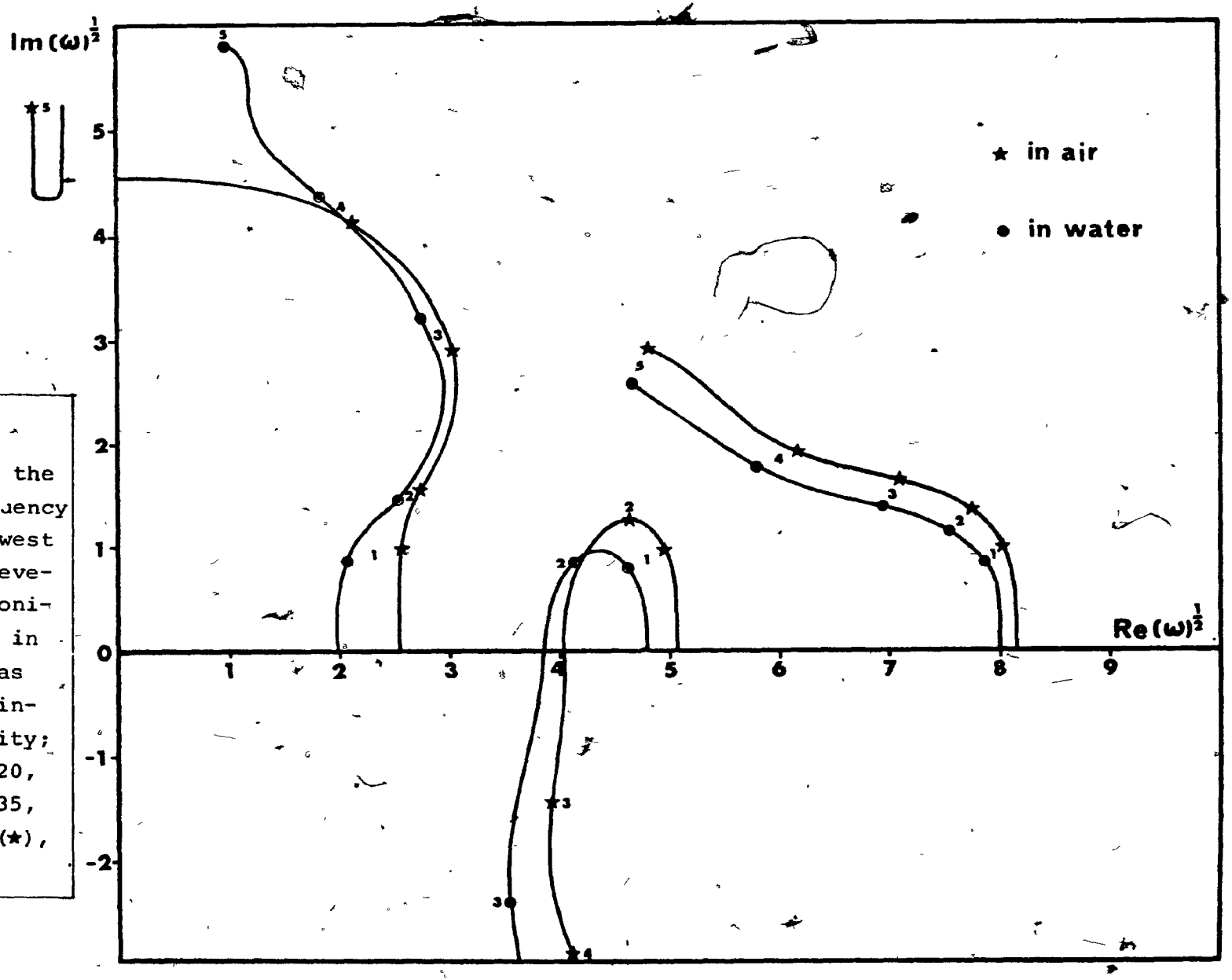

Fig. 4

Argand diagram of the complex eigenfrequency ω of the three lowest modes of a cantilevered cylindrical-conical tube, hanging in water or in air, as functions of the internal flow velocity; $\alpha_e=0$, $\alpha_i=-0.5$, $\tilde{\varepsilon}=20$, $\gamma_i=-0.03$, $\gamma=0.00235$, $\gamma_e=1.9$ (●), $\gamma_e=1$ (★), $\delta=0.5$, $\chi_e=\mu=\nu=0$.

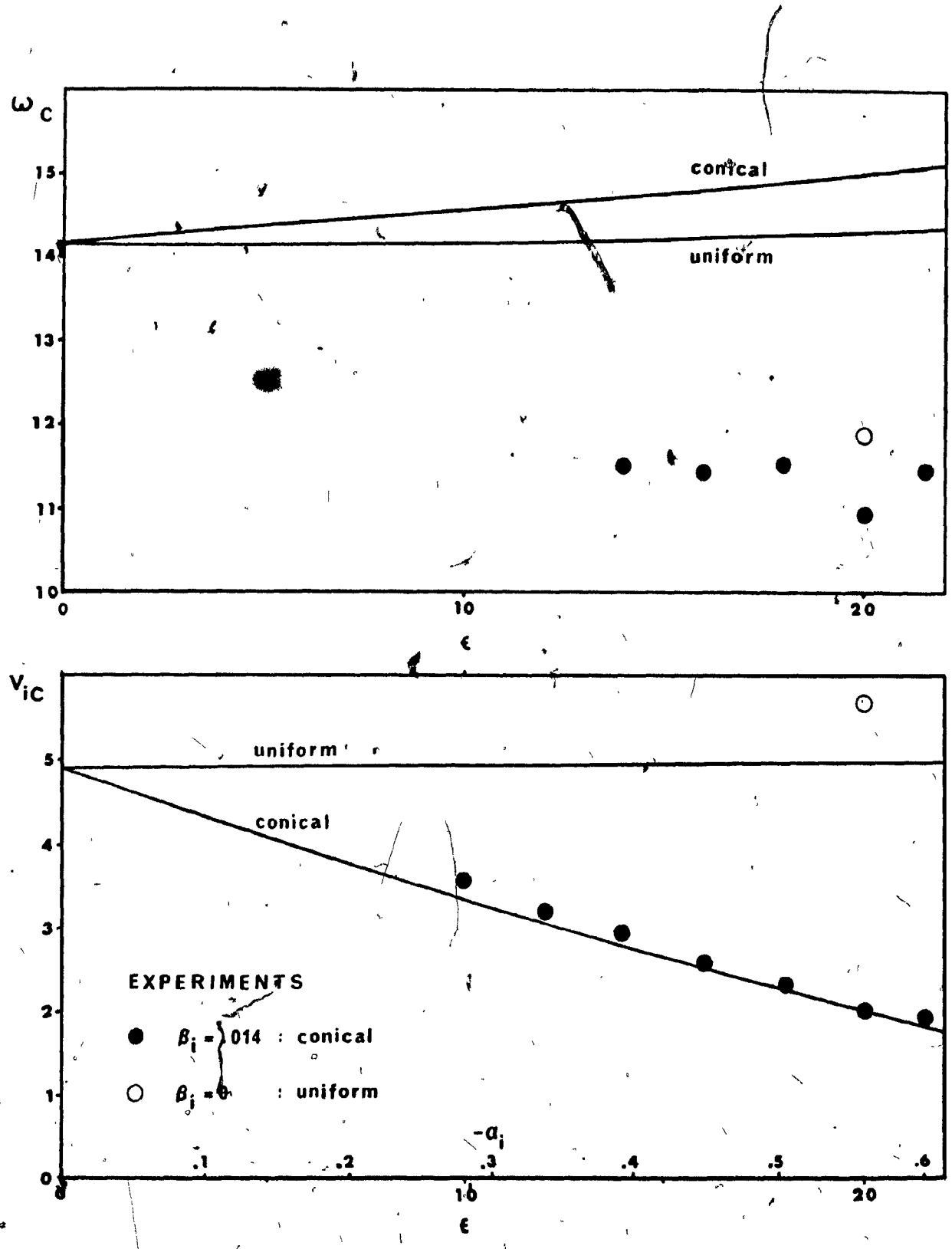

Fig. 5 Comparison, for various slenderness ratios ϵ, between the experimental and theoretical critical flow velocities, v_{ic}, and eigenfrequencies, ω_c, of a cantilevered, either cylindrical or cylindrical-conical (β_e=0, β_i=0.014) tube hanging in water (δ=0.5, γ=0.00235, γ_e=1.9, γ_i=-0.03, χ_e=u_e=μ=ν=0).

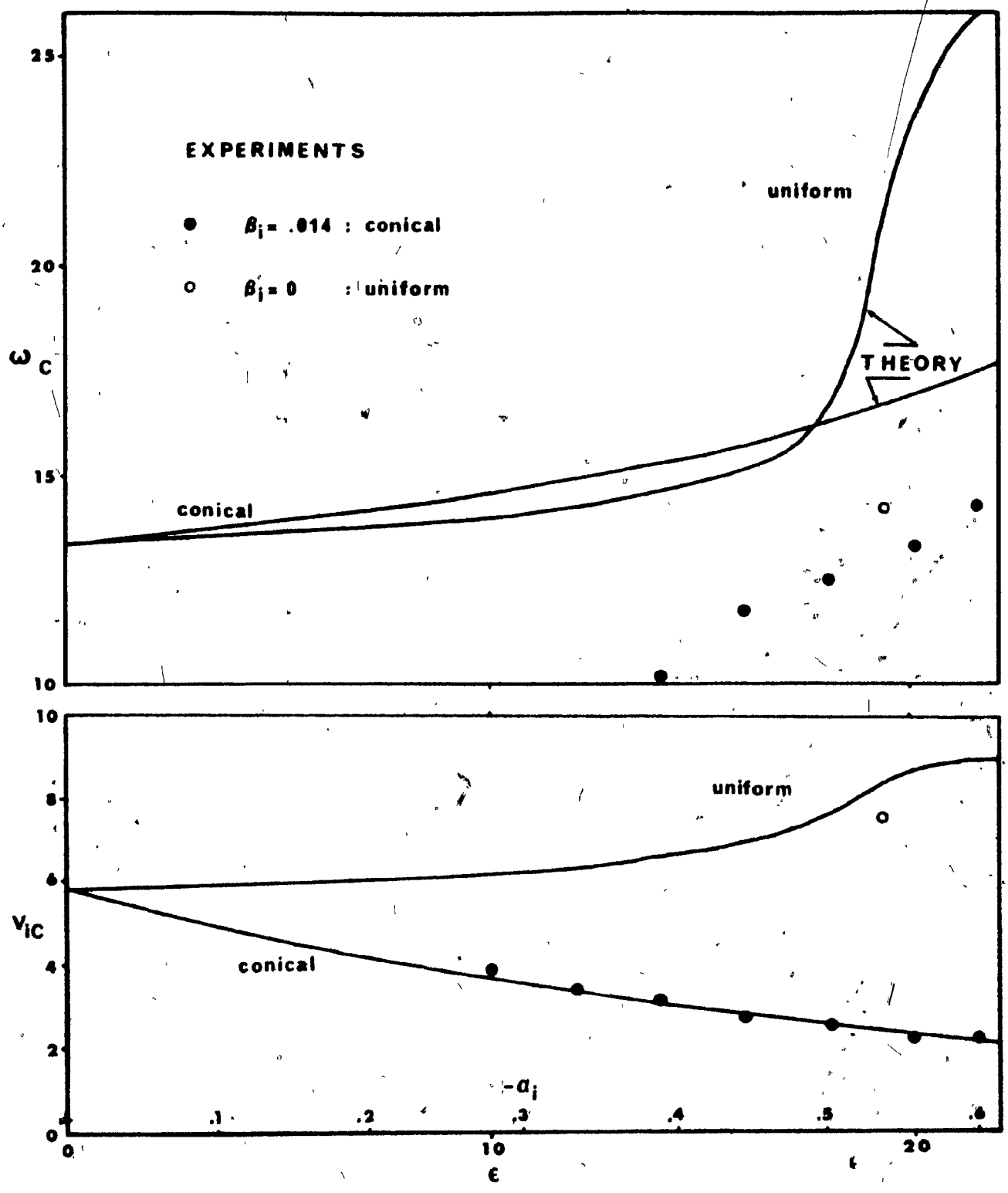

Fig.6 Comparison, for various slenderness ratios ϵ, between the experimental and theoretical critical flow velocities, v_{ic}, and eigenfrequencies, ω_c, of a cantilevered, either cylindrical or cylindrical-conical (β_e=0,β_i=0.014) tube hanging in air (δ=0.5, γ=0.00235, γ_e=1.0, γ_i=-0.03, χ_e=u_e=μ=ν=0).

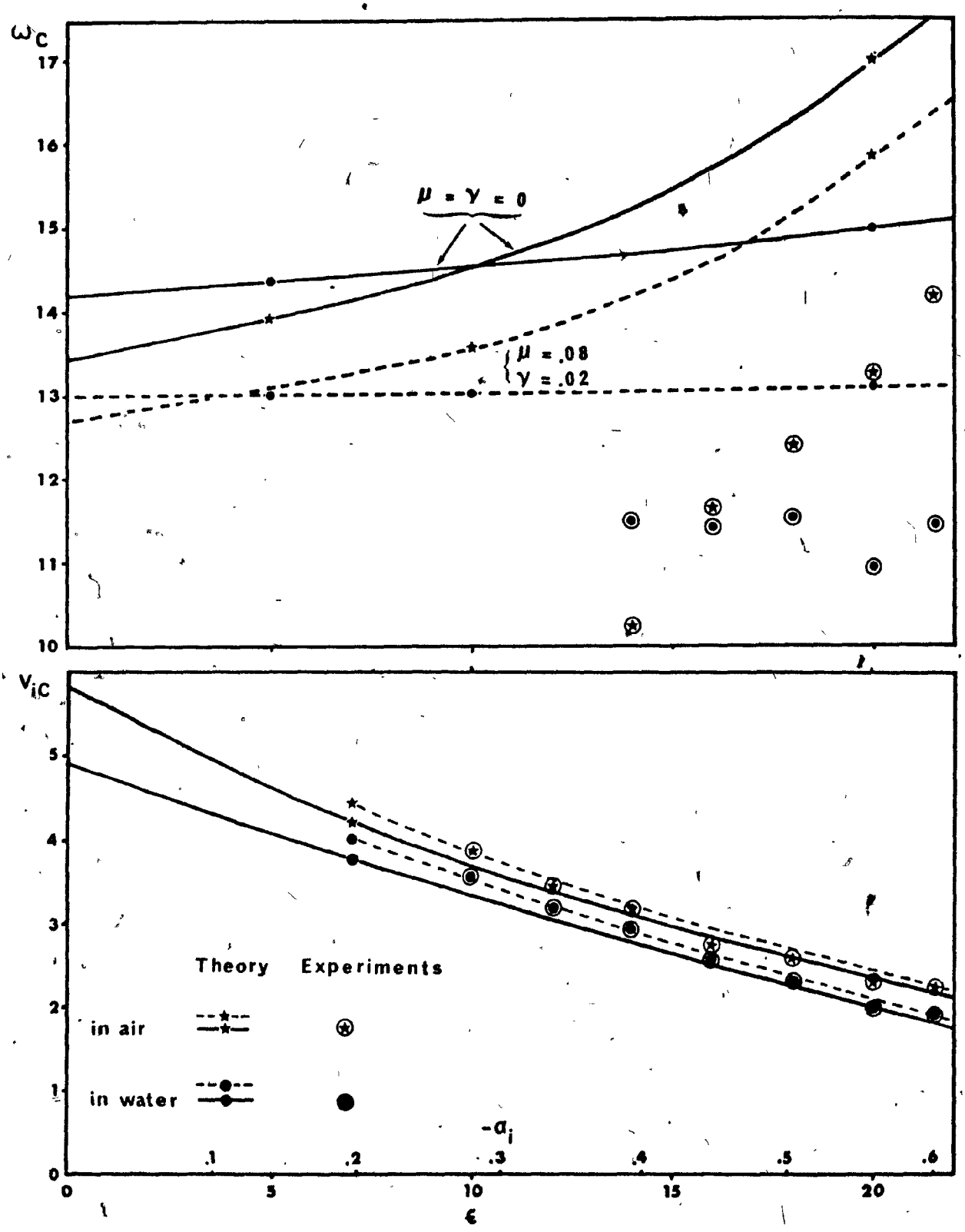

Fig.7 Comparison, for various slenderness ratios ε, between the experimental critical flow velocities, v_{ic}, and eigenfrequencies, ω_c, of a cantilevered vertical cylindrical-conical tube and the theoretical values obtained with viscohysteretic damping ($\mu=4\nu=0.08$) or no damping ($\mu=\nu=0$), and $\beta_i=0.014, \delta=0.5, \gamma=0.00235, \gamma_i=-0.03$.

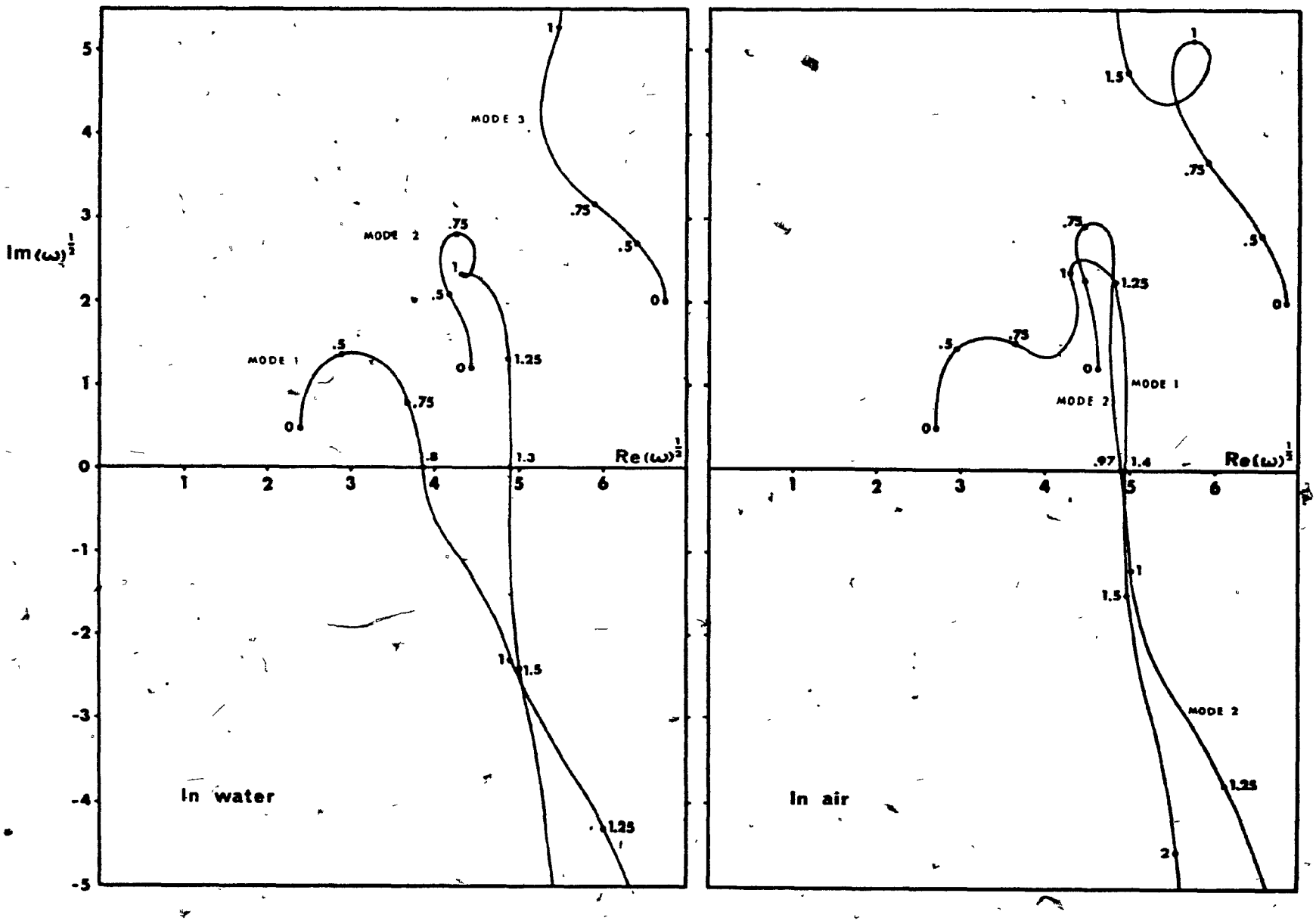

Fig.6 . Argand diagrams of the complex eigenfrequencies ω of a cantilevered vertical conical tube, immersed in water or in air, as functions of the internal flow velocity, for β_e=0.03, β_i=0.016, δ=0.5, ε=22, γ=0.00145, χ_e=u_e=0, μ=0.2 and γ_e=1.7, ν=0.04 (in water) or γ_e=1, ν=0.05 (in air).

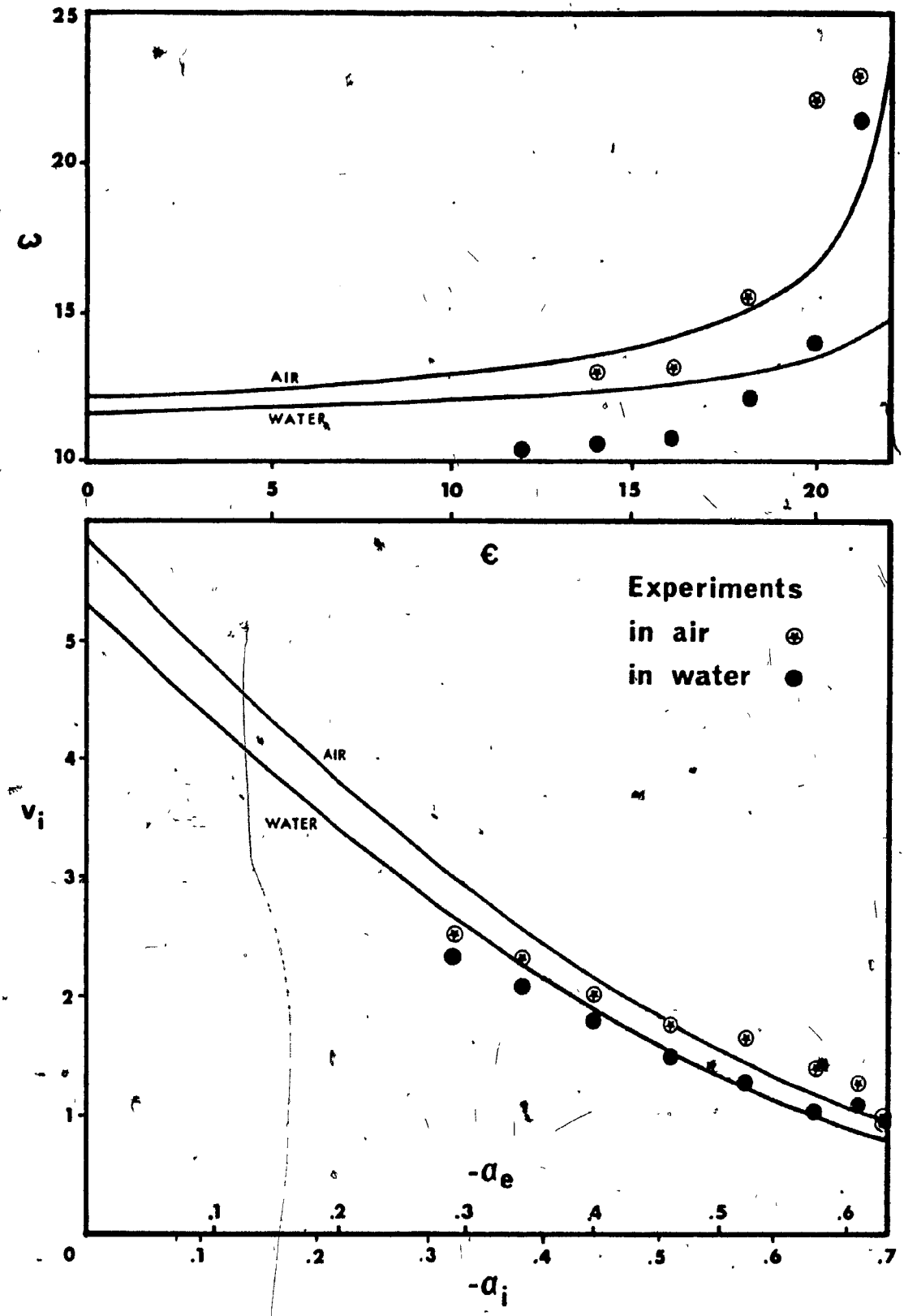

Fig.9 Effect of ε on the critical values of v_i and ω for a conical cantilever hanging in water or in air, with $\beta_e=0.03$, $\beta_i=0.016$, $\delta=0.5$, $\gamma=0.00145$, $\chi_e=u_e=0$, $\mu=0.2$, $\gamma_i=-0.08$ and $\gamma_e=1.7$, $\nu=0.04$ (in water).

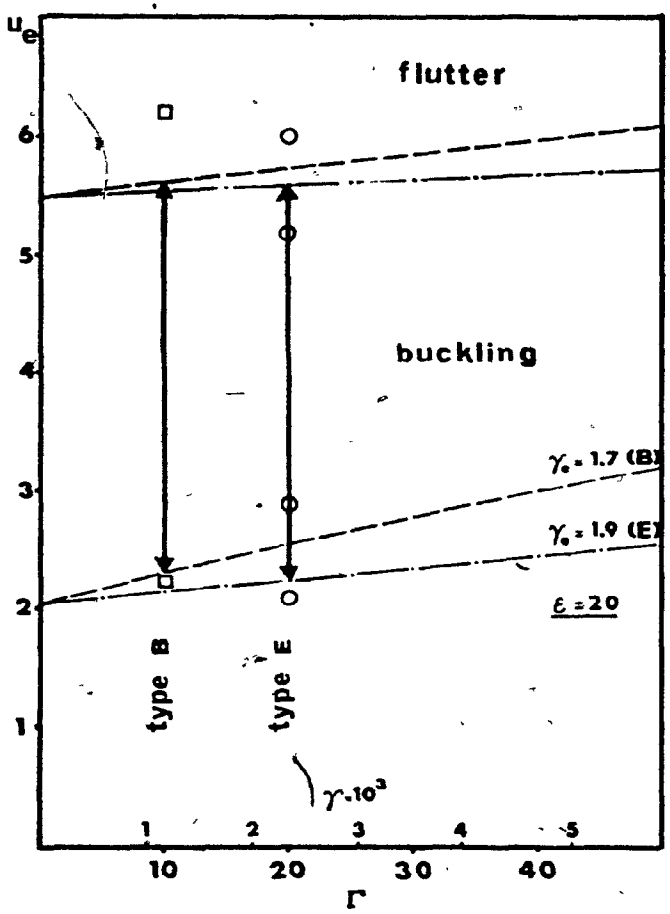

Fig.10 Influence of the parameters γ and Γ on the critical flow velocities for two values of γ_e. Comparison with experimental results, for material type B (γ_e=1.7, γ=0.0012) and E (γ_e=1.9, γ=0.0024); other parameters: $c_n=c_t=0.008$, $\varepsilon=20$, $\varepsilon_o=10$, $\delta=0.5$, $\chi_e=1.5$, $\gamma_i=(\gamma_e-2)\delta^2$.

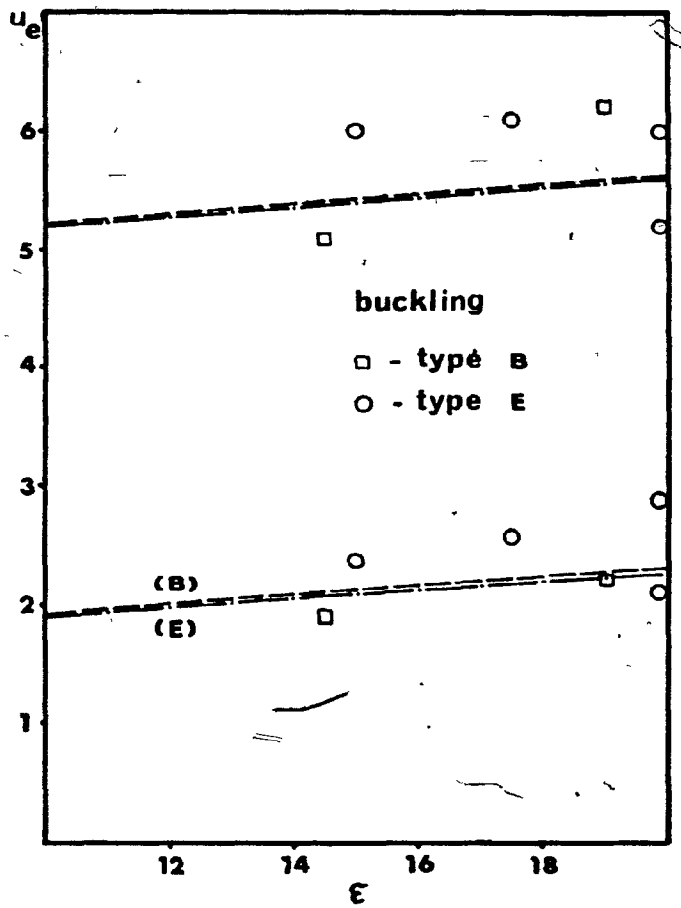

Fig.11 Comparison, for several length ratios, ε, between experimental and theoretical critical flow velocities for cylindrical cantilevers cast with two types of material, i.e. B and E; parameters as in Fig.10.

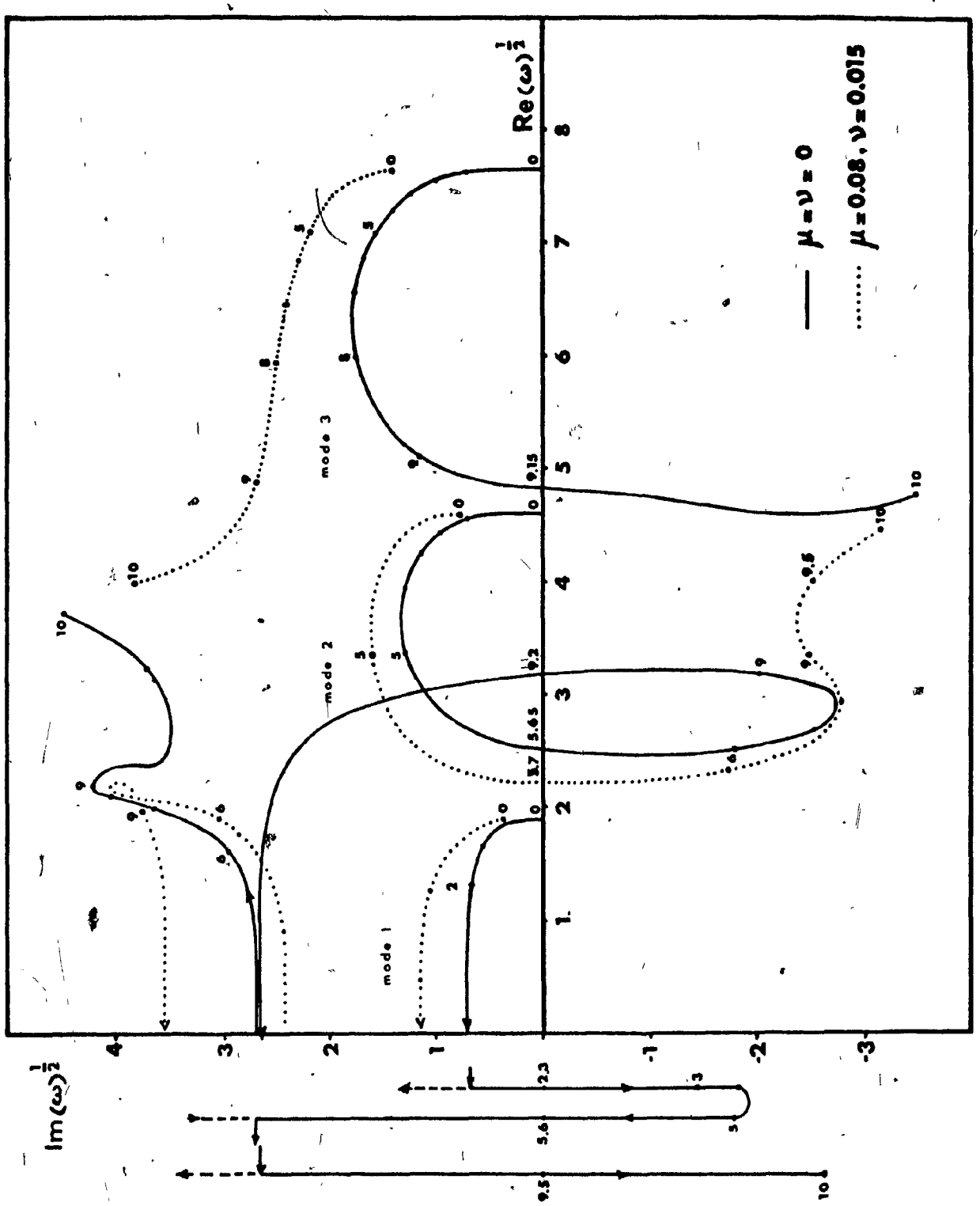

Fig.12 The complex eigenfrequencies of the three lowest modes of a vertical cantilevered cylindrical beam as functions of the flow velocity when, either with no internal damping ($\mu=\nu=0$) or with internal damping ($\mu=0.08$, $\nu=0.015$, as for material E); $c_n=c_t=0.008$, $\varepsilon=20$, $\varepsilon_o=10$, $\delta=0$, $\chi_c=1.5$, $\gamma_c=1.9$, $\gamma=0.0024$.

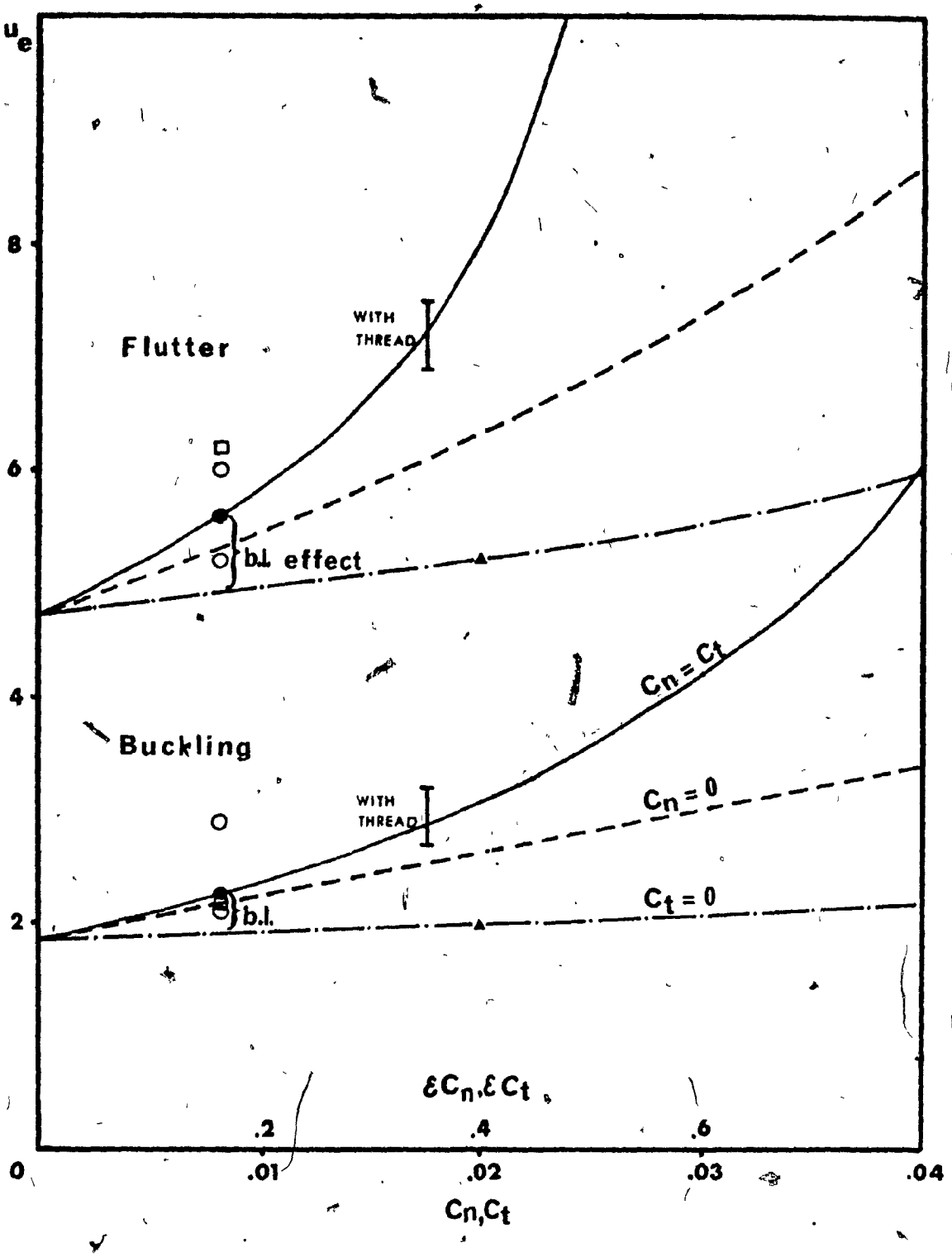

Fig.13 Comparative influence of skin friction and boundary layer thickness on the critical flow velocities of a cantilevered cylindrical beam ($\alpha_e=\alpha_i=0$, $\delta=0.5$, $\chi_e=1.5$, $\gamma=0.0024$, $\varepsilon=20$, $\varepsilon_o=10$, $\mu=\nu=0$). The symbols ● and ▲ indicate the theoretical critical velocities for $c_n=c_t=0.008$ (present work) and $c_n=c_t=0.02$ (Paidoussis), respectively; effect of skin friction alone, —·—, boundary layer alone, - - -, and both, ——. Comparison with experimental data.

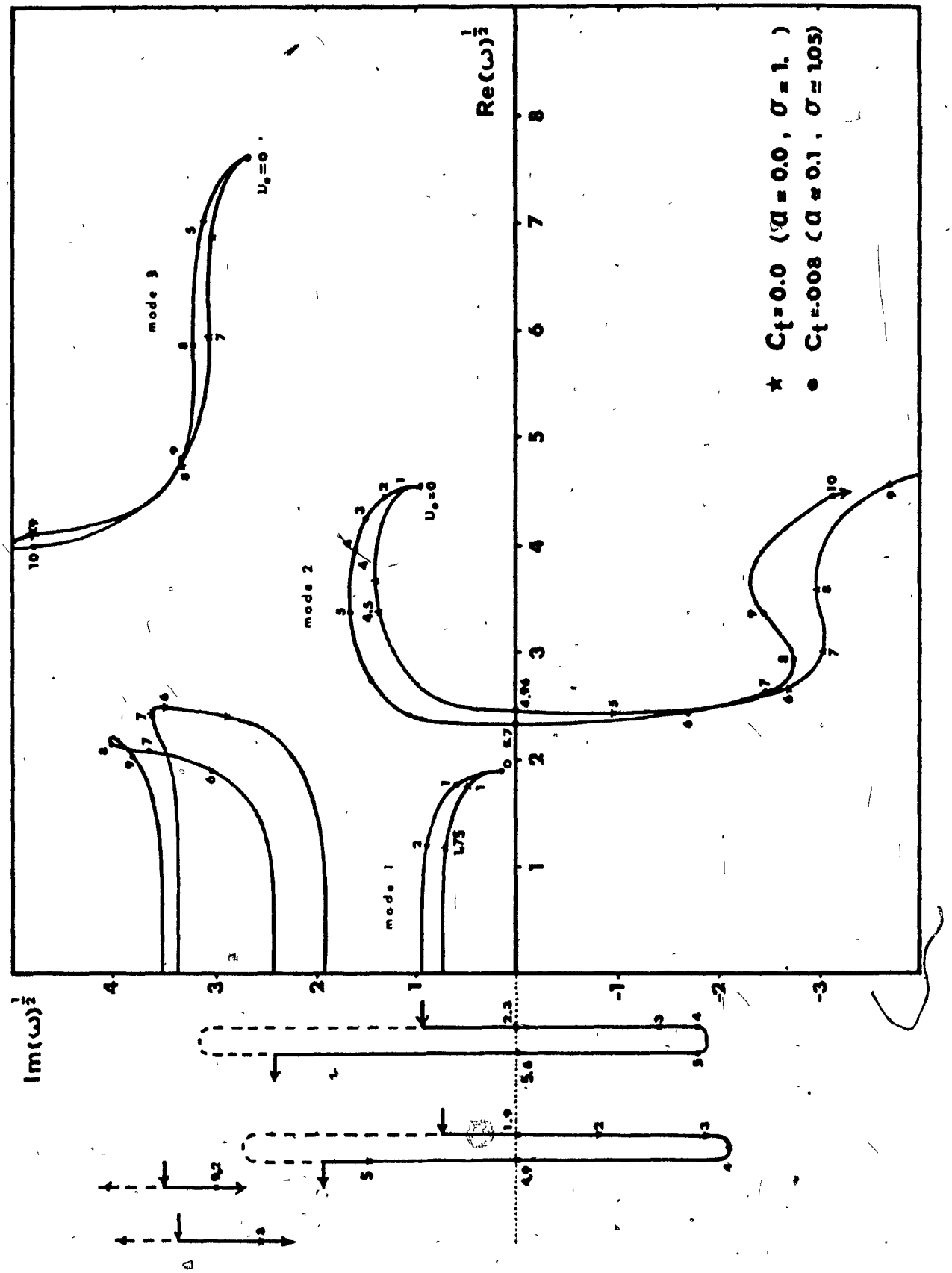

Fig.14 Influence of the boundary layer thickness on the three lowest modes of a cylindrical beam in external flow ($\alpha_e=\alpha_i=0$, $\delta=0.5$, $c_n=0.008$, $\chi_e=1.5$, $\gamma=0.0024$, $\varepsilon=20$, $\varepsilon_o=10$, $\mu=\infty$, $\nu=0.005$).

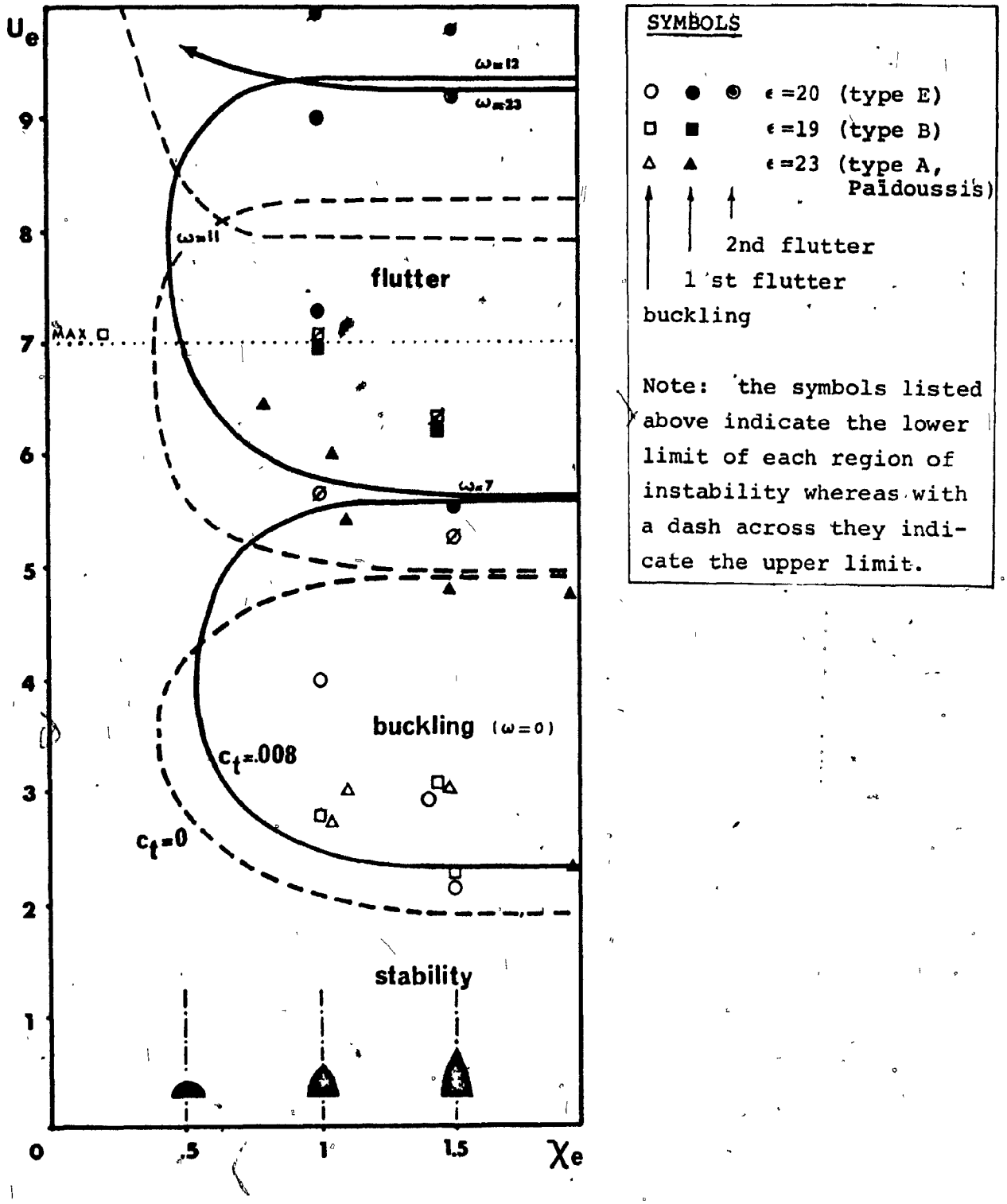

Fig.15 Effect of the size of the tapered end-piece on the critical flow velocities of the three lowest modes of cantilevered cylindrical beams. Comparison with theoretical results obtained with no boundary layer (c_t=0) and with boundary layer (c_t=0.008); $\alpha_c=\alpha_i$= 0, c_n=0.008, ε=20, ε_o=10, δ=0.5, γ_i=-0.03, γ_c=1.9, γ=0.0024, ν=0.

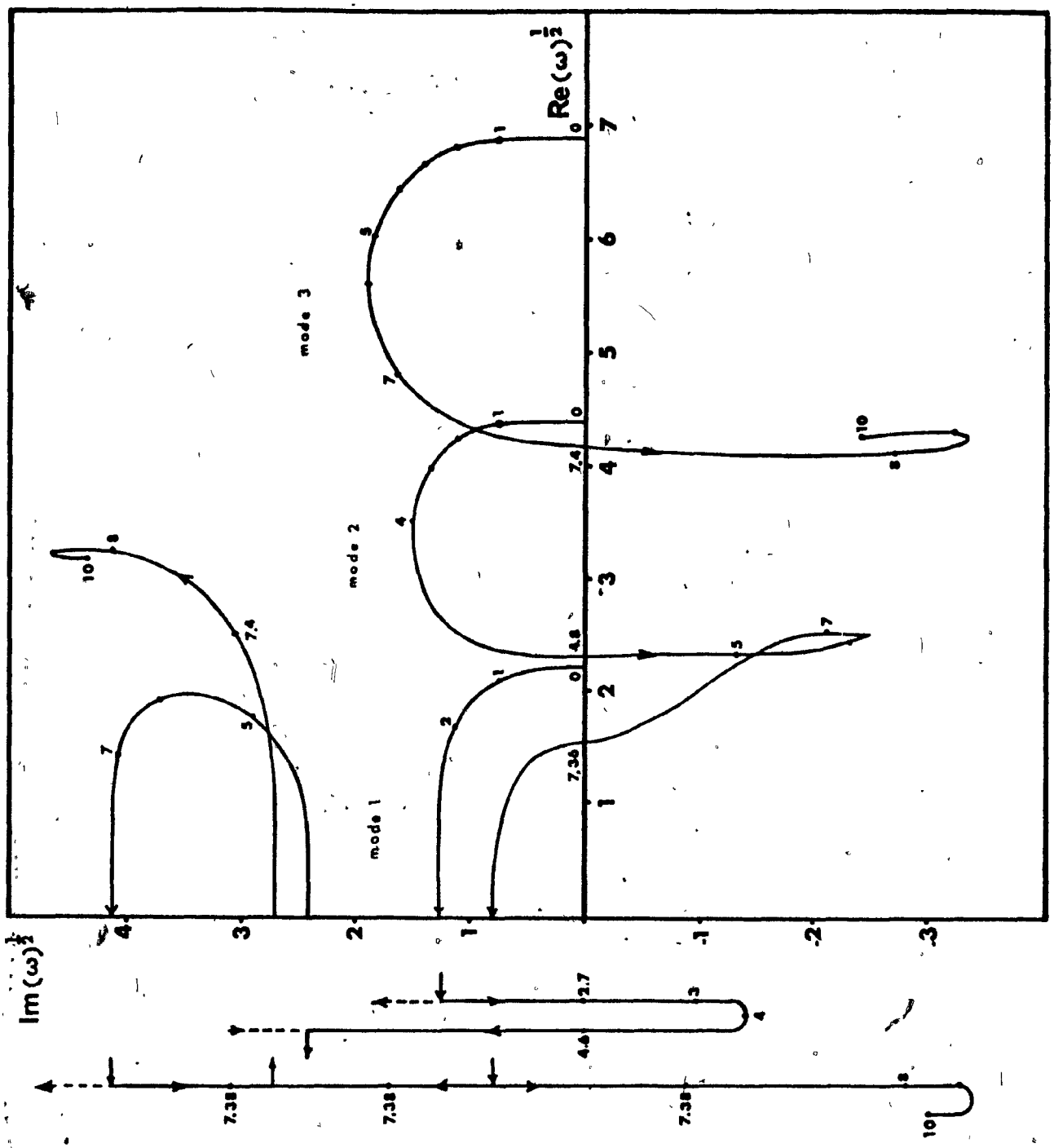

Fig.16 The complex eigenfrequencies of the three lowest modes of a vertical cantilevered conical beam (α_e=-0.5) as functions of the external flow velocity (parameters as in Fig.12 and ν=0).

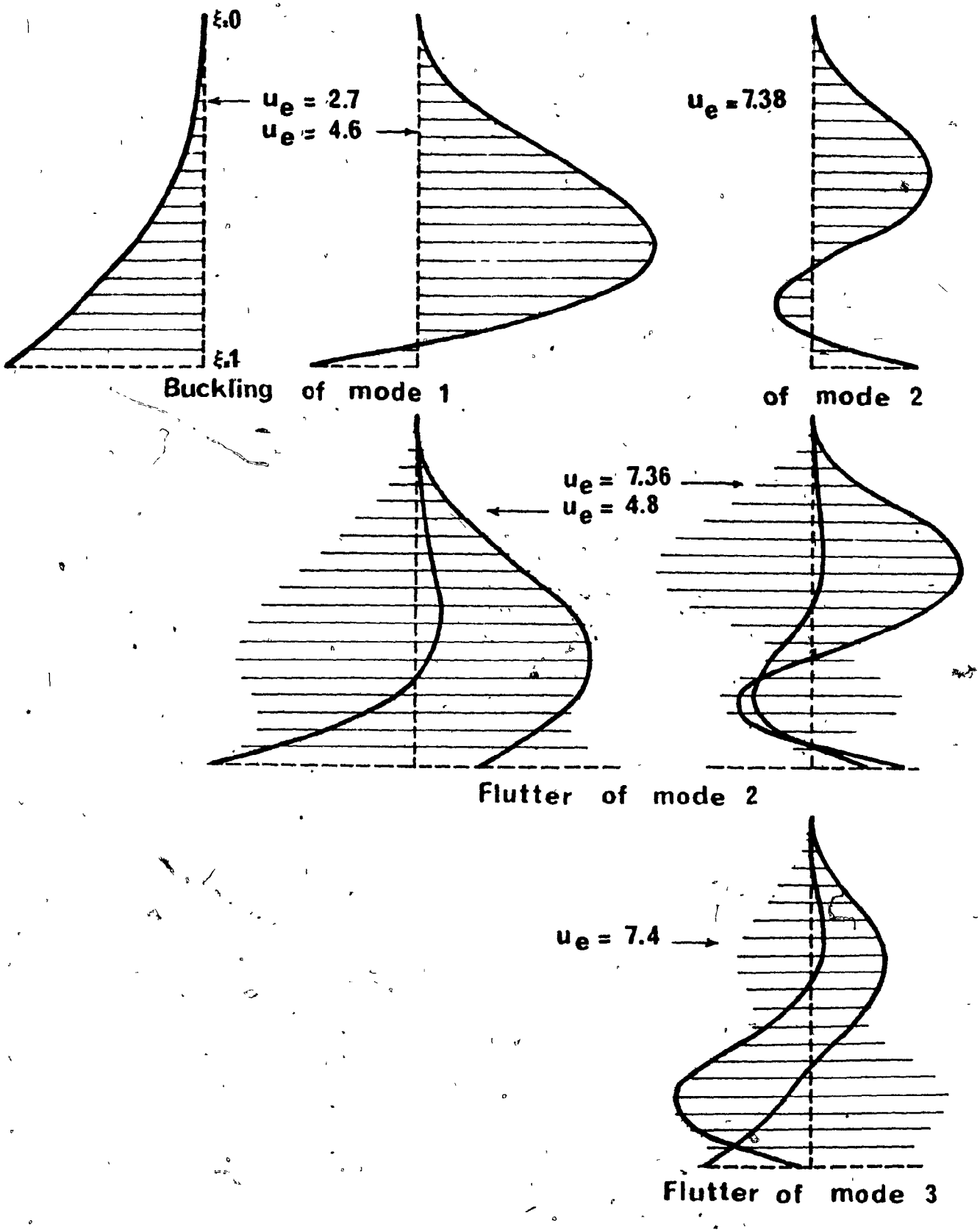

Fig.17 Modal shapes of a conical cantilevered beam computed at the threshold of the following instabilities: buckling of mode 1, flutter of mode 2 (lower and upper limits), buckling of mode 2 and flutter of mode 3 (parameters as in Fig.16).

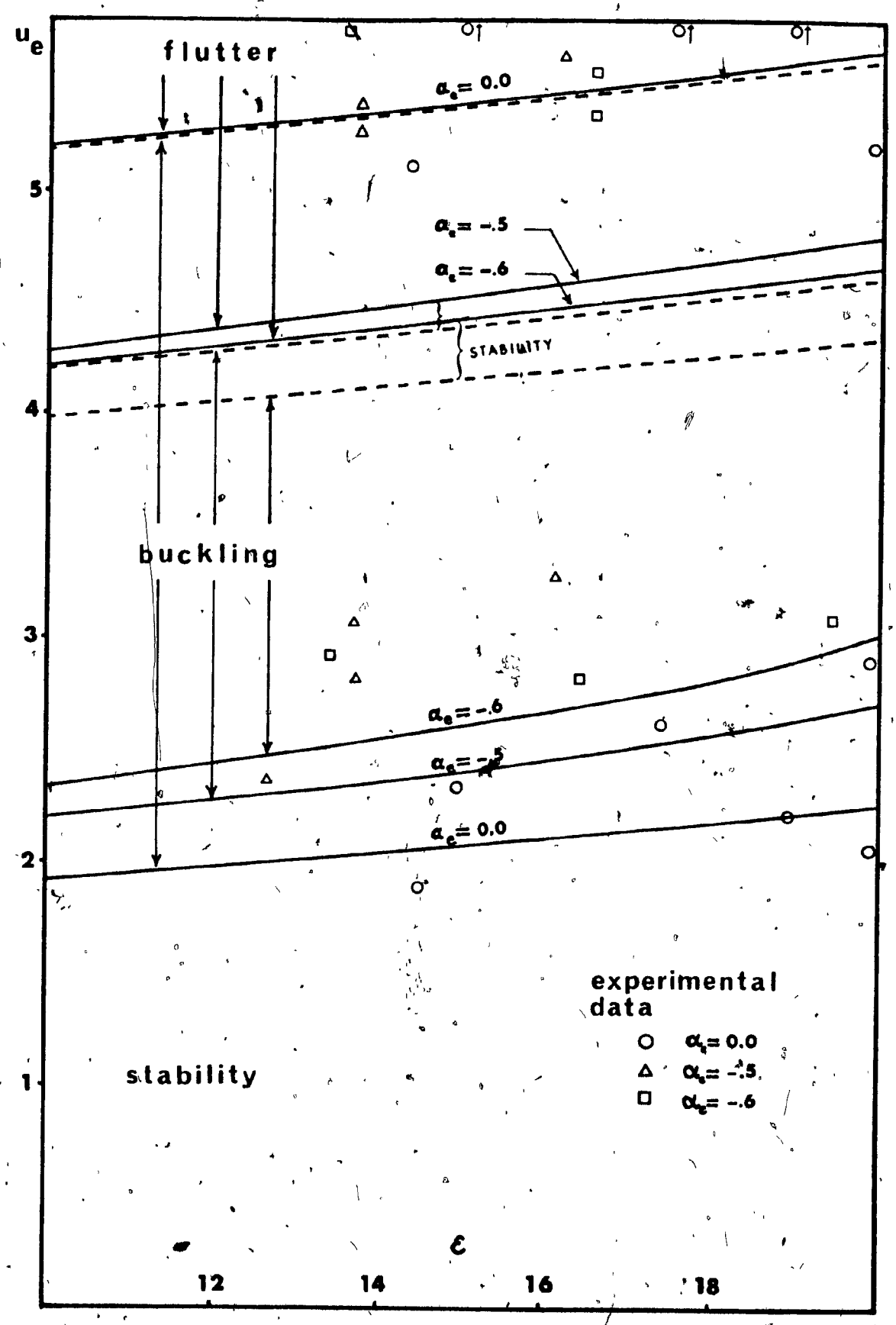

Fig.18 Influence of ε on the critical external flow velocities for three values of the taper ratio with $c_n=c_t=0.008$, $\varepsilon_o=10$, $\gamma_c=1.9$, $\gamma=0.0024$, $\chi_e=1.5$; comparison with the experiments.

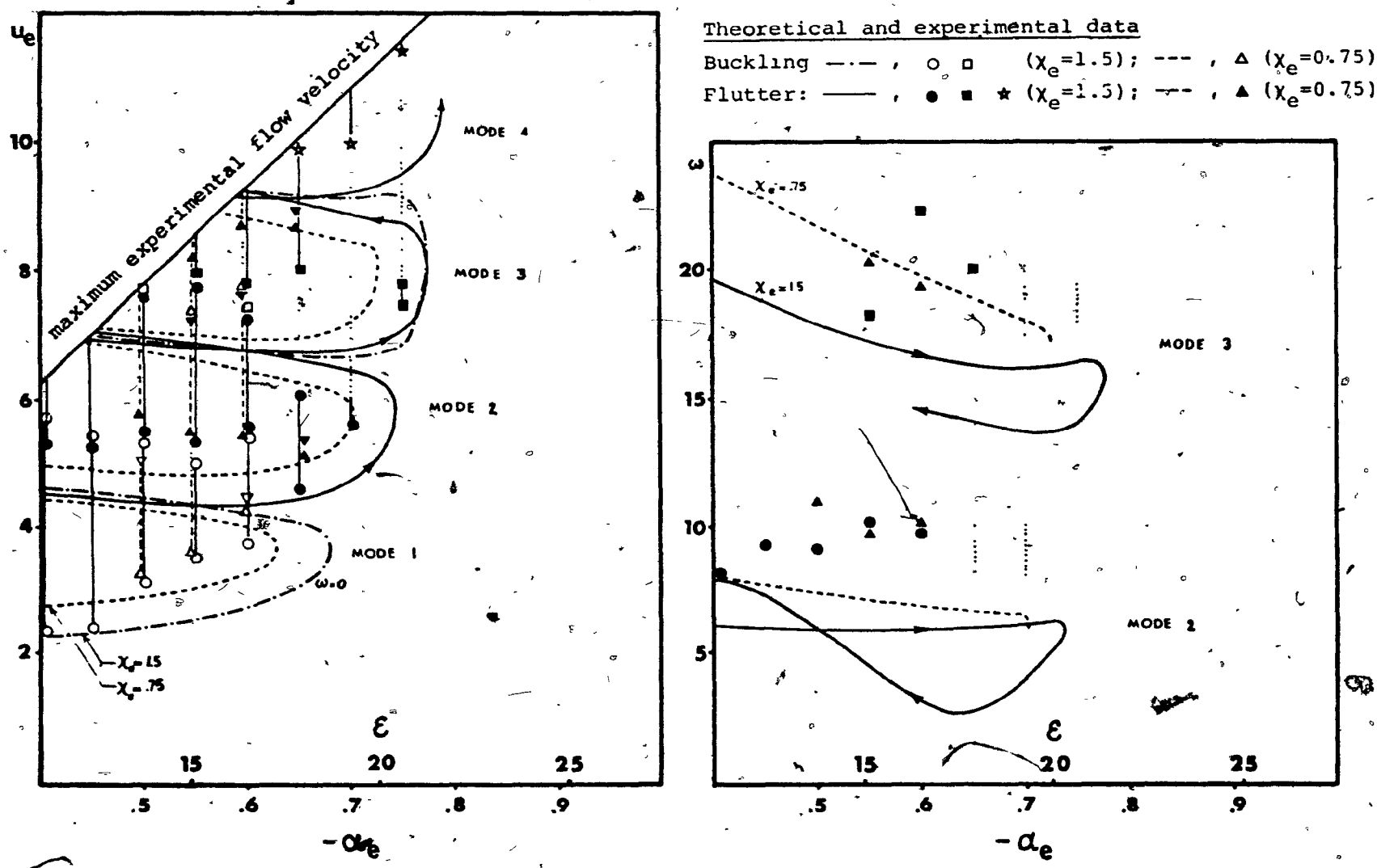

Fig.19 Diagrams of the critical flow velocities and frequencies of a conical beam truncated at various lengths, as functions of ε and $-\alpha_e$; other parameters: β_e=0.04, c_n=c_t=0.008, τ_o=10, γ_e=1.9, γ=0.0024, ν=0, χ_e=0.75 or 1.5; comparison with the experiments.

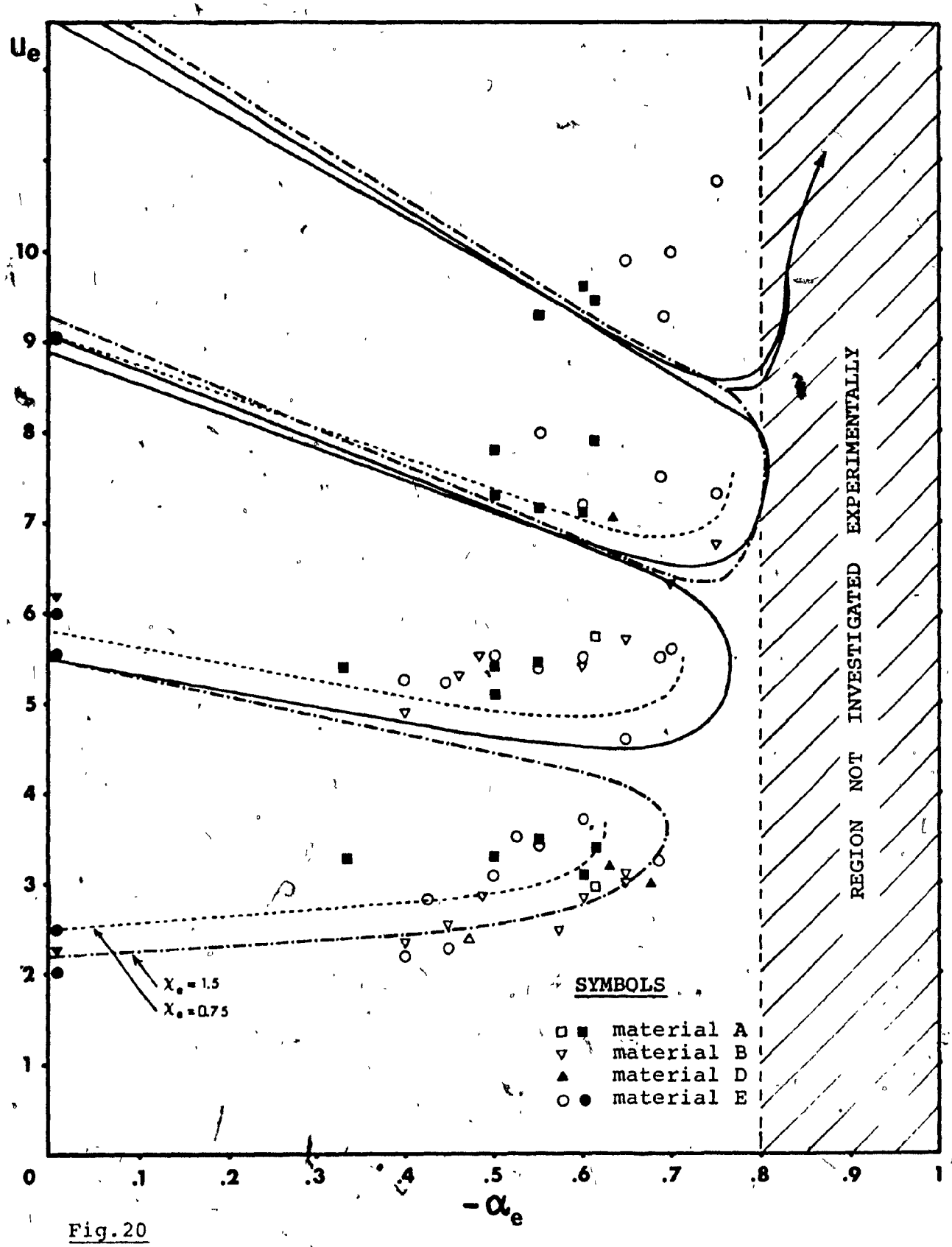

Fig.20

Effect of the truncation ratio, $-\alpha_e$, on the stability of conical beams. Comparison between the experimental data and the critical external flow velocities computed, assuming constant slenderness (ε=17), for two end pieces, i.e. χ_e=0.75 and χ_e=1.5. Other parameters: $c_n=c_t$=0.008, δ=0, ε_o=10, γ_e=1.9, γ=0.0024, $\mu=\nu$=0.

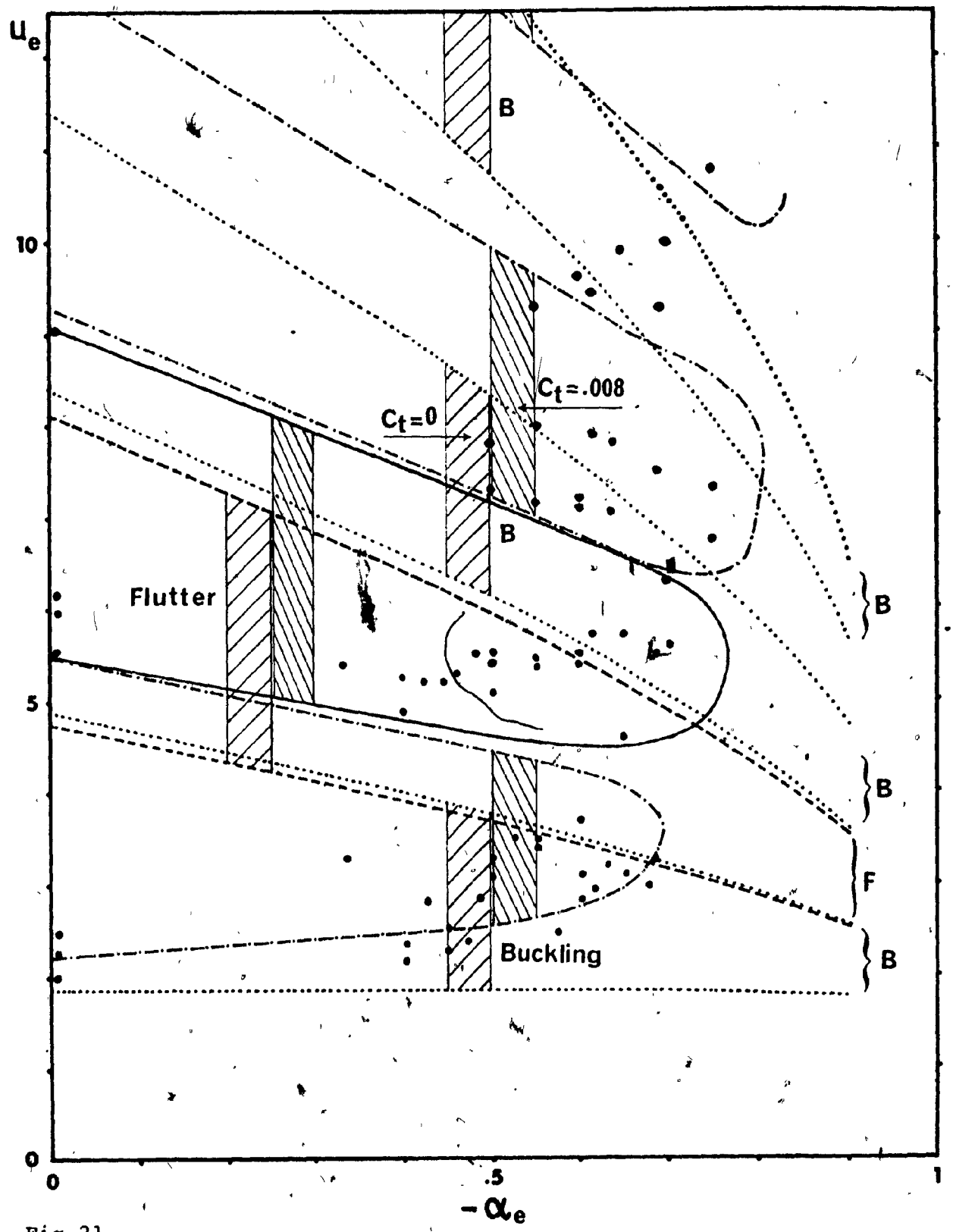

Fig.21

Effect of the boundary layer on the stability of conical beams of constant length (ε=17). Comparison between the experimental data and the critical external flow velocities of the three lower buckling and first flutter instabilities computed with c_t=0.008 and c_t=0 (zero thickness). Other parameters: c_n=0.008, ε_o=10, χ_e=1.5, γ_e=1.9, γ=0.0024, μ=ν=0.

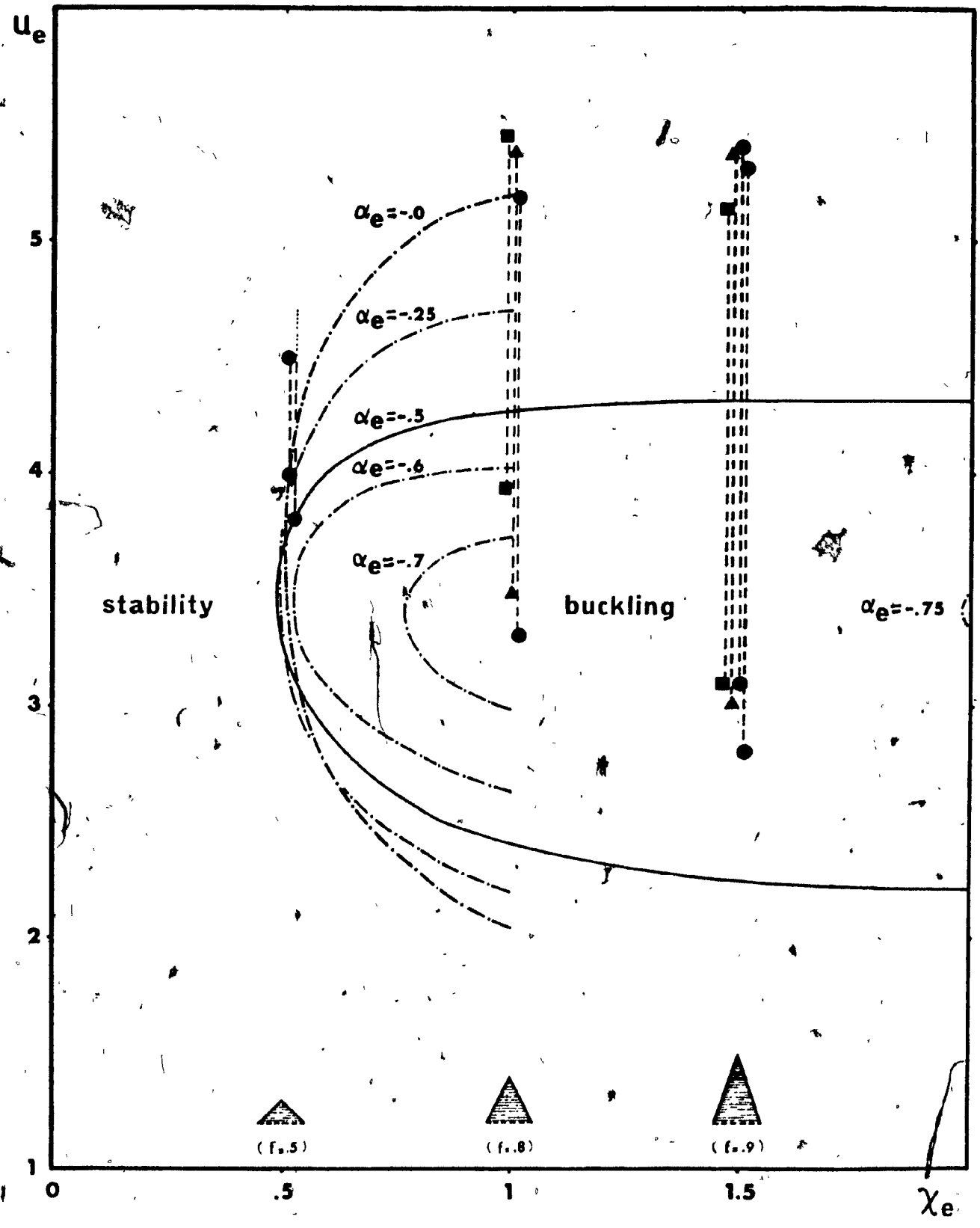

Fig.22

Effect of the size of the tapered end-piece on buckling for several conical horizontal cantilevered beams of equal length (c=14); comparison of experiments with theory for α_e=-0.5. Other parameters: c_n=c_t=0.008, ε_o=10, γ_e=1.9, γ=μ=ν=0.

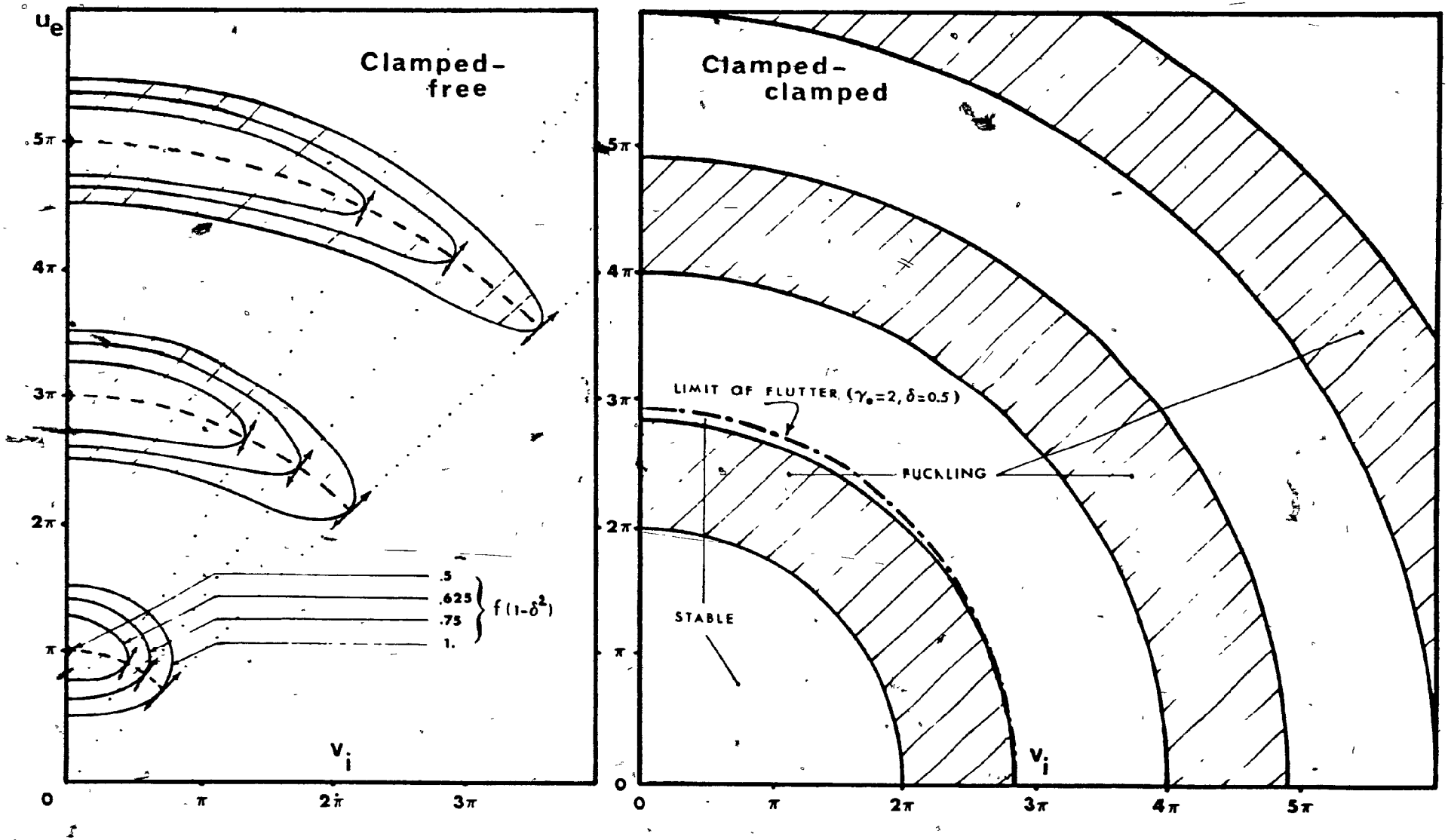

Fig. 23 Critical theoretical internal and external flow velocities for buckling of clamped-free and clamped-clamped tubular beams subject to flexural and hydrodynamic forces only ($c_n=c_t=\gamma=\theta=\nu=0$).

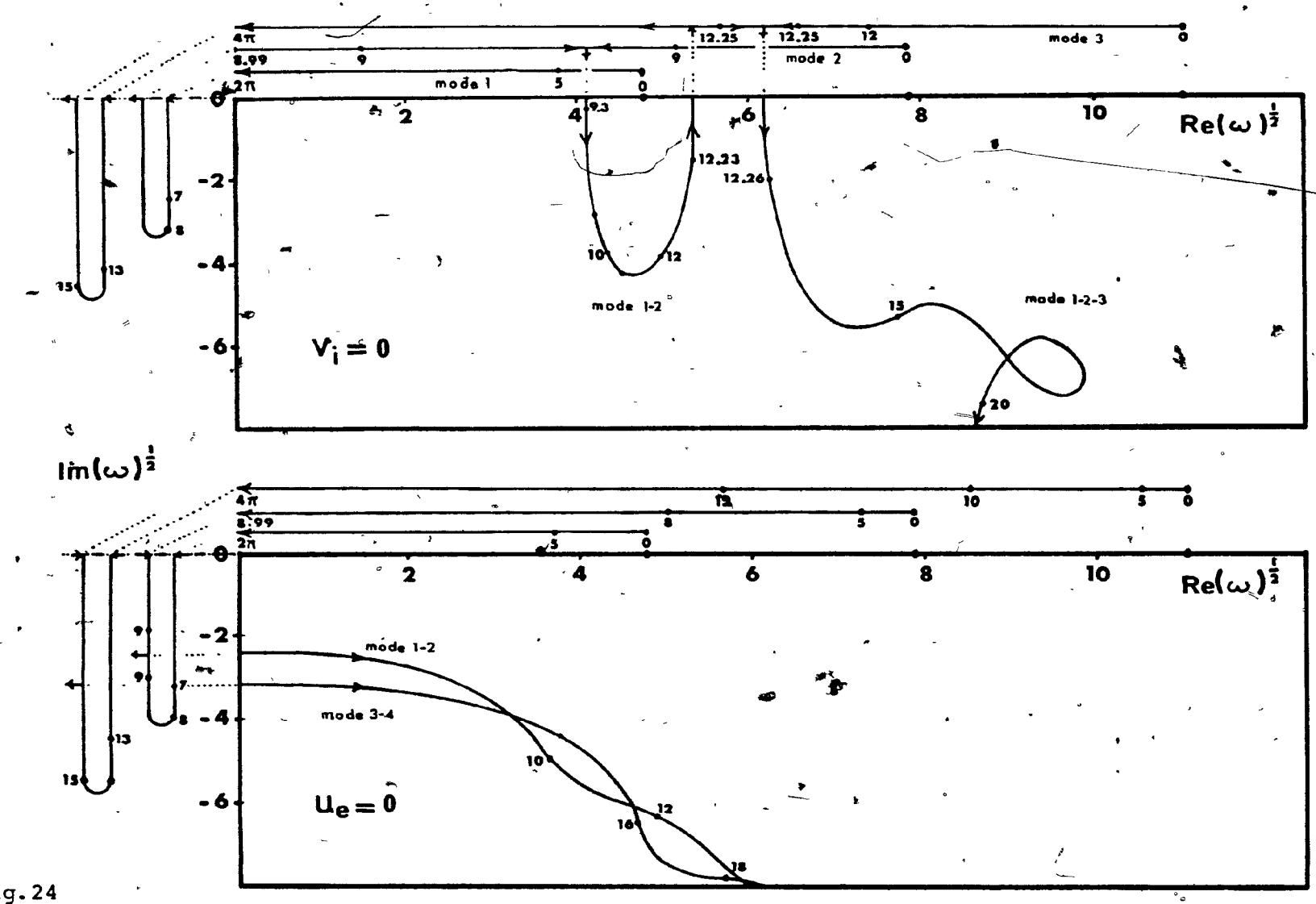

Fig.24

Complex frequency diagrams of a clamped-clamped tubular beam subject to flexural, hydrodynamic and inertial forces only ($c_n=c_t=\theta=\mu=\nu=\gamma_i=0$, $\gamma_e=2$, $\delta=0.5$), when either internal or external fluid is at rest.

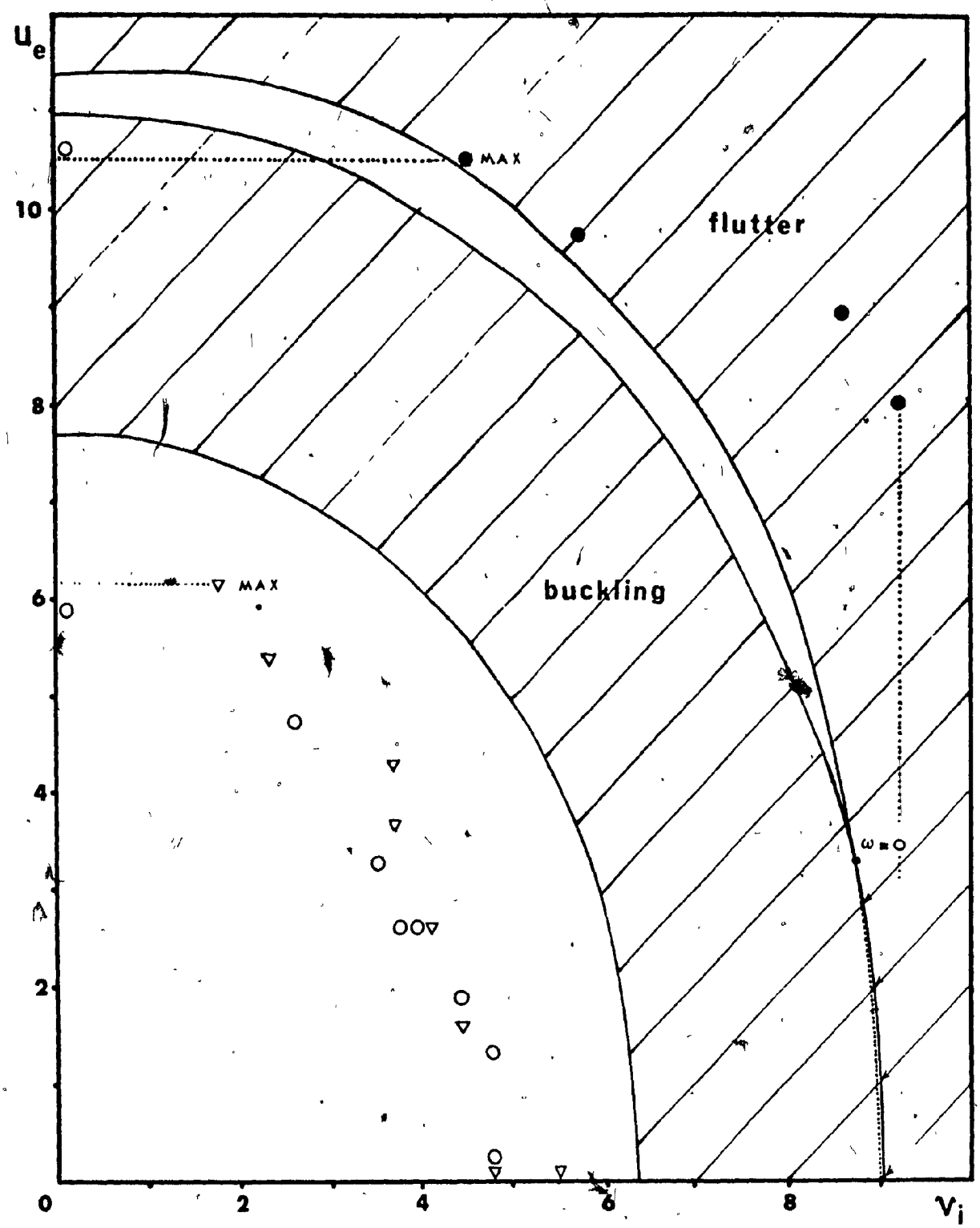

Fig.25 The effect of internal and external flow velocities on stability of clamped-clamped tubular beams; comparison of experiments with theory ($\alpha_e=\alpha_i=0$, $c_n=c_t=0.008$, $\varepsilon=18$, $c_o=10$, $\delta=0.5$, $\gamma_e=1.9$, $\gamma_i=0.03$, $\gamma=0.0024$, $\chi_e=\mu=\nu=0$).

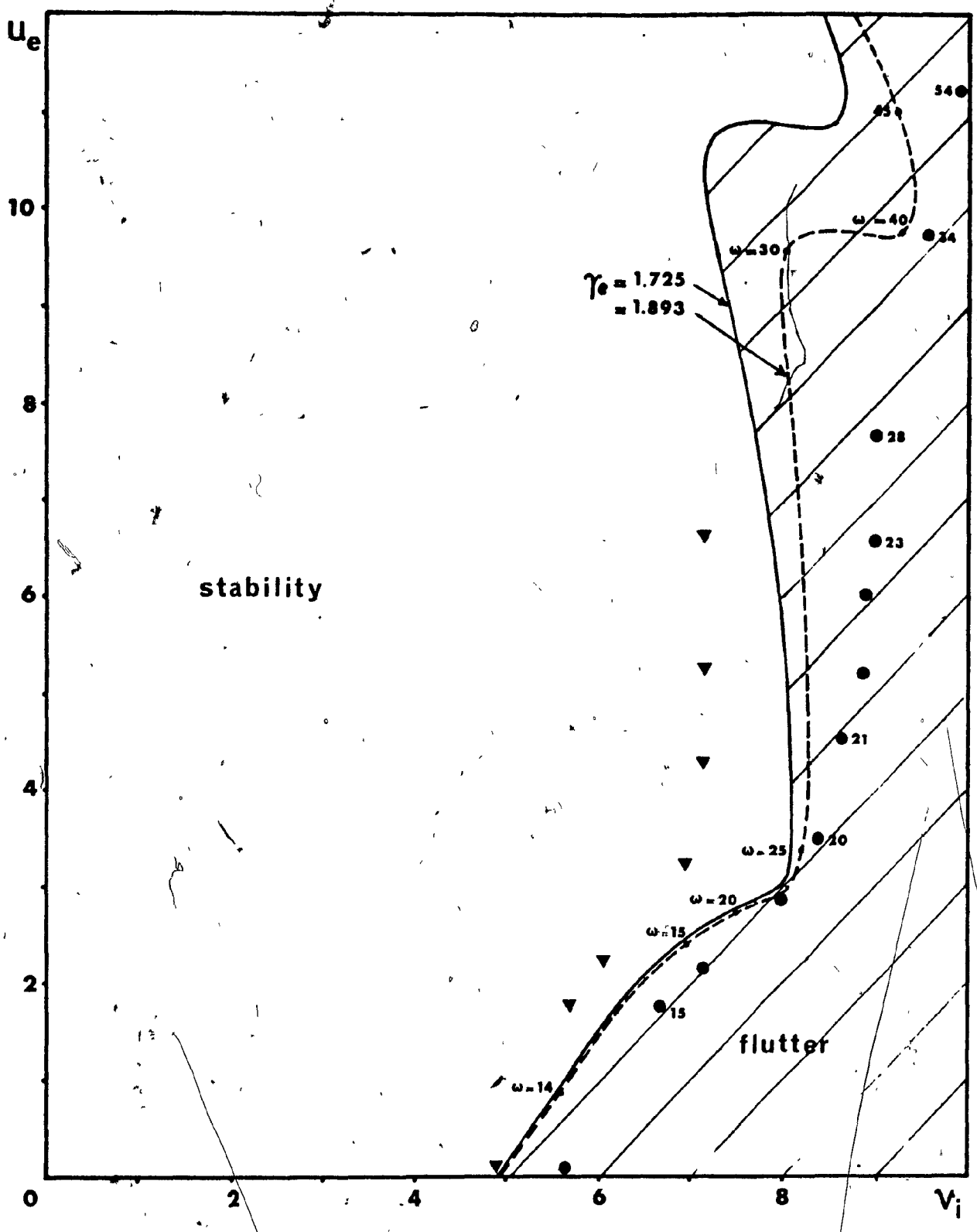

Fig.26 The effect of internal and external flow velocities on stability of cantilevered tubular beams with a blunt base; comparison of experiments with theory ($\alpha_c=\alpha_i=0$, $c_n=c_t=0.008$, $\varepsilon=20$, $\varepsilon_o=10$, $\delta=0.5$, $\chi_c=\mu=\nu=0$) for beams of two different materials, i.e. $\gamma_c=1.9, \gamma_i=-0.03, \gamma=0.0024$ (rubber E, ●) and $\gamma_c=1.7, \gamma_i=-0.07, \gamma=0.001$ (rubber B, ▼).

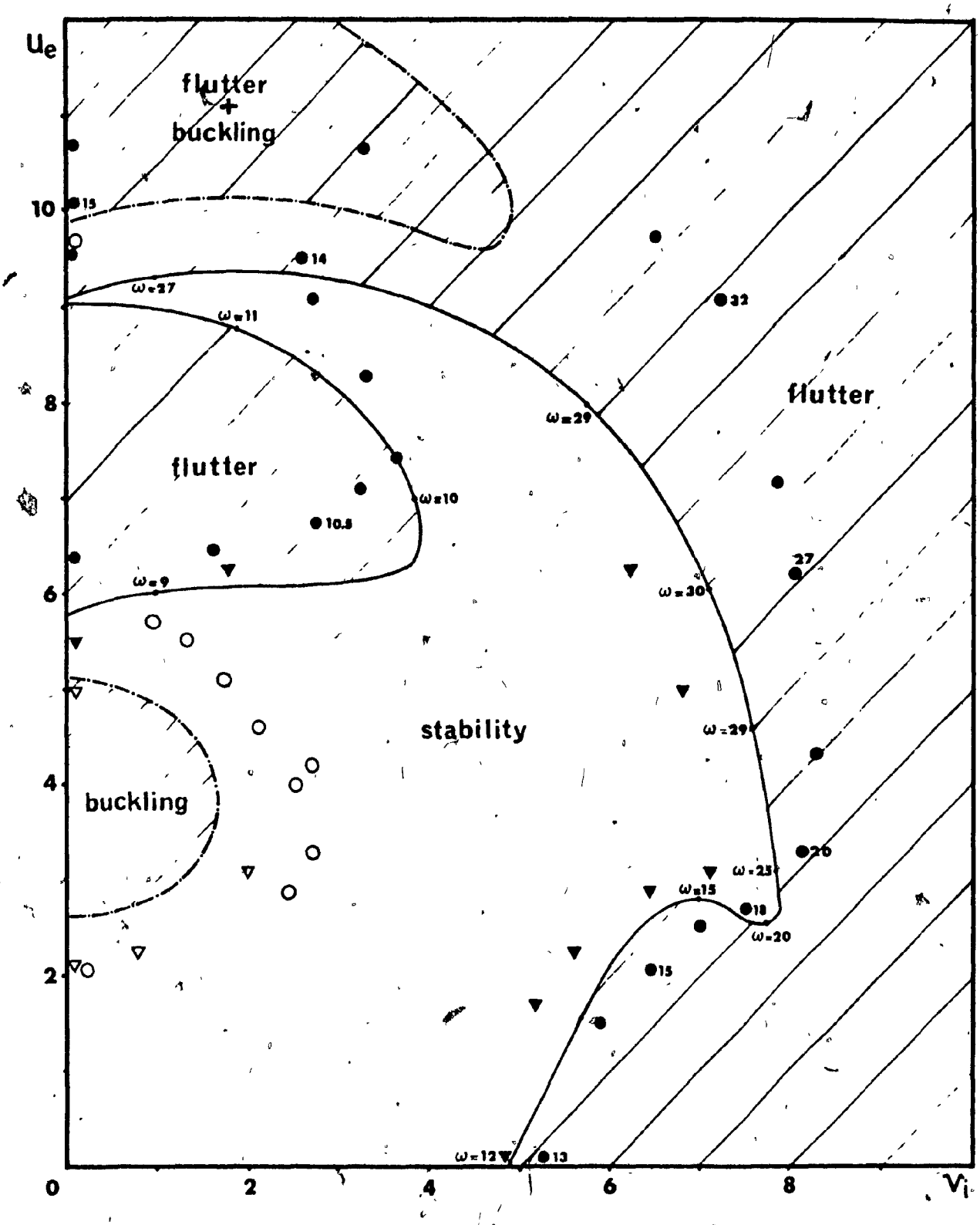

Fig.27 The effect of internal and external flow velocities on stability of cantilevered tubular beams with a tapered base; comparison of experiments with theory ($\alpha_e=\alpha_i=0$, $c_n=c_t=0.008$, $\chi_c=1$, $\varepsilon=19$, $\varepsilon_o=10$, $\delta=0.5$, $\mu=\nu=0$). Rubber B: ▽ (buckling) and ▼ (flutter); rubber E: ○ (buckling) and ● (flutter).

APPENDIX A

DIMENSIONAL ANALYSIS

APPENDIX A: DIMENSIONAL ANALYSIS

In this Appendix we shall render dimensionless the equation of motion and the boundary condition given by eq.(5.13), which were derived in the main text. To this end we shall define a number of dimensionless parameters; let the superscript ^{o} denote quantities at $x=0$, and let us define

$$\xi = x/L, \quad \eta = y/L, \quad \tau = \left[\frac{EI^{o}}{\Sigma\rho A^{o}}\right]^{\frac{1}{2}} \frac{t}{L^{2}} \quad \text{with} \quad \Sigma\rho A^{o} = \rho A^{o}+\rho_{e}A_{e}^{o}+\rho_{i}A_{i}^{o},$$

$$\sigma(\xi) = A/A^{o}, \quad \sigma_{e}(\xi) = A_{e}/A_{e}^{o}, \quad \sigma_{i}(\xi) = A_{i}/A_{i}^{o}, \quad j(\xi) = I/I^{o},$$

$$u_{i} = \left[\frac{\rho_{i}A_{i}^{o}}{EI^{o}}\right]^{\frac{1}{2}} U_{i}L, \quad u_{e} = \left[\frac{\rho_{e}A_{e}^{o}}{EI^{o}}\right]^{\frac{1}{2}} U_{e}L, \quad u_{e}^{*} = u_{e}\frac{A_{e}}{A_{e}^{*}}, \quad C_{f} = \left[\frac{\rho_{e}A_{e}^{o}}{EI^{o}}\right]^{\frac{1}{2}} U_{v}L.$$

which, substituted into equation (5.14), give

$$\rho A^{o}\sigma\frac{EI^{o}}{L^{3}\Sigma\rho A^{o}}\frac{\partial^{2}\eta}{\partial\tau^{2}} = -\frac{EI^{o}}{L^{3}}\left[1+\frac{k}{L^{2}}\left(\frac{EI^{o}}{\Sigma\rho A^{o}}\right)^{\frac{1}{2}}\frac{\partial}{\partial\tau}\right]\left\{\frac{\partial^{2}}{\partial\xi^{2}}\left(j\frac{\partial^{2}\eta}{\partial\xi^{2}}\right)\right\}$$

$$+\frac{\rho_{i}A_{i}^{o\,2}}{2\pi L^{2}}\sigma_{i}\frac{d\sigma_{i}}{d\xi}\left[\frac{EI^{o}}{L^{3}\Sigma\rho A^{o}}\frac{\partial^{3}\eta}{\partial\xi\partial\tau^{2}}+\frac{2u_{i}EI^{o}}{L^{3}(\rho_{i}A_{i}^{o}\Sigma\rho A^{o})^{\frac{1}{2}}}\frac{\partial^{3}\eta}{\partial\xi^{2}\partial\tau}+\frac{u_{i}^{2}EI^{o}}{L^{3}\rho_{i}A_{i}^{o}}\frac{\partial^{3}\eta}{\partial\xi^{3}}\right]$$

$$+\frac{\rho_{e}A_{e}^{o\,2}}{2\pi L^{2}}\sigma_{e}\frac{d\sigma_{e}}{d\xi}\left[\frac{EI^{o}}{L^{3}\Sigma\rho A^{o}}\frac{\partial^{3}\eta}{\partial\xi\partial\tau^{2}}+\frac{2u_{e}EI^{o}}{L^{3}(\rho_{e}A_{e}^{o}\Sigma\rho A^{o})^{\frac{1}{2}}}\frac{\partial^{3}\eta}{\partial\xi^{2}\partial\tau}+\frac{u_{e}^{2}EI^{o}}{L^{3}\rho_{e}A_{e}^{o}}\frac{\partial^{3}\eta}{\partial\xi^{3}}\right]$$

$$-\rho_{i}A_{i}^{o}\sigma_{i}\left[\frac{EI^{o}}{L^{3}\Sigma\rho A^{o}}\frac{\partial^{2}\eta}{\partial\tau^{2}}+\frac{2u_{i}EI^{o}}{L^{3}(\rho_{i}A_{i}^{o}\Sigma\rho A^{o})^{\frac{1}{2}}}\frac{\partial^{2}\eta}{\partial\xi\partial\tau}+\frac{u_{i}^{2}EI^{o}}{L^{3}\rho_{i}A_{i}^{o}}\frac{\partial^{2}\eta}{\partial\xi^{2}}\right]$$

$$-\rho_{e}A_{e}^{o}\sigma_{e}\left[\frac{EI^{o}}{L^{3}\Sigma\rho A^{o}}\frac{\partial^{2}\eta}{\partial\tau^{2}}+\frac{(u_{e}+u_{e}^{*})EI^{o}}{L^{3}(\rho_{e}A_{e}^{o}\Sigma\rho A^{o})^{\frac{1}{2}}}\frac{\partial^{2}\eta}{\partial\xi\partial\tau}+\frac{u_{e}u_{e}^{*}EI^{o}}{L^{3}\rho_{e}A_{e}^{o}}\frac{\partial^{2}\eta}{\partial\xi^{2}}\right]$$

$$-\rho_{e}A_{e}^{o}\frac{d\sigma_{e}}{d\xi}\left[\frac{u_{e}^{*}EI^{o}}{L^{3}(\rho_{e}A_{e}^{o}\Sigma\rho A^{o})^{\frac{1}{2}}}\frac{\partial\eta}{\partial\tau}+\frac{u_{e}u_{e}^{*}EI^{o}}{L^{3}\rho_{e}A_{e}^{o}}\frac{\partial\eta}{\partial\xi}\right]-\left[\rho A^{o}\sigma+\rho_{i}A_{i}^{o}\sigma_{i}-\rho_{e}A_{e}^{o}\sigma_{e}\right]g\frac{\partial\eta}{\partial\xi}$$

$$+\frac{T_{1}}{L}\frac{\partial^{2}\eta}{\partial\xi^{2}}-\frac{\rho_{e}D_{e}\sigma_{e}^{\frac{1}{2}}}{2L^{2}}\left\{\frac{EI^{o}}{(\rho_{e}A_{e}^{o}\Sigma\rho A^{o})^{\frac{1}{2}}}(C_{fn}u_{e}+C_{f})\frac{\partial\eta}{\partial\tau}+\frac{EI^{o}}{\rho_{e}A_{e}^{o}}C_{fn}u_{e}^{2}\frac{\partial\eta}{\partial\xi}\right\},$$

where we kept the label T_{1} for the expression given in eq.(5.3).

We next divide the previous equation by $\frac{EI^o}{L^3}$, expand $T_1(\xi)$ and set

$$\nu = \left[\frac{EI^o}{\Sigma\rho A^o}\right]^{\frac{1}{2}} \frac{k}{L^2}, \quad \Gamma = \frac{\rho A_e^o}{EI^o} gL^3, \quad \Theta = \frac{T_1(L)L^2}{EI^o},$$

and we now obtain

$$\left\{\frac{\rho A^o\sigma+\rho_i A_i\sigma_i+\rho_e A_e^o\sigma_e}{\Sigma\rho A^o}\right\}\frac{\partial^2\eta}{\partial\tau^2} - \left\{\frac{\rho_i(A_i^o)^2\sigma_i}{2\pi L^2\Sigma\rho A^o}\frac{d\sigma_i}{d\xi} + \frac{\rho_e(A_e^o)^2\sigma_e}{2\pi L^2\Sigma\rho A^o}\frac{d\sigma_e}{d\xi}\right\}\frac{\partial^3\eta}{\partial\xi\partial\tau^2}$$

$$+ \left\{2\left[\frac{\rho_i A_i^o}{\Sigma\rho A^o}\right]^{\frac{1}{2}} u_i\sigma_i + \left[\frac{\rho_e A_e^o}{\Sigma\rho A^o}\right]^{\frac{1}{2}} (u_e+u_e^*)\sigma_e\right\}\frac{\partial^2\eta}{\partial\xi\partial\tau}$$

$$- \left\{\left[\frac{\rho_i A_i}{\Sigma\rho A^o}\right]^{\frac{1}{2}} \frac{A_i^o u_i\sigma_i}{\pi L^2}\frac{d\sigma_i}{d\xi} + \left[\frac{\rho_e A_e^o}{\Sigma\rho A^o}\right]^{\frac{1}{2}} \frac{A_e^o u_e\sigma_e}{\pi L^2}\frac{d\sigma_e}{d\xi}\right\}\frac{\partial^3\eta}{\partial\xi^2\partial\tau}$$

$$+ \left\{\sigma_i u_i^2+\sigma_e u_e u_e^*\right\}\frac{\partial^2\eta}{\partial\xi^2} - \left\{\frac{A_i^o u_i^2\sigma_i}{2\pi L^2}\frac{d\sigma_i}{d\xi} + \frac{A_e^o u_e^2\sigma_e}{2\pi L^2}\frac{d\sigma_e}{d\xi}\right\}\frac{\partial^3\eta}{\partial\xi^3} \qquad (A.1)$$

$$+ u_e^*\frac{d\sigma_e}{d\xi}\left\{\left[\frac{\rho_e A_e^o}{\Sigma\rho A^o}\right]^{\frac{1}{2}}\frac{\partial\eta}{\partial\tau} + u_e\frac{\partial\eta}{\partial\xi}\right\} + \Gamma\frac{\rho A^o\sigma+\rho_i A_i^o\sigma_i-\rho_e A_e^o\sigma_e}{\rho A_e^o}\frac{\partial\eta}{\partial\xi}$$

$$- \left\{\Theta+\sigma_i u_i[u_i-u_i(1)] + \int_1^\xi\left[\Gamma\frac{\rho_e A_e^o\sigma_e-\rho_i A_i^o\sigma_i-\rho A^o\sigma}{\rho A_e^o} - \frac{2\sigma_e^{\frac{1}{2}}L}{\pi D_e^o}C_{ft}u_e^2\right]d\xi\right\}\frac{\partial^2\eta}{\partial\xi^2}$$

$$+ \frac{\sigma_e^{\frac{1}{2}}}{2}\left\{\left[\frac{4\rho_e L^2}{\pi\Sigma\rho A^o}\right]^{\frac{1}{2}}(C_{fn}u_e+C_f)\frac{\partial\eta}{\partial\tau} + \frac{4L}{\pi D_e^o}C_{fn}u_e^2\frac{\partial\eta}{\partial\xi}\right\} + (1+\nu\frac{\partial}{\partial\tau})\frac{\partial^2}{\partial\xi^2}(j\frac{\partial^2\eta}{\partial\xi^2}) = 0 .$$

We next consider the boundary condition given by eq.(5.13). Dividing it by $\frac{EI^o}{L^2}$ we obtain the following, valid at $\xi=1$:

$$\left\{(\rho+f\rho_e)S_e + (\rho_i-\rho)A_i^o\sigma_i\right\}\frac{\ell}{L\Sigma\rho A^o}\left[\frac{\partial^2\eta}{\partial\tau^2}\right] - f\rho_e\frac{A_e^o\sigma_e-A_i^o\sigma_i}{(\rho_e A_e^o)^{\frac{1}{2}}(\Sigma\rho A^o)^{\frac{1}{2}}}u_e^*\left[\frac{\partial\eta}{\partial\tau}\right]$$

$$+ \left\{f\rho_e\frac{A_i^o\sigma_i u_e^*+S_e u_e}{(\rho_e A_e^o)^{\frac{1}{2}}} + \frac{2\rho_i A_i^o u_i\sigma_i}{(\rho_i A_i^o)^{\frac{1}{2}}}\right\}\frac{\ell}{L(\Sigma\rho A^o)^{\frac{1}{2}}}\left[\frac{\partial^2\eta}{\partial\xi\partial\tau}\right] - j(1+\nu\frac{\partial}{\partial\tau})\left[\frac{\partial^3\eta}{\partial\xi^3}\right] \qquad (A.2)$$

$$- \left\{f\rho_e u_e^* u_e\frac{A_e^o\sigma_e-A_i^o\sigma_i}{\rho_e A_e^o} + \Gamma\frac{\ell}{L}\left[\frac{\rho_e-\rho}{\rho}\frac{S_e}{A_e^o} + \frac{\rho-\rho_i}{\rho}\frac{A_i^o}{A_e^o}\sigma_i\right]\right\}\left[\frac{\partial\eta}{\partial\xi}\right] = 0.$$

We next proceed to simplify the form of eqs.(A.1) and (A.2) further. Defining

$$v_i = u_i\sigma_i,\quad \delta^2 = \frac{A_i^o}{A_e^o},\quad \gamma_e = 1 + \frac{\rho_e}{\rho},\quad \gamma_i = \left(\frac{\rho_i}{\rho} - 1\right)\delta^2,\quad \varepsilon = \frac{L}{D_e^o} = \left[\frac{\pi L^2}{4A_e^o}\right]^{\frac{1}{2}}$$

the coefficients of eq.(A.1) may now be expressed as follows:

$$\frac{\rho A^o\sigma+\rho_i A_i^o\sigma_i+\rho_e A_e^o\sigma_e}{\Sigma\rho A^o} = \frac{(\rho+\rho_e)A_e^o\sigma_e+(\rho_i-\rho)A_i^o\sigma_i}{(\rho+\rho_e)A_e^o + (\rho_i-\rho)A_i^o} = \frac{\gamma_e\sigma_e+\gamma_i\sigma_i}{\gamma_e+\gamma_i},$$

$$\frac{\rho_i A_i^o}{\Sigma\rho A^o} = \frac{(\rho_i/\rho)(A_i^o/A_e^o)}{\gamma_e+\gamma_i} = \frac{\delta^2+\gamma_i}{\gamma_e+\gamma_i},\quad \frac{\rho_e A_e^o}{\Sigma\rho A^o} = \frac{\gamma_e-1}{\gamma_e+\gamma_i},\quad \frac{\rho A_e^o}{\Sigma\rho A^o} = \frac{1}{\gamma_e+\gamma_i},$$

$$\frac{A_i^o}{2\pi L^2} = \frac{\delta^2}{8\varepsilon^2},\qquad \frac{A_e^o}{2\pi L^2} = \frac{1}{8\varepsilon^2},$$

$$\frac{\rho A^o\sigma+\rho_i A_i^o\sigma_i-\rho_e A_e^o\sigma_e}{\rho A_e^o} = \frac{(\rho-\rho_e)A_e^o\sigma_e+(\rho_i-\rho)A_i^o\sigma_i}{\rho A_e^o} = (2-\gamma_e)\sigma_e + \gamma_i\sigma_i,$$

$$j = \frac{I}{I_o} = \frac{D_e^4-D_i^4}{(D_e^o)^4-(D_i^o)^4} = \frac{(A^o)^2\sigma_e^2-(A_i^o)^2\sigma_i^2}{(A_e^o)^2-(A_i^o)^2} = \frac{\sigma_e^2-\delta^4\sigma_i^2}{1-\delta^4}.$$

Similarly, in connection with eq.(A.2) let us define

$$\chi_e = \frac{\ell}{D_e(1)},$$

$$\chi = \frac{\ell}{L} = \frac{\ell}{D_e(1)}\frac{D_e(1)}{D_e(0)}\frac{D_e(0)}{L} = \chi_e\sigma_e^{\frac{1}{2}}(1)\frac{1}{\varepsilon},$$

$$s_e = \frac{S_e}{A_e^o} = \frac{1}{3A_e^o}\frac{[A_e^o\sigma_e(1)]^{\frac{3}{2}} - [A_i^o\sigma_i(1)]^{\frac{3}{2}}}{[A_e^o\sigma_e(1)]^{\frac{1}{2}} - [A_i^o\sigma_i(1)]^{\frac{1}{2}}} = \frac{1}{3}\frac{\sigma_e(1)^{\frac{3}{2}} - \delta^3\sigma_i(1)^{\frac{3}{2}}}{\sigma_e(1)^{\frac{1}{2}} - \delta\sigma_i(1)^{\frac{1}{2}}}.$$

Equation (A.1) now becomes

$$\frac{\gamma_e\sigma_e+\gamma_i\sigma_i}{\gamma_e+\gamma_i}\frac{\partial^2\eta}{\partial\tau^2} - \{\frac{\delta^2+\gamma_i}{\gamma_e+\gamma_i}\frac{\delta^2\sigma_i}{8\varepsilon^2}\frac{d\sigma_i}{d\xi} + \frac{\gamma_e-1}{\gamma_e+\gamma_i}\frac{\sigma_e}{8\varepsilon^2}\frac{d\sigma_e}{d\xi}\}\frac{\partial^3\eta}{\partial\xi\partial\tau^2}$$

$$+ \{2[\frac{\delta^2+\gamma_i}{\gamma_e+\gamma_i}]^{\frac{1}{2}} v_i + [\frac{\gamma_e-1}{\gamma_e+\gamma_i}]^{\frac{1}{2}}(u_e+u_e^*)\sigma_e\}\frac{\partial^2\eta}{\partial\xi\partial\tau}$$

$$- \{[\frac{\delta^2+\gamma_i}{\gamma_e+\gamma_i}]^{\frac{1}{2}}\frac{\delta^2 v_i}{4\varepsilon^2}\frac{d\sigma_i}{d\xi} + [\frac{\gamma_e-1}{\gamma_e+\gamma_i}]^{\frac{1}{2}}\frac{u_e\sigma_e}{4\varepsilon^2}\frac{d\sigma_e}{d\xi}\}\frac{\partial^3\eta}{\partial\xi^2\partial\tau}$$

$$+ \{\sigma_e u_e u_e^* + \frac{v_i^2}{\sigma_i(1)} - \Theta + \int_1^\xi [\Gamma(2-\gamma_e)\sigma_e+\Gamma\gamma_i\sigma_i + \frac{2\varepsilon}{\pi}\sigma_e^{\frac{1}{2}} C_{ft}u_e^2]d\xi\}\frac{\partial^2\eta}{\partial\xi^2}$$

$$- \{\frac{\delta^2 v_i^2}{8\varepsilon^2\sigma_i}\frac{d\sigma_i}{d\xi} + \frac{\sigma_e u_e^2}{8\varepsilon^2}\frac{d\sigma_e}{d\xi}\}\frac{\partial^3\eta}{\partial\xi^3} + \Gamma[(2-\gamma_e)\sigma_e+\gamma_i\sigma_i]\frac{\partial\eta}{\partial\xi} \qquad \text{(A.3)}$$

$$+ u_e^*\frac{d\sigma_e}{d\xi}[(\frac{\gamma_e-1}{\gamma_e+\gamma_i})^{\frac{1}{2}}\frac{\partial\eta}{\partial\tau} + u_e\frac{\partial\eta}{\partial\xi}] + (1+\nu\frac{\partial}{\partial\tau})\frac{\partial^2}{\partial\xi^2}\{\frac{\sigma_e^2-\delta^4\sigma_i^2}{1-\delta^4}\frac{\partial^2\eta}{\partial\xi^2}\}$$

$$+ \frac{2\varepsilon}{\pi}\sigma_e^{\frac{1}{2}}\{(\frac{\gamma_e-1}{\gamma_e+\gamma_i})^{\frac{1}{2}}[C_{fn}u_e+C_f]\frac{\partial\eta}{\partial\tau} + C_{fn}u_e^2\frac{\partial\eta}{\partial\xi}\} = 0 .$$

From eq. (5.10) and upon introducing $\Pi = \frac{T_o L^2}{EI^o}$, we write

$$\Theta = \Pi + \tfrac{1}{2}C_{fe}\sigma_e(1)u_e^2 + \tfrac{1}{2}C_{fi}\frac{v_i^2}{\sigma_i(1)} + \tfrac{1}{2}C_{fx}[\frac{\sigma_e(1)}{\sigma_i(1)}]^{\frac{1}{2}} u_e v_i \ , \qquad \text{(A.4)}$$

and, accordingly, for free or supported downstream ends, we have

a) for free end: $\Pi = \chi\Gamma[(2-\gamma_e)s_e + \gamma_i\sigma_i(1)]$

(*vide* Appendix H)

$$C_{fe} = 1.35\ [9 + (2\chi_e)^3]^{-1},$$

$$C_{fi} = 0.016\ [1 + (2\chi_e)^{\frac{1}{2}}]^{-1},$$

$$C_{fx} = 0.05(0.1 + \chi_e)(0.05+\chi_e)^{-1} ;$$

b) for supported end: (as from eq.(5.9))

$$\Pi = T_o L^2/EI^o,$$

$$C_{fe} = -\alpha_e' \frac{2\varepsilon}{\pi} C_{ft},$$

$$C_{fi} = 2\alpha_i',$$

$$C_{fx} = 0 .$$

The boundary condition at $\xi=1$ for a free end given by eq.(A.2) may be written in its final form

$$\frac{[1+f(\gamma_e-1)]s_e+\gamma_i\sigma_i}{\gamma_e+\gamma_i}\chi[\frac{\partial^2\eta}{\partial\tau^2}] - fu_e^*(\frac{\gamma_e-1}{\gamma_e+\gamma_i})^{\frac{1}{2}}(\sigma_e-\delta^2\sigma_i)[\frac{\partial\eta}{\partial\tau}]$$

$$+ \{f(s_e u_e+\delta^2\sigma_i u_e^*)(\frac{\gamma_e-1}{\gamma_e+\gamma_i})^{\frac{1}{2}} + 2v_i(\frac{\delta^2+\gamma_i}{\gamma_e+\gamma_i})^{\frac{1}{2}}\}\chi[\frac{\partial^2\eta}{\partial\xi\partial\tau}] - (1+\nu\frac{\partial}{\partial\tau})\frac{\sigma_e^2-\delta^4\sigma_i^2}{1-\delta^4}[\frac{\partial^3\eta}{\partial\xi^3}]$$

$$- \{fu_e u_e^*[\sigma_e-\delta^2\sigma_i] + \Gamma[(\sigma_e-2)s_e - \gamma_i\sigma_i]\chi\}[\frac{\partial\eta}{\partial\xi}] = 0 . \qquad (A.5)$$

Finally, denoting

$$c_n = \frac{2}{\pi} C_{fn}, \quad c_t = \frac{2}{\pi} C_{ft} \text{ and } c_v = \frac{2}{\pi} C_f ,$$

the differential equation may be written in its final dimensionless form

$$\frac{\gamma_e\sigma_e+\gamma_i\sigma_i}{\gamma_e+\gamma_i}\frac{\partial^2\eta}{\partial\tau^2} - \{\frac{\delta^2+\gamma_i}{\gamma_e+\gamma_i}\frac{\delta^2\sigma_i}{8\varepsilon^2}\frac{d\sigma_i}{d\xi} + \frac{\gamma_e-1}{\gamma_e+\gamma_i}\frac{\sigma_e}{8\varepsilon^2}\frac{d\sigma_e}{d\xi}\}\frac{\partial^3\eta}{\partial\xi\partial\tau^2}$$

$$+ \{2[\frac{\delta^2+\gamma_i}{\gamma_e+\gamma_i}]^{\frac{1}{2}}v_i + [\frac{\gamma_e-1}{\gamma_e+\gamma_i}]^{\frac{1}{2}}(u_e+u_e^*)\sigma_e\}\frac{\partial^2\eta}{\partial\xi\partial\tau}$$

$$- \{[\frac{\delta^2+\gamma_i}{\gamma_e+\gamma_i}]^{\frac{1}{2}}\frac{\delta^2 v_i}{4\varepsilon^2}\frac{d\sigma_i}{d\xi} + [\frac{\gamma_e-1}{\gamma_e+\gamma_i}]^{\frac{1}{2}}\frac{u_e\sigma_e}{4\varepsilon^2}\frac{d\sigma_e}{d\xi}\}\frac{\partial^3\eta}{\partial\xi^2\partial\tau}$$

$$+ \{u_e u_e^* \sigma_e + \frac{v_i^2}{\sigma_i(1)} - \Theta - \int_\xi^1 \{\Gamma[(2-\gamma_e)\sigma_e + \gamma_i \sigma_i] + \varepsilon c_t u_e^2 \sigma_e^{\frac{1}{2}}\} d\xi\} \frac{\partial^2 \eta}{\partial \xi^2}$$

$$\pm \{\frac{\delta^2 v_i^2}{8\varepsilon^2 \sigma_i} \frac{d\sigma_i}{d\xi} + \frac{\sigma_e u_e^2}{8\varepsilon^2} \frac{d\sigma_e}{d\xi}\} \frac{\partial^3 \eta}{\partial \xi^3} + \Gamma[(2-\gamma_e)\sigma_e + \gamma_i \sigma_i] \frac{\partial \eta}{\partial \xi} \qquad \text{(A.6)}$$

$$+ u_e^* \frac{d\sigma_e}{d\xi} \{(\frac{\gamma_e - 1}{\gamma_e + \gamma_i})^{\frac{1}{2}} \frac{\partial \eta}{\partial \tau} + u_e \frac{\partial \eta}{\partial \xi}\} + (1 + \nu \frac{\partial}{\partial \tau}) \frac{\partial^2}{\partial \xi^2} \{\frac{\sigma_e^2 - \delta^4 \sigma_i^2}{1 - \delta^4} \frac{\partial^2 \eta}{\partial \xi^2}\}$$

$$+ \varepsilon \sigma_e^{\frac{1}{2}} \{[\frac{\gamma_e - 1}{\gamma_e + \gamma_i}]^{\frac{1}{2}} (c_n u_e + c_v) \frac{\partial \eta}{\partial \tau} + c_n u_e^2 \frac{\partial \eta}{\partial \xi}\} = 0 .$$

APPENDIX B

SOLUTION OF THE DIFFERENTIAL EQUATION IN TERMS OF AN EIGENVALUE MATRIX EQUATION

APPENDIX B: SOLUTION OF THE DIFFERENTIAL EQUATION IN TERMS OF AN EIGENVALUE MATRIX EQUATION.

Within the next pages we shall develop a new technique to solve differential equations of the form

$$\sum_{r=0}^{M} f_r(\xi,\omega)\,\psi^{(r)}(\xi) = 0 \qquad \text{(B.1)}$$

involving M linear boundary conditions at $\xi=0$ and 1,

$$\sum_{r=0}^{M-1} g_r^j(\omega)\,\psi^{(r)}(\xi_j) = 0 \text{ with } j=1 \text{ to } M \qquad \text{(B.2)}$$

and $\xi_j=0$ or 1.

B.1 SOLUTION BY SERIES

A classical approach to the resolution of such eigenvalue problems is to investigate solutions in terms of series of real admissible functions; we would thus set

$$\psi(\xi) = \sum_{n=0}^{\infty} a_n \phi_n(\xi),$$

where the a's are complex coefficients. Assuming the series and its derivatives to be absolutely convergent, we then write

$$\psi^{(r)}(\xi) = \sum_{n=0}^{\infty} a_n \phi_n^{(r)}(\xi)$$

and then expand in series the terms of the differential equation as follows:

$$f_r(\xi,\omega)\,\phi_n^{(r)}(\xi) = \sum_{p=0}^{\infty} b_{np}^r(\omega)\,\phi_p(\xi) \ ,$$

so that the initial differential equation now becomes

$$\sum_{r=0}^{M} \sum_{n=0}^{\infty} a_n \sum_{p=0}^{\infty} b_{np}^{r}(\omega)\,\phi_r(\xi) = 0 \;.$$

For orthogonal comparison functions, the previous equation is finally equivalent to the following homogeneous linear system:

$$\sum_{n=0}^{\infty} \left\{ \sum_{r=0}^{M} b_{np}^{r}(\omega) \right\} a_n = 0 \quad (p = 0, +\infty) \;.$$

In previous work, mainly power series and uniform-beam eigenfunction series had been used [50],[66]; however, slow convergence of the a's must be expected from the power series, as shown later in section B.5; and by extension, any series of polynomials, such as shifted Chebyshev polynomials (cf. [68]), is also likely to lead to problems of convergence; on the other hand, the satisfactory convergence obtained through uniform-beam eigenfunctions deteriorates quickly as we depart either from a uniform shape or zero-flow boundary conditions (poor convergence of the b_{np}^{r} coefficients).

B.2 SOLUTION BY FOURIER SERIES

In searching for a proper set of comparison functions, the next simplest alternative appeared to be Fourier series, which are obviously easy to differentiate and can be expected to require relatively few terms in order to match actual modal shapes; yet, in order to satisfy distinct boundary conditions at $\xi=0$ and $\xi=1$, these Fourier series will be required to have a periodicity

greater than 1. We finally opted to express the solution in terms of Fourier series of periodicity 2 as follows:

$$\Psi(\xi) = \sum_{-\infty}^{\infty} a_n \frac{e^{in\pi\xi}}{\sqrt{2}},$$

and we have $$a_n = \int_0^2 \Psi(\xi) \frac{e^{-in\pi\xi}}{\sqrt{2}} d\xi.$$

Yet, $\Psi(\xi)$ only needs to satisfy the differential equation in the domain $0 \leq \xi \leq 1$. By choosing a periodicity of 2, instead of 1, we may require Ψ, Ψ' ... $\Psi^{(k)}$ ... to be continuous over $0 \leq \xi \leq 2$, and $\Psi^{(k)}(0) = \Psi^{(k)}(2)$ for any value of k, so that, if we expand the derivative of order k as

$$\Psi^{(k)}(\xi) = \sum_{-\infty}^{\infty} a_n^k \frac{e^{in\pi\xi}}{\sqrt{2}}$$

then we simply have

$$a_n^k = (in\pi)^k a_n.$$

Let it be noted that such simple relations could not have been obtained had the periodicity of Ψ been chosen equal to 1, because of the discontinuity of Ψ or its derivatives at both ends of the inteval $0<\xi<1$. Moreover, the continuity of Ψ and its derivatives will also obviously improve the convergence of the solution as illustrated in the two diagrams on the next page, (these two diagrams illustrate the periodic solutions for the first mode of a cantilevered beam clamped at x=0 and free at x=1).

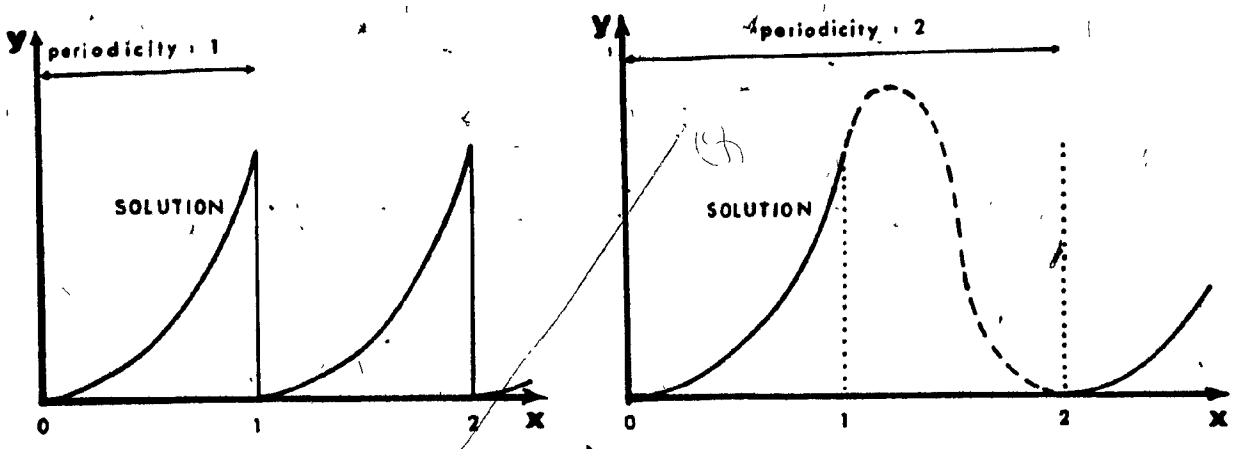

Once $\Psi, \Psi' \ldots \Psi^{(M)}$ have been replaced in (B.1) and (B.2) by their respective Fourier expansions, we obtain

$$D[\xi,\omega] = \sum_{r=0}^{M} f_r(\xi,\omega) \sum_{n=-\infty}^{\infty} (in\pi)^r a_n \frac{e^{in\pi\xi}}{\sqrt{2}} = 0,$$

and $$b_j(\omega) = \sum_{r=0}^{M-1} g_r^j(\omega) \sum_{n=-\infty}^{\infty} (in\pi)^r a_n \frac{e^{in\pi\xi}}{\sqrt{2}} j = 0, \quad j=1,\ldots M.$$

We then proceed as in the Galerkin method to eliminate ξ from the former equation by equating to zero the following coefficients, calculated over the interval $0<\xi<1$ of application of the expression $D(\xi,\omega)$,

$$d_p = \int_0^1 \sqrt{2}\, D(\xi,\omega) e^{ip\pi\xi}\, d\xi = 0, \quad p\ [-\infty,+\infty].$$

As pointed out in a previous paper [69], it is only necessary to set $d_{2p}=0$, but less coefficients were ultimately required when we added the conditions $d_{2p+1}=0$. The differential equation and its boundary conditions have now been replaced by an infinite homogenous system of equations, linear with respect to the a's and dependent upon ω.

It will now be convenient (for computing purposes) to switch back to real eigenfunctions with complex coefficients by setting

$$\Psi(\xi) = \sum_{n=0}^{\infty} (\gamma_{2n-1}\sin n\pi\xi + \gamma_{2n}\cos n\pi\xi)/\sqrt{2}. \qquad (B.3)$$

The correspondence between the γ's and the a's is

$$\gamma_{2n} = a_n + a_{-n},$$
$$\gamma_{2n-1} = i(a_n - a_{-n}). \qquad (B.4)$$

In order to have these relations and the following equations also valid for n=0 we shall break a_o into two equal components, i.e. $a_{+o}=a_{-o}=\frac{1}{2}a_o$; hence we shall have $\gamma_o=a_o$ & $\gamma_{-1}=0$.

We then calculate

$$D_{2p} = d_p+d'_{-p} = \sum_{r=0}^{M}\sum_{n=0}^{\infty} (in\pi)^r\{a_n\int_0^1 2\, f_r(\xi,\omega)\cos p\pi\xi\, e^{in\pi\xi}d\xi +$$
$$(-1)^r a_{-n}\int_o^1 2\, f_r(\xi,\omega)\cos p\pi\xi\, e^{-in\pi\xi}d\xi\}$$

and

$$D_{2p-1} = i(d'_{-p}-d_p),$$

which is derived from D_{2p} by substituting sin $p\pi\xi$ instead of cos $p\pi\xi$. We now set

$$D_{2p} = \sum_{r=0}^{M}\sum_{n=0}^{\infty} C^r_{pn}$$
$$D_{2p-1} = \sum_{r=0}^{M}\sum_{n=0}^{\infty} S^r_{pn}, \qquad (B.5)$$

with

$$C^r_{pn} = (in\pi)^r\{a_n\int_o^1 2f_r(\xi,\omega)\cos\ p\pi\xi\ e^{in\pi\xi}d\xi$$

$$+ (-1)^r a_{-n}\int_o^1 2f_r(\xi,\omega)\cos\ p\pi\xi\ e^{-in\pi\xi}d\xi\} ,$$

$$S^r_{pn} = (in\pi)^r\{a_n\int_o^1 2f_r(\xi,\omega)\sin\ p\pi\xi\ e^{in\pi\xi}d\xi$$

$$+ (-1)^r a_{-n}\int_o^1 2f_r(\xi,\omega)\sin\ p\pi\xi\ e^{-in\rho\xi}d\xi\} .$$

These constants may be expressed in the form

$$C^r_{pn} = (in\pi)^r\{[a_n+(-1)^r a_{-n}]FCC^r_{pn} + i[a_n-(-1)^r a_{-n}]FCS^r_{pn}\} ,$$

$$S^r_{pn} = (in\pi)^r\{[a_n+(-1)^r a_{-n}]FSC^r_{pn} + i[a_n-(-1)^r a_{-n}]FSS^r_{pn}\} ,$$

with

$$FCC^r_{pn} = \int_o^1 2f_r(\xi,\omega)\cos\ p\pi\xi\cos\ n\pi\xi\ d\xi ,$$

$$FCS^r_{pn} = \int_o^1 2f_r(\xi,\omega)\cos\ p\pi\xi\sin\ n\pi\xi\ d\xi ,$$

$$FSC^r_{pn} = \int_o^1 2f_r(\xi,\omega)\sin\ p\pi\xi\cos\ n\pi\xi\ d\xi = FCS^r_{np} , \qquad (B.6)$$

$$FSS^r_{pn} = \int_o^1 2f_r(\xi,\omega)\sin\ p\pi\xi\sin\ n\pi\xi\ d\xi ,$$

the evaluation of which reduces to the computation of the following two types of integrals:

$$\int_0^1 f_r(\xi,\omega)\cos k\pi\xi d\xi \quad \text{and} \quad \int_0^1 f_r(\xi,\omega)\sin k\pi\xi d\xi ,$$

where k takes on the values $p + n$ or $p - n$.

According to the parity of r we have two cases,

a) if $r = 2s$

$$(i)^r[a_n+(-1)^r a_{-n}] = (-1)^s \gamma_{2n} ,$$

$$(i)^{r+1}[a_n-(-1)^r a_{-n}] = (-1)^s \gamma_{2n-1} ,$$

and accordingly

$$C^r_{pn} = (-1)^s (n\pi)^r [\gamma_{2n} FCC^r_{pn} + \gamma_{2n-1} FCS^r_{pn}] ,$$

$$S^r_{pn} = (-1)^s (n\pi)^r [\gamma_{2n} FSC^r_{pn} + \gamma_{2n-1} FSS^r_{pn}] ;$$

b) if $r = 2s+1$

$$(i)^r[a_n+(-1)^r a_{-n}] = (-1)^s \gamma_{2n-1} ,$$

$$(i)^{r+1}[a_n-(-1)^r a_{-n}] = -(-1)^s \gamma_{2n} ,$$

and, accordingly,

$$C^r_{pn} = (-1)^s (n\pi)^r [\gamma_{2n-1} FCC^r_{pn} - \gamma_{2n} FCS^r_{pn}] ,$$

$$S^r_{pn} = (-1)^s (n\pi)^r [\gamma_{2n-1} FSC^r_{pn} - \gamma_{2n} FSS^r_{pn}] .$$

B.3 THE EIGENVALUE MATRIX EQUATION

For the purpose of solving our specific differential equation, where M=4, we finally end up with the following system, consisting of (a) two boundary conditions at each end, which yield

$$\sum_{n=0}^{\infty} \{[g_i^o - (n\pi)^2 g_i^2]\gamma_{2n} + n\pi[g_i^1 - (n\pi)^2 g_i^3]\gamma_{2n-1}\} = 0,$$

at $\xi = 0$, for $i = 1,2$, and

$$\sum_{n=0}^{\infty} (-1)^n\{[g_i^o - (n\pi)^2 g_i^2]\gamma_{2n} + n\pi[g_i^1 - (n\pi)^2 g_i^3]\gamma_{2n-1}\} = 0$$

at $\xi = 1$, for $i = 3,4$,

and (b) the following equations to represent the differential equation:

$$D_{2p-1} = \sum_{n=0}^{\infty} \{[FSS_{pn}^o + n\pi FSC_{pn}^1 - (n\pi)^2 FSS_{pn}^2 - (n\pi)^3 FSC_{pn}^3 + (n\pi)^4 FSS_{pn}^4]\gamma_{2n-1}$$
$$+[FSC_{pn}^o - n\pi FSS_{pn}^1 - (n\pi)^2 FSC_{pn}^2 + (n\pi)^3 FSS_{pn}^3 + (n\pi)^4 FSC_{pn}^4]\gamma_{2n}\} = 0,$$

$$D_{2p} = \sum_{n=0}^{\infty} \{[FCS_{pn}^o + n\pi FCC_{pn}^1 - (n\pi)^2 FCS_{pn}^2 - (n\pi)^3 FCC_{pn}^3 + (n\pi)^4 FCS_{pn}^4]\gamma_{2n-1}$$
$$+[FCC_{pn}^o - n\pi FCS_{pn}^1 - (n\pi)^2 FCC_{pn}^2 + (n\pi)^3 FCS_{pn}^3 + (n\pi)^4 FCC_{pn}^4]\gamma_{2n}\} = 0.$$

The calculation of the FCC, FCS, FSC, FSS and g coefficients is performed in Appendix C. This system will now be represented by the matrix equation

$$[A][\Gamma] = [0]$$

with $[\Gamma] = \begin{bmatrix} \gamma_o \\ \gamma_i \\ \gamma_n \end{bmatrix}$ and $[A] =$ a matrix whose 4 rows of boundary conditions are followed by the rows $p = 0$, $p = 1$, ..., $p = m$.

We next solve the equation $\det[A] = 0$ to obtain the eigenfrequencies, and then determine $[\Gamma]$ and the modal shapes if required.

B.4 STANDARDIZATION OF THE SOLUTIONS

Since the system is linear and homogeneous, any solution vector $[\Gamma^*]$ is defined within a complex constant factor. We set $\gamma_o^* = 1$ and compute the corresponding solution set (provided $\gamma_o = 0$ is not a solution) and then calculate a complex factor which both normalizes $\Psi(\xi)$ and sets $\Psi(0)$ real. These two steps are elaborated upon in (i) and (ii) below.

(i) Although Ψ should be normalized on $0<\xi<1$, for purposes of comparing the various solutions, i.e. by setting

$$\int_0^1 \Psi\bar{\Psi}d\xi = 1 \ , \qquad (B.7)$$

it will be much easier to set

$$\int_0^2 \Psi\bar{\Psi}d\xi = 2 \ , \qquad (B.8)$$

even though eq.(B.7) will no longer be satisfied for most cases. From the computed vector $[\Gamma^*]$ we then calculate

$$N^2 = \frac{1}{2}\int_0^2 \sum_{-\infty}^{n=\infty}\sum_{-\infty}^{p=\infty} \frac{1}{2} a_n^{*-*} a_p e^{i(n-p)\pi\xi} d\xi = \frac{1}{2}\sum_{-\infty}^{n=\infty} a_n^{*-*} a_n ,$$

which, by use of eq.(B.4), becomes

$$N^2 = \frac{1}{2}[\gamma_o^{*-*}\gamma_o + \sum_{p=1}^{\infty} \frac{\gamma_p^{*-*}\gamma_p}{2}] = \frac{1}{2} + \sum_{p=1}^{\infty} \frac{\gamma_p^{*-*}\gamma_p}{4} ,$$

and the previously computed solution $\Psi^*(\xi)$ must be divided by N; hence by use of eq.(B.3), the amplitude-normalized solution becomes

$$\Psi_1(\xi) = \frac{\Psi^*(\xi)}{N} = \frac{1 + \sum_{n=1}^{\infty} [\gamma_{2n-1}^* \sin(n\pi\xi) + \gamma_{2n}^* \cos(n\rho\xi)]}{[1 + \sum_{p=1}^{\infty} \frac{\gamma_p^* \bar{\gamma}_p^*}{2}]^{\frac{1}{2}}} .$$

(ii) We may express $\Psi_1(\xi)$ in terms of a real amplitude function $\zeta(\xi)$ and a real phase angle function $\phi_1(\xi)$ as follows:

$$\Psi_1(\xi) = \zeta(\xi)\, e^{i\phi_1(\xi)} .$$

Whereas in the previous step we normalized $\zeta(\xi)$, we now wish to standardize the phase functions in order to obtain a zero phase angle at $\xi = 0$. Hence, we need to apply to $\Psi_1(\xi)$ a correcting factor $e^{-i\phi_o}$, where ϕ_o will be given by

$$\tan\phi_o = \lim_{\xi \to 0} \frac{\mathrm{Im}\{\Psi_1(\xi)\}}{\mathrm{Re}\{\Psi_1(\xi)\}} .$$

If we now have $\Psi_1(0) = \Psi_1'(0) = \ldots = \Psi_1^{(p-1)}(0) = 0$ and $\Psi_1^{(p)}(0) \neq 0$ then, when $\xi \to 0$, a MacLaurin's expansion yields

$$\Psi_1(\xi) \sim \frac{\xi^p}{p!} \Psi_1^{(p)}(\xi)$$

(for example, the boundary conditions for a clamped beam yield $p = 2$, since $\Psi_1(0) = \Psi_1'(0) = 0$), and therefore

$$\tan \phi_0 = \frac{\mathrm{Im}\{\Psi_1^{(p)}(0)\}}{\mathrm{Re}\{\Psi_1^{(p)}(0)\}} = \frac{\sum_0^\infty n^p \mathrm{Im}\{\gamma_{2n+m}\}}{\sum_0^\infty n^p \mathrm{Re}\{\gamma_{2n+m+1}\}},$$

with $m = 0$ if p is even,

$m = -1$ if p is odd,

as obtained upon differentiating (B.3) for $\xi = 0$.

B.5 COMPARISON BETWEEN FOURIER AND POWER SERIES IN SOLVING THE BEAM EQUATION

In this section we apply the new method of solution to the beam eigenvalue problem for which closed-form solutions are available. We shall first consider the solution of this problem by power series, and shall discuss the convergence of such series. Then, the solution will be obtained by the new method and its efficiency will be compared to the power series solution.

B.5.1 Solution by power series; analysis of convergence

We consider the beam eigenvalue problem

$$y^{(4)}(x) = \lambda^4 y(x) \tag{B.9}$$

to which we seek absolutely convergent solutions of the form

$$y(x) = \sum_{0}^{\infty} a_n x^n \qquad \text{over} \qquad 0 \leq x \leq 1,$$

where the a_n's are thus given by Taylor's expansion

$$a_n = [y^{(n)}(x)/n!]_{x=0} .$$

Now, differentiating eq.(B.9) n-4 times gives

$$y^{(n)} = \lambda^4 y^{(n-4)};$$

hence

$$a_n = [\frac{y^{(n)}}{(n)!}]_{x=0} = [\frac{\lambda^4 y^{(n-4)}}{(n)!}]_{x=0} = \frac{\lambda^4 a_{n-4} \times (n-4)!}{(n)!}$$

and then

$$a_n = \frac{\lambda^4}{n(n-1)(n-2)(n-3)} a_{n-4} . \qquad \text{(B.10)}$$

All coefficients can thus be expressed in terms of the first four as follows:

$$a_{4p} = \frac{\lambda^{4p}}{(4p)!} a_o; \quad a_{4p+1} = \frac{\lambda^{4p}}{(4p+1)!} a_1;$$

$$a_{4p+2} = \frac{\lambda^{4p}}{(4p+2)!} (2a_2); \quad a_{4p+3} = \frac{\lambda^{4p}}{(4p+3)!}(6a_3) .$$

One may notice that if λ is large, the magnitude of the coefficients goes through a maximum and then goes to zero as p increases. (in eq.(B.10) the ratio a_n/a_{n-4} is smaller than 1 if $n>\lambda+2$, and greater than 1 if $n<\lambda+1$).

B.5.1.a Truncation error

Let us now study the convergence of the theoretical series (i.e. with infinite number of terms) at x=1,

$$y(1) = \sum_{p=0}^{\infty} \lambda^{4p} \left[\frac{a_o}{(4p)!} + \frac{a_1}{(4p+1)!} + \frac{2a_2}{(4p+2)!} + \frac{6a_3}{(4p+3)!}\right].$$

If we truncate the expansion at N = 4n, the error made in evaluating the first sum associated with coefficient a_o is

$$\varepsilon_o = a_o \sum_{p=n}^{\infty} \frac{\lambda^{4p}}{(4p)!} = a_o \frac{\lambda^{4n}}{(4n)!} \left[1 + \frac{\lambda^4 (4n)!}{(4n+4)!} + \ldots\right].$$

If we set

$$q_{4n} = (4n+4)(4n+3)(4n+2)(4n+1),$$

we have

$$\varepsilon_o = a_o \frac{\lambda^{4n}}{(4n)!} \left[1 + \frac{\lambda^4}{q_{4n}} + \frac{\lambda^8}{q_{4n} \cdot q_{4n+4}} + \ldots\right];$$

hence ε_o is bounded as follows:

$$a_o \frac{\lambda^{4n}}{(4n)!} < \varepsilon_o < a_o \frac{\lambda^{4n}}{(4n)!} \left[1 + \frac{\lambda^4}{q_{4n}} + \left(\frac{\lambda^4}{q_{4n}}\right)^2 + \ldots\right] = \frac{a_o \lambda^{4n}}{(4n)! \left(1 - \frac{\lambda^4}{q_{4n}}\right)}.$$

The condition $\lambda < 4n$ usually yields $\lambda^4 \ll q_{4n}$; hence

$$\varepsilon_o \sim \frac{a_o \lambda^{4n}}{(4n)!}.$$

Finally, the total error for estimating y(1) is

$$\delta_{4n} = \varepsilon_o + \varepsilon_1 + \varepsilon_2 + \varepsilon_3 \simeq \lambda^{4n} \sum_{k=0}^{3} \frac{(k)! a_k}{(4n+k)!}. \qquad (B.11)$$

B.5.1.b. Magnitude of coefficients

As previously mentioned, the size of the a_n's reaches a maximum for some value of n depending upon λ_r. If we assume n to be large, from equation (B.10) we obtain

$$\frac{a_n}{a_{n-4}} \sim \frac{\lambda^4}{(n-1.5)^4} = \left[\frac{\lambda}{n-1.5} \right]^4 ;$$

hence, each of the four series of a_n's, related to a_o, a_1, a_2, a_3 respectively will start decreasing when n becomes larger than a value n_1 which is approximately

$$n_1 \sim 1.5 + \lambda . \qquad (B.12)$$

In each series the maximum value of a_{4p+k} will be

$$a_{4p_1+k} = \frac{\lambda^{4p_1}}{(4p_1+k)!}\, k!\, a_k \qquad (B.13)$$

with k = 0, 1, 2, 3 for each series, and $4(p_1+1)+k > \lambda + 1.5 > 4p_1+k$.

If λ is large, equation (B.13) may be transformed and expressed in terms of λ and k alone. By use of Stirling's formula we obtain

$$(4p_1+k)! \sim \sqrt{2\pi}\, e^{-(4p_1+k)}\, (4p_1+k)^{4p_1+k+1/2} ,$$

and we set

$$4p_1+k = \lambda+\mu$$

where, because of eq. (B.12), μ satisfies

$$1.5 > \mu > -2.5 ;$$

hence, assuming $\mu << \lambda$ yields

$$(4p_1+k)^{4p_1+k+\frac{1}{2}} = (\lambda+\mu)^{\lambda+\mu+\frac{1}{2}} = \lambda^{\lambda+\mu+\frac{1}{2}} \left[1+\frac{\mu}{\lambda}\right]^{\lambda+\mu+\frac{1}{2}} \sim \lambda^{\lambda+\mu+\frac{1}{2}} e^{\mu} ,$$

and finally

$$\frac{a_{4p_1+k}}{k!a_k} \sim \frac{\lambda^{\lambda-k+\mu}}{\sqrt{2\pi}\, e^{-(\lambda+\mu)} \lambda^{\lambda+\mu+1/2}\, e^{\mu}} = \frac{\lambda^{-k}}{\sqrt{2\pi}\, e^{-\lambda} \lambda^{1/2}} .$$

This may be written as follows:

$$[a_{4p+k}]_{max} \sim \frac{e^{\lambda}}{\sqrt{2\pi\lambda}} \cdot \frac{k!a_k}{\lambda^k} , \qquad (B.14)$$

and for usual boundary conditions a_k/λ^k will almost be a constant, independent of λ; this arises because the solution y is a combination of sinusoidal and hyperbolic functions of λx, therefore each successive derivative is of order λ with respect to the previous one, and $a_o, a_1, 2a_2, 6a_3$ are the values of $y(0), y'(0), y''(0)$ and $y'''(0)$ respectively. One now sees that this maximum increases almost exponentially with λ and therefore the calculation of the larger a_n coefficients may require high precision to obtain $y(x) = \Sigma a_n x^n$ within good limits of precision.

B.5.1.c. Application to a cantilevered beam

Let us now consider a specific set of boundary conditions, those corresponding to a cantilever beam. Application of the boundary conditions in this case gives for the normalized solution

$$a_o = a_1 = 0,$$

$$a_2 = \lambda_r^2,\ a_3 = -\sigma_r \lambda_r^3/3,$$

for the rth mode, and

$$\sigma_r = [\sinh(\lambda_r) - \sin(\lambda_r)]/[\cosh(\lambda_r) + \cos(\lambda_r)].$$

Let us now consider the truncation error in this case. From equation (B.11) the total error in y at x=1 is

$$\delta_{4n} = \lambda_r^{4n} \left[\frac{2a_2}{(4n+2)!} + \frac{6a_3}{(4n+3)!}\right] = \frac{2\lambda_r^{4n+2}}{(4n+2)!}\left[1 - \frac{\sigma_r \lambda_r}{4n+3}\right].$$

The value of σ_r is close to 1, and we have assumed previously $\lambda<4n$; hence, the order of magnitude of δ_{4n} may be estimated by calculating

$$\varepsilon_{4n} = \lambda_r^{4n+2} / (4n+2)!$$

We shall not attempt to solve an inequality such as $\varepsilon_{4n}<10^{-s}$, where s would be the order of accuracy, but rather report a few quick rules which have been obtained. In order to have $\varepsilon_{4n}<10^{-3}$ we must choose $n \geq n_1$ such that

$$4n_1 - 6 \leq e\lambda_r < 4n_1 - 2 \qquad \text{where } e = 2.718; \tag{B.15}$$

if, however, such accuracy is not satisfactory enough, by increasing n_1 by 1 the accuracy approximately increases to another two decimal places since

$$\frac{\varepsilon_{4n+4}}{\varepsilon_{4n}} = \frac{\lambda_r^4}{(4n_1+6)(4n_1+5)(4n_1+4)(4n_1+3)} < \left(\frac{\lambda_r}{4n_1-2}\right)^4 < e^{-4} \sim 10^{-2}.$$

We next consider the magnitude of the largest coefficient. From equation (B.14) we obtain

$$(a_{4p+2})_{max} \sim \frac{e^{\lambda_r}}{\sqrt{2\pi\lambda_r}} \times (2) \text{ for } k=2,$$

and

$$(a_{4p+3})_{max} \sim \frac{e^{\lambda_r}}{\sqrt{2\pi\lambda_r}} \times (-2) \text{ for } k=3.$$

Let us now consider a numerical application; let us investigate the fifth mode (r=5) of the cantilever; accordingly, $\lambda_r \sim (2r-1)\frac{\pi}{2} \sim 14.15$.

We calculate $e^{\times\lambda_r} \sim 38.4$; hence we must choose $n_1 = 11$ in eq.(B.15). The accuracy is expected to be between 10^{-3} and 10^{-5}, but closer to 10^{-5}, since in eq.(B.15) $e\lambda_r$ is close to the lower limit of the inequality; actually, exact calculation yields $\delta_{44} \sim 2.5\times10^{-5}$. Hence, although half of them are null, we must still calculate the first 43 a_n coefficients!

As far as the maxima are concerned, we obtain from eq.(B.13) $p_1=3$ for both cases k=2 and k=3; hence,

$$a_{14} \sim -a_{15} \sim \frac{2e^{14.15}}{\sqrt{2\pi\ 14.15}} \sim 3\times10^{+6},$$

whereas exact calculation yields $a_{14} \sim -a_{15} \sim 3.3\times10^{+6}$. (Let us recall that the exact solution, y(x) sought hereby, varies between -2 and +2, hence the previous calculations require accuracy to seven digits, at least.)

B.5.1.d Determination of the eigenvalues

Up to this point we proceeded as if λ were known. In practice we must find both λ and the a_n coefficients. Let us now recall how λ may be calculated.

Since all coefficients may be expressed in terms of the lower four, i.e. a_o, a_1, a_2, a_3, we may express the boundary conditions in terms of those, and obtain a matrix, the determinant of which has to be equated to zero for a non-trivial solution of a_o, a_1, a_2, a_3.

For instance, for a cantilever beam we write

$$\begin{aligned} y(0) &= 0 && a_o = 0, \\ y'(0) &= 0 && a_1 = 0, \\ y''(1) &= 0 && \sum_{n=2}^{\infty} n(n-1)a_n = 0, \\ y'''(1) &= 0 && \sum_{n=3}^{\infty} n(n-1)(n-2)a_n = 0 . \end{aligned}$$

The second and third lines may be rewritten as follows:

$$\sum_{p} \sum_{k=0}^{3} \frac{(4p+k)(4p+k-1)\lambda^{4p}k!}{(4p+k)!} a_k = \sum_{k=2}^{3} \sum_{p=0}^{\infty} \frac{\lambda^{4p}k! a_k}{(4p+k-2)!} ;$$

$$\sum_{p} \sum_{k=0}^{3} \frac{(4p+k)(4p+k-1)(4p+k-2)\lambda^{4p}k!}{(4p+k)!} a_k = \sum_{k=2}^{3} \sum_{p=3-k}^{\infty} \frac{\lambda^{4p}k! a_k}{(4p+k-3)!} ;$$

hence, the characteristic equation in λ is derived from the determinant of the coefficients of a_2 and a_3 in the two equations, i.e.

$$\{\sum_{p=0}^{\infty} \frac{\lambda^{4p}}{4p!}\}^2 - \{\sum_{p=1}^{\infty} \frac{\lambda^{4p}}{(4p-1)!}\}\{\sum_{p=0}^{\infty} \frac{\lambda^{4p}}{(4p+1)!}\} = 0 .$$

The first six positive roots have been computed for increasing values of p, and reported in the first table of this Appendix. One may observe that the convergence of $y(x)$, discussed previously, and that of λ require approximately the same number of terms. E.g. for the fifth mode, in order to get both $y(x)$ and λ within 0.01 percent we require 43 terms.

B.5.2 Solution by the new method

We now consider the analysis of the beam eigenvalue problem by the new method.

An analysis of convergence, such as was done in the case of solution by power series, is not available; we shall merely present an application of the new method. Obviously, the case of a beam with simply supported ends would not be representative of the general efficiency of the method since the modal shapes are pure sine curves and thus included among the series of eigenfunctions used; we thus selected the case of the uniform cantilever beam.

We have $$\frac{d^4y}{dx^4} - \lambda^4 y = 0$$

and

$$y(0) = y'(0) = \bar{y}''(1) = y'''(1) = 0 .$$

Using the notation of §B.5 we write

$$D_{2p} = \sum_{n=0}^{\infty} \sum_{r=0}^{M} C_{pn}^{r} = \sum_{n=0}^{\infty} (C_{pn}^{0} + C_{pn}^{4}) ,$$

$$D_{2p-1} = \sum_{n=0}^{\infty} \sum_{r=0}^{M} S_{pn}^{r} = \sum_{n=0}^{\infty} (S_{pn}^{o} + S_{pn}^{4}).$$

Because the two values of r are even we have

$$C_{pn}^{o} = \gamma_{2n} FCC_{pn}^{o} + \gamma_{2n-1} FSC_{np}^{o},$$

$$S_{pn}^{o} = \gamma_{2n} FSC_{pn}^{o} + \gamma_{2n-1} FSS_{pn}^{o},$$

and

$$C_{pn}^{4} = (n\pi)^4 (\gamma_{2n} FCC_{pn}^{4} + \gamma_{2n-1} FSC_{np}^{4}),$$

$$S_{pn}^{4} = (n\pi)^4 (\gamma_{2n} FSC_{pn}^{4} + \gamma_{2n-1} FSS_{pn}^{4}).$$

We have defined

$$FCC_{pn}^{r} = \int_0^1 f_r(x) [\cos(p+n)\pi x + \cos(p-n)\pi x] dx,$$

$$FSC_{pn}^{r} = \int_0^1 f_r(x) [\sin(p+n)\pi x + \sin(p-n)\pi x] dx,$$

$$FSS_{pn}^{r} = \int_0^1 f_r(x) [\cos(p-n)\pi x - \cos(p+n)\pi x] dx,$$

The coefficients of the differential equation are simply

$$f_4(x) = 1 \qquad \text{and} \qquad f_0(x) = -\lambda^4.$$

We now introduce and calculate

$$CC_{pn} = \int_0^1 [\cos(p+n)\pi x + \cos(p-n)\pi x] dx = \begin{cases} 0 \text{ if } p \neq n \\ 1 \text{ if } p = n \neq 0 \\ 2 \text{ if } p = n = 0 \end{cases}$$

$$SS_{pn} = \int_0^1 [\cos(p-n)\pi x - \cos(p+n)\pi x] dx = \begin{cases} 0 \text{ if } p \neq n \\ 1 \text{ if } p = n \neq 0 \\ 2 \text{ if } p = n = 0 \end{cases}$$

$$SC_{pn} = \int_0^1 [\sin(p+n)\pi x + \sin(p-n)\pi x] dx = \begin{cases} 0 \text{ if } p+n \text{ is even; otherwise} \\ \frac{2}{(p+n)\pi} + \frac{2}{(p-n)\pi} \end{cases}$$

Finally, we obtain

$$D_{2p} = \sum_{0}^{\infty} (n^4\pi^4 - \lambda^4)\,[\gamma_{2n}\, CC_{pn} + \gamma_{2n-1}\, SC_{np}] = 0,$$

and

$$D_{2p-1} = \sum_{0}^{\infty} (n^4\pi^4 - \lambda^4)\,(\gamma_{2n}\, SC_{pn} + \gamma_{2n-1}\, SS_{pn}] = 0,$$

and four boundary conditions

$$\left.\begin{aligned} &\sum_{0}^{\infty} \gamma_{2n} = 0 \\ &\sum_{1}^{\infty} n\pi\gamma_{2n-1} = 0 \end{aligned}\right\} \text{ for } y(x=0) = y'(x=0) = 0$$

$$\left.\begin{aligned} &\sum_{1}^{\infty} -n^2\pi^2(-1)^n\gamma_{2n} = 0 \\ &\sum_{1}^{\infty} -n^3\pi^3(-1)^n\gamma_{2n-1} = 0 \end{aligned}\right\} \text{ for } y''(x=1) = y'''(x=1) = 0$$

We now build the matrix of the coefficients of the γ's, which must be singular for non trivial solutions to exist, as shown in the computer programme listing; the first four rows contain the boundary conditions; the next row represents the case of p=0. We then calculate

$$CC_{pn},\ SC_{pn},\ SS_{pn} \text{ for } p \ \&\ n = 1, 2, \ldots$$

and the matrix is filled by groups of 4 elements, corresponding to the coefficients of γ_{2n} and γ_{2n-1} in D_{2p} and D_{2p-1}; exception is made for the first element of each row, which is filled in separately for convenience as it corresponds to a null index, n = 0.

On the last page of this Appendix is a listing of the short program required for the purpose of filling the matrix. The results of computation for a cantilever beam have been printed as follows:

a) On page B.26 we tabulated the lowest eigenvalues, up to the sixth, for matrix sizes of 7x7 up to 19x19. The convergence achieved by this method, compared to that of power series can be appreciated; for an error $<10^{-5}$ the number of terms required by the two methods has been summarized in the following table:

Series \ Mode	1	2	3	4	5	6
Fourier	14	17	15	17	16	18
Power	14	22	31	39	47	55

b) On page B.27 and B.28 the fifth and sixth modes have been tabulated from a 17 term expansion. The γ's were normalized and the accuracy on y is within 1.5×10^{-4} as compared with the exact solution [70].

For the sake of curiosity, the values of $y(x)$ for $1<x<2$ have been listed in the right-most column of the same tables. The shape is simple, (one node at most) yet, the amplitude, subject to implicit conditions which have not been elaborated upon, is much larger than on the [0,1] interval.

B.5.3 The conical cantilever beam

The equation of motion for a full cone is

$$\frac{d^2}{dx^2}(1-x)^4\frac{d^2y}{dx^2} - \lambda^4(1-x)^2y = 0,$$

which may be transformed and re-written conveniently as

$$\xi^2\frac{d^4\psi}{d\xi^4} - \lambda^4\psi = 0;$$

the values of λ compatible with the boundary conditions are obtained from the following equation (cf. [71],[72]):

$$J_2(2\lambda)\cdot I_3(2\lambda) + J_3(2\lambda)\cdot I_2(2\lambda) = 0,$$

where I_2, I_3 and J_2, J_3 are Bessel functions of first and second types.

The values of λ computed by use of the previous equations and by use of the new method are tabulated on page B.29. Clearly, for the same mode number we observe that the convergence of λ requires more terms in the Fourier series in this case compared to the case of a uniform cantilever.

B.5.4 Conclusion.

Because the new method involves usually large determinants it is not the most economic tool for most common applications. For instance, if one is only concerned with the very first eigenvalues of a differential equation with almost

constant coefficients, the eigenfunctions are likely to be smoothly shaped (i.e. with few inflexion points), and power series, although they may require more terms than Fourier series, may be more economical since the determinants involved can be calculated by other techniques than full size matrix inversion. Furthermore, the differential equation may be of low order or of simple form, and it may allow easier solution by means of classical methods such as Laplace transforms. On the other hand, this method becomes competitive as the order of the differential equations and the complexity of the coefficients increases, or when higher order eigenvalues are involved (as observed on the previous page, one additional term per additional mode being enough to maintain accuracy), or when accurate modal shapes are required. Moreover, since the method only transforms the differential equation coefficients by use of integration, these coefficients need not be continuous functions of the independent coordinate, although this was never the case in the present work.

EIGENVALUES OF DIFFERENTIAL EQUATION :

$$Y^{(4)} - \lambda^4 Y = 0 ,$$

WITH BOUNDARY CONDITIONS : $Y(0) = Y'(0) = Y''(1) = Y'''(1) = 0$.

CONVERGENCE OF λ WITH RESPECT TO THE TERMS $A_2, A_3, A_6, A_7 \ldots A_{4p+2}, A_{4p+3} \ldots$ IN THE SOLUTION

$$Y(x) = A_2x^2 + A_3x^3 + A_6x^6 + A_7x^7 + \ldots\ldots\ldots + A_{4p+2}x^{4p+2} + A_{4p+3}x^{4p+3} \ldots$$

	MODE 1	MODE 2	MODE 3	MODE 4	MODE 5	MODE 6
JP TJ A 6:	1.681793					
JP TJ A 7:	1.886615	3.882977				
JP TJ A10:	1.872788					
JP TJ A11:	1.875124	4.536286				
JP TJ A14:	1.875101	5.022475	5.236689			
JP TJ A15:	1.875104	4.689718				
JP TJ A18:	1.875104	4.696020	6.942553			
JP TJ A19:	1.875104	4.694064				
JP TJ A22:	1.875104	4.694100	7.714088			
JP TJ A23:	1.875104	4.694091	7.861682	9,83118		
JP TJ A26:	1.875104	4.694091	7.851498			
JP TJ A27:	1.875104	4.694091	7.854828	10,74722		
JP TJ A30:	1.875104	4.694091	7.854730			
JP TJ A31:	1.875104	4.694091	7.854758	10,98582		
JP TJ A34:	1.875104	4.694091	7.854757	11,00077	12,97264	
JP TJ A35:	1.875104	4.694091	7.854757	10,99541		
JP TJ A38:	1.875104	4.694091	7.854757	10,99560	13,90426	
JP TJ A39:	1.875104	4.694091	7.854757	10,99554	14,15293	15,79146
JP TJ A42:	1.875104	4.694091	7.854757	10,99554	14,12927	
JP TJ A43:	1.875104	4.694091	7.854757	10,99554	14,13739	16,88387
JP TJ A46:	1.875104	4.694091	7.854757	10,99554	14,13706	
JP TJ A47:	1.875104	4.694091	7.854757	10,99554	14,13717	17,25679
THEORY* :	1.875104	4.694091	7.854757	10,99554	14,13717	17,27875

* Values obtained from Bishop and Johnson [70]

EIGENVALUES OF DIFFERENTIAL EQUATION :

$$Y^{(4)} - \lambda^4 Y = 0 ,$$

WITH BOUNDARY CONDITIONS : $Y(0) = Y'(0) = Y''(1) = Y'''(1) = 0$.

CONVERGENCE OF λ WITH RESPECT TO THE NUMBER OF TERMS $\gamma_0, \gamma_1, \gamma_2 \ldots \gamma_p \ldots$ IN THE SERIES

$$Y(x) = \gamma_0 + \gamma_1 \sin(\pi x) + \gamma_2 \cos(\pi x) + \gamma_3 \sin(2\pi x) + \gamma_4 \cos(2\pi x) + \ldots + \gamma_{2n} \cos(n\pi x) \ldots$$

	MODE 1	MODE 2	MODE 3	MODE 4	MODE 5	MODE 6
7 TERMS:	2.324349					
8 TERMS:	2.320479	6.283185	6.451220	11.28642		
9 TERMS:	1.935021	4.805770	7.895980	11.18346	15.65789	
10 TERMS:	1.878046	4.701601	7.862592	10.97480	14.16087	
11 TERMS:	1.878353	4.701230	7.855705	11.01267	14.09325	17.51883
12 TERMS:	1.878334	4.701222	7.855315	11.01226	14.09612	17.29963
13 TERMS:	1.875257	4.694484	7.854792	10.99701	14.13786	17.28173
14 TERMS:	1.875112	4.694111	7.854777	10.99565	14.13739	17.27737
15 TERMS:	1.875111	4.694111	7.854759	10.99564	14.13719	17.27926
16 TERMS:	1.875111	4.694111	7.854758	10.99564	14.13717	17.27925
17 TERMS:	1.875104	4.694092	7.854757	10.99555	14.13717	17.27880
18 TERMS:	1.875104	4.694091	7.854757	10.99554	14.13717	17.27876
19 TERMS:	1.875104	4.694091	7.854757	10.99554	14.13717	17.27876
THEORY * :	1.875104	4.694091	7.854757	10.99554	14.13717	17.27875

* Values obtained from Bishop and Johnson

FIFTH MODE

X=0.0 : Y= 0.00000	X=0.50 : Y= 0.0[illegible]	X=1.00 : Y= 2.00000
X=0.01 : Y= 0.01904	X=0.51 : Y= 0.20111	X=1.02 : Y= 2.56605
X=0.02 : Y= 0.07241	X=0.52 : Y= 0.33543	X=1.04 : Y= 3.14031
X=0.03 : Y= 0.15446	X=0.53 : Y= 0.55389	X=1.06 : Y= 3.74571
X=0.04 : Y= 0.25954	X=0.54 : Y= 0.75978	X=1.08 : Y= 4.42334
X=0.05 : Y= 0.38222	X=0.55 : Y= 0.97058	X=1.10 : Y= 5.23376
X=0.06 : Y= 0.51696	X=0.56 : Y= 1.06711	X=1.12 : Y= 6.25690
X=0.07 : Y= 0.65850	X=0.57 : Y= 1.12452	X=1.14 : Y= 7.54085
X=0.08 : Y= 0.80177	X=0.58 : Y= 1.20241	X=1.16 : Y= 9.34260
X=0.09 : Y= 0.94194	X=0.59 : Y= 1.35484	X=1.18 : Y= 11.63120
X=0.10 : Y= 1.07452	X=0.60 : Y= 1.40038	X=1.20 : Y= 14.56868
X=0.11 : Y= 1.19537	X=0.61 : Y= 1.41814	X=1.22 : Y= 18.25398
X=0.12 : Y= 1.30082	X=0.62 : Y= 1.40778	X=1.24 : Y= 22.75974
X=0.13 : Y= 1.38764	X=0.63 : Y= 1.36953	X=1.26 : Y= 28.11994
X=0.14 : Y= 1.45312	X=0.64 : Y= 1.30417	X=1.28 : Y= 34.31874
X=0.15 : Y= 1.49513	X=0.65 : Y= 1.21305	X=1.30 : Y= 41.22192
X=0.16 : Y= 1.51209	X=0.66 : Y= 1.09801	X=1.32 : Y= 48.87272
X=0.17 : Y= 1.50305	X=0.67 : Y= 0.96138	X=1.34 : Y= 56.89171
X=0.18 : Y= 1.46763	X=0.68 : Y= 0.81594	X=1.36 : Y= 65.08393
X=0.19 : Y= 1.40607	X=0.69 : Y= 0.66464	X=1.38 : Y= 73.15067
X=0.20 : Y= 1.31918	X=0.70 : Y= 0.51137	X=1.40 : Y= 80.76691
X=0.21 : Y= 1.20834	X=0.71 : Y= 0.35936	X=1.42 : Y= 87.60264
X=0.22 : Y= 1.07546	X=0.72 : Y= 0.20362	X=1.44 : Y= 93.34607
X=0.23 : Y= 0.92290	X=0.73 : Y= -0.13313	X=1.46 : Y= 97.76677
X=0.24 : Y= 0.75349	X=0.74 : Y= -0.32634	X=1.48 : Y=100.53[illegible]
X=0.25 : Y= 0.57040	X=0.75 : Y= -0.51203	X=1.50 : Y=101.64879
X=0.26 : Y= 0.37709	X=0.76 : Y= -0.6 633	X=1.52 : Y=101.00619
X=0.27 : Y= 0.17727	X=0.77 : Y= -0.84556	X=1.54 : Y= 98.[illegible]
X=0.28 : Y= -0.02521	X=0.78 : Y= -0.98661	X=1.56 : Y= 94.76603
X=0.29 : Y= -0.22643	X=0.79 : Y= -1.10575	X=1.58 : Y= 89.49801
X=0.30 : Y= -0.42247	X=0.80 : Y= -1.20697	X=1.60 : Y= 83.12[illegible]
X=0.31 : Y= -0.60752	X=0.81 : Y= -1.2[illegible]86	X=1.62 : Y= 75.9[illegible]
X=0.32 : Y= -0.73391	X=0.82 : Y= -1.31066	X=1.64 : Y= 68.24491
X=0.33 : Y= -0.9.223	X=0.83 : Y= -1.32222	X=1.66 : Y= 60.33346
X=0.34 : Y= -1.0 139	X=0.84 : Y= -1.3 376	X=1.68 : Y= 52.49219
X=0.35 : Y= -1.1[illegible]63	X=0.85 : Y= -1.25513	X=1.70 : Y= 44.93147
X=0.36 : Y= -1.2[illegible]167	X=0.86 : Y= -1.17666	X=1.72 : Y= 37.5[illegible]
X=0.37 : Y= -1.3[illegible]869	X=0.87 : Y= -1.0[illegible]21	X=1.74 : Y= 31.33753
X=0.38 : Y= -1.39337	X=0.88 : Y= -0.9[illegible]404	X=1.76 : Y= 25.51[illegible]
X=0.39 : Y= -1.[illegible]0[illegible]95	X=0.89 : Y= -0.77[illegible]96	X=1.78 : Y= 20.3[illegible]
X=0.40 : Y= -1.[illegible]222	X=0.90 : Y= -0.5 [illegible]93	X=1.80 : Y= 15.9[illegible]
X=0.41 : Y= -1.3[illegible]359	X=0.91 : Y= -0.3[illegible]157	X=1.82 : Y= 12.2[illegible]
X=0.42 : Y= -1.27679	X=0.92 : Y= -0.1[illegible]33	X=1.84 : Y= 9.11[illegible]
X=0.43 : Y= -1.17946	X=0.93 : Y= 0.0 493	X=1.86 : Y= 6.56505
X=0.44 : Y= -1.0[illegible]445	X=0.94 : Y= 0.33930	X=1.88 : Y= 4.5[illegible]03
X=0.45 : Y= -0.9[illegible]28	X=0.95 : Y= 0.6 414	X=1.90 : Y= 2.[illegible]481
X=0.46 : Y= -0.75572	X=0.96 : Y= 0.[illegible]7653	X=1.92 : Y= 1.76292
X=0.47 : Y= -0.[illegible]3[illegible]90	X=0.97 : Y= 1.15424	X=1.94 : Y= 1.[illegible]230
X=0.48 : Y= -0.[illegible]0[illegible]65	X=0.98 : Y= 1.43502	X=1.96 : Y= 1.[illegible]0[illegible]
X=0.49 : Y= -0.19740	X=0.99 : Y= 1.71729	X=1.98 : Y= 0.[illegible]

SIXTH MODE

X=0.0 : Y= 0.00019	X=0.50 : Y= -1.41407	X=1.00 : Y= 1.99992
X=0.01 : Y= -0.02793	X=0.51 : Y= -1.39285	X=1.02 : Y= 2.69230
X=0.02 : Y= -0.10546	X=0.52 : Y= -1.33016	X=1.04 : Y= 3.40335
X=0.03 : Y= -0.22213	X=0.53 : Y= -1.22788	X=1.06 : Y= 4.18507
X=0.04 : Y= -0.36775	X=0.54 : Y= -1.08905	X=1.08 : Y= 5.13008
X=0.05 : Y= -0.53233	X=0.55 : Y= -0.91779	X=1.10 : Y= 6.37207
X=0.06 : Y= -0.70628	X=0.56 : Y= -0.71922	X=1.12 : Y= 8.07917
X=0.07 : Y= -0.88038	X=0.57 : Y= -0.49922	X=1.14 : Y= 10.44039
X=0.08 : Y= -1.04610	X=0.58 : Y= -0.26435	X=1.16 : Y= 13.64344
X=0.09 : Y= -1.19568	X=0.59 : Y= -0.02156	X=1.18 : Y= 17.84586
X=0.10 : Y= -1.32227	X=0.60 : Y= 0.22193	X=1.20 : Y= 23.14108
X=0.11 : Y= -1.42007	X=0.61 : Y= 0.45887	X=1.22 : Y= 29.52214
X=0.12 : Y= -1.48449	X=0.62 : Y= 0.68226	X=1.24 : Y= 36.85120
X=0.13 : Y= -1.51217	X=0.63 : Y= 0.88543	X=1.26 : Y= 44.84036
X=0.14 : Y= -1.50113	X=0.64 : Y= 1.06239	X=1.28 : Y= 53.04654
X=0.15 : Y= -1.45067	X=0.65 : Y= 1.20785	X=1.30 : Y= 60.88818
X=0.16 : Y= -1.36148	X=0.66 : Y= 1.31751	X=1.32 : Y= 67.68332
X=0.17 : Y= -1.23550	X=0.67 : Y= 1.38813	X=1.34 : Y= 72.71164
X=0.18 : Y= -1.07584	X=0.68 : Y= 1.41760	X=1.36 : Y= 75.26659
X=0.19 : Y= -0.88686	X=0.69 : Y= 1.40508	X=1.38 : Y= 74.83792
X=0.20 : Y= -0.67371	X=0.70 : Y= 1.35100	X=1.40 : Y= 70.98996
X=0.21 : Y= -0.44243	X=0.71 : Y= 1.25696	X=1.42 : Y= 63.62253
X=0.22 : Y= -0.19958	X=0.72 : Y= 1.12588	X=1.44 : Y= 52.90637
X=0.23 : Y= 0.04786	X=0.73 : Y= 0.96168	X=1.46 : Y= 39.30869
X=0.24 : Y= 0.29275	X=0.74 : Y= 0.76939	X=1.48 : Y= 23.55997
X=0.25 : Y= 0.52796	X=0.75 : Y= 0.55483	X=1.50 : Y= 6.58801
X=0.26 : Y= 0.74664	X=0.76 : Y= 0.32451	X=1.52 : Y=-10.57013
X=0.27 : Y= 0.94242	X=0.77 : Y= 0.08549	X=1.54 : Y=-26.86905
X=0.28 : Y= 1.10961	X=0.78 : Y= -0.15494	X=1.56 : Y=-41.36056
X=0.29 : Y= 1.24333	X=0.79 : Y= -0.38945	X=1.58 : Y=-53.27869
X=0.30 : Y= 1.33960	X=0.80 : Y= -0.61070	X=1.60 : Y=-62.11008
X=0.31 : Y= 1.39568	X=0.81 : Y= -0.81186	X=1.62 : Y=-67.61646
X=0.32 : Y= 1.40991	X=0.82 : Y= -0.98659	X=1.64 : Y=-69.83899
X=0.33 : Y= 1.38193	X=0.83 : Y= -1.12923	X=1.66 : Y=-69.06287
X=0.34 : Y= 1.31262	X=0.84 : Y= -1.23510	X=1.68 : Y=-65.76025
X=0.35 : Y= 1.20402	X=0.85 : Y= -1.30038	X=1.70 : Y=-60.51917
X=0.36 : Y= 1.05941	X=0.86 : Y= -1.32247	X=1.72 : Y=-53.97125
X=0.37 : Y= 0.88310	X=0.87 : Y= -1.29989	X=1.74 : Y=-46.72501
X=0.38 : Y= 0.68036	X=0.88 : Y= -1.23227	X=1.76 : Y=-39.31253
X=0.39 : Y= 0.45728	X=0.89 : Y= -1.12052	X=1.78 : Y=-32.15964
X=0.40 : Y= 0.22049	X=0.90 : Y= -0.96646	X=1.80 : Y=-25.57190
X=0.41 : Y= -0.02292	X=0.91 : Y= -0.77303	X=1.82 : Y=-19.73824
X=0.42 : Y= -0.26568	X=0.92 : Y= -0.54396	X=1.84 : Y=-14.74681
X=0.43 : Y= -0.50054	X=0.93 : Y= -0.28367	X=1.86 : Y=-10.61972
X=0.44 : Y= -0.72051	X=0.94 : Y= 0.00286	X=1.88 : Y= -7.28746
X=0.45 : Y= -0.91902	X=0.95 : Y= 0.31048	X=1.90 : Y= -4.70917
X=0.46 : Y= -1.09014	X=0.96 : Y= 0.63401	X=1.92 : Y= -2.79105
X=0.47 : Y= -1.22878	X=0.97 : Y= 0.96863	X=1.94 : Y= -1.44563
X=0.48 : Y= -1.33080	X=0.98 : Y= 1.30992	X=1.96 : Y= -0.57754
X=0.49 : Y= -1.39319	X=0.99 : Y= 1.65444	X=1.98 : Y= -0.13319

EIGENVALUES OF DIFFERENTIAL EQUATION :

$$\frac{d^2}{dx^2}\left[(1-x)^4 \frac{d^2Y}{dx^2}\right] - \lambda^4(1-x)^2 Y = 0 \qquad \text{(FULL CONE)}$$

BOUNDARY CONDITIONS : $Y(0)=Y'(0)=Y''(1)=Y'''(1)=0$.

CONVERGENCE OF λ WITH NUMBER OF TERMS G0,G1,D1,G2,.... IN SOLUTION

$Y(X) = G0 + G1\ COS(\pi X) + D1\ SIN(\pi X) + G2\ COS(2\pi X) + D2\ SIN(2\pi X) + \ldots + DN\ SIN(N\pi X)$

	MODE 1	MODE 2	MODE 3	MODE 4	MODE 5
15 TERMS:	2.952867	4.599338	6.212342	7.873621	9.701466
16 TERMS:	2.952845	4.598701	6.205439	7.827411	9.556300
17 TERMS:	2.952842	4.598577	6.203266	7.809033	9.473924
19 TERMS:	2.952839	4.598461	6.201459	7.793540	9.398042
21 TERMS:	2.952839	4.598442	6.201146	7.790419	9.377611
23 TERMS:	2.952839	4.598441	6.201115	7.789859	9.373061
THEORY* :	2.952839	4.598438	6.201107	7.789742	9.371971

*VALUES COMPUTED FROM: $J_2(2\lambda)\times I_3(2\lambda) + J_3(2\lambda)\times I_2(2\lambda) = 0$

```
      SUBROUTINE MATDET(B,X,Y,IY,N)
      IMPLICIT REAL*8(A-H,O-Z)
      DIMENSION B(N,N),CC(20,20),SC(20,20),SS(9,20),L(20),M(20),A(20,20)
      PI=3.1415926536
      NIN=N/2
      NIP=NIN-2
      DO 11 I=1,N
      DO 11 J=1,N
11    A(I,J)=0.D0
C
C  4 rows of boundary conditions.
C
      A(1,1)       =1
      DO 12 IN=1,NIN
      A(1,2*IN)    =1
      A(2,2*IN+1)=IN*PI
      A(3,2*IN)    =(IN*PI)**2*(-1)**IN
12    A(4,2*IN+1)=(IN*PI)**3*(-1)**IN
C
C  1 row corresponding to p=0
C  1 col corresponding to n=0.
C
      A(5,1)       =-2*X**4
      DO 13 IN=1,NIN,2
13    A(5,2*IN+1)=4*(-X**4+(IN*PI)**4)/(IN*PI)
      DO 15 IP=1,NIN
      DO 14 IN=1,NIN
      IF(IN.EQ.IP)  GO TO 14
      SS(IN,IP)=0
      SC(IN,IP)=(1-(-1)**(IN+IP))*2*IN/(PI*(IN**2-IP**2))
      CC(IN,IP)=0
14    CONTINUE
      SS(IP,IP)=1
      SC(IP,IP)=0
15    CC(IP,IP)=1
      DO 8 IP=1,NIP
      A(4+2*IP,1) = 0
      A(4+2*IP+1,1) =2*X**4*((-1)**IP-1)/(IP*PI)
      DO 8 IN=1,NIN
      PIN4 =(IN*PI)**4-X**4
      A(4+2*IP,2*IN)    =PIN4*CC(IP,IN)
      A(4+2*IP,2*IN+1) =PIN4*SC(IN,IP)
      A(5+2*IP,2*IN)    =PIN4*SC(IP,IN)
8     A(5+2*IP,2*IN+1) =PIN4*SS(IP,IN)
      DO 20 I=1,N
      DO 20 J=1,N
20    B(I,J)=A(I,J)/PI**4
      IF(IY.EQ.0) GO TO 30
      Y=RDET(B,L,M,N)
30    RETURN
      END
```

APPENDIX C

CALCULATION OF THE FCC, FCS, FSC, FSS AND g_r COEFFICIENTS

APPENDIX C: CALCULATION OF FCC^r_{pn}, FCS^r_{pn}, FSC^r_{pn}, FSS^r_{pn}, g_r

C.1 VALUES OF f_r

Using the notation of eq. (B.1) we write the coefficients of eq. (6.8) in ascending order with respect to powers of $(1+\alpha_e\xi)$, $(1+\alpha_i\xi)$ and $(1-\alpha\xi)^2$ as follows:

$$f_4(\xi,\omega) = \frac{1}{1-\delta^4}\left(1+\frac{i\omega\mu\nu}{\mu+\nu|\omega|}\right)\left[(1+\alpha_e\xi)^4 - \delta^4(1+\alpha_i\xi)^4\right],$$

$$f_3(\xi,\omega) = \frac{8}{1-\delta^4}\left(1+\frac{i\omega\mu\nu}{\mu+\nu|\omega|}\right)\left[(1+\alpha_e\xi)^3 - \delta^4(1+\alpha_i\xi)^3\right],$$

$$f_2(\xi,\omega) = \left[\frac{v_i}{1+\alpha_i}\right]^2 - \Theta + u_e^2\left(\frac{1-\alpha\xi}{\sigma}\right)^2(1+\alpha_e\xi)^2$$

$$+ \frac{12}{1-\delta^4}\left(1+\frac{i\omega\mu\nu}{\mu+\nu|\omega|}\right)\left[(1+\alpha_e\xi)^2 - \delta^4(1+\alpha_i\xi)^2\right]$$

$$- \left\{\varepsilon c_t u_e^2\,\frac{(1+\alpha_e\xi)^3}{2\alpha_e} - \Gamma(2-\gamma_e)\frac{(1+\alpha_i\xi)^3}{3\alpha_e} + \Gamma\gamma_i\,\frac{(1+\alpha_i\xi)^3}{3\alpha_i}\right\}_{\xi}^{\xi=1},$$

$$f_1(\xi,\omega) = 2i\omega\left[\frac{\delta^{2+\gamma_i}}{\gamma_e+\gamma_i}\right]^{\frac{1}{2}} v_i + u_e^2\left[\varepsilon c_n(1+\alpha_e\xi) + 2\alpha_e(1+\alpha_e\xi)\left(\frac{1-\alpha\xi}{\sigma}\right)^2\right]$$

$$+ \left[\Gamma(2-\gamma_e) + i\omega\left(\frac{\gamma_e-1}{\gamma_e+\gamma_i}\right)^{\frac{1}{2}} u_e\right](1+\alpha_e\xi)^2 + \gamma\gamma_i(1+\alpha_i\xi)^2$$

$$+ i\omega\left[\frac{\gamma_e-1}{\gamma_e+\gamma_i}\right]^{\frac{1}{2}} u_e(1+\alpha_e\xi)^2\left(\frac{1-\alpha\xi}{\sigma}\right)^2,$$

$$f_0(\xi,\omega) = i\omega\left[\frac{\gamma_e-1}{\gamma_e+\gamma_i}\right]^{\frac{1}{2}}\left[\varepsilon(c_n u_e + c_v) + 2u_e\alpha_e\left(\frac{1-\alpha\xi}{\sigma}\right)^2\right](1+\alpha_e\xi)$$

$$- \frac{\omega^2}{\gamma_e+\gamma_i}\left[\gamma_e(1+\alpha_e\xi)^2 + \gamma_i(1+\alpha_i\xi)^2\right];$$

and each of the preceding functions may be written as

$$f_r(\xi,\omega) = \sum_{i=1}^{3} \sum_{m=0}^{4} b_{im}^{r}(\omega)(1+a_i\xi)^m \ , \qquad (C.1)$$

where a_i may take the values $a_1=\alpha_e$, $a_2=\alpha_i$, $a_3=-\alpha$.

C.2 CALCULATION OF FCC, FCS, FSC, FSS

In the calculation of the FCC, FCS, FSC and FSS coefficients as defined by eq.(B.6) we shall thus encounter two major types of integrals, namely

$$I_k^m(a) = \int_0^1 (1+a\xi)^m \cos k\pi\xi d\xi \ ,$$

and

$$J_k^m(a) = \int_0^1 (1+a\xi)^m \sin k\pi\xi d\xi \ .$$

Because $m \leq 4$, we obtain

$$I_k^m(a) = \frac{am}{k^2\pi^2}[(-1)^k(1+a)^{m-1}-1] - \frac{a^3m}{k^4\pi^4}(m-1)(m-2)[(-1)^k(1+a)^{m-1}-1],$$

and

$$J_k^m(a) = \frac{1-(-1)^k(1+a)^m}{k\pi} + \frac{a^2m}{k^3\pi^3}(m-1)[(-1)^k(1+a)^{m-2} - 1]$$

$$- \frac{a^4m}{k^3\pi^3}(m-1)(m-2)(m-3)[(-1)^k(1+a)^{m-4} - 1] \ ,$$

provided that k is not equal to zero; otherwise, if k=0

$$I_o^m(a) = 1 + m\frac{a}{2}[1+(m-1)\frac{a}{3}[1+(m-2)\frac{a}{4}[1+(m-3)\frac{a}{5})]],$$

and

$$J_o^m(a) = 0 \ .$$

We now introduce the following coefficients:

$$CC^m_{pn}(a_i) = I^m_{p+n}(a_i) + I^m_{p-n}(a_i) \ ,$$

$$CS^m_{pn}(a_i) = J^m_{n+p}(a_i) + J^m_{n-p}(a_i) \ ,$$

$$SC^m_{pn}(a_i) = J^m_{p+n}(a_i) + J^m_{p-n}(a_i) = CS^m_{np}(a_i) \ ,$$

$$SS^m_{pn}(a_i) = I^m_{p-n}(a_i) - I^m_{p+n}(a_i) \ ,$$

so that, by use of eq.(C.1) we finally obtain

$$FCC^r_{pn} = \sum_{i=1}^{3} \sum_{m=0}^{4} b^r_{im} CC^m_{pn}(a_i) \ ,$$

$$FCS^r_{pn} = \sum_{i=1}^{3} \sum_{m=0}^{4} b^r_{im} CS^m_{pn}(a_i) = FSC^r_{np} \ ,$$

$$FSS^r_{pn} = \sum_{i=1}^{3} \sum_{m=0}^{4} b^r_{im} SS^m_{pn}(a_i) \ .$$

C.3 VALUES OF g^j_r

a) The upstream end, at $\xi=0$, is supported, hence $\Psi(0) = 0$, and by use of eq.(B.2), the first boundary condition yields

$$g^1_0 = 1 \quad \& \quad g^1_1 = g^1_2 = g^1_3 = 0 \ ;$$

if it is pinned, we also assume that $\Psi''(0) = 0$, then

$$g^2_2 = 1 \quad \& \quad g^2_0 = g^2_1 = g^2_3 = 0 \ ,$$

and if it is clamped, then $\Psi'(0) = 0$, and

$$g^2_1 = 1 \quad \& \quad g^2_0 = g^2_2 = g^2_3 = 0 \ .$$

b) If the downstream end, at $\xi=1$, is also supported, pinned or clamped, we obtain for g^3 and g^4 the same conditions as above for g^1 and g^2 ; if however it is free then we obtain

α) by condition of zero moment, i.e. $\Psi''(1) = 0$,

$$g_2^3 = 1 \;\&\; g_0^3 = g_1^3 = g_3^3 = 0,$$

β) by the relation between Ψ, Ψ' & $\Psi^{(3)}$ at $\xi=1$, as in eq.(6.7),

$$g_0^4 = i\omega f u_e \left(\frac{1-\alpha}{\sigma}\right)^2 [(1+\alpha_e)^2 - \delta^2(1+\alpha_i)^2] \left(\frac{\gamma_e-1}{\gamma_e+\gamma_i}\right)^{\frac{1}{2}} + \omega^2\chi \frac{[1+f(\gamma_e-1)]s_e+\gamma_i(1+\alpha_i)^2}{\gamma_e+\gamma_i},$$

$$g_1^4 = f[(1+\alpha_e)^2 - \delta^2(1+\alpha_i)]\left(\frac{1-\alpha}{\sigma}\right)^2 u_e - \chi\Gamma[2-\gamma_e)s_e + \gamma_i(1+\alpha_i)^2] - i\omega\{f[s_e+\delta^2\left(\frac{1-\alpha}{\sigma}\right)^2(1+\alpha_i)^2]\left(\frac{\gamma_e-1}{\gamma_e+\gamma_i}\right)^{\frac{1}{2}} u_e + 2\left(\frac{\delta^2+\gamma_i}{\gamma_e+\gamma_i}\right)^{\frac{1}{2}} v_i\}\chi,$$

$$g_2^4 = 0,$$

$$g_3^4 = \left(1+\frac{i\omega\mu\nu}{\mu+\nu|\omega|}\right)\frac{(1+\alpha_e)^4 - \delta^4(1+\alpha_i)^4}{1-\delta^4}.$$

APPENDIX D

CALCULATION OF α_i' AND α_e'

APPENDIX D: CALCULATION OF α_i' & α_e'

D.1 Using dimensionless notation we write

$$\int_0^L \frac{dx}{A_e - A_i} = \frac{L}{A_e^o} \int_0^1 \frac{d\xi}{\sigma(\xi)} .$$

Assuming slender bodies and small taper angles we develop the inverse of the cross section up to the second order, as follows:

$$\frac{1}{\sigma(\xi)} \sim \left[\frac{1}{\sigma}\right]_{\xi=0} - \xi\left[\frac{\sigma'}{\sigma^2}\right]_{\xi=0} + \frac{1}{2}\xi^2\left[\frac{2\sigma'^2}{\sigma^3} - \frac{\sigma''}{\sigma^2}\right]_{\xi=0} ;$$

hence

$$\int_0^1 \frac{d\xi}{\sigma(\xi)} \sim \left[\frac{1}{\sigma}\right]_{\xi=0} \times \left[1 - \frac{1}{2}\frac{\sigma'}{\sigma} + \frac{1}{6}\frac{2\sigma'^2 - \sigma\sigma''}{\sigma^2}\right]_{\xi=0} . \qquad (D.1)$$

D.2 We now calculate

$$\int_0^L \frac{U_i(x)}{A_e - A_i}\, dx = \frac{LU_i(0)}{A_e^o} \int_0^L \frac{d\xi}{\sigma\sigma_i} .$$

As in the previous paragraph, we write

$$\left[\frac{1}{\sigma\sigma_i}\right]_\xi \sim \left[\frac{1}{\sigma\sigma_i}\right]_0 - \xi\left[\frac{\sigma'}{\sigma^2\sigma_i} + \frac{\sigma_i'}{\sigma\sigma_i^2}\right]_0 + \frac{1}{2}\xi^2\left[\frac{2\sigma'^2 - \sigma''\sigma}{\sigma^3\sigma_i} + \frac{2\sigma_i'^2 - \sigma_i''\sigma_i}{\sigma\sigma_i^3} + \frac{2\sigma'\sigma_i'}{\sigma^2\sigma_i^2}\right]_0 ,$$

and, therefore,

$$\int_0^1 \frac{d\xi}{\sigma\sigma_i(\xi)} \sim \left\{\frac{1}{\sigma\sigma_i}\left[1 - \frac{1}{2}\left(\frac{\sigma'}{\sigma} + \frac{\sigma_i'}{\sigma_i}\right) + \frac{1}{6}\left(\frac{2\sigma'^2 - \sigma\sigma''}{\sigma^2} + \frac{2\sigma'\sigma_i'}{\sigma\sigma_i} + \frac{2\sigma_i'^2 - \sigma_i\sigma_i''}{\sigma_i^2}\right)\right]\right\}_{\xi=0} .$$

According to notation in eq.(5,8) we write

$$\alpha_i' = 1 - \int_0^L \frac{U_i(x)dx}{A_e-A_i} \Big/ \int_0^L \frac{U_i(L)dx}{A_e-A_i} = 1 - \frac{U_i(0)}{U_i(L)} \int_0^1 \frac{d\xi}{\sigma\sigma_i} \Big/ \int_0^1 \frac{d\xi}{\sigma}$$

$$\sim 1 - \frac{\sigma_i(1)}{\sigma_i(0)} \frac{1 - \frac{1}{2}(\frac{\sigma'}{\sigma} + \frac{\sigma_i'}{\sigma_i}) + \frac{1}{6}(\frac{2\sigma'^2-\sigma\sigma''}{\sigma^2} + \frac{2\sigma'\sigma_i'}{\sigma\sigma_i} + \frac{2\sigma_i'^2-\sigma_i\sigma_i''}{\sigma_i^2})}{1 - \frac{1}{2}\frac{\sigma'}{\sigma} + \frac{1}{6}\frac{2\sigma'^2-\sigma\sigma''}{\sigma^2}}$$

$$\sim 1 - \frac{\sigma_i(1)}{\sigma_i(0)} [1 - \frac{\frac{1}{2}\frac{\sigma_i'}{\sigma_i} - \frac{1}{6}(\frac{2\sigma'\sigma_i'}{\sigma\sigma_i} + \frac{2\sigma_i'^2-\sigma_i'\sigma_i''}{\sigma_i^2})}{1 - \frac{1}{2}\frac{\sigma'}{\sigma} + \frac{1}{6}\frac{2\sigma'^2-\sigma\sigma''}{\sigma^2}}]$$

$$\sim 1 - \frac{\sigma_i(1)}{\sigma_i(0)} [1 - \frac{1}{2}\frac{\sigma_i'}{\sigma_i} + \frac{\sigma'\sigma_i'}{12\sigma\sigma_i} + \frac{1}{6}\frac{2\sigma_i'^2-\sigma_i\sigma_i''}{\sigma_i^2}] .$$

For conical elements, as in §2.6.2, we will set

$$\sigma(\xi) = (1+\alpha_e\xi)^2 - \delta^2(1+\alpha_i\xi)^2 \text{ and } \sigma_i(\xi) = (1+\alpha_i\xi)^2;$$

then

$$\sigma(0) = 1-\delta^2 \qquad \sigma_i(0) = 1 \qquad , \sigma_i(1) = (1+\alpha_i)^2$$

$$\sigma'(0) = 2(\alpha_e-\delta^2\alpha_i) \qquad \sigma_i'(0) = 2\alpha_i$$

$$\sigma''(0) = 2(\alpha_e^2-\delta^2\alpha_i^2) \qquad \sigma_i''(0) = 2\alpha_i^2 .$$

We thus obtain

$$\alpha_i \sim 1 - (1+\alpha_i)^2[1 - \alpha_i + \frac{1}{3}\frac{\alpha_e-\delta^2\alpha_i}{1-\delta^2}\alpha_i + \alpha_i^2]$$

$$\sim 1 - [1 + \alpha_i(2+\alpha_i)]\{1 - \alpha_i[1-\alpha_i-\frac{\alpha_e-\delta^2\alpha_i}{3(1-\delta^2)}]\} ,$$

$$\sim 1 - \{1 + \alpha_i[1 + \frac{\alpha_e-\delta^2\alpha_i}{3(1-\delta^2)}]\} ;$$

hence

$$\alpha_i' \sim -\alpha_i\left[1 + \frac{\alpha_e - \delta^2\alpha_i}{3(1-\delta^2)}\right] . \qquad (D.2)$$

For quasicylindrical tubular beams we obtain $\alpha_i' \sim -\alpha_i$. At this point we recall that for a convergent taper we have $\alpha_i < 0$ and hence α_i' is positive.

D.3 We now calculate α_e'; from eq. (5.8) we write

$$\alpha_e' = \frac{2}{Lq_{et}(0)}\int_0^L \left\{\int_x^L q_{et}dx\right\} \frac{dx}{A_e - A_i} \Big/ \int_0^L \frac{dx}{A_e - A_i} ;$$

from the expression of friction in eq. (3.7) we write

$$q_{et}(x) = q_{et}(0) \frac{D_e(x)}{D_e(0)} ,$$

and introduce the function $f(\xi)$ such that

$$\int_x^L q_{et}dx = Lq_{et}(0)\int_\xi^1 \frac{D_e(\xi)}{D_e(0)} d\xi = Lq_{et}(0)f(\xi).$$

We now write α_e' as follows:

$$\alpha_e' = 2\int_0^1 \frac{f(\xi)}{\sigma(\xi)} d\xi \Big/ \int_0^1 \frac{d\xi}{\sigma(\xi)} ; \qquad (D.3)$$

as previously, we expand the following term

$$\left[\frac{f}{\sigma}\right]_\xi = \left[\frac{f}{\sigma}\right]_0 + \xi\left[\frac{f'}{\sigma} - \frac{f\sigma'}{\sigma^2}\right]_0 + \frac{1}{2}\xi^2\left[\frac{f''}{\sigma} - \frac{2f'\sigma'}{\sigma^2} + \frac{(2\sigma'^2 - \sigma\sigma'')f}{\sigma^3}\right]_0$$

and, hence, by use of eq. (D.1), we rewrite (D.3) as follows:

$$\alpha_e' = 2\left[f + \frac{\frac{f'}{2} + \frac{f''\sigma - 2f'\sigma'}{6\sigma}}{1 - \frac{\sigma'}{2\sigma} + \frac{2\sigma'^2 - \sigma\sigma''}{6\sigma}}\right]_{\xi=0} .$$

For conical shapes we have

$$D_e(\xi) = D_e(0)[1+\alpha_e\xi]$$

and hence,

$$f(\xi) = 1 + \tfrac{1}{2}\alpha_e - \xi - \tfrac{1}{2}\alpha_e\xi^2 ;$$

therefore,

$$\alpha_e' = 2\left[1 + \frac{\alpha_e}{2} + \frac{-\frac{1}{2} - \frac{\alpha_e}{6} + \frac{2}{3}\frac{\alpha_e - \delta^2\alpha_i}{1-\delta^2}}{1 - \frac{\alpha_e - \delta^2\alpha_i}{1-\delta^2}}\right]$$

$$\sim 2 + \alpha_e - \left[1 + \frac{\alpha_e}{3} - \frac{4}{3}\frac{\alpha_e - \delta^2\alpha_i}{1-\delta^2} + \frac{\alpha_e - \delta^2\alpha_i}{1-\delta^2}\right]$$

$$\sim 1 + \frac{2}{3}\alpha_e - \frac{\alpha_e - \delta^2\alpha_i}{3(1-\delta^2)} ,$$

or

$$\alpha_e' \sim 1 + \frac{\alpha_e - \delta^2(2\alpha_e - \alpha_i)}{3(1-\delta^2)} . \qquad (D.4)$$

For quasicylindrical tubular beams we obtain $\alpha_e' \sim 1$.

APPENDIX E

PERTURBATION METHOD AND INITIALIZATION OF COMPUTATIONS

APPENDIX E: PERTURBATION METHOD AND INITIALIZATION OF COMPUTATIONS

In this Appendix, the perturbation method will be used to obtain simple approximate expressions of the eigenfrequencies for small flow velocities and small internal damping, which will be used in initializing the calculations in the computer programs.

E.1 SMALL VELOCITIES

Although it has been previously mentioned that we are mainly interested in critical flow velocities, the following analysis will provide some useful insight about the behaviour of natural frequencies at small flow velocities.

For simplicity, we shall restrict ourselves to

- almost uniform tubes: $\alpha_e \sim \alpha_i \sim 0$;
- negligible gravity forces: $\gamma \sim 0$;
- no external tension: $\theta \sim 0$;
- pure viscoelastic damping ($\nu/\mu \sim 0$).

We set $\lambda_e = \left(\frac{\gamma_e - 1}{\gamma_e + \gamma_i}\right)^{\frac{1}{2}}$, $\lambda_i = \left(\frac{\delta^2 + \gamma_i}{\gamma_e + \gamma_i}\right)^{\frac{1}{2}}$ and rewrite eq.(6.8) as follows:

$$(1+i\omega\nu)\frac{d^4\Phi}{d\xi^4} + \left\{\left(\frac{1-\alpha\xi}{\sigma}\right)^2 u_e^2 + v_i^2 + \varepsilon c_t u_e^2 (1-\xi)\right\}\frac{d^2\Phi}{d\xi^2}$$

$$+ \left\{\varepsilon c_n u_e^2 + i\omega\left[2\lambda_i v_i + \left[1+\left(\frac{1-\alpha\xi}{\sigma}\right)^2 \lambda_e u_e\right]\right\}\frac{d\Phi}{d\xi}\right.$$

$$+ \left\{i\omega\,\varepsilon(c_n u_e + c_v)\lambda_e - \omega^2\right\}\Phi = 0 \ .$$

We now write a first order perturbation approximation with respect to u_e & v_i in the form

$$\Phi = \Phi_o + u_e \Phi_e + v_i \Phi_i \ ,$$

$$\omega = \omega_o + u_e \omega_e + v_i \omega_i \ ,$$

where Φ_o and ω_o may represent any of the modal eigenfunctions and matching eigenfrequencies at zero flow.

For zero flow, i.e. $u_e = v_i = 0$, we have

$$(1+i\omega_o \nu)\,\Phi_o^{(4)} + \{i\omega_o \varepsilon c_v \lambda_e - \omega_o^2\}\Phi_o = 0 \ ; \qquad \text{(E.1)}$$

and for no internal flow, i.e. $v_i = 0$, but small external flow velocity, u_e, first order terms in u_e yield

$$(1+i\omega_o \nu)\,\Phi_e^{(4)} + \{i\omega_o \varepsilon c_v \lambda_e - \omega_o^2\}\Phi_e =$$

$$- i\omega_e \nu\, \Phi_o^{(4)} - i\omega_o [1+(\tfrac{1-\alpha\xi}{\sigma})^2]\lambda_e\, \Phi_o' - [i\omega_e \varepsilon c_v \lambda_e - 2\omega_o \omega_e + i\omega_o \varepsilon c_n \lambda_e]\Phi_o \ ; \qquad \text{(E.2)}$$

finally, for no external flow, i.e. $u_e = 0$, first order terms in v_i yield

$$(1+i\omega_o \nu)\,\Phi_i^{(4)} + [i\omega_o \varepsilon c_v \lambda_e - \omega_o^2]\Phi_i =$$

$$- i\omega_i \nu\, \Phi_o^{(4)} - i\omega_o\, 2\lambda_i\, \Phi_o' - [i\omega_i \varepsilon c_v \lambda_e - 2\omega_o \omega_i]\Phi_o \ . \qquad \text{(E.3)}$$

Let us now premultiply eq.(E.1) by Φ_e, and add it to eq.(E.2) premultiplied by $-\Phi_o$; we get

$$(1+i\omega_o \nu)[\Phi_o^{(4)}\Phi_e - \Phi_o \Phi_e^{(4)}] =$$

$$i\omega_e \nu \Phi_o \Phi_o^{(4)} + i\omega_o [1 + (\tfrac{1-\alpha\xi}{\sigma})^2]\lambda_e \Phi_o \Phi_o' + [i\omega_e \varepsilon c_v \lambda_e - 2\omega_o \omega_e + i\omega_o \varepsilon c_n \lambda_e]\Phi_o^2 \ .$$

Similarly, premultiplying eq.(E.1) by Φ_i and adding eq.(E.3) multiplied by $-\Phi_o$, we obtain

$$(1+i\omega_o\nu)[\Phi_o^{(4)}\Phi_i - \Phi_o\Phi_i^{(4)}] =$$

$$i\omega_i\nu\Phi_o\Phi_o^{(4)} + i\omega_o 2\lambda_i\Phi_o\Phi_o' + [i\omega_i\varepsilon c_v\lambda_e - 2\omega_o\omega_i]\Phi_o^2 .$$

In these last two equations, by use of eq.(E.1), we shall write

$$\Phi_o\Phi_o^{(4)} = -\frac{i\omega_o\varepsilon c_v\lambda_e-\omega_o^2}{1+i\omega_o\nu}\Phi_o^2$$

We shall now integrate these two equations over the interval [0,1]; the integration by parts of the following term yields

$$\int_0^1 [\Phi_o^{(4)}\Phi-\Phi_o\Phi^{(4)}]d\xi = [\Phi_o^{(3)}\Phi-\Phi_o\Phi^{(3)}-\Phi_o^{(2)}\Phi' + \Phi_o'\Phi^{(2)}]_o^1 ,$$

and the last two equations, once integrated over the interval [0,1], thus yield

$$(1+i\omega_o\nu)[\Phi_o^{(3)}\Phi_e - \Phi_o\Phi_e^{(3)} - \Phi_o^{(2)}\Phi_e' + \Phi_o'\Phi_e^{(2)}]_{\xi=0}^{\xi=1} =$$

$$\{i\omega_e\nu\frac{\omega_o^2-i\omega_o\varepsilon c_v\lambda_e}{1+i\omega_o\nu} + i\omega_e\varepsilon c_v\lambda_e - 2\omega_o\omega_e + i\omega_o\varepsilon c_n\lambda_e\}\int_0^1 \Phi_o^2 d\xi .$$

$$+ i\omega_o\lambda_e\int_0^1 [1+(\frac{1-\alpha\xi}{\sigma})^2]\Phi_o\Phi_o'd\xi ,$$

and

$$(1+i\omega_o\nu)[\Phi_o^{(3)}\Phi_i - \Phi_o\Phi_i^{(3)} - \Phi_o^{(2)}\Phi_i' + \Phi_o'\Phi_i^{(2)}]_{\xi=0}^{\xi=1} =$$

$$\{i\omega_i\nu\frac{\omega_o^2-i\omega_o\varepsilon c_v\lambda_e}{1+i\omega_o\nu} + \imath\omega_i\varepsilon c_v\lambda_e - 2\omega_o\omega_i\}\int_0^1 \Phi_o^2 d\xi + i\omega_o\lambda_i[\Phi_o^2]_{\xi=0}^{\xi=1} .$$

From hereon we shall assume that the beam is supported at $\xi=0$, i.e. $\Phi_o(0)=\Phi_e(0)=\Phi_i(0)=0$; also that Φ_o is normalized, i.e. $\int_0^1\Phi_o^2 d\xi=1$. We may now calculate the following integral which appears in the former equation,

$$\int_0^1 [1 + (\frac{1-\alpha\xi}{\sigma})^2]\Phi_o'\Phi_o d\xi = \left\{\frac{1}{2}[1 + (\frac{1-\alpha\xi}{\sigma})^2]\Phi_o^2\right\}_0^1 + \frac{\alpha}{\sigma^2}\int_0^1 (1-\alpha\xi)\Phi_o^2\, d\xi$$

$$= \frac{1}{2\sigma^2}(\sigma^2+1-2\alpha+\alpha^2)\Phi_o^2(1) + \frac{\alpha}{\sigma^2}(1-\alpha\int_0^1\Phi_o^2\xi d\xi)$$

$$\sim \frac{\sigma^2+1-2\alpha}{2\sigma^2}\Phi_o^2(1) + \frac{\alpha}{\sigma^2} ;$$

neglecting the terms containing α^2 is indeed of little consequence since α, which accounts for the slope of the boundary layer, is much smaller than 1. We thus rewrite our two equations as

$$(1+i\omega_o\nu)[\Phi_o^{(3)}\Phi_e - \Phi_o\Phi_e^{(3)} - \Phi_o^{(2)}\Phi_e' + \Phi_o'\Phi_e^{(2)}]_{\xi=0}^{\xi=1} \qquad (E.4)$$

$$= i\omega_e[\varepsilon c_v\lambda_e - \nu\frac{i\omega_o\varepsilon c_v\lambda_e-\omega_o^2}{1+i\omega_o\nu} + 2i\omega_o] + i\omega_o\lambda_e[\varepsilon c_n + \frac{\alpha}{\alpha^2} + \frac{\sigma^2+1-2\alpha}{2\sigma^2}\Phi_o^2(1)],$$

and,

$$(1+i\omega_o\nu)[\Phi_o^{(3)}\Phi_i - \Phi_o\Phi_i^{(3)} - \Phi_o^{(2)}\Phi_i' - \Phi_o'\Phi_i^{(2)}]_{\xi=0}^{\xi=1}$$

$$= i\omega_i[\varepsilon c_v\lambda_e - \nu\frac{i\omega_o\varepsilon c_v\lambda_e-\omega_o^2}{1+i\omega_o\nu} + 2i\omega_o] + i\omega_o\lambda_i\,\Phi_o^2(1) . \qquad (E.5)$$

E.1.1 Applications: Tubular beams supported at both ends.

Φ_o, Φ_e and Φ_i satisfy the same boundary conditions as Φ, i.e.

$\Phi(0) = \Phi''(0) = \Phi(1) = \Phi''(1) = 0$ for pinned-pinned, and

$\Phi(0) = \Phi'(0) = \Phi(1) = \Phi'(1) = 0$ for clamped-clamped beams;

hence, eq.(E.4) yields in both cases

$$i\omega_e[\varepsilon c_v \lambda_e + 2i\omega_o - \nu\frac{i\omega_o \varepsilon c_v \lambda_e - \omega_o^2}{1+\omega i\nu_o}] + i\omega_o\lambda_e[\varepsilon c_n + \frac{\alpha}{\sigma^2}] = 0 ,$$

or

$$\omega_e = \frac{i\lambda_e[\varepsilon c_n + \frac{\alpha}{\sigma^2}]}{2 + \frac{\varepsilon c_v \lambda_e}{i\omega_o} - \nu\frac{\varepsilon c_v \lambda_e + i\omega_o}{(1+i\omega_o\nu)}} ;$$

similarly, eq.(E.5) simply yields

$$\omega_i = 0 .$$

Thus, for negligible flow viscosity effects and negligible viscoelastic damping, i.e. for $c_v \sim 0$ and $\nu \sim 0$, we obtain

$$\omega_e \sim i\frac{\lambda_e}{2}[\varepsilon c_n + \frac{\alpha}{\sigma^2}]$$

$$\omega_i = 0 .$$

It is seen that ω_e is purely imaginary and independent of the natural frequencies ω_o, and that the imaginary part of ω_e is positive. Hence, small external flow velocities produce damping which is the same for all the modes and introduce no change in the frequencies of oscillations. The hydrodynamic damping predicted by the

perturbation method is proportional to the flow velocity since $\omega = \omega_o + \omega_e u_e$. However, the perturbation method only applies if $\omega_e u_e << \omega_o$. Nevertheless, the range of velocities which satisfy this condition is proportional to ω_o and thus increases rapidly from one mode to the next one above.

Because α is proportional to c_t (§2.6.2), ω_e is proportional to c_n and c_t and therefore damping at low flow velocities will be proportional to normal and tangential friction; furthermore, ω_e being proportional to λ_e, it can be shown that damping diminishes as the ratio ρ_e/ρ of the density of the fluid to that of the beam increases.

With respect to the internal flow, since $\omega_i = 0$, small flow velocities have little influence on the eigenfrequencies; in other words, small internal flows do not create damping nor do they affect the natural frequencies of oscillations.

E.1.2 Applications: Clamped-free beams.

From eq. (6.7) we obtain, neglecting all second order terms in u_e or v_i, at $\xi = 1$

$$(1+i\omega_o\nu)\frac{d^3\Phi}{d\xi^3} - i\omega\chi\{f[s_e + \delta^2(\frac{1-\alpha}{\sigma})^2]\lambda_e u_e + 2\lambda_i v_i\}\frac{d\Phi}{d\xi} + \{i\omega f u_e[1-\delta^2]\lambda_e(\frac{1-\alpha}{\sigma})^2 + \omega^2\chi\lambda\}\Phi = 0 , \tag{E.6}$$

$$\text{with } \lambda = \frac{[1+f(\gamma_e-1)]s_e+\gamma_i}{\gamma_e+\gamma_i} \sim \frac{1+f(\gamma_e-1)+3\gamma_i}{3(\gamma_e+\gamma_i)} ,$$

and we have for Φ the following relation:

$$\Phi(0) = \Phi'(0) = \Phi''(1) = 0 .$$

From eq. (E.6) we further obtain

$$(1+i\omega_o\nu)\Phi_o^{(3)}(1) + \omega_o^2\chi\lambda\ \Phi_o(1) = 0\ , \tag{E.7}$$

$$(1+i\omega_o\nu)\Phi_e^{(3)}(1) + \omega_o^2\chi\lambda\ \Phi_e(1) =$$

$$- [i\omega_o f(1-\delta^2)\lambda_e(\frac{1-\alpha}{\sigma})^2 + 2\omega_o\omega_e\chi\lambda]\Phi_o(1) \tag{E.8}$$

$$+ i\omega_o\chi f[s_e+\delta^2(\frac{1-\alpha}{\sigma})^2]\lambda_e\ \Phi_o'(1) - i\omega_e\nu\Phi_o^{(3)}(1)\ ,$$

$$(1+i\omega_o\nu)\Phi_i^{(3)}(1) + \omega_o^2\chi\lambda\ \Phi_i(1) =$$

$$- 2\omega_o\omega_i\chi\lambda\ \Phi_o(1) + 2i\omega_o\chi\lambda_i\ \Phi_o'(1) - i\omega_i\nu\Phi_o^{(3)}(1)\ ; \tag{E.9}$$

subsequently, we shall eliminate $\Phi_o^{(3)}(1)$ from eqs. (E.8) and (E.9) by use of eq. (E.7).

In order to evaluate eqs. (E.4) and (E.5) we calculate

$$(1+i\omega_o\nu)[\Phi_o^{(3)}\Phi_e - \Phi_o\Phi_e^{(3)}]_{\xi=1} \quad \text{and} \quad (1+i\omega_o\nu)[\Phi_o^{(3)}\Phi_i - \Phi_o\Phi_i^{(3)}]_{\xi=1}$$

$$(1+i\omega_o\nu)[\Phi_o^{(3)}\Phi_e - \Phi_o\Phi_e^{(3)}]_{\xi=1} =$$

$$[i\omega_o f[1-\delta^2)\Phi_e(\frac{1-\alpha}{\sigma})^2 + 2\omega_o\omega_e\chi\lambda - \omega_o^2\chi\lambda\frac{i\omega_e\nu}{1+i\omega_o\nu}]\Phi_o^2(1)$$

$$- i\omega_o\chi f[s_e+\delta^2(\frac{1-\alpha}{\sigma})^2]\lambda_e\Phi_o\Phi_o'(1)$$

and

$$(1+i\omega_o\nu)\,[\Phi_o^{(3)}\Phi_i - \Phi_o\Phi_i^{(3)}]_{\xi=1} =$$

$$[2\omega_o\omega_i\chi\lambda - \omega_o^2\chi\lambda\frac{i\omega_i\nu}{1+i\omega_o\nu}]\Phi_o^2(1) - 2i\omega_o\chi\lambda_i\Phi_o'\Phi_o(1)\ .$$

We may now rewrite eq.(E.4) and (E.5) at $\xi=1$ as follows:

$$(1+i\omega_o\nu)\{[i\omega_o f(1-\delta^2)\lambda_e(\frac{1-\alpha}{\sigma})^2 + 2\omega_o\omega_e\chi\lambda - \omega_o^2\chi\lambda\frac{i\omega_e\nu}{1+i\omega_o\nu}]\Phi_o^2$$

$$- i\omega_o\chi f\,[s_e+\delta^2(\frac{1-\alpha}{\sigma})^2]\lambda_e\Phi_o\Phi_o'\} = \qquad \text{(E.10)}$$

$$i\omega_e[2i\omega_o+\varepsilon c_v\lambda_e-\nu\frac{i\omega_o\varepsilon c_v\lambda_e-\omega_o^2}{1+i\omega_o\nu}] + i\omega_o\lambda_e[\varepsilon c_n + \frac{\alpha}{\sigma^2} + \frac{\sigma^2+1-2\alpha}{2\sigma^2}\Phi_o^2]\ ,$$

and

$$(1+i\omega_o\nu)\{[2\omega_o\omega_i\chi\lambda - \omega_o^2\chi\lambda\frac{i\omega_i\nu}{1+i\omega_o\nu}]\Phi_o^2 - 2i\omega_o\chi\lambda_i\Phi_o'\Phi_o\} =$$

$$\qquad \text{(E.11)}$$

$$i\omega_i[2i\omega_o + \varepsilon c_v\lambda_e - \nu\frac{i\omega_o\varepsilon c_v\lambda_e-\omega_o^2}{1+i\omega_o\nu}] + i\omega_o\lambda_i\Phi_o^2\ .$$

We now need to calculate $\Phi_o(1)$ and $\Phi_o'(1)$; this could be done theoretically by solving eq.(E.1) with the boundary conditions $\Phi_o(0) = \Phi_o'(0) = \Phi_o'(1) = (1+i\omega_o\nu)\Phi_o^{(3)}(1) + \omega_o^2\chi\lambda\Phi_o(1) = 0$.

For the sake of simplicity we shall now assume that $c_v\sim\nu\sim0$ and $\chi<<1$ so that the eigenfunctions Φ_o are close to those of the classical uniform beam; hence, the normalized solution yields

$$\Phi_o(1) \sim \pm 2\ ,$$

$$\Phi_o'(1) \sim \Phi_o(1)\omega_o^{\frac{1}{2}}\ ,$$ where the positive or negative sign depends upon the mode number corresponding to ω_o.

We now rewrite eq. (E.10) as follows:

$$f(1-\delta^2)\lambda_e\left(\frac{1-\alpha}{\sigma}\right)^2 4 - \chi f\left[s_e+\delta^2\left(\frac{1-\alpha}{\sigma}\right)^2\right]\lambda_e 4\omega_o^{\frac{1}{2}} - \lambda_e\left[\varepsilon c_n + 2\frac{\sigma^2+1}{\sigma^2} - 3\frac{\alpha}{\sigma^2}\right]$$

$$\sim 2i\omega_e(1+4\chi\lambda) \ ;$$

hence, we get

$$\omega_e \sim \frac{i\lambda_e}{2(1+4\chi\lambda)}\left\{ - 4f(1-\delta^2)\left(\frac{1-\alpha}{\sigma}\right)^2 + 4\chi\omega_o^{\frac{1}{2}} f\left[s_e+\delta^2\left(\frac{1-\alpha}{\sigma}\right)^2\right] \right.$$

$$\left. + \varepsilon c_n + 2 + \frac{2-3\alpha}{\sigma^2} \right\}. \qquad \text{(E.12)}$$

Apart from the fact that it is imaginary, little can be concluded concerning the value of ω_e; however, provided that $\chi\omega_o^{\frac{1}{2}} << 1$ and $\chi << 1$, and provided that we neglect the boundary layer ($\sigma \sim 1, \alpha \sim 0$), the previous expression reduces to

$$\omega_e \sim i\frac{\lambda_e}{2}[\varepsilon c_n + 4(f\delta^2+1-f)];$$

and similarly eq. (E.11) yields

$$- 4i\omega_o\lambda_i - 2i\omega_o\chi\lambda_i\, 4\omega_o^{\frac{1}{2}} \sim i\omega_i[2i\omega_o(1+4\chi\lambda)] \ ;$$

hence

$$\omega_i \sim i\lambda_i\frac{4+8\chi\omega_o^{\frac{1}{2}}}{2(1+4\chi\lambda)} \sim 2i\lambda_i \ . \qquad \text{(E.13)}$$

We thus note that both ω_e and ω_i are imaginary and positive (since $\lambda_e, \lambda_i, \varepsilon c_n, \delta > 0$ and $0 < f < 1$), and therefore small flow velocities will have a stabilizing (damping) effect on

cantilevers; such hydrodynamic damping will be larger with larger local shear (larger friction coefficients c_n), slender beams and blunter end pieces (smaller values of f). As previously noted, in the case of clamped-clamped beams, here again hydrodynamic damping is independent of the natural modal frequencies ω_o provided that the end piece is small enough to have $f\chi\omega_o^{\frac{1}{2}} \ll 1$.

In summary, these sets of formulae in their simplest form could be successfully applied to velocities up to 1 with less than 1% error; in their more elaborate form, e.g. in eq. (E.12), they can be used over a larger range of velocities provided that the conditions

$$v_i\omega_i \ll \omega_o \text{ and } u_e\omega_e \ll \omega_o$$

for perturbation solutions are not violated.

On page E-15, the eigenvalues of the five lowest modes have been plotted with respect to the internal flow velocity in the simple case were $c_v=\nu=\chi=0$ and $\lambda_i=.5$; eq. (E.13) yields $\omega_i=i$, and the approximate solution reads

$$\omega = \omega_o + i v_i \ ;$$

as can be seen from the graph, the higher the mode, the larger the range of velocities over which this solution appears to be valid.

E.2 SMALL INTERNAL DAMPING

We shall now investigate the effect of small viscoelastic and hysteretical damping involving the terms with coefficient

$$1 + \frac{i\omega\mu\nu}{\mu+\nu|\omega|}$$

upon the natural frequencies at zero flow conditions. We shall also relax the assumption $\alpha_e=\alpha_i=0$ and eq.(6.8) may be rewritten at zero flows as

$$(1 + \frac{i\omega\mu\nu}{\mu+\nu|\omega|})\frac{d^2}{d\xi^2}\{j(\xi)\frac{d^2\phi}{d\xi^2}\} - \omega^2 m(\xi)\phi = 0 , \qquad (E.14)$$

with

$$j(\xi) = \frac{(1+\alpha_e\xi)^4 - \delta^4(1+\alpha_i\xi)^4}{1 - \delta^4} , \quad m(\xi) = \frac{\gamma_e(1+\alpha_e\xi)^2 + \gamma_i(1+\alpha_i\xi)^2}{\gamma_e + \gamma_i} .$$

We shall consider the viscoelastic coefficient ν as the only perturbation variable, and we set

$$\phi = \phi_o + \nu\phi_1 ,$$

$$\omega = \omega_o + \nu\omega_1 .$$

Let $\beta=\nu/\mu$, the damping coefficient becomes

$$1 + \frac{i\omega\mu\nu}{\mu+\nu|\omega|} \sim 1 + \frac{i\omega_o\nu}{1+\beta\omega_o}$$

where β will be considered as a parameter, i.e. independent of ν.

We now obtain the following differential equations

$$\frac{d^2}{d\xi^2}\{j(\xi)\phi_o^{(2)}\} - \omega_o^2 m(\xi)\phi_o = 0 ,$$

$$\frac{d^2}{d\xi^2}\{j(\xi)\phi_1^{(2)}\} - \omega_o^2 m(\xi)\phi_1 - \frac{-i\omega_o}{1+\beta\omega_o}\frac{d^2}{d\xi^2}\{j(\xi)\phi_o^{(2)}\} + 2\omega_o\omega_1 m(\xi)\phi_o$$

$$= [\frac{-i\omega_o^3}{1+\beta\omega_o} + 2\omega_o\omega_1]m(\xi)\phi_o ,$$

which may be combined and integrated to give

$$[\Phi_1 \frac{d}{d\xi}\{j(\xi)\Phi_o^{(2)}\} - \Phi_o \frac{d}{d\xi}\{j(\xi)\Phi_1^{(2)}\} - \Phi_1' j(\xi)\Phi_o^{(2)} + \Phi_o' j(\xi)\Phi_1^{(2)}]_o^1$$

$$= [\frac{+i\omega_o^3}{1+\beta\omega_o} - 2\omega_o\omega_1] \int_o^1 m(\xi)\Phi_o^2(\xi)d\xi \ . \qquad \text{(E.15)}$$

Let us now apply the boundary conditions.

a) For clamped-clamped or pinned-pinned beams:

The left-hand-side of eq.(E.15) is null, hence we need have:

$$\omega_1 = \frac{1}{2}\ \omega_o^2 i/(1+\beta\omega_o)$$

b) For clamped-free beams: $\Phi(0) = \Phi'(0) = \Phi''(1) = 0$,

and $[1 + \frac{i\omega_o\nu}{1+\beta\omega_o}] j(1)\Phi^{(3)}(1) + \omega_o^2\ \chi\lambda\ \Phi(1) \qquad = 0$,

with $\lambda = \dfrac{[1+f(\gamma_e-1)]s_e+\gamma_i s_i}{\gamma_e + \gamma_i}$, as obtained from eq.(6,7).

Hence, we derive the two boundary conditions

$$j(1)\Phi_o^{(3)}(1) + \omega_o^2\ \chi\lambda\ \Phi_o(1) = 0 \ , \qquad \text{(E.16)}$$

$$j(1)\Phi_1^{(3)}(1) + \omega_o^2\ \chi\lambda\ \Phi_1(1) = -\frac{i\omega_o}{1+\beta\omega_o}\ j(1)\Phi_o^{(3)}(1)$$

$$- 2\omega_o\omega_1\ \chi\lambda\ \Phi_o(1) \ ; \qquad \text{(E.17)}$$

Since either slope or moment is null at the extremeties, eq.(E.15) reduces to

$$[\Phi_1\Phi_o^{(3)} - \Phi_o\Phi_1^{(3)}]_1 j(1) = [\frac{i\omega_o^3}{1+\beta\omega_o} - 2\omega_o\omega_1] \int_0^1 m(\xi)\Phi_o^2 d\xi .$$

The left-hand side, calculated by combining eq.(E.16) and (E.17), yields

$$\left(\frac{-i\omega_o^3}{1+\beta\omega_o} + 2\omega_o\omega_1\right)\chi\lambda\ \Phi_o^2(1);$$

hence, we obtain

$$\left(\frac{i\omega_o^3}{1+\beta\omega_o} - 2\omega_o\omega_1\right)\int_0^1 m(\xi)\Phi_o^2 d\xi = \left(2\omega_o\omega_1 - \frac{i\omega_o^3}{1+\beta\omega_o}\right)\chi\lambda\Phi_o^2(1)\ ;$$

since the integral and $\Phi_o^2(1)$ are both positive and not zero, once more we must have

$$\omega_1 = \frac{i\omega_o^2}{2(1+\beta\omega_o)}\ .$$

It thus appears that damping resulting from visco-hysteretic characteristics in the material, unlike hydrodynamic damping, increases with the mode number; it is proportional to the modal eigenfrequency for purely hysteretic damping and proportional to the eigenfrequency squared for viscoelastic damping. In summary we obtain

$$\begin{aligned}
\omega &= \omega_o + \tfrac{1}{2}i\mu\omega_o && \text{for hysteretic damping,}\\
\omega &= \omega_o + \tfrac{1}{2}i\nu\omega_o^2 && \text{for viscoelastic damping,}\\
\omega &= \omega_o + \frac{i\mu\nu\omega_o^2}{2(\mu+\nu\omega_o)} && \text{for viscohysteretic damping.}
\end{aligned} \qquad \text{(E.18)}$$

These results are illustrated on page E-16 and compared to the three lowest eigenfrequencies of a conical tube (the

characteristics of which are given in Fig.8) for each type of damping. Although gravity effects were not negligible ($\gamma=1.45\times10^{-3}$) and although relatively large damping coefficients were selected, the agreement between eq.(E.18) (dotted lines) and the corresponding eigenfrequencies actually computed (data points) is good. In addition, it can be verified that viscohysteretic damping is equivalent to viscoelastic damping at low frequencies ($\omega_o<<\mu/\nu=40$) and tends towards hysteretic damping at high frequencies ($\omega_o>>\mu/\nu$).

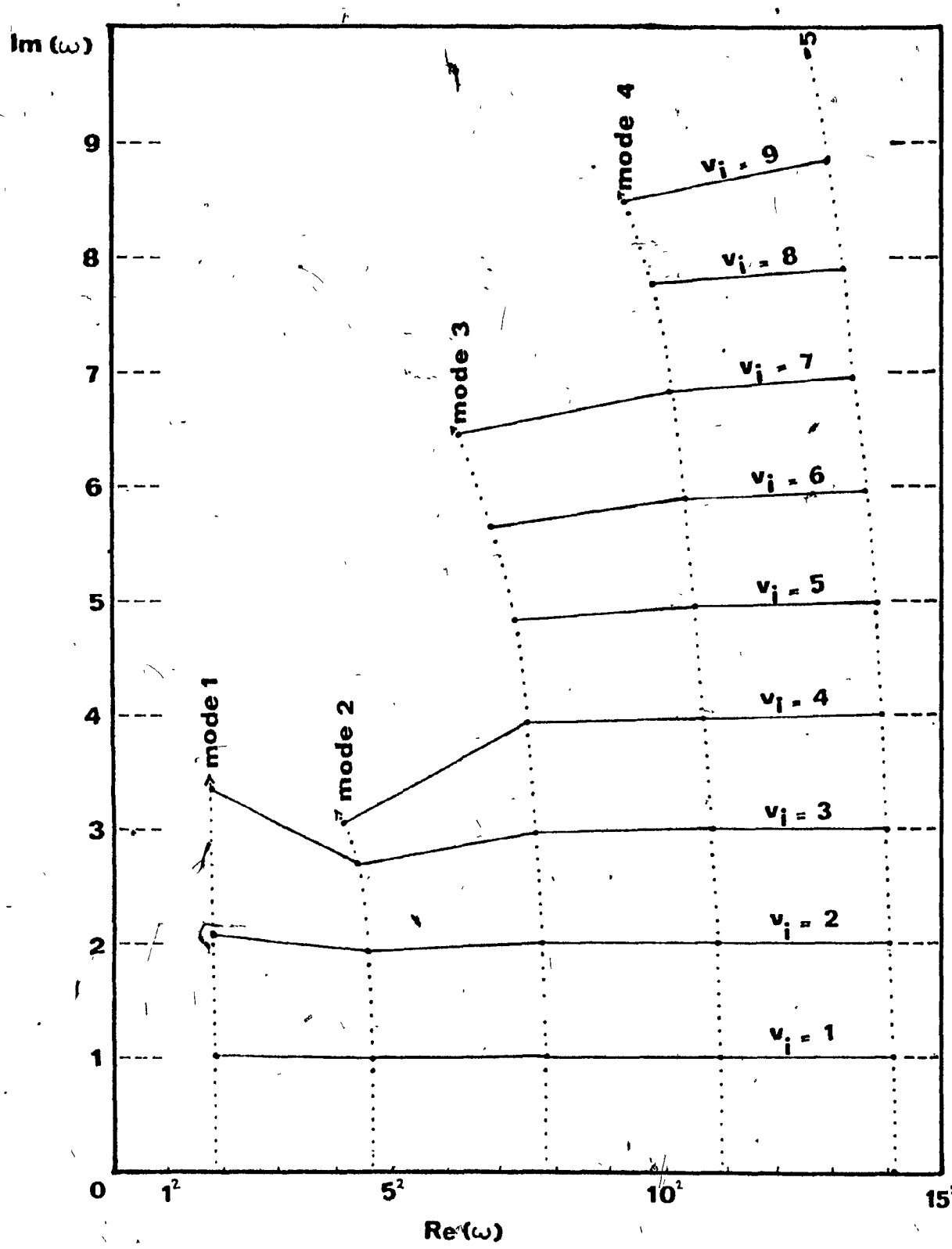

HYDRODYNAMIC DAMPING RESULTING FROM SMALL INTERNAL FLOW VELOCITIES FOR A CYLINDRICAL CANTILEVERED TUBE.

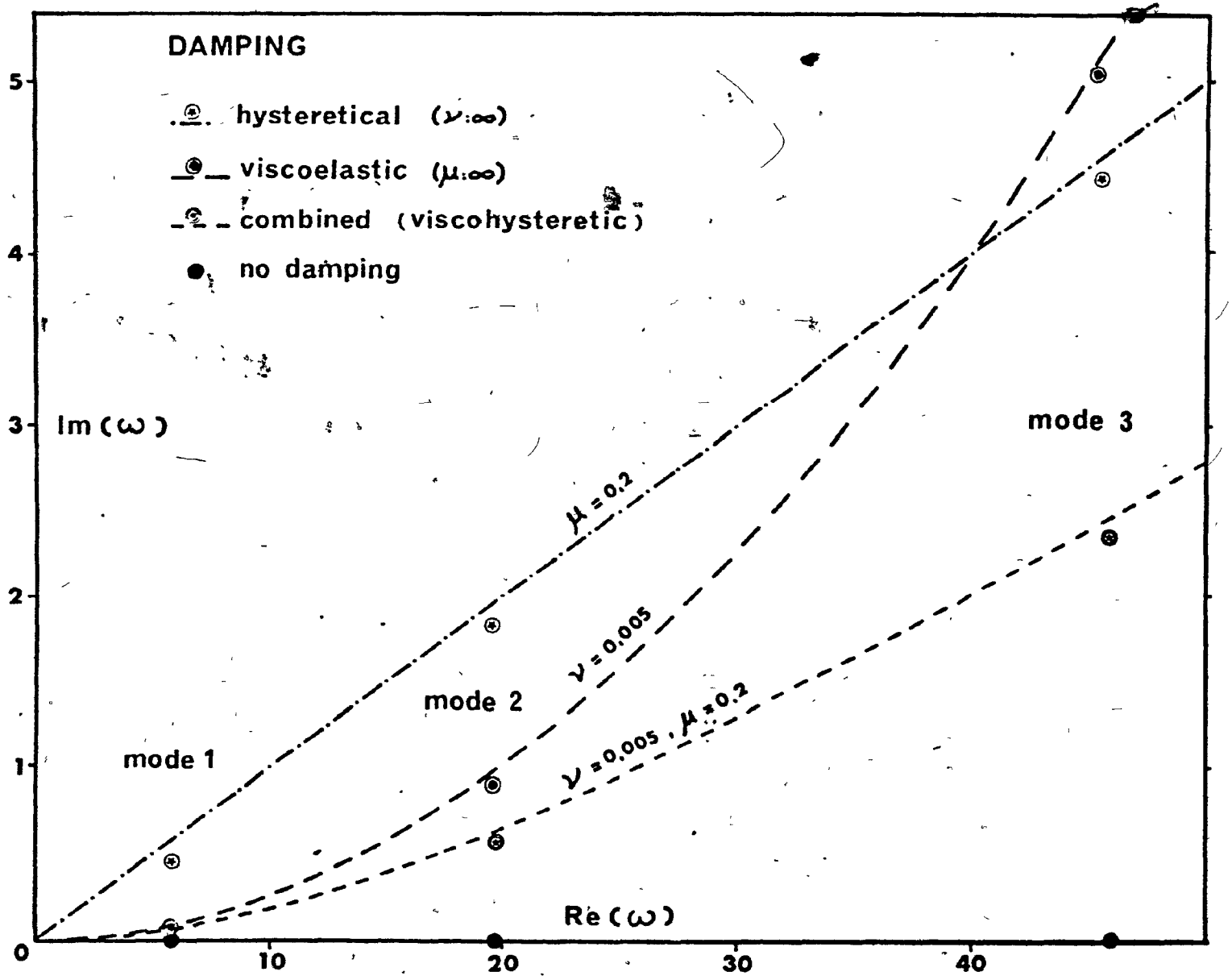

COMPARATIVE EFFECTS OF VISCOELASTIC, HYSTERETIC AND VISCOHYSTERETIC DAMPING ON NATURAL EIGENFREQUENCIES.

APPENDIX F

CALCULATION OF THE CORRECTIVE PRESSURE COEFFICIENT c_p FOR SLENDER BODIES

APPENDIX F: CALCULATION OF THE CORRECTIVE PRESSURE COEFFICIENT c_p FOR SLENDER BODIES

We shall now show that the pressure terms involving $\frac{dc_p}{dx}$, which were neglected in eq.(3.4), are indeed quite small, vis-à-vis the friction terms involving q_{et}. As given by Sears [73], the perturbation potential of the flow pattern for Mach numbers <<1 is

$$\Phi(x,r) = -\frac{U}{4\pi}\int_0^L \frac{S'(u)\,du}{[(x-u)^2 + r^2]^{\frac{1}{2}}}$$

As illustrated on the right, U is the (positive) flow velocity, S(x) is the cross-section area, x=0 and x=L are the abscissae of the nose and tail of the beam.

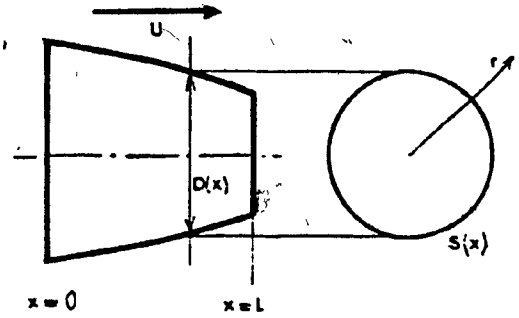

The pressure coefficient for points near the surface of a slender body of revolution is

$$c_p = -\frac{2}{U}\frac{\partial\Phi}{\partial x} - \frac{1}{U^2}\left[\frac{\partial\Phi}{\partial r}\right]^2 . \qquad (F.1)$$

For a conical structum we write for the diameter

$$D(x) = D_o\left[1 + \alpha\frac{x}{L}\right]$$

and we now set the following dimensionless parameters:

$$\xi = x/L, \quad \rho = r/L, \quad \varepsilon = L/D_o .$$

Hence, we write

$$\Phi(x,r) = -\frac{\alpha U D_o^2}{8L}\int_0^1 \frac{(1+\alpha u)\,du}{[(\xi-u)^2+\rho^2]^{\frac{1}{2}}} = -\frac{\alpha U L}{8\varepsilon^2}\,\Psi(\xi,\rho) \qquad (F.2)$$

and

$$c_p = \frac{\alpha}{4\varepsilon^2}\frac{\partial\Psi}{\partial\xi} - \frac{\alpha^2}{64\varepsilon^4}\left(\frac{\partial\Psi}{\partial\rho}\right)^2 . \qquad (F.3)$$

The value of $\frac{dc_p}{dx}$ at the wall is

$$\frac{dc_p}{dx} = \frac{\partial c_p}{\partial x} + \frac{\partial c_p}{\partial r}\left[\frac{\partial r}{\partial x}\right]_w = \frac{\partial c_p}{\partial x} + \frac{\partial c_p}{\partial r}\times\frac{\alpha}{2\varepsilon} ;$$

hence, by use of eq.(F.3)

$$\frac{dc_p}{d\xi} = \frac{\alpha}{4\varepsilon^2}\left[\frac{\partial^2\Psi}{\partial\xi^2} + \frac{\alpha}{2\varepsilon}\frac{\partial^2\Psi}{\partial\xi\partial\rho}\right] - \frac{\alpha^2}{32\varepsilon^4}\frac{\partial\Psi}{\partial\rho}\left[\frac{\partial^2\Psi}{\partial\xi\partial\rho} + \frac{\alpha}{2\varepsilon}\frac{\partial^2\Psi}{\partial\rho^2}\right] .$$

F.1 CALCULATION OF $\frac{\partial\Psi}{\partial\rho}$

$$\frac{\partial\Psi}{\partial\rho} = \int_0^1 \frac{(1+\alpha u)(-\rho)\,du}{[(\xi-u)^2+\rho^2]^{\frac{3}{2}}} = \int_0^1 \frac{[\alpha\rho(\xi-u) - (\rho+\rho\alpha\xi)]\,du}{[(\xi-u)^2+\rho^2]^{\frac{3}{2}}} ,$$

which yields, upon setting $v=\xi-u$,

$$\frac{\partial\Psi}{\partial\rho} = [\rho+\alpha\rho\xi]\int_\xi^{\xi-1}\frac{dv}{[v^2+\rho^2]^{\frac{3}{2}}} - \alpha\rho\int_\xi^{\xi-1}\frac{v\,dv}{[v^2+\rho^2]^{\frac{3}{2}}}$$

$$= \frac{(1+\alpha\xi)}{\rho}\left\{\frac{v}{[v^2+\rho^2]^{\frac{1}{2}}}\right\}_{v=\xi}^{v=\xi-1} + \alpha\rho\left\{\frac{1}{[v^2+\rho^2]^{\frac{1}{2}}}\right\}_{v=\xi}^{v=\xi-1}$$

or

$$\frac{\partial\Psi}{\partial\rho} = \frac{1+\alpha\xi}{\rho}\,\frac{\xi-1}{[(\xi-1)^2+\rho^2]} - \frac{\xi}{[\xi^2+\rho^2]} + \alpha\rho\,\frac{1}{[(\xi-1)^2+\rho^2]} - \frac{1}{[\xi^2+\rho^2]} \qquad (F.4)$$

At the wall $\rho = \frac{1+\alpha\xi}{2} << 1$, hence the second term which is pre-multiplied by $\alpha\rho$ will usually be small compared to the first one, and $[\frac{\partial\Psi}{\partial\rho}]$ at the wall will be of the order of ε.

F.2 CALCULATION OF $\frac{\partial^2\Psi}{\partial\rho^2}$

From eq. (F.4) we may now derive $\frac{\partial^2\Psi}{\partial\rho^2}$

$$\frac{\partial^2\Psi}{\partial\rho^2} = -\frac{1+\alpha\xi}{\rho^2}\left[\frac{\xi-1}{[(\xi-1)^2+\rho^2]^{\frac{1}{2}}} - \frac{\xi}{[\xi^2+\rho^2]^{\frac{1}{2}}}\right] + \alpha\left[\frac{1}{[(\xi-1)^2+\rho^2]^{\frac{1}{2}}} - \frac{1}{[\xi^2+\rho^2]^{\frac{1}{2}}}\right]$$

$$+[(1+\alpha\xi)\xi + \alpha\rho^2][\xi^2+\rho^2]^{-\frac{3}{2}} - [(1+\alpha\xi)(\xi-1) + \alpha\rho^2][(\xi-1)^2+\rho^2]^{-\frac{3}{2}};$$

hence, $\frac{\partial^2\Psi}{\partial\rho^2}$ at the wall is of the order of ε^2.

F.3 CALCULATION OF $\frac{\partial^2\Psi}{\partial\rho\partial\xi}$

Upon differentiating eq. (F.4) with respect to ξ we obtain

$$\frac{\partial^2\Psi}{\partial\rho\partial\xi} = \{[\frac{1+\alpha\xi}{\rho}(\xi-1)+\alpha\rho](1-\xi) + \frac{1-\alpha+2\alpha\xi}{\rho}[(\xi-1)^2+\rho^2]\}[(\xi-1)^2+\rho^2]^{-\frac{3}{2}}$$

$$- \{[\frac{1+\alpha\xi}{\rho}\xi+\alpha\rho](-\xi) + \frac{1+2\alpha\xi}{\rho}[\xi^2+\rho^2]\}[\xi^2+\rho^2]^{-\frac{3}{2}},$$

which can be re-written as

$$\frac{\partial^2\Psi}{\partial\rho\partial\xi} = \frac{\frac{\alpha}{\rho}(\xi-1)^3 + \rho(1+\alpha\xi)}{[(\xi-1)^2+\rho^2]^{\frac{3}{2}}} - \frac{\frac{\alpha}{\rho}\xi^3 + \rho(1+\alpha\xi)}{[\xi^2+\rho^2]^{\frac{3}{2}}}.$$

F.4 CALCULATION OF $\frac{\partial^2\psi}{\partial\xi^2}$

Because of symmetry between ξ and u,

$$\frac{\partial^2\psi}{\partial\xi^2} = \int_0^1 (1+\alpha u)\frac{\partial^2}{\partial\xi^2}[(\xi-u)^2+\rho^2]^{-\frac{1}{2}}du = \int_0^1 (1+\alpha u)\frac{\partial^2}{\partial u^2}[(\xi-u)^2+\rho^2]^{-\frac{1}{2}}du,$$

which may be integrated by parts, and yields after two integrations

$$\frac{\partial^2\psi}{\partial\xi^2} = [(1+\alpha u)\frac{\partial}{\partial u}[(\xi-u)^2+\rho^2]^{-\frac{1}{2}} - \alpha[(\xi-u)^2+\rho^2]^{-\frac{1}{2}}]_{u=0}^{u=1}$$

$$= [\frac{(1+\alpha u)(\xi-u)}{[(\xi-u)^2+\rho^2]^{\frac{1}{2}}} - \frac{\alpha}{[(\xi-u)^2+\rho^2]^{\frac{1}{2}}}]_{u=0}^{u=1}$$

$$= \frac{(\xi-1)(1+\alpha) - \alpha[(\xi-1)^2+\rho^2]}{[(\xi-1)^2+\rho^2]^{\frac{1}{2}}} - \frac{\xi - \alpha(\xi^2+\rho^2)}{[\xi^2+\rho^2]^{\frac{1}{2}}}.$$

F.5 CALCULATION OF $\frac{dc_p}{d\xi}$

Upon setting

$$\frac{dc_p}{d\xi} = \frac{\alpha}{4\varepsilon^2}\{\frac{\partial^2\psi}{\partial\xi^2} + \frac{\alpha}{2\varepsilon}\frac{\partial^2\psi}{\partial\xi\partial\rho}(1 - \frac{1}{4\varepsilon}\frac{\partial\psi}{\partial\rho}) - \frac{\alpha^2}{32\varepsilon^3}\frac{\partial\psi}{\partial\rho}\frac{\partial^2\psi}{\partial\rho^2}\}$$

we may expect $\frac{dc_p}{d\xi}$ to be of the order of ε^{-2}, and no term within the bracket may be neglected a priori.

If we now wish to compare q_{et} and $\frac{1}{2}\rho U_e^2 A_e \frac{\partial c_p}{\partial x}$ (as it would appear) in eq. (3.4), we consider the ratio

$$q = \frac{\frac{1}{2}\rho_e U_e^2 A_e \frac{\partial c_p}{\partial x}}{q_{et}} = \frac{A_e}{D_e C_{ft}}\frac{\partial c_p}{\partial x} = \frac{\pi D_e}{4C_{ft}}\frac{\partial c_p}{\partial x}$$

and, upon using the dimensionless notation defined in §2.6, we obtain

$$q = \frac{(1+\alpha\xi)}{2\varepsilon c_t} \frac{\partial c_p}{\partial \xi} .$$

On the next pages we shall present some specific values of qc_t and the short computer program used to calculate them. The calculations were performed for three values of ε, using nine truncation ratios (ranging from $\alpha=-0.1$ for an almost cylindrical beam to $\alpha=-0.9$ for an almost fully conical beam); the values of the taper angle, β, which are equal to $-\alpha/\varepsilon$, are listed below the values of α. Because the experiments were conducted with beams which normally satisfied the conditions $\varepsilon>15$ and $\beta<2^{o}=0.035$ rd and, since the tables indicate that the value of qc_t diminishes with increasingly larger values of ε and increases with larger values of $-\alpha$, hence, the maximum average value of qc_t is obtained for $\varepsilon=15$ and $\alpha=-0.5$. For $\varepsilon=15$ and $\alpha=-0.5$ we obtain

$$qc_t = 5.3\ 10^{-4} ;$$

hence, for a typical value $c_t=8.10^{-3}$, the average value of q will satisfy

$$q<0.07 \quad \text{for} \quad \varepsilon>15 \quad \text{and} \quad \beta<0.035 .$$

Although this ratio is not really negligible with respect to 1, it is argued that the theoretical calculation has assumed a uniform cylinder, both upstream ($\xi<0$) and downstream ($\xi>1$) of

the conical structure, as illustrated below, whereas the real calculation of c_p would require the addition to the conical profile of the boundary layer displacement thickness; this would eliminate the slope discontinuities at $\xi=0$ & $\xi=1$* which boosted the values of $\frac{dc_p}{d\xi}$ in the neighbourhood of $\xi=0$ & $\xi=1$, as observed on the tables. Accordingly, in reality q is substantially less than 1 and may be considered to be negligible.

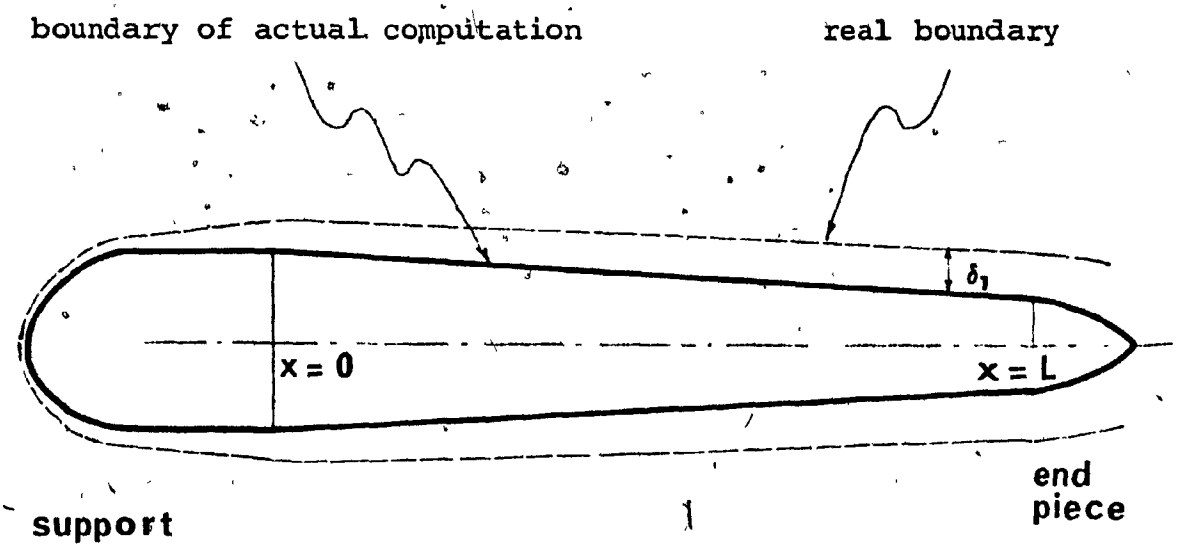

* The perturbation potential assumes that the slender body is inserted between two axial infinite uniform cylinders.

CALCULATION OF $\partial C_P/\partial X$ & $q_\infty C_t$

```
C
      DIMENSION Y(21),H(21,9),Z(9),BETA(9)
      DO 101 IEPS=1,3
      EPS=10+IEPS*5
C     EPS=L/D0
      EPS=IPS
      DO 11 IALP=1,9
      ALP=-0.1*IALP
C     TAPER ANGLE
      BETA(IALP)=-ALP/EPS
      Y(IALP)=-ALP
      S=0
      DO 10 IX=1,21
      X=0.05*(IX-1)
      R=(1+ALP*X)/(2*EPS)
      ER =2*EPS*((X-1)/SQRT((X-1)**2+R**2)-X/SQRT(X**2+R**2))+ALP*R*(1./
     1     SQRT((X-1)**2+R**2)-1./SQRT(X**2+R**2))
      ERR=2*EPS/R*((/SQRT(X**2+R**2)-(X-1)/SQRT((X-1)**2+R**2))+ALP*(1./
     1     SQRT((X-1)**2+R**2)-1./SQRT(X**2+R**2))+(X+ALP*(X**2+R**2))/(X
     1     **2+R**2)**1.5-((1+ALP*X)*(X-1)+ALP*R**2)/((X-1)**2+R**2)**1.5
      ERX=(ALP/R*(X-1)**3+R**2*2*EPS)/((X-1)**2+R**2)**1.5
     1     -(ALP/R*X**3+R**2*2*EPS)/(X**2+R**2)**1.5
      ERXX=((X-1)*(1+ALP)-ALP*((X-1)**2+R**2))/((X-1)**2+R**2)**1.5
     1     -(X-ALP*(X**2+R**2))/(X**2+R**2)**1.5
      H(IX,IALP)=(ALP/(4*EPS**2)*(ERX+ALP/(2*EPS)*ERR)
     1           -ALP**2/(32*EPS**4)*ER**(ERX+ALP/(2*EPS)*ERR))*R
10    S=S+H(IX,IALP)
11    Z(IALP)=S/21
      WRITE(6,202) (PS,(Y(I),I=1,9),(BETA(I),I=1,9)
202   FORMAT('1',////////T54,I2///T6,9F10.1/T7,9F10.3/)
      DO 100 I=1,21
      Y(I)=0.05*(I-1)
100   WRITE(6,203) Y(I),(H(I,IALP),IALP=1,9)
203   FORMAT(F6.2,1X,1P9E10.1)
101   WRITE(6,204) (Z(I),I=1,9)
204   FORMAT('0',6X,1P9E10.1/////////////)
      STOP
      END
```

VALUES OF $q\,c_t$

$\varepsilon = 15$

ξ \ −α / β	0.1 0.007	0.2 0.013	0.3 0.020	0.4 0.027	0.5 0.033	0.6 0.040	0.7 0.047	0.8 0.053	0.9 0.060
0.00	-2.5E-06	-1.7E-05	-4.4E-05	-8.2E-05	-1.3E-04	-1.9E-04	-2.6E-04	-3.5E-04	-4.4E-04
0.05	8.6E-04	1.7E-03	2.6E-03	3.5E-03	4.3E-03	5.2E-03	6.1E-03	7.0E-03	7.9E-03
0.10	3.2E-04	6.4E-04	9.6E-04	1.3E-03	1.6E-03	1.9E-03	2.2E-03	2.6E-03	2.9E-03
0.15	1.6E-04	3.1E-04	4.7E-04	6.2E-04	7.8E-04	9.3E-04	1.1E-03	1.2E-03	1.4E-03
0.20	9.4E-05	1.9E-04	2.8E-04	3.7E-04	4.5E-04	5.4E-04	6.3E-04	7.2E-04	8.1E-04
0.25	6.3E-05	1.2E-04	1.8E-04	2.4E-04	3.0E-04	3.5E-04	4.1E-04	4.7E-04	5.2E-04
0.30	4.7E-05	9.1E-05	1.3E-04	1.7E-04	2.1E-04	2.5E-04	2.9E-04	3.3E-04	3.7E-04
0.35	3.7E-05	7.1E-05	1.0E-04	1.3E-04	1.6E-04	1.9E-04	2.2E-04	2.4E-04	2.7E-04
0.40	3.1E-05	5.9E-05	8.4E-05	1.1E-04	1.3E-04	1.5E-04	1.7E-04	1.9E-04	2.1E-04
0.45	2.8E-05	5.2E-05	7.2E-05	9.0E-05	1.1E-04	1.2E-04	1.4E-04	1.5E-04	1.7E-04
0.50	2.7E-05	4.8E-05	6.6E-05	8.0E-05	9.2E-05	1.0E-04	1.1E-04	1.2E-04	1.3E-04
0.55	2.7E-05	4.8E-05	6.3E-05	7.5E-05	8.4E-05	9.1E-05	9.7E-05	1.0E-04	1.1E-04
0.60	2.9E-05	5.0E-05	6.5E-05	7.4E-05	8.0E-05	8.4E-05	8.6E-05	9.0E-05	9.5E-05
0.65	3.3E-05	5.6E-05	7.0E-05	7.8E-05	8.1E-05	8.1E-05	8.0E-05	8.0E-05	8.2E-05
0.70	4.0E-05	6.7E-05	8.2E-05	8.9E-05	8.9E-05	8.5E-05	7.9E-05	7.4E-05	7.2E-05
0.75	5.4E-05	8.8E-05	1.1E-04	1.1E-04	1.1E-04	9.6E-05	8.3E-05	7.2E-05	6.5E-05
0.80	7.8E-05	1.3E-04	1.5E-04	1.5E-04	1.4E-04	1.2E-04	9.8E-05	7.6E-05	6.0E-05
0.85	1.3E-04	2.1E-04	2.5E-04	2.5E-04	2.3E-04	1.9E-04	1.4E-04	9.3E-05	6.1E-05
0.90	2.7E-04	4.4E-04	5.1E-04	5.2E-04	4.6E-04	3.7E-04	2.6E-04	1.5E-04	7.4E-05
0.95	7.6E-04	1.3E-03	1.6E-03	1.7E-03	1.6E-03	1.3E-03	9.0E-04	4.9E-04	1.7E-04
1.00	9.3E-06	3.0E-05	6.2E-05	1.0E-04	1.6E-04	2.3E-04	3.0E-04	3.9E-04	5.0E-04
Average	1.5E-04	2.7E-04	3.7E-04	4.6E-04	5.3E-04	5.8E-04	6.3E-04	6.8E-04	7.4E-04

VALUES OF $q\,c_t$

$\varepsilon=20$

ξ \ −α, β	0.1 C.CC5	0.2 C.C10	0.3 0.015	0.4 0.020	0.5 0.025	0.6 0.030	0.7 0.035	0.8 C.040	0.9 C.C45
0.00	-1.9E-06	-1.0E-05	-2.6E-05	-4.7E-05	-7.5E-05	-1.1E-04	-1.5E-04	-2.0E-04	-2.5E-04
C.C5	4.5E-04	9.0E-04	1.4E-03	1.8E-03	2.3E-03	2.7E-03	3.2E-03	3.6E-03	4.1E-03
0.10	1.4E-04	2.9E-04	4.3E-04	5.8E-04	7.2E-04	8.6E-04	1.0E-03	1.2E-03	1.3E-03
C.15	6.8E-05	1.4E-04	2.0E-04	2.7E-04	3.4E-04	4.0E-04	4.7E-04	5.4E-04	6.CE-04
0.2C	4.CE-C5	8.CE-05	1.2E-C4	1.6E-04	1.9E-04	2.3E-04	2.7E-04	3.1E-04	3.5E-C4
0.25	2.7E-05	5.3E-05	7.8E-05	1.0E-04	1.3E-04	1.5E-04	1.7E-04	2.0E-04	2.2E-04
C.3C	2.0E-05	3.8E-05	5.6E-05	7.3E-05	9.0E-05	1.1E-04	1.2E-04	1.4E-04	1.6E-04
C.35	1.6E-C5	3.CE-05	4.3E-05	5.6E-05	6.8E-05	8.0E-05	9.1E-05	1.0E-04	1.1E-C4
0.40	1.3E-05	2.5E-05	3.6E-05	4.5E-05	5.4E-05	6.3E-05	7.1E-05	7.9E-05	8.8E-05
0.45	1.2E-05	2.2E-05	3.1E-05	3.8E-05	4.5E-05	5.1E-05	5.7E-05	6.3E-05	7.0E-05
C.5C	1.1E-C5	2.CE-05	2.8E-05	3.4E-05	3.9E-05	4.3E-05	4.8E-05	5.2E-05	5.7E-05
0.55	1.1E-C5	2.CE-05	2.7E-C5	3.2E-05	3.5E-05	3.8E-05	4.1E-05	4.4E-05	4.7E-05
0.60	1.2E-05	2.1E-05	2.7E-05	3.1E-05	3.4E-05	3.5E-05	3.6E-C5	3.8E-05	4.0E-05
0.65	1.4E-05	2.4E-05	3.0E-05	3.3E-05	3.4E-05	3.4E-05	3.4E-05	3.4E-05	3.4E-05
0.7C	1.7E-C5	2.8E-05	3.5E-C5	3.8E-05	3.8E-05	3.6E-05	3.3E-05	3.1E-05	3.CE-C5
0.75	2.3E-05	3.7E-05	4.5E-05	4.7E-05	4.5E-05	4.1E-05	3.5E-05	3.0E-05	2.7E-05
0.8C	3.3E-05	5.4E-05	6.4E-05	6.5E-05	6.1E-05	5.2E-C5	4.2E-C5	3.2E-05	2.5E-05
0.85	5.7E-C5	9.1E-05	1.1E-04	1.1E-04	9.7E-05	7.9E-05	5.9E-05	3.9E-05	2.6E-05
0.90	1.2E-04	1.9E-04	2.2E-C4	2.2E-04	2.0E-C4	1.6E-04	1.1E-04	6.5E-05	3.1E-05
0.95	3.8E-04	6.4E-04	7.7E-04	7.9E-04	7.2E-04	5.7E-04	3.9E-C4	2.1E-04	7.1E-05
1.CC	4.7E-C6	1.6E-05	3.3E-05	5.7E-05	8.7E-05	1.2E-04	1.7E-C4	2.2E-C4	2.7E-C4
Average	7.0E-05	1.3E-04	1.8E-C4	2.2E-04	2.5E-04	2.7E-04	3.0E-04	3.2E-04	3.5E-04

VALUES OF $q\ c_t$

$\varepsilon = 25$

ξ \ $-\alpha$ / β	0.1 0.004	0.2 0.008	0.3 0.012	0.4 0.016	0.5 0.020	0.6 0.024	0.7 0.028	0.8 0.032	0.9 0.036
0.00	-1.3E-06	-6.9E-06	-1.7E-05	-3.1E-05	-4.9E-05	-7.0E-05	-9.6E-05	-1.3E-04	-1.6E-04
0.05	2.6E-04	5.1E-04	7.7E-04	1.0E-03	1.3E-03	1.5E-03	1.8E-03	2.1E-03	2.3E-03
0.10	7.6E-05	1.5E-04	2.3E-04	3.0E-04	3.8E-04	4.6E-04	5.3E-04	6.1E-04	6.8E-04
0.15	3.6E-05	7.1E-05	1.1E-04	1.4E-04	1.7E-04	2.1E-04	2.4E-04	2.8E-04	3.1E-04
0.20	2.1E-05	4.1E-05	6.1E-05	8.1E-05	1.0E-04	1.2E-04	1.4E-04	1.6E-04	1.8E-04
0.25	1.4E-05	2.7E-05	4.0E-05	5.3E-05	6.5E-05	7.8E-05	9.0E-05	1.0E-04	1.1E-04
0.30	1.0E-05	2.0E-05	2.9E-05	3.8E-05	4.6E-05	5.5E-05	6.3E-05	7.1E-05	8.0E-05
0.35	8.0E-06	1.5E-05	2.2E-05	2.9E-05	3.5E-05	4.1E-05	4.7E-05	5.3E-05	5.9E-05
0.40	6.8E-06	1.3E-05	1.8E-05	2.3E-05	2.8E-05	3.2E-05	3.6E-05	4.1E-05	4.5E-05
0.45	6.1E-06	1.1E-05	1.6E-05	2.0E-05	2.3E-05	2.6E-05	2.9E-05	3.2E-05	3.6E-05
0.50	5.8E-06	1.0E-05	1.4E-05	1.7E-05	2.0E-05	2.2E-05	2.4E-05	2.7E-05	2.9E-05
0.55	5.8E-06	1.0E-05	1.4E-05	1.6E-05	1.8E-05	2.0E-05	2.1E-05	2.2E-05	2.4E-05
0.60	6.3E-06	1.1E-05	1.4E-05	1.6E-05	1.7E-05	1.8E-05	1.9E-05	1.9E-05	2.0E-05
0.65	7.2E-06	1.2E-05	1.5E-05	1.7E-05	1.8E-05	1.8E-05	1.7E-05	1.7E-05	1.8E-05
0.70	8.8E-06	1.5E-05	1.8E-05	1.9E-05	1.9E-05	1.8E-05	1.7E-05	1.6E-05	1.5E-05
0.75	1.2E-05	1.9E-05	2.3E-05	2.4E-05	2.3E-05	2.1E-05	1.8E-05	1.5E-05	1.4E-05
0.80	1.7E-05	2.8E-05	3.3E-05	3.4E-05	3.1E-05	2.7E-05	2.1E-05	1.6E-05	1.3E-05
0.85	2.9E-05	4.7E-05	5.5E-05	5.5E-05	5.0E-05	4.1E-05	3.0E-05	2.0E-05	1.3E-05
0.90	6.3E-05	1.0E-04	1.2E-04	1.2E-04	1.0E-04	8.2E-05	5.7E-05	3.3E-05	1.6E-05
0.95	2.2E-04	3.5E-04	4.2E-04	4.3E-04	3.8E-04	3.0E-04	2.0E-04	1.1E-04	3.7E-05
1.00	2.8E-06	9.6E-06	2.1E-05	3.5E-05	5.4E-05	7.8E-05	1.0E-04	1.4E-04	1.7E-04
Average	3.8E-05	7.0E-05	9.6E-05	1.2E-04	1.3E-04	1.5E-04	1.6E-04	1.8E-04	1.9E-04

APPENDIX G

BOUNDARY LAYER AND FRICTION COEFFICIENTS

APPENDIX G: BOUNDARY LAYER AND FRICTION COEFFICIENTS

In the first sections of this Appendix we shall calculate the boundary layer thickness and friction coefficients when the beam is at zero incidence and in a two-dimensional flow. The last part of the Appendix deals with boundary-layer suction.

G.1. General

We first proceed as in the case of a flat plate to calculate the drag and the boundary-layer momentum thickness. For this purpose we draw a cylindrical control volume as illustrated below; the section S_1 and the outer surface S_3 are placed at such a distance from the beam that they lie in a region where the axial velocity, U, may be assumed undisturbed and equal to U_e.

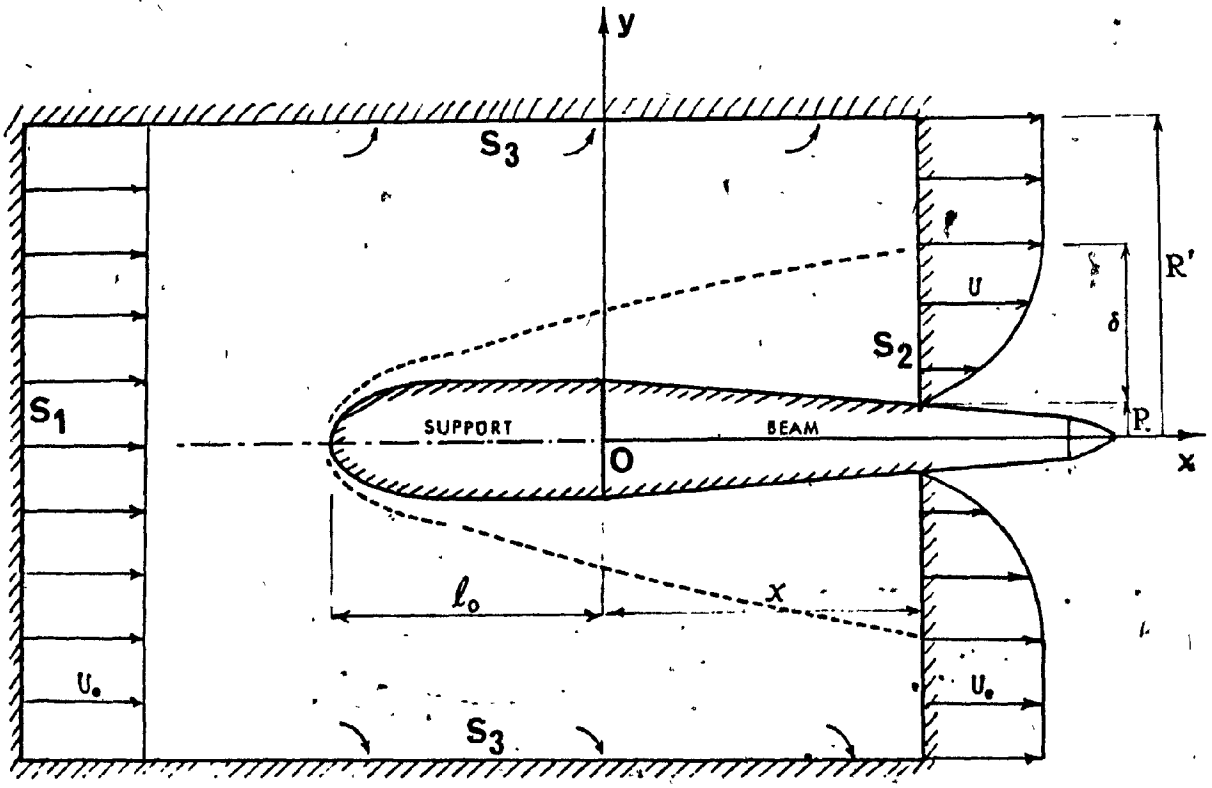

The momentum balance is given in tabular form as follows:

cross-section	rate of flow	momemtum in x-direction
S_1	$Q_1=\int_0^{R'} U_e 2\pi r dr$	$\rho\int_0^{R'} U_e^2 2\pi r dr$
S_2	$-Q_2= -\int_R^{R'} U 2\pi r dr$	$-\rho\int_R^{R'} U^2 2\pi r dr$
S_3	Q_2-Q_1	$U_e(Q_2-Q_1)$

Hence, the total axial momentum flux is

$$M = \rho\int_R^{R'} U(U_e-U)2\pi r dr$$

which can be expressed in terms of the momentum boundary layer thickness, δ_2, as follows:

$$M = \rho\int_R^{R+\delta} U(U_e-U)2\pi r dr = \int_R^{R+\delta_2} U_e^2\, 2\pi r dr$$

$$= \rho\pi\delta_2(2R+\delta_2)U_e^2 \sim 2\pi R\delta_2\rho U_e^2 \text{ if } \delta_2 << 2R.$$

Provided that the adverse pressure gradient introduced by the taper of the beam may be neglected, the rate of change of this momentum is simply equal to local friction force per unit length, and we thus write

$$2\pi R\,\tau_o = \frac{d}{dx}(2\pi R\delta_2\rho U_e^2)$$

where τ_0 is the local shear stress; upon rewriting it as

$$\tau_0 = \frac{1}{2}\rho U_e^2 c_f'$$

we obtain

$$\frac{1}{2} R c_f' = \frac{d}{dx} (R\delta_2) \qquad (G.1)$$

and in order to obtain δ_2 we will now calculate c_f' as for a uniform cylinder at zero incidence.

Using classical notation we write

$$c_f' = 2\frac{d\delta_2}{dx} \quad \text{and} \quad c_f = 2\frac{\delta_2(L^*)}{L^*}$$

where $L^* = L + x_o$, and x_o approximately represents the length ℓ_o of the upstream support of the beam corrected for edge effects; δ_2 is the momentum thickness. Provided that δ_2 remains small with respect to the beam diameter, we may apply the Prandtl-Schlichting skin friction formula [74] for a smooth flat plate at zero incidence. Thus,

$$c_f = \frac{0.455}{[\text{Log}_{10} N_R]^{2.58}} - \frac{A}{N_R} \qquad \text{for } N_R > 5 \times 10^5, \qquad (G.2)$$

where N_R is the Reynolds number at abscissa $L+x_o$, and A is the correction for the laminar skin friction up to the point of transition; for values of the critical (transition) Reynolds number below 3×10^5, we have $A<1050$; typically for $N_R = 10^7$, we have $c_f \sim 2.9 \times 10^{-3}$ independently of the critical Reynolds number, but for $N_R = 10^6$ then c_f may vary from 3×10^{-3} to 4×10^{-3}.

It will be convenient to approximate c_f over a specific range of velocities. We may do that, either by considering a range of dimensionless velocities, or by taking an empirical average Reynolds number. First, we write the Reynolds number in terms of the dimensionless velocity u_e introduced in §2.6.1, as follows:

$$N_R(x) = \left[\frac{EI}{\rho_e A_e}\right]_0^{\frac{1}{4}} u_e \frac{x+x_o}{L\nu_e}, \quad (\nu_e \text{ is the kinematic viscosity of the fluid}).$$

Then select N_R for the median velocity $u_e = 5$, since our dimensionless velocity range will commonly be $0<u_e<10$, and set for $x=L$

$$\bar{N}_R = \frac{1}{\nu_e}\left[\frac{EI}{\rho_e A_e}\right]_{x=0}^{\frac{1}{4}} 5\left(1 + \frac{x_o}{L}\right).$$

Upon setting $N_R=\bar{N}_R$ in eq. (G.2) we can calculate an average value of c_f. In practice, for the purpose of this work, we derived c_f from an average experimental value of $N_R=2\times10^6$ obtained at $x=0.3$ m with $\varepsilon_o=x_o/D_e=10$ and $U_e=3$m/s, which yields $c_f\sim4\times10^{-3}$ by the logarithmic law. Incidentally, for turbulent axial flow over a cylinder rather than a flat plate, Hoerner [75] proposes a corrective increment to c_f, namely $\Delta c_f=0.0008\ L/R\ (N_R)^{2/5}$; such a correction is negligible in our case.

G.2 Calculation of friction coefficients

The local shearing stress at the surface of the beam being

$$\tau_o = \frac{1}{2}\rho_e U_e^2 c_f',$$

the frictional tangential force per unit length of beam is

$$q_{et} = \pi D_e \tau_o = \frac{1}{2}\rho_e U_e^2 D_e \pi c_f' .$$

By comparing to equation (3.7) we obtain $C_{ft} = \pi c_f'$ and from the dimensionless notation of §2.6.1

$$c_n \sim c_t = 2c_f'$$

For turbulent Reynolds number we shall approximate c_f' by $c_f \sim 4\times10^{-3}$.

G.3 Displacement thickness

By the n=7 power law we may relate the displacement thickness, δ_1, and the momentum thickness, δ_2, of the boundary layer as follows:

$$\delta_1 = (1+2/n)\delta_2 \sim 1.3\delta_2;$$

we then integrate (G.1) to obtain δ_2 at a distance ℓ from the leading edge

$$\delta_2 = \frac{1}{2}c_f' \frac{\int_0^{\ell} R(u)du}{R(\ell)} . \qquad (G.3)$$

As previously, we account for the edge effects and the short laminar boundary layer (transition will occur very close to the edge) by correcting the actual length ℓ_o by x_o. We further assume the support to be cylindrical and the beam attached to it to be of a conical shape as in §2.6.2; hence, upon setting $\ell = x_o + x$ in eq.(G.3) we obtain.

$$\delta_2(x) = \frac{1}{2}c_f'\left[x_o + \frac{\int_0^x (1+\alpha_e x/L)\,dx}{1+\alpha_e x/L}\right]$$

$$= \frac{1}{2}c_f'\left[x_o + \left(x+\frac{\alpha_e x^2}{2L}\right)\left(1+\alpha_e \frac{x}{L}\right)^{-1}\right]$$

$$\sim \frac{1}{2}c_f'\left[x_o+x\left(1 - \frac{\alpha_e x}{2L}\right)\right] .$$

In order to simplify further calculations associated with the boundary layer we shall only retain a linear expression for δ_2 by assuming $\alpha_e x/(2L) << 1$; hence,

$$\delta_2(x) \sim \frac{1}{2}c_f'(x_o+x) = 2\times10^{-3}(x_o+x) ,$$

and

$$\delta_1(x) \sim 1.3\ \delta_2(x) = 2.6\times10^{-3}(x_o+x) . \qquad (G.4)$$

G.4 Boundary layer suction

Based on uniform suction, the theoretical velocity profile of a laminar flow on a flat plate develops towards an asymptotic suction profile which is fuller than a typical Blasius profile; in terms of the characteristic velocity defined by quantity of fluid removed by wetted area, $-v_o$ and viscosity, ν_e, the velocity obtained thereby at a distance, y, from the wall, is

$$U_e = U_{e\infty}\left\{1 - e^{\frac{v_o y}{\nu_e}}\right\} \qquad (G.5)$$

the asymptotic displacement thickness, $\delta_{1\infty}$, is equal to $-\frac{\nu_e}{v_o}$, as given by Schlichting*.

* op. cit. [74], Chapter XIV, b

Many technical difficulties made it almost impossible for us to obtain such a profile; for instance the Reynolds numbers in the tests are too large to expect a laminar boundary layer over the beam, even with the help of suction; in addition, the ideal conditions for a uniform and axisymmetric suction are difficult to approach, especially in dynamic rather than static tests. Moreover, theoretical difficulties are encountered; for example, suction implies that friction coefficients should be reduced in the calculations, and more seriously still, the lift calculated in eq.(3.1) no longer applies because of sink effects and the presence of an internal adverse (accelerated) flow, as illustrated in the diagram.

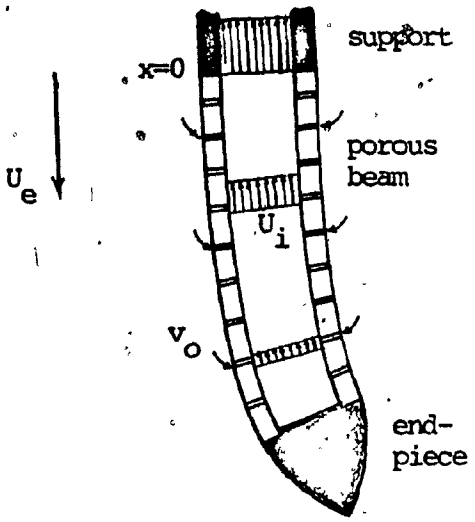

Nevertheless, let us proceed and estimate the amount of suction required to produce a significant reduction of the boundary layer on cylindrical tubes. Two methods will be investigated.

(a) We first apply the theoretical results for a laminar boundary; eq.(G.5), applied to water at 20°C yields

$$v_o = \sqrt{\frac{3.3\times10^{-6}}{\delta_{1\infty}}} \text{ (m/s)} ,$$

which may be rewritten in terms of the maximum internal flow, i.e. $A_i U_i$ at x=0 (assuming no suction for x<0), and the wetted area, $\pi D_e L$, as follows:

$$v_o = \frac{U_i(0)\, A_i}{\pi D_e L} = U_i(0)\, \frac{A_i}{A_e}\, \frac{D_e}{4L} ,$$

by use of dimensionless notation (§2.6.1),

$$v_o = U_i(0)\,\frac{\delta^2}{4\varepsilon}\ ;$$

hence,

$$U_i(0) = -\frac{1.3\varepsilon\times10^{-5}}{\delta^2\delta_{1\infty}}\ .$$

Let us now assume that the cross-sectional area of the asymptotic displacement thickness, $A_e^*-A_e$, should not be larger than 5% of that of the beam, A_e; hence

$$\frac{A_e^*-A_e}{A_e} = \left(1+\frac{2\delta_{1\infty}}{D_e}\right)^2 - 1 < 0.05\ ,$$

which yields, for a 2.54 cm O.D., $\delta_{1\infty}<0.032$ cm; this value would be approximately 6 times smaller than the present value of 0.2 cm, derived from eq.(G.4) for δ_1 at the downstream end of the same beam (preceded by a 25 cm support, and without suction). For $\delta=0.5$ and $\varepsilon=20$, as in our tests, we would thus require

$$U_i(0)>1 \text{ m/s}.$$

(b) Alternatively, because neither the boundary layer is laminar nor the suction uniform, the following rule of thumb may be used: let us draw from the external flow, the rate of flow displaced by the boundary layer thickness, i.e. $[A_e^* - A_e]_L U_{e\infty}$; we would then expect the velocity profile to be significantly fuller. We now obtain

$$U_i(0) = \frac{[A_e^*-A_e]}{A_i}L \times U_{e\infty} \sim \frac{A_e}{A_i}\,\frac{4\delta_1(L)}{D_e}\,U_{e\infty}\ ,$$

which yields for the data of the previous paragraph and $\delta_1(L)=0.2$ cm the following condition:

$$U_i(0) > 1.25 \times U_{e\infty}.$$

As opposed to the previous condition for U_i, this one depends on the velocity of the external flow; however, since the values of the external velocities required to observe instabilities of the beams are generally above 1 m/s, both conditions yield internal flows of at least 1 m/s. Such velocities were too large for our apparatus, since, in practice, we could never draw more than 20 cm/s.

APPENDIX H

BASE DRAG EVALUATION

APPENDIX H: BASE DRAG EVALUATION

It was decided to evaluate the base drag coefficients, C_{fe}, C_{fi} and C_{fx} introduced in equation (5.6), experimentally. To this end, rigid cylindrical tubes equipped with pressure taps were designed, which, for convenience, were tested in a wind tunnel rather than in a water tunnel.

H.1 Geometric similarity

In order to reproduce similar external flow conditions in both water and air, the Reynolds numbers based both on diameter and length were scaled separately, i.e. it was required that

$$\frac{U_w D_w}{\nu_w} = \frac{U_a D_a}{\nu_a} \quad \text{and} \quad \frac{U_w L_w}{\nu_w} = \frac{U_a L_a}{\nu_a},$$

where U, D and L denote external velocities, diameters and lengths, respectively, and subscripts w and a refer to water and air.

Clearly, it follows that $L_w/D_w = L_a/D_a$ and, therefore, the two models must be geometrically similar; in fact the geometric similarity further extends to the boundary layer, as shown by the following dimensional analysis: the ratio δ^*/D, i.e. the boundary layer thickness divided by diameter, is (in incompressible flow) a given function of x/L, D/L, UD/ν and of a critical Reynolds number which accounts for transition (and which depends mainly upon the level of turbulence for similar and smooth surfaces). Hence, provided that either the levels of turbulence in the two tunnels are similar or the transition points close to the leading edge, the ratio δ^*/D will be very close, especially at the downstream end

where they are relevant for base drag. It is noted that for the external flow, velocities will remain low enough to neglect the compressibility of air.

With respect to the internal flow, geometric similarity must be satisfied in this case also, to provide similar flow conditions. Ultimately the scale factor L_a/L_w was chosen equal to 2 for a velocity factor of 8 at $70^{\circ}F$.

H.2 Experiments

Experiments were conducted on rigid tubes, cylindrical both outside and inside; the ratio of internal to external diameter was kept constant and equal to $D_i/D_e=0.4$ (i.e. $D_i=2$ cm and $D_e=5$ cm) and the ratio $\varepsilon=L/D$ was equal to 15. Three different downstream end pieces were used, as illustrated below on the right; one was elongated, another was hemispherical, and the last one was very blunt. In each end piece, six pressure taps were drilled at different radial positions and connected to an alcohol manometer; the support strut was placed next to the upstream end of the tube, so as not to interfere significantly with the base drag measurements.

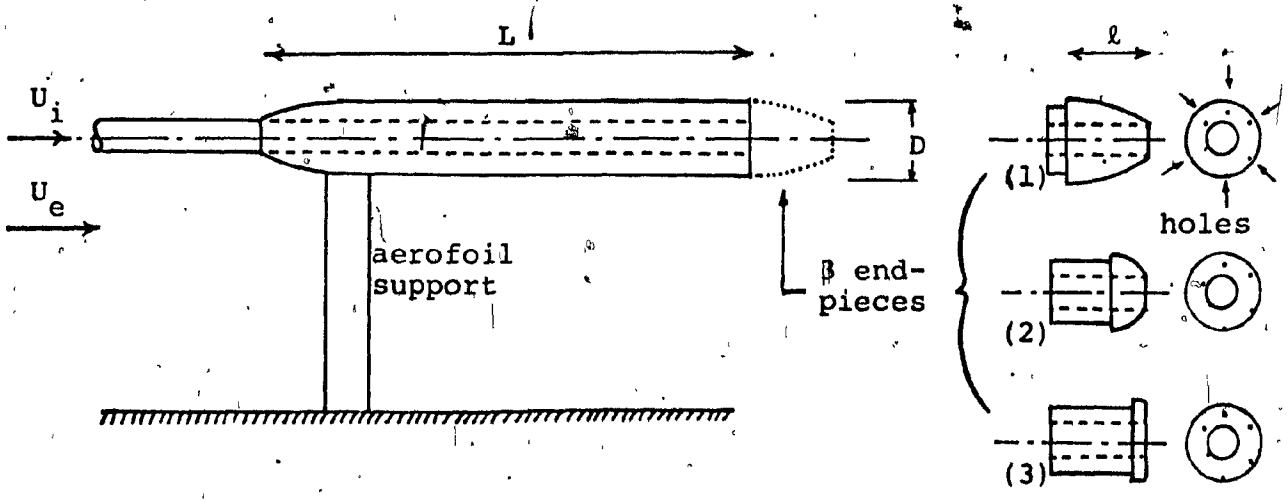

The range of external flow velocities was 0 to 50 m/s and that of internal flow was 0 to 100 m/s (in order to scale ranges of 0→6 m/s and 0→12 m/s in water, respectively). The pressure measurements from the six pressure taps and the main pressure in the wind tunnel were then recorded for each pair of velocities and the total base drag calculated.

H.3 Quadratic fit

A homogeneous second-order approximation was then selected to fit the experimental points (the average relative deviation was less than 10%) leading to

$$D_b = \frac{1}{2}\rho_{air}\{A_e U_e^2 C_{fe} + A_i U_i^2 C_{fi} + [A_e A_i]^{\frac{1}{2}} U_e U_i C_{fx}\}.$$

The values of the coefficients for each end piece are tabulated below.

	C_{fe}	C_{fi}	C_{fx}
blunt	0.15	0.016	0.109
hemispherical	0.13	0.009	0.054
elongated	0.03	0.007	0.053

As may be observed they are all positive, thus suggesting that drag increases with either internal or external flow velocity; however, experiments indicated that for the larger Reynolds numbers of the external flow, the drag for zero internal flow was always 10% higher than predicted by the expression above. Furthermore, those coefficients should also depend to some extent upon the ratio $\varepsilon = L/D$

and on the actual velocities, since the thicker the boundary layer ratio δ/D, the more "insulated" is the base; as suggested by Hoerner*, the base drag coefficient for a slender body varies as the inverse of the square root of the forebody drag coefficient; however, in this study, we shall assume that they are reasonably constant, because of the limited ranges of Reynolds numbers and slenderness ratios ε.

Nevertheless, these coefficients still yield, if not a very accurate, at least a representative evaluation of the base drag of our tubular beams.

It will now be convenient to find semi-empirical expressions for each of the three coefficients, according to the shape of the end piece, to be supplied to the computer program.

(a) For elongated semi-ellipsoidal end pieces, without internal flow, the following formula for C_{fe} has been suggested by Chank as reported by Hoerner*

$$C_{fe} = 0.06 \left[\frac{2\ell}{D}\right]^{-\frac{3}{2}},$$

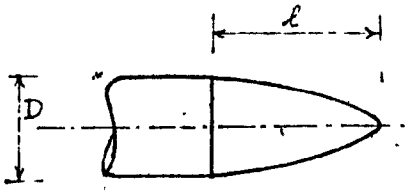

where, as illustrated above, ℓ is the length of the end piece, and D, the diameter; as could be expected it only agrees with our data for the most elongated end piece; thus we proceeded to derive our own formula to fit the range $\ell = 0$ to $\ell = 3D/2$, namely

$$C_{fe} = \frac{1.35}{9+(2\ell/D)^3}.$$

---

* Op. Cit. [75] p.2-7.

(b) Similarly, the following formula was obtained for C_{fi}

$$C_{fi} = \frac{0.02}{1.25+(2\ell/D)^{\frac{1}{2}}}$$

however, it is noted that since C_{fi} is of the order of $C_{fe}/10$, it will add little to the total drag whenever $A_iU_i^2$ remains below or is comparable to $A_eU_e^2$.

(c) We now consider C_{fx}. Its magnitude tends to indicate that there is a strong interaction between internal and external flow with respect to base drag: for similar magnitudes of $A_iU_i^2$ and $A_eU_e^2$, the contributions to drag from the C_{fe} and the C_{fx} terms are similar. As previously, we established our own semi-empirical formula for C_{fx} as follows:

$$C_{fx} = 0.05\,\frac{0.2 + 2\ell/D}{0.1 + 2\ell/D}\,.$$

The applicability of these three formulae should further be restricted to cases where the diameter ratio is close to 0.4 (actually in the experiments conducted in the water tunnel this ratio was equal to 0.5).

APPENDIX I

IMPORTANCE OF ROTATORY INERTIA AND MOMENTS DUE TO CONVERGENT FLOW

APPENDIX I: IMPORTANCE OF ROTATORY INERTIA AND MOMENTS DUE TO CONVERGENT FLOW

I.1 Rotatory inertia

The moment arising from rotatory inertia of the beam is

$$\rho I \frac{\partial^3 y}{\partial x \partial t^2} \tag{I.1}$$

per unit length, and the corresponding flexural moment is

$$\frac{\partial}{\partial x}\left[EI \frac{\partial^2 y}{\partial x^2}\right] \sim EI \frac{\partial^3 y}{\partial x^3} \tag{I.2}$$

for slender bodies.

If we set $y(x,t) = Re\{Y(x)e^{i\omega t}\}$, Re{} denoting the real part, eq. (I.1) yields

$$\rho I \frac{\partial^3 y}{\partial x \partial t^2} = \rho I \, Re\{-\omega^2 \frac{\partial Y}{\partial x} e^{i\omega t}\} .$$

If we now assume $Y(x) \sim e^{i\lambda x}$, that is to say that some wavelength can be found associated with the modal shape, then eq. (I.2) yields

$$EI \frac{\partial^3 y}{\partial x^3} \sim EI \, Re\{-\lambda^2 \frac{\partial Y}{\partial x} e^{i\omega t}\} .$$

Hence, provided that λ^2 and ω^2 are approximately real, the ratio of these two terms is

$$\frac{\rho}{E} \frac{\partial^3 y/\partial x \partial t^2}{\partial^3 y/\partial x^3} \sim \frac{\rho}{E} \frac{|\omega|^2}{|\lambda|^2} . \tag{I.3}$$

Provided that this ratio is well below unity, it may be assumed that rotatory inertia will have a small effect compared to flexural inertia.

Let us consider quasi-uniform beams *at zero flow velocity*; then, $\omega^2 \simeq (\lambda L)^4 \, EI/(\rho A L^4)$, and eq. (I.3) becomes

$$\frac{\rho}{E}\left|\frac{\omega}{\lambda}\right|^2 \simeq \frac{\rho}{E}\frac{\lambda^4 EI}{\rho A \lambda^2} = \left(\frac{\lambda L}{L}\right)^2 \frac{D^2}{16} = \left(\frac{\lambda L}{4\varepsilon}\right)^2 ,$$

where, for standard boundary conditions, λL takes well-known values.

Thus, for pinned-pinned beams, for mode k, $\lambda L = k\pi$; hence

$$\frac{\rho}{E}\left(\frac{\omega}{\lambda}\right)^2 = \left(\frac{k\pi}{4\varepsilon}\right)^2 ,$$

and in order to neglect rotatory inertia we need to have $\varepsilon >> k$; for instance, if $\varepsilon > 8k$ then the error will be less than one percent.

For clamped-free beams,

$$\lambda L \simeq (2k-1)\frac{\pi}{2} \quad \text{and} \quad \frac{\rho}{E}\left(\frac{\omega}{\lambda}\right)^2 = \left\{\frac{(k-\frac{1}{2})\pi}{4\varepsilon}\right\}^2$$

hence, we need $\varepsilon >> k-\frac{1}{2}$, and $\varepsilon > 8k-4$ will yield less than one percent error. In fact, provided that $\varepsilon > 25$ Rosinger and Ritchie [76] found that the errors resulting from neglecting rotatory inertia and shear deformation are less than 5% for the natural frequencies (up to the fifth) of a cantilever beam; furthermore, such errors vary approximately like ε^{-2}, and somewhat proportionally to the mode number.

Unfortunately, when we depart from the zero flow velocity condition or from the case of a uniform beam λ becomes a function of x, and the relation between ω and λ is no longer straightforward.

The longest wavelength, X, should then be measured empirically from the experimental modal shape and λ estimated from the value $\lambda m = \frac{2\pi}{X}$; then, one should check that

$$\frac{\rho}{E} \left(\frac{\omega}{\lambda m}\right)^2 << 1 \ .$$

In practice we shall choose large length ratios (ε>15), and only consider the first set of instabilities, which occur at critical velocities where only the lowest modes can be excited; as a result, the corresponding critical frequencies remain small, i.e. generally lower than at zero flow; in addition, the wavelengths never increased significantly and therefore, the inequality stated above could be satisfied.

I.2 Moments due to convergent flows

Let us prove that the terms resulting from the moments induced by the combination of flow and taper (either internal or external), may be neglected in the differential equation of motion.

In eq.(5.2) these terms have the form

$$\frac{\rho_o A_o}{2\pi} \frac{\partial A_o}{\partial x} \frac{\partial}{\partial x}\{V_o^2(y)\} \ , \qquad (I.4)$$

where the subscript o stands for either i or e, referring to internal and external flow respectively. We shall now compare the terms to

similar ones associated with the hydrodynamic forces, which have the form

$$\rho_o A_o \mathcal{D}_o^2(y) \quad . \tag{I.5}$$

As in the previous section, we assume a solution $y \sim e^{i\lambda x}\, e^{i\omega t}$; the ratio between the terms in (I.4) and (1.5) gives

$$\left|\frac{\lambda}{2\pi}\frac{\partial A_o}{\partial x}\right| = \left|\frac{\lambda}{4}\frac{\alpha_o}{L}\left(1+\alpha_o\frac{x}{L}\right) D_o^2(0)\right| < \left|\alpha_o \frac{\lambda L}{4\varepsilon^2}\right| \quad .$$

This ratio will always be very small because (i) we have already satisfied the conditions $4\varepsilon > \lambda L$, in order to neglect rotatory inertia, (ii) $\varepsilon >> 1$ for slender bodies, and (iii) $|\alpha_o| < 1$ for the tapered beams under consideration.

Incidentally, it is not always necessary to make assumptions regarding y in order to neglect the fluid-induced moments. For instance, when the frequency, ω, is very small, as in the neighbourhood of buckling, the expansion of (I.4) with respect to the operator $\mathcal{D}$ reduces to a single term, i.e. one containing $\frac{\partial^3 y}{\partial x^3}$; as stated at the end of §2.6.1 such a term is negligibly small compared to the term resulting from the flexural moment, provided that the flow velocities remain below the slenderness ratio ε. This can be shown by comparing the following two terms in eq.(6.3)

$$\frac{2}{1-\delta^4}\left[\sigma_e \frac{d\sigma_e}{d\xi} - \delta^4 \sigma_i \frac{d\sigma_i}{d\xi}\right] \frac{d^3\psi}{d\xi^3} \quad ,$$

$$\frac{1}{8\varepsilon^2}\left[u_e^2 \sigma_e \frac{d\sigma_e}{d\xi} + \frac{\delta^2 v_i^2}{\sigma_i}\frac{d\sigma_i}{d\xi}\right] \frac{d^3\psi}{d\xi^3} \quad ,$$

for the flexural and fluid-induced moments, respectively. Therefore, if,

$$u_e^2 << \frac{16\varepsilon^2}{1-\delta^4} \text{ , and; } \quad \left(\frac{v_i}{\sigma_i}\right)^2 << \frac{16\varepsilon^2\delta^2}{1-\delta^4} \text{ ,}$$

then, necessarily, the second term will be negligible. In terms of the true flow velocities U_e, U_i, and the wave-propagation velocity, c, these inequalities yield

$$U_e^2 << \frac{2\rho}{\rho_e} c^2 \text{ , } \quad U_i^2(0) << \frac{2\rho}{\rho_i} c^2 \text{ .}$$

These conditions were satisfied in our tests since the maximum flow velocities were around 6 m/s and the smallest of the values of c, listed for different materials in §4.2, was 40 m/s.

APPENDIX J

CALCULATION OF THE CORRECTIVE HYDRODYNAMIC COEFFICIENT f

APPENDIX J: CALCULATION OF THE CORRECTIVE HYDRODYNAMIC COEFFICIENT f.

R.H. Upson and W.A. Klikoff [77] proposed an analysis of the forces exerted on half bodies of revolution which has also later been reported by H.R. Kelly [78] to be more appropriate than Munk's [45]. In brief, it is suggested to replace Munk's virtual mass factor k_2-k_1 by the following factor

$$f = \frac{1}{2}(1+k_1)(1+k_2)\cos^2\frac{\beta}{2}$$

where β is the full taper angle, i.e. $\tan\frac{\beta}{2} = \frac{1}{2}dD/dx$, D being the diameter of a cross-section. This factor would then be variable along the body except for conical shapes. For practical purposes, the product $(1+k_1)(1+k_2)$ decreases very rapidly to a value of 2 as the slenderness of the body increases; this is illustrated in the table below for half ellipsoids of revolution: the initial value of 2.25 is obtained for a hemispherical body (a and b are the lengths of the major and minor axes respectively).

a/b	1	1.5	2	3	4	5	10	∞
k_1	0.500	0.305	0.209	0.122	0.082	0.059	0.021	0.0
k_2	0.500	0.621	0.702	0.803	0.860	0.895	0.960	1.0
$(1+k_1)(1+k_2)$	2.250	2.115	2.058	2.023	2.013	2.007	2.001	2

Over the major portion of the beam which is conical we thus take $(1+k_1)(1+k_2) = 2$, since the conical shape may be considered as the envelope of a family of infinitely long ellipsoids, hence

$$f = \cos^2\frac{\beta}{2} = \frac{1}{1+\tan^2\frac{\beta}{2}} \sim 1 - \tan^2\frac{\beta}{2} \; ;$$

since $\tan\frac{\beta}{2} = \frac{1}{2}\frac{dD_2}{dx} = \frac{\alpha_e}{2\varepsilon}$, then $f \sim 1 - (\frac{\alpha_e}{2\varepsilon})^2$.

We shall always consider cases where $|\frac{\alpha_e}{2\varepsilon}| < \frac{1}{30}$, then $f \sim 1$ and no corrective factor need be applied to the lift exerted on the beam along its length; however at the downstream end, the angle β is no longer negligible.

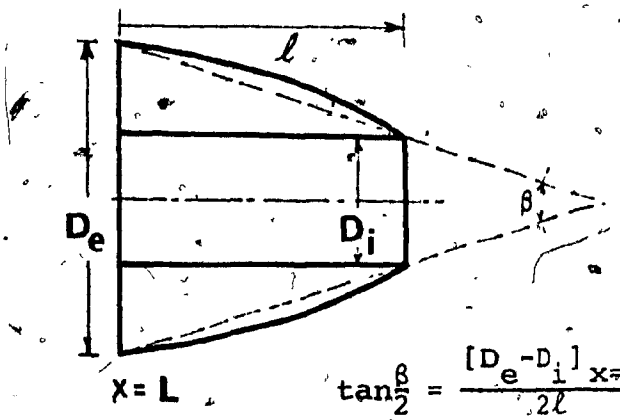

As in §2.5.3, and for the sake of simplicity, we shall assume that the end piece may be represented by a truncated cone, and then $(1+k_1)(1+k_2) \sim 2$ and β is given by

$$\tan\frac{\beta}{2} = \frac{[D_e - D_i]_{x=L}}{2\ell} = \frac{D_e(L)}{2\ell}\left[1-\frac{D_i}{D_e}\right]_{x=L} = \frac{1}{2\chi_e}\left[1-\delta\frac{1+\alpha_i}{1+\alpha_e}\right] \; ;$$

hence,

$$f = \cos^2\frac{\beta}{2} = \frac{4\chi_e^2}{4\chi_e^2+[1-\delta(1+\alpha_i)/(1+\alpha_e)]^2} \; . \qquad (J.1)$$

Clearly, the evaluation of the hydrodynamic force over the end piece and the calculation of the corrective factor, f, have been oversimplified in the present work. For example, in §2.5.3 of the main text, we accounted for a constant boundary

layer effect over the end piece in terms of a reduced flow velocity, U_e^* obtained at x=L, whereas the boundary layer grows rapidly over the end piece. In addition, the eventuality of flow separation must be considered.

Recent studies have investigated the thick turbulent boundary layer near the tail of bodies of revolution [79], [80], [81]. Nakayama, Patel and Landweber [80] found that the rapid growth of the thick boundary layer over the conical tail section of a modified spheroid is sufficient to relieve the potential flow pressure gradients and thereby avoid separation altogether. Incidentally, those results were obtained with experimental data very similar to ours; for instance, Reynolds numbers were in the vicinity of 10^6, the displacement thickness measured prior to the tail section was of the order of 5% of the local diameter and the taper angle of the conical tail piece was $\beta=45^\circ$. Although this study does not consider transverse motion, it is nonetheless useful to calculate base drags and to predict that flow separation will probably not occur for sufficiently small motions (provided that the boundary layer remains stable).

Another approximation made in §2.5.3 and previous studies [38], [40], [77], was to consider a constant value of the parameter f, independent of the type of motion. More sophisticated approaches are now available to calculate the ideal flow around bodies of revolution. Very recently, Paidoussis and Yu [82] investigated the effect of nose and tail shapes on the stability of towed bodies. They presented an analysis giving the forces and moment distribution

on an ellipsoid undergoing plane motion. An interesting feature of their work is that they considered truncated tails. Unfortunately, our theory is difficult to compare to theirs, because, on one hand, our parameter f is insufficient to account for the refinements introduced by their theory, and, on the other hand, they did not account for the insulation effect of the boundary layer. Nevertheless, comparing the new theory with an older theory, which is similar to ours for zero-boundary layer thickness, Paidoussis and Yu noted that, for appropriate values of the parameter f, the correspondance of the two theories is quite good, at least up to the first oscillatory instability. The values of f thus required are generally lower than those derived by use of eq.(J.1) since they vary from 0 up to a maximum value which, for very elongated bodies, is shown to be less than 1, whereas eq.(J.1) yields f~1 when $\chi_e > 2$ (f=1, asymptotically). However, in our boundary conditions, e.g. eq.(10.7), f is compounded by the factor $(\frac{1-\alpha}{\sigma})^2$, due to the boundary layer, which is smaller than unity, as a result, the two theories are expected to yield quite similar results for the lower instabilities.

APPENDIX K

DETERMINATION OF THE COMPLEX ELASTIC MODULUS AND OTHER RELATED FACTORS; VISCOHYSTERETICAL DAMPING

APPENDIX K. DETERMINATION OF THE COMPLEX ELASTIC MODULUS AND OTHER RELATED FACTORS; VISCOHYSTERETICAL DAMPING.

In order to calculate the dimensionless parameters defined on p.60 we need determine Young's modulus, E, and the damping coefficient, k; the remaining characteristics, such as friction coefficients have been obtained in Appendix G, whereas flow velocities, specific gravities and geometric ratios may be measured easily and accurately.

K.1 Velocity and Time Scales

The quantities by which the velocities and true frequencies should be divided to yield dimensionless values may be expressed in terms of the velocity of wave propagation, $c=[E/\rho]^{\frac{1}{2}}$ as follows:

a) Reference external velocity V_e,

$$V_e = \left[\frac{EI}{\rho_e A_e}\right]_0^{\frac{1}{2}} \frac{1}{L} = \left[\frac{ED_e^2(1-\delta^4)}{16\rho_e}\right]_0^{\frac{1}{2}} \frac{1}{L} = \left[\frac{E}{\rho}\right]^{\frac{1}{2}} \left[\frac{\rho}{\rho_e}(1-\delta^4)\right]^{\frac{1}{2}} \frac{1}{4\varepsilon} = \frac{c}{4\varepsilon}\left[\frac{1-\delta^4}{\gamma_e-1}\right]^{\frac{1}{2}}.$$

b) Reference internal velocity V_i,

$$V_i = \left[\frac{EI}{\rho_i A_i}\right]_0^{\frac{1}{2}} \frac{1}{L} = \left[\frac{E}{\rho}\right]^{\frac{1}{2}} \left[\frac{\rho}{\delta^2\rho_i}(1-\delta^4)\right]^{\frac{1}{2}} \frac{1}{4\varepsilon} = \frac{c}{4\varepsilon}\left[\frac{1-\delta^4}{\gamma_i+\delta^2}\right]^{\frac{1}{2}}.$$

If external and internal fluids have the same density, then $V_e = \delta V_i$.

c) Reference frequency F,

$$F = \left[\frac{EI}{\Sigma\rho A}\right]_0^{\frac{1}{2}} \frac{1}{L^2} = \left[\frac{ED_e^2}{16\rho}\right]_0^{\frac{1}{2}} \left[\frac{(1-\delta^4)\rho A_e}{\rho A+\rho_e A_e+\rho_i A_i}\right]_0^{\frac{1}{2}} \frac{1}{L^2} = \frac{c}{4\varepsilon L}\left[\frac{1-\delta^4}{\gamma_e+\gamma_i}\right]^{\frac{1}{2}}.$$

It will also be useful to express this quantity in terms of Γ, which has been defined in §2.6.1 as

$$\Gamma = \left[\frac{\rho A_e}{EI}\right]_0 gL^3 ;$$

we then obtain

$$F = \left[\frac{gL^3}{\Gamma}\right]^{\frac{1}{3}} \left[\frac{\rho A_e}{\rho A+\rho_e A_e+\rho_i A_i}\right]_0^{\frac{1}{3}} \frac{1}{L^2} = \left[\frac{g}{\Gamma L}\right]^{\frac{1}{3}} \left[\gamma_e+\gamma_i\right]^{-\frac{1}{3}} .$$

Finally, the three reference quantities may also be expressed in terms of a dimensionless parameter γ which relates to c and Γ as follows:

$$\gamma = \frac{16g\, D_e(0)}{c^2} \quad \text{or} \quad \gamma = \Gamma \frac{1-\delta^4}{\varepsilon^3} .$$

Clearly, γ is independent of the length and thickness ratios. The upstream diameter of beams had to be one inch (because of our apparatus); hence γ may be used as a characteristic of the material.

K.2 Determination of the viscoelastic constants

Starting from the general relation between stresses and strains for a viscoelastic material, i.e. (cf. [83])

$$\left(a_0 + a_1\frac{\partial}{\partial t} + a_2\frac{\partial^2}{\partial t^2} + \ldots\right)\sigma = \left(b_0 + b_1\frac{\partial}{\partial t} + b_2\frac{\partial^2}{\partial t^2} + \ldots\right)\varepsilon$$

we restrict ourselves to the Kelvin-Voigt first order model and obtain for sinusoidal motions the following complex Young's modulus:

$$E^* = E(1+ki\Omega) \quad , \qquad (k.1)$$

where Ω is the circular frequency, and E and k are characteristic constants of the material. Clearly, E can be measured by static tests; however, we opted for dynamic tests from which both E and k could be derived at the same time. The method involved the measurement of the natural frequency of the first, and sometimes the second and third, transverse mode and the corresponding logarithmic decrement.

For convenience, the measurements were performed on cantilevers hanging in air rather than in the water tunnel; the free end was displaced and then released; the ensuing free decaying sinusoidal motion was sensed by a fibre - optic sensor, recorded on an oscilloscope and finally photographed, once all but the oscillations of the specific mode investigated were damped out. Support pins had to be adjusted experimentally at the nodes for exciting the second and the third modes. The natural frequencies, Ω, and the logarithmic decrement, δ, were thus obtained for up to three different modes.

In the next step, for no flow velocity and no damping, eq.(6.8) was solved numerically in terms of the dimensionless frequency ω for the corresponding beam and corresponding modes; to this end a trial value for Γ was selected and iterations were carried out until the experimental frequency Ω could be matched; namely, until the following ratio was reached:

$$\frac{\Omega_{exp}}{\omega} = F.$$

Then we calculated $\Gamma = \frac{g}{L(\gamma_e+\gamma_i)} \times \frac{\omega^2}{\Omega^2_{exp}}$

and we obtained $c = [\frac{E}{\rho}]^{\frac{1}{2}} = [\frac{AgL^3}{I\ \Gamma}]^{\frac{1}{2}}_0$ and calculated V_e and V_i.

If we now consider damping and a logarithmic decrement δ, we have

$$\frac{Im(\omega)}{Re(\omega)} = \frac{Im(\Omega_{exp})}{Re(\Omega_{exp})} = \frac{\delta}{2\pi} .$$

Fortunately, the real part of ω is almost independent of damping for small values of the dimensionless damping parameter ν, as shown in Appendix E, and the imaginary part of ω is almost proportional to ν, *ceteris paribus* . We thus select an arbitrary small trial value of ν, compute $Im(\omega)$ and compare with the required value $\frac{\delta}{2\pi}Re(\omega)$ to obtain the proper factor to be applied to the initial trial value. We then derive k by dividing ν by the reference frequency, i.e.

$$k = \nu/F .$$

However, it should be pointed out that the damping characteristic of the material is k and not the dimensionless term ν; for example, ν will vary with the truncation ratio, for the same beam.

It was found that the value of the elastic modulus E of each beam was often larger for higher modes, as is generally the case for a material with viscoelastic properties, but the variation of the values of E seldom exceeded 10% between the first and the third modes. The first order viscoelastic

approximation cannot account for variations of the real part of the modulus; anyway, this approximation is not satisfactory, mainly because the supposedly constant value of k was found to drop rapidly with the modal frequencies Ω.

K.3 Viscohysteretical damping

We have plotted on page K-8 the typical results obtained from tests on several beams made of a rubber-like material; rather than presenting k versus Ω, we chose k as the ordinate versus $k\Omega$ as the abscissa, in order to compare the data for the material tested with either the case of pure Voigt type viscoelastic damping, i.e. k independent of Ω (a horizontal line on this diagram), or with the case of hysteretical damping, i.e. k inversely proportional to Ω (a vertical line on the diagram). Beams with different lengths and different taper angles were tested, and the points corresponding to the modes of the same beam have been joined together. We observe that the relative change in k is larger than the change of $k\Omega$, thus implying that dissipation follows the hysteretical model more closely than the viscoelastic one; but there is little evidence of a single analytical relation between k and Ω.

The search for other parameters involved in relating k to Ω is beyond the scope of this work; therefore, we shall simply assume a linear relationship between k and $k\Omega$; for each material we obtain a least-square-fit relation, namely

$$k = k_0 - b(k\Omega) \quad \text{or} \quad k = \frac{k_0}{1+b\Omega} \ .$$

This relation between k and Ω implies visco-hysteretical properties,

(a) when $\Omega \to 0$, then $k \sim k_0$; in other words, for low eigenfrequencies the complex modulus accounts for Kelvin-Voigt viscoelastic damping and $E^* = E(1+ik_0\Omega)$;

(b) when $\Omega \to \infty$, then $k \to 0$ and $k\Omega \sim k_0/b$; the complex modulus will thus account for hysteretical damping, and $E^* = E[1+ik_0/b]$;

(c) for the general case we will have a combination of the two effects and

$$E^* = E\left[1 + \frac{ik_0\Omega}{1+b\Omega}\right].$$

We now define two dimensionless parameters, namely

$$\nu = k_0 \times \tau/t, \text{ and } \mu = k_0/b$$

and we obtain

$$\frac{E^*}{E} = 1 + \frac{i\nu\omega}{1+\frac{\nu}{\mu}\omega}.$$

In fact, the denominator of the expression above should contain the real part of ω, rather than ω, because we derived eq.(k.1) using the actual real frequencies of oscillations; however, we are mainly interested in the critical velocities which occur when the imaginary part of ω goes to zero, at which point the expression above is valid; moreover, as the frequency loci exhibit symmetry with respect to the imaginary axis, only if damping is a real function of $i\omega$ (see §7), we choose the magnitude $|\omega|$, rather than ω or its real part; again the critical

values will not be altered since the semi-empirical expression for the modulus will be exact. Finally, we write

$$\frac{E^*}{E} = 1 + \frac{i\omega\mu\nu}{\mu+\nu|\omega|} \qquad (k.2)$$

so that in eq.(6,6) we need only perform the following substitution:

$$\nu \to \nu\mu/(\mu+\nu|\omega|).$$

Remarks

(a) It should be noticed that this expression yields pure viscoelastic and hysteretical properties for $\omega \sim 0$ and $\omega \to \infty$ respectively, whereas a linear combination such as $E^* = E(1+i\omega\nu+i\mu)$ would yield the opposite properties for $\omega \sim 0$ and $\omega \to \infty$, respectively.

(b) Pure hysteretical damping is also obtained if $\nu \to \frac{\mu}{\omega}$ whereas viscoelastic damping requires $\mu \to \nu\omega$; hence it should be realized that visco-hysteretical damping is viscoelastic if the hysteretical constant μ is infinite; and vice versa, it is hysteretical if the viscoelastic parameter ν is infinite.

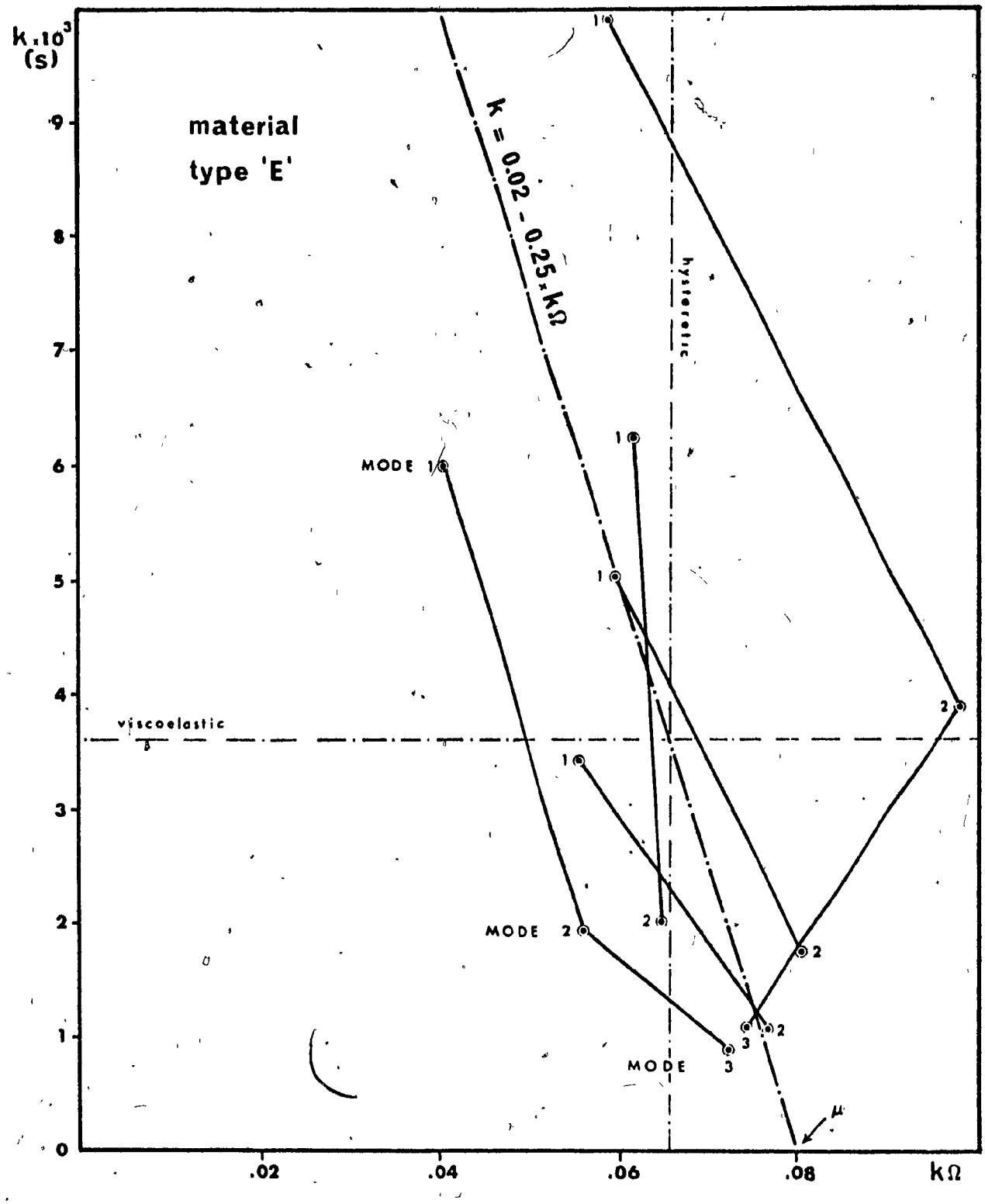

DAMPING COEFFICIENTS K VERSUS KΩ FOR THE LOWEST NATURAL FREQUENCIES OF CANTILEVER BEAMS CAST FROM THE SAME MATERIAL. VISCOHYSTERETICAL LINEAR FIT THROUGH THE EXPERIMENTAL DATA.

APPENDIX L

COMPUTER LISTINGS

APPENDIX L: COMPUTER LISTINGS

L.1 Search for eigenfrequencies with increasing flow

These are the "class A" operations defined in §3.3, and the program consists of the following sequence:

1.	main program	listing on page L3,
2.	subroutines COEFIL & BLCOEF	listing on pages L4-6,
3.	subroutine MAT	similar to MATRIX,
4.	subfunction DET	listing on page L7,
5.	subroutine SECANT	similar to LAGRAN,
6.	subroutine PREDIC	listing on pages L8-10.

The main program is used for input-output purposes, and the next two subroutines calculate the integrals defined in Appendix C; subroutine MAT fills the matrix [A] of eq.(7.2) for given values of the flow velocity and ω; its determinant is then calculated by use of the subfunction DET, and the nearest eigenvalue of [A] is obtained by secant iterations on ω performed by subroutine SECANT. (A more elaborate version of this last subroutine, using the Lagrange method is introduced in the next subsection.) Finally, subroutine PREDIC chooses adequate velocity step sizes and predicts new values of ω to initialize the next secant iterations.

L.2 Calculations of critical eigenfrequencies

These are class B operations which deal with the following three cases:

a) critical velocities for flutter,

b) critical velocities for buckling,

c) velocities for singular eigenfrequencies.

In the first case we must iterate both on velocity and the corresponding eigenfrequency to find the critical velocity, whereas in the second case we may set $\omega=0$ and iterate on velocity alone; in the latter case storage is cut by half (the matrices being real, rather than complex). Because the predictions are not as accurate as in the previous section, the Lagrange method rather than the secant method is used to reduce the number of iterations. For the first case the program comprises the following:

1.	main program	listing on pages L11-12,
2.	subroutines COEFIL & BLCOEF	(same as previously)
3.	subroutine MATRIX	listing on pages L13-15
4.	subfunctions DET	(same as previously)
5.	subroutine LAGRAN	listing on pages L16-17
6.	subroutine AXROOT	listing on pages L18-20.

For the second case, the sequence is identical but the subroutines are simpler and real. For the third case, iterations are performed on the frequencies to find the extremum of the determinant and then iterations on the velocity are performed until this extremum is found to be null. The last two subroutines in the sequence listed above are now replaced by

5.	IMROOT	listing on pages L21-22,
6.	MINIMI	listing on page L22,
7.	VELSEC	listing on page L23

EIGENVALUES FOR INCREASING FLOW

```
      MAIN
      IMPLICIT COMPLEX*16(D),REAL*8 (A-H,P-Z)
      COMMON /COEFFS/ CCEX(5,9,9),SCEX(5,9,9),SSEX(5,9,9),CCIN(5,9,9),
     1SCIN(5,9,9),SSIN(5,9,9),CCINP(3,9,9),SCINP(3,9,9),SSINP(3,9,9),CCE
     1XP(3,9,9),SCEXP(3,9,9),SSEXP(3,9,9) /COEFBL/ CCBL(3,9,9),SCBL(3,9,
     191),SSBL(3,9,9) /PRMTRS/ PAR(22),IV,IBC
      DIMENSION DA(17,17),OMEGA(5),PARAM(24),L(17),M(17)
      DATA PARAM/'ALPHA(E)','ALPHA(I)','RL  0/0=','      CN=','      CT=',
     1           '      MU=','GAMM(I)=','GAMM(E)=','DELTA1/E','DI,END/L',
     1           '(L/D)END','G*/-PSI=','EPS(L/D)','EP(X0/D)','K(OMPG)=',
     1           'PI(TEN)=','U.INT  =','U.EXT  =','ALPHABI=','     EE=',
     1           'NU     =','SIGMA  =','CLA-CLAM','CLA-FREE'/
C  READ PARAMETERS.
      READ(5,101) MAXPAR,IBC
      DO 1000 IPRMTR=1,MAXPAR
      READ(5,100) (PAR(J),J=1,18)
100   FORMAT(8D10.3)
      PAR(22)=1+0.65*PAR(14)*PAR(5)*PAR(3)
      PAR(19)=(PAR(1)+0.65*PAR(13)*PAR(5)*PAR(3))/PAR(22)
C  READ NB OF LOCI,N,INDEX OF VARIABLE (DI=17,UE=18) & MAXIMUM VELOCITY.
      READ(5,101) ITEMAX,N,IV,UM
101   FORMAT(3I5,2F10.6)
      IF(ITEMAX.GT.0)  GO TO 5
      ITEMAX=-ITEMAX
      GO TO 6
5     CALL COEFIL(PAR(1),PAR(2),N)
      CALL ALGOEF(PAR(1),PAR(19),N)
6     PAR(20)=PAR(11)**2/(PAR(11)**2+0.2500*(1-PAR(9)*PAR(10)*(1+PAR(2))
     1/(1+PAR(1)))**2)
      GAMSP=PAR(12)/(1-PAR(9)**4)
      PAR(21)=DSQRT(386.400/GAMSP  /(PAR(7)+PAR(8)))/PAR(13)**2 *PAR(15)
      WRITE(6,200) (PARAM(23+IBC),(PARAM(I),PAR(J),J=1,22)
200   FORMAT('1',A8/4(/6(2X,A8,1PD12.5)))
      DO 1000 ITERAT=1,ITEMAX
C  READ MODE,PARAMETERS FOR SUBROUTINE PREDIC (CF:DESCRIPTION IN PREDIC)
      READ(5,102) MODE,IDUP ,KM,KEY,IEEND,OM
102   FORMAT(5I5,D10.3)
C  READ INITIAL VELOCITY&INCREMENT,FREQUENCIES(2 FOR SECANT)&INCREMENT.
      READ(5,103) U,DU,OM1,OM,OD1
103   FORMAT(8F10.6)
      WRITE(6,201) PARAM(35-IV),PAR(35-IV),MODE,N,OM
201   FORMAT('1**',A8,F4.2,' ** MODE=',I1,' ** N=',I2,',OM=',1PD7.1 //)
      DO 1 IN=1,IEEND
      CALL PREDIC(OM1,OM,OD1,OD2,U,DU,OM,IN,N,K2,K1,K,IAX,IDUP ,KM,KEY)
      EIGIM=(0.D0,-1.D0) *OM1
      EIGIM=DSIGN(DSQRT(DABS(EIGIM)),EIGIM)
      EIGRE=OM1
      EIGRE=DSQRT(DABS(EIGRE))
      WRITE(6,10) PARAM(IV),U,OM1,EIGRE,EIGIM,K
10    FORMAT(' ',A8,F10.7,4X,'OM-GA=',1P2D14.6,11X,'SQRT(OMEGA)=',4P2E9.
     16,13X,I3,' ITERATIONS'/)
      EI=EIGIM**2
      IF((K.GE.KM+1).OR.((U-UM)*DU.GT.0.D0).OR.(EI.GT.5.D1)) GO TO 1000
1     CONTINUE
1000  CONTINUE
      STOP
      END
```

```
      SUBROUTINE COEFIL(AE,AI,N)
      IMPLICIT REAL*8 (A-C,P,S)
      COMMON /COEFFS/ CCEX(5,9,9),SCEX(5,9,9),SSEX(5,9,9),CCIN(5,9,9),
     1SCIN(5,9,9),SSIN(5,9,9),CCINP(3,9,9),SCINP(3,9,9),SSINP(3,9,9),CCE
     1XP(3,9,9),SCEXP(3,9,9),SSEXP(3,9,9)
      PI=3.14159265360D
      L=N/2+1
      DO 1 M=1,5
      CCEX(M,1,1)=2*(1+(M-1)*AE/2*(1+(M-2)*AE/3*(1+(M-3)*AE/4*(1+(M-4)*A
     1E/5))))
      CCIN(M,1,1)=2*(1+(M-1)*AI/2*(1+(M-2)*AI/3*(1+(M-3)*AI/4*(1+(M-4)*A
     1I/5))))
      SCEX(M,1,1)=0
      SCIN(M,1,1)=0
      SSIN(M,1,1)=0
      SSEX(M,1,1)=0
      IF(M.GT.3) GO TO 6
      CCEXP(M,1,1)=2*(0.5D0+(M-1)*AE/3+(M-1)*(M-2)*AE**2/8)
      CCINP(M,1,1)=2*(0.5D0+(M-1)*AI/3+(M-1)*(M-2)*AI**2/8)
      SCEXP(M,1,1)=0
      SCINP(M,1,1)=0
      SSEXP(M,1,1)=0
      SSINP(M,1,1)=0
6     CONTINUE
      DO 1 I=1,L
      IF(I.EQ.1) GO TO 7
      CCEX(M,I,1)=CCEX(M,1,1)/2.D0 -AE*(M-1)*(1-(1+AE)**(M-2))/((2*I-2)*
     1PI)**2+AE**3*(M-1)*(M-2)*(M-3)*(1-(1+AE)**(M-4))/((2*I-2)*PI)**4
      CCIN(M,I,1)=CCIN(M,1,1)/2.D0 -AI*(M-1)*(1-(1+AI)**(M-2))/((2*I-2)*
     1PI)**2+AI**3*(M-1)*(M-2)*(M-3)*(1-(1+AI)**(M-4))/((2*I-2)*PI)**4
      SCEX(M,I,1)=(1-(1+AE)**(M-1))/((2*I-2)*PI)-AE**2*(M-1)*(M-2)*(1-
     1(1+AE)**(M-3))/((2*I-2)*PI)**3+AE**4*(M-1)*(M-2)*(M-3)*(M-4)*(1-
     1(1+AE)**(M-5))/((2*I-2)*PI)**5
      SCIN(M,I,1)=(1-(1+AI)**(M-1))/((2*I-2)*PI)-AI**2*(M-1)*(M-2)*(1-
     1(1+AI)**(M-3))/((2*I-2)*PI)**3+AI**4*(M-1)*(M-2)*(M-3)*(M-4)*(1-
     1(1+AI)**(M-5))/((2*I-2)*PI)**5
      SSEX(M,I,1)=-CCEX(M,I,1)+CCEX(M,1,1)
      SSIN(M,I,1)=-CCIN(M,I,1)+CCIN(M,1,1)
7     DO 1 J=1,L
      IF(I.EQ.J) GO TO 2
      CCEX(M,I,J)=-AE*(M-1)*(1-(-1)**(I+J)*(1+AE)**(M-2))*(1/((I+J-2)*PI
     1)**2+1/((I-J)*PI)**2)+AE**3*(M-3)*(M-1)*(M-2)*(1-(-1)**(I+J)*(1+AE
     1)**(M-4))*(1/((I+J-2)*PI)**4+1/((I-J)*PI)**4)
      CCIN(M,I,J)=-AI*(M-1)*(1-(-1)**(I+J)*(1+AI)**(M-2))*(1/((I+J-2)*PI
     1)**2+1/((I-J)*PI)**2)+AI**3*(M-3)*(M-1)*(M-2)*(1-(-1)**(I+J)*(1+AI
     1)**(M-4))*(1/((I+J-2)*PI)**4+1/((I-J)*PI)**4)
      SCEX(M,I,J)=(1-(-1)**(I+J)*(1+AE)**(M-1))*(1/((I+J-2)*PI)+1/((I-J)
     1*PI))-AE**2*(M-1)*(M-2)*(1-(-1)**(I+J)*(1+AE)**(M-3))*(1/((I+J-2)*
     1PI)**3+1/((I-J)*PI)**3) + AE**4*(M-4)*(M-1)*(M-2)*(M-3)*(1-(-1)**(
     1I+J)*(1+AE)**(M-5))*(1/((I+J-2)*PI)**5+1/((I-J)*PI)**5)
      SCIN(M,I,J)=((1-(-1)**(I+J)*(1+AI)**(M-1))*(1/((I+J-2)*PI)+1/((I-J)
     1*PI))-AI**2*(M-1)*(M-2)*(1-(-1)**(I+J)*(1+AI)**(M-3))*(1/((I+J-2)*
     1PI)**3+1/((I-J)*PI)**3) + AI**4*(M-4)*(M-1)*(M-2)*(M-3)*(1-(-1)**(
```

```
     1I+J)*(1+AI)**(M-6))*(1/((I+J-2)*PI)**5+1/((I-J)*PI)**5)
      SSEX(M,I,J)=-AE*(M-1)*(1-(-1)**(I+J)*(1+AE)**(M-2))*(1/((I-J)*PI
     1)**2-1/((I+J-2)*PI)**2)+AE**3*(M-3)*(M-1)*(M-2)*(1-(-1)**(I+1)*(1+
     1AE)**(M-4))*(1/((I-J)*PI)**4-1/((I+J-2)*PI)**4)
      SSIN(M,I,J)=-AI*(M-1)*(1-(-1)**(I+J)*(1+AI)**(M-2))*(1/((I-J)*PI
     1)**2-1/((I+J-2)*PI)**2)+AI**3*(M-3)*(M-1)*(M-2)*(1-(-1)**(I+1)*(1+
     1AI)**(M-4))*(1/((I-J)*PI)**4-1/((I+J-2)*PI)**4)
2     IF(((M-3)*(M-4) .GT. 0) .OR. (I*J.EQ.1)) GO TO 1
      IF(DABS(AE) .LT. 1.D-5) GO TO 3
      CCEXP(M-1,I,J)=((1+AE)**(M-1)*CCEX(I,I,J)-CCEX(M,I,I))/((M-1)*AE)
      SCEXP(M-1,I,I)=((1+AE)**(M-1)*SCEX(I,I,J)-SCEX(M,I,J))/((M-1)*AE)
      SSEXP(M-1,I,J)=((1+AE)**(M-1)*SSEX(I,I,J)-SSEX(M,I,J))/((M-1)*AE)
      GO TO 4
3     IF(I.EQ.J) GO TO 30
      CCEXP(M-1,I,J)=(1-(-1)**(I+J))*(1/((I+J-2)*PI)**2+1/((I-J)*PI)**2)
      SSEXP(M-1,I,J)=(1-(-1)**(I-J))*(1/((I-J)*PI)**2-1/((I+J-2)*PI)**2)
      SCEXP(M-1,I,J)=1/((I+J-2)*PI)+1/((I-J)*PI)
      GO TO 4
30    CCEXP(M-1,I,I)= 0.5D0
      SSEXP(M-1,I,I)= 0.5D0
      SCEXP(M-1,I,I)= 1/((2*I-2)*PI)
4     IF(DABS(AI) .LT. 1.D-5) GO TO 5
      CCINP(M-1,I,J)=((1+AI)**(M-1)*CCIN(I,I,J)-CCIN(M,I,J))/((M-1)*AI)
      SCINP(M-1,I,J)=((1+AI)**(M-1)*SCIN(I,I,J)-SCIN(M,I,J))/((M-1)*AI)
      SSINP(M-1,I,J)=((1+AI)**(M-1)*SSIN(I,I,J)-SSIN(M,I,J))/((M-1)*AI)
      GO TO 1
5     IF(I.EQ.J) GO TO 50
      CCINP(M-1,I,J)=(1-(-1)**(I+J))*(1/((I+J-2)*PI)**2+1/((I-J)*PI)**2)
      SSINP(M-1,I,J)=(1-(-1)**(I+J))*(1/((I-J)*PI)**2-1/((I+J-2)*PI)**2)
      SCINP(M-1,I,J)=1/((I+J-2)*PI)+1/((I-J)*PI)
      GO TO 1
50    CCINP(M-1,I,I)= 0.5D0
      SSINP(M-1,I,I)= 0.5D0
      SCINP(M-1,I,I)= 1/((2*I-2)*PI)
1     CONTINUE
      RETURN
      END
      SUBROUTINE RLCOEF(AE,ALP,N)
      IMPLICIT REAL*8 (A-C,P-S)
      COMMON /COEFRL/ CCRL(3,9,9),SCRL(3,9,9),SSRL(3,9,9)
      PI=3.14159265360D
      L=N/2+1
      DO 1 M=2,3
      A=(5-M)*AE - (4-M)*ALP
      DO 1 I=1,L
      DO 2 J=1,L
      IF(I.EQ.J) GO TO 2
      CCRL(M,I,J)=-A *(M-1)*(1-(-1)**(I+J)*(1+A )**(M-2))*(1/((I+J-2)*PI
     1)**2+1/((I-J)*PI)**2)
      SCRL(M,I,J)=(1-(-1)**(I+J)*(1+A )**(M-1))*(1/((I+J-2)*PI)+1/((I-J)
     1*PI))-A **2*(M-1)*(M-2)*(1-(-1)**(I+J)*(1+A )**(M-3))*(1/((I+J-2)*
     1PI)**3+1/((I-J)*PI)**3 )
      SSRL(M,I,J)=-A *(M-1)*(1-(-1)**(I+J)*(1+A )**(M-2))*(1/((I-J)*PI
     1)**2-1/((I+J-2)*PI)**2)
2     CONTINUE
      IF(I.EQ.1) GO TO 7
      CCRL(M,I,I)=CCRL(M,I,I)/2.D0 -A *(M-1)*(1-(1+A )**(M-2))/((2*I-2)*
     1PI)**2
      SCRL(M,I,I)=(1-(1+A )**(M-1))/((2*I-2)*PI)-A **2*(M-1)*(M-2)*(1-
     1(1+A )**(M-3))/((2*I-2)*PI)**3
      SSRL(M,I,I)=-CCRL(M,I,I)+CCRL(M,1,1)
```

```
      GO TO 1
7     CCAL(M,1,1)=2*(1+(M-1)*A /2*(1+(M-2)*A/3))
      SCAL(M,1,1)=0
      SSAL(M,1,1)=0
1     CONTINUE
      RETURN
      END
```

```
      COMPLEX FUNCTION DET*16(A,L,M,N)
      DIMENSION A(N,N),L(N),M(N)
      COMPLEX*16 A,PIVOT,HOLD
      INTEGER END, ROW, COL, PIVROW, PIVCOL
    1 END  = N - 1
      DET =(1.00,0.00)
      DO 10 I = 1,N
      L(I)  = I
   10 M(I)  = I
      DO 100 LMNT  = 3,END
      PIVOT=(0.00,0.00)
      DO 20 I = LMNT,N
      ROW  = L(I)
      DO 20 J = LMNT,N
      COL  =M(J)
      IF (CDABS(PIVOT) .GE. CDABS(A(ROW,COL)))  GO TO 20
      PIVROW  = I
      PIVCOL  = J
      PIVOT  = A(ROW,COL)
   20 CONTINUE
      IF(PIVROW.EQ.LMNT) GO TO 22
      DET  = - DET
      KEEP  = L(PIVROW)
      L(PIVROW)  = L(LMNT)
      L(LMNT)  = KEEP
   22 IF(PIVCOL.EQ.LMNT) GO TO 26
      DET  = - DET
      KEEP  = M(PIVCOL)
      M(PIVCOL)  = M(LMNT)
      M(LMNT)  = KEEP
   26 DET  = DET * PIVOT
      IF(CDABS(PIVOT) .EQ.0.00)  GO TO 333
      JAUG  = LMNT + 1
      PIVROW  = L(LMNT)
      PIVCOL  = M(LMNT)
      DO 100 I = JAUG,N
      ROW  = L(I)
      HOLD  = A(ROW,PIVCOL)/PIVOT
      DO 100 J = JAUG,N
      COL  = M(J)
  100 A(ROW,COL)  = A(ROW,COL) - HOLD*A(PIVROW,COL)
      DET  = DET * A(ROW,COL)
  333 RETURN
      END
```

```
      SUBROUTINE PREDIC(DM1,DM,D1,D,U,DU,RM,IN,N,I2,I1,I,IAX,IUP,IM,KEY)
      DIMENSION A(19,19),L(19),M(19)
      COMPLEX*16 A,DM1,DM0,DM,D1,D,GI
      REAL*8 U,DU,R4,DDR,R0,R1,R1),DUM
      GI=(0.D0,1.D0)
      J1=1
      J=0
      DUM=DABS(IUP*RM)/128
      IF(DABS(DU/DUM).GT.64.D0) I1=9
C  INITIAL VELOCITY . INITIAL CHARACTERISTICS KEPT FOR NEXT STEP.
      R1=DM1
      IF(IN .GT. 1) GO TO 1000
      IUP=IUP*(DABS(DU/RM)+1)
      DM0=DM
      IAX=0
      IF(DABS(R1).LT.10.*RM) IAX=5
      R1=D1
      IF((DABS(R1).GT.10.*RM).AND.(IAX.EQ.5)) IAX=-3
      GO TO 81
1000  R0=DM
      IF(I.LT.IM) GO TO 1
C  SPECIAL CASES OF DIVERGENCE.
      IF(IN.EQ.1) GO TO 101
      IF(IAX) 101, 8,11
C  SPECIAL CASES OF CONVERGENCE.
1     IF( KEY.LT.0 ) I=2
      IF(IN.LE.3) GO TO 50
      JAX=IAX+5
      GO TO (12,5,5,5,2,9,5,5,5),JAX
2     IF((R1.GT.RM*10. ).AND.(R0.LT.RM*10. )) GO TO 12
      IF((R1.LT.RM*10. ).AND.(R0.GT.RM*10. )) GO TO 50
      IF(IAX.GT.4) GO TO 20
      IF( R1+ RM .GT.  R0/2.) GO TO 19
      IF( R1+ RM .LT.  R0/4.) I=I-1
      I=MAX0(2,1+I/2+I/7)
      I2=9
19    I=I-I/5
      R2=0.75*R1+5*D1-3*D
      IF(R2.LT.0.0  ) I2=9
20    IF((I.LE.4+4/IN).OR.(DABS(DU/4.D0).LT.DUM  )) GO TO 4
C  SLOW CONVERGENCE . DIVISION OF STEP BY 4.
3     U=U-0.75D0*DU
      DU=DU/4.D0
      D =(5*D+3*D1)/32
      D1=(5*D1+3*D)/32
      DM1=(DM+D1)
      WRITE(6,99) U
99    FORMAT(' -PREDIC- VELOCITY SET BACK TO',F9.6,' BECAUSE TOO MANY IT
     1ERATIONS IN PREVIOUS STEP')
      I=I-1
      GO TO 79
C  SPECIAL  THIRD & FOURTH POINTS ON OR OFF IM-AXIS.
5     D=(D+DM1-DM)/2.D0
      DDR=1
      I=3
      GO TO 7
```

```
C  SPECIAL PROCEDURE TO FACE TOO QUICK VARIATIONS OF FREQUENCY.
4      IF(KEY.LT.0) GO TO 6
       IF(IN.EQ.4) GO TO 64
       IF(IAX.EQ.0) GO TO 63
       F=(DM1-DM)/D
       IF((ABS(F).LT.0.5).AND.(I.LE.2)) J=-1
       I=I-J
       IF(IAX.LE.4) GO TO 5
63     IF((I.GT.3).OR.((I.EQ.3 .AND. I1*I2.GT.I)) GO TO 6
       IF( I*I1*I2.LE.8) GO TO 64
       IF(I.EQ.1) GO TO 65
       GO TO 6
64     KU=(U+RM/5.00)/DU
       IF(KEY.EQ.0) KU=0
       IF(KU-(KU/2)*2 .EQ. 0 ) GO TO 66
65     J=I-2-(4/IN)*MIN0(I-3,2)
       GO TO 67
66     J=I/2 - (I/4)*(IN/4)
       IF(((I*(I-1.EQ.1).AND.(KU-(KU/4)*4 .EQ. 0) ) J=1
67     I=I-J
C  PREDICTED STEP FACTOR . NEW CHARACTERISTICS.
6      DDR=2.00**(2-I)
       MINDDR=DABS(DU/DUM)+0.1
       IF(MINDDR*DDR.LT.1.00) DDR=2.00**(-MINDDR/2)
       DU=DU*DDR
       F=(DM1-DM0)/D1
       IF(F.GT.0.) JJ=-1
7      DD1=(DM)-DM-D1)*(1-4/IN)*8.**(2-I)*D1/D
       D1 =(3*(DM1-DM)-D + (DM1-DM-D)*DDR)*DDR/2.00
       D  =(3*(DM1-DM)-D - (DM1-DM-D)*DDR)*DDR/2.00
       I2=I1-I+1/I1
       I1=I+J
       U=U+DU
       DM1=DM1+D1+DD1
       IF(IAX.NE.0) IAX=IAX+1
       GO TO 80
C  FIRST POINT ON IM-AXIS.
8      H1=D1
       IF(((R0+3.00*H1).GT.0.00) .AND. (I.EQ.IM)) GO TO 10
       DM0=DM-R0   +    (D1-H1)*R0/(R0-H1)
       D1=     GI*CDABS(IUP*(R0-D))/(2*IUP)
       R0=(R0-D)/2
84     IAX=1
       DM1=DM0+D1
       DM0=DM1    - GI* DABS(IUP*R0     )/(2*IUP)
       GO TO 81
85     H1=D1
       D1=DM0-DM1
       DM0=DM-R0    +    (D1-H1)*R0/(R0-H1)
       R0=-D1*GI/5
       IF(R0*IUP.GT.0.00) GO TO 84
C  SECOND POINT ON IM-AXIS.
9      IAX=2
       D1=CDABS(IUP*(DM1-DM+D))*GI/(2*IUP)
       D=CDABS (IUP*(DM1-DM))/IUP*GI
       GO TO 50
10     IF(CDABS(DM-R0).GT.RM) GO TO 3
C  FIRST POINT OFF AXIS (TO BE R-CALCULATED)
11     IAX=-4
       D1=(CDABS(D) + D1/2.00)*1.500
       IF(R0.GT.10.00*RM) D1=(GI*CDABS(D/IUP)*IUP+H1)*0.7500
```

```
      DM1=DM
      GO TO 52
C  SECOND POINT OFF IM-AXIS (TO BE PREDICTED)
12    IAX=-3
      D1=CDABS(DM1-DM)
50    U=U+DU
      IF(IN-3) 51,53,52
53    D1=DM1-DM
51    D=D1
52    DM1=DM1+D1
      IF(IN.GT.3) J1=-1-IABS(IAX+1)
79    I2=2
      I1=2
      DD1=0
80    DM=DM1-D1-DD1
      R1=DM1
      R0=DM
C  INVESTIGATION OF A NEGATIVE PREDICTION BEYOND IM-AXIS.
      IF((R1.LT.10.00*RM) .AND. (IAX .EQ.0)) GO TO 8
      DM0=DM +D1+DD1-J1*D1/IM
      J1=I
81    CALL SECANT(A,DM1,DM0,U,RM,IM,L,M,N,I,KEY)
      IF(I*J1 .GE. IM*IM) I=IM+1
      IF((I.LT.IM) .OR. (DABS(DU).LT.2*DUM ) .OR. (IN.LT.4)) GO TO 100
      IF((IAX-1)*(IAX+4)) 91,90,100
90    D1=0
      IF(IAX.EQ.1) D1=H1
      D=D1
      IAX=-IAX+1
      GO TO 92
91    IF(IAX.EQ.0) GO TO 100
92    IF(DABS(DU).GT.4*DUM) GO TO 3
101   I=IM+1
100   IF(I.EQ.IM) GO TO 1000
      RETURN
      END
```

CRITICAL CHARACTERISTICS

```
      MAIN
      IMPLICIT COMPLEX*16 (C),REAL*8 (A-H,P-Z)
      COMMON /COEFFS/ CCEX(5,9,9),SCEX(5,9,9),SSEX(5,9,9),CCIN(5,9,9),
     1SCIN(5,9,9),SSIN(5,9,9),CCINP(3,9,9),SCINP(3,9,9),SSINP(3,9,9),CCE
     1XP(3,9,9),SCEXP(3,9,9),SSEXP(3,9,9) /COEFAL/ CCAL(3,9,9),SCAL(3,9,
     19),SSAL(3,9,9) /PRMTRS/ PAR(22),IP3,IP2,IMC
      DIMENSION OMEG(3),P3(3),PARAM(24)
      DATA PARAM/'ALPHA(E)','ALPHA(I)','RL  0/0=','      GN=','      GT=',
     1           '      MU=','GAMM(I)=','GAMM(E)=','DELTAT/E','DI.END/L',
     1           '(L/D)END','G*/EPS3=','EPS(L/D)','EP(X0/D)','K(OMPG)=',
     1           'P((TEN)=','U.INT  =','U.EXT  =','ALPHANL=','     EFE=',
     1           'NU     =','SIGMA  =','CLA-CLAM','CLA-FREE'/
C  READ NUMBER OF DIFFERENT SETS OF PARAMETERS,INDEX FOR MC (CL-CL:0,CL
      READ(5,13) NPMAX,IMC
      DO 100 IPAR=1,NPMAX
C  READ COMPLETE SET OF PARAMETERS.NOTE:READ EPS<0 FOR CONSTANT ANGLE.
      READ(5,12) (PAR(J),J=1,18)
12    FORMAT(8D10.3)
C  READ FIRST PARAMETER'S LOCATION,STEPS(OR BRANCHES),STEP SIZE(OR 0.0)
      READ(5,13) IP1,NP1,DP1
13    FORMAT(2I5,4E10.5,4I5)
      IPR=0
      DO 100 NPAR1=1,NP1
C  READ SECOND PARAMETER'S LOCATION,STEPS,INITIAL VALUE:INITIAL,MINIMUM
C  (SAME SIGN UNLESS UPPER BRANCH):ACCURACY , MAX OF ITERATIONS,MATRIX
      READ(5,13) IP2,NP2,P2,DP2,DP2MIN,DM,IM,N,KEY
      GAMSP=PAR(12)/(1-PAR(9)**4)+1.D-20
      PAR(21)=DSQRT(384.4D0/GAMSP  /(PAR(7)+PAR(8)))/PAR(13)**2 *PAR(15)
      PAR(20)=PAR(11)**2/(PAR(11)**2+0.2500*(1-PAR(9)*PAR(10)*(1+PAR(7))
     1/(1+PAR(1)))**2)
      PAR(22)=1+0.65*PAR(14)*PAR(5)*PAR(3)
      PAR(19)=(PAR(1)+0.65*DABS(PAR(13))*PAR(5)*PAR(3))/PAR(22)
      IF((IP1-1)*(IP1-2)*(IP1-3)*(IP1-5)*(IP1-13)*(IP1-14)*(NPAR1-1),NE.
     10) GO TO 51
      IF((NPAR1-1)*(IP1-1)*(IP1-2).NE.0) GO TO 50
      CALL COEFIL(PAR(1),PAR(2),N)
      IF(NPAR1 .GT. 1) GO TO (50,51),IP1
      EPS=PAR(13)
50    CALL ALCOEF(PAR(1),PAR(19),N)
51    IF((DABS(DP1).LT.1.D-7) .AND.(IPR.EQ.IP2)) GO TO 49
      WRITE(6,15)  PARAM(23+IMC),(PARAM(I),PAR(J),J=1,22)
15    FORMAT('1 ',A8,'. REAL INT-RCEDTS          '/4(/6(2X,A8,1PD12.5))//)
C  READ THIRD PARAMETER'S LOCATION,2 VALUES IN CRITICAL ZONE,INCREMENT,
C  APPROXIMATE (CORRESPONDING) FREQUENCIES,EXPECTED INCREMENT (REAL):
49    READ(5,17) IP3,P3(1),P3(2),DP3,P3,OMEG(1),OMEG(2),DOMP2
17    FORMAT(I2,7E10.6,E8.4)
      WRITE(6,16) N,DM ,PARAM(IP1),PAR(IP1),PARAM(IP2),P2,DP2,PARAM(IP3)
16    FORMAT('-*** N=',I2,' , ACCURACY=',1PD8.1,T39,'P1:',A8,D12.5/
     1T39,'P2:',A8,D12.5,'   BY DP2=',D12.5/T39,'P3:',A8,' ?'/)
      IF((IP3-1)*(IP3-2)*(IP3-3)*(IP3-5)*(IP3-13)*(IP3-14))56,55,56
55    WRITE(6,19) PARAM(IP3)
19    FORMAT(' COEFFICIENTS WON'T MATCH THIRD PARAMETER !',A8/)
```

```
      SUBROUTINE MATRIX(A,X,P3,P2,N)
      IMPLICIT COMPLEX*16(A,X),R-AL*8(B-H,O-W)
      REAL*8  NU,AE,AI,ALP
      COMMON /COEFFS/ CCEX(5,9,9),SCEX(5,9,9),SSEX(5,9,9),CCIN(5,9,9),
     1SCIN(5,9,9),SSIN(5,9,9),CCINP(3,9,9),SCINP(3,9,9),SSINP(3,9,9),CCE
     1XP(3,9,9),SCEXP(3,9,9),SSEXP(3,9,9), /COEFHL/ CCHL(3,9,9),SCHL(3,9,
     19),SSHL(3,9,9) /PRMTRS/ P(22),IP3,IP2,IRC
      DIMENSION A(N,N),ACC4(9,9),ASC4(9,9),ASS4(9,9),ACC3(9,9),ASC3(9,9)
     1,ASS3(9,9),ACC2(9,9),ASC2(9,9),ASS2(9,9),ACC1(9,9),ASC1(9,9),ASS1(
     19,9),ACC0(9,9),ASC0(9,9),ASS0(9,9)
      XI=(0.D0,1.D0)
      PI=3.14159265358979300
      P(IP3)=P3
      P(IP2)=P2
      AE=P(1)
      AI=P(2)
      UI=P(17)
      UE=P(18)
      SIGMA=1+0.65*P  (14)*P  (5)*P  (3)
      ALP     =(P  (1)+0.65*P  (13)*P  (5)*P  (3))/SIGMA
      GAMMA=P(12)*P(13)**3/(1-P(9)**4)+1.D-10
      NU=DSQRT(386.400/GAMMA/(P(7)+P(8))/P(13))*P(15)
      DMUNU=P(6) + NU*CDABS(X)
      IF(DMUNU.LT.1.D-9) DMUNU=1.
      NU=NU*P(6)/DMUNU
      XB=(1+XI*X*NU    )/(1-P(9)**4)
      V2=UE**2
      WE=((1+AE)/(1+ALP)/SIGMA)**2
      U2=V2/SIGMA**2
      CHI=P(11)*(1+AE)/P(13)
      B2=P(13)*P(5)*V2
      SE =((1+AE)**3-P(9)**3*(1+AI)**3)/3.D0/(1+AE-P(9)*(1+AI))
      CFE=0.675/(9.+(2*P(11)))**3)*V2
      CFI=0.01/(1.25+DSQRT(2.D0*P(11)))*UI**2
      CFX=0.025*(0.1+P(11))/(0.05+P(11))*UE*UI
      THETA=CFE*(1+AE)**2   +CFI/(1+AI)**2    +CFX*(1+AE)/(1+AI) +P(16)
      B3=UI**2/(1+A()**2-THETA-CHI*GAMMA*((2-P(8))* SE +P(7)*(1+AI)**2)
      B4=-GAMMA*(2.D0-P(8))
      B5=-GAMMA*P(7)
      B6=2.D0*DSQRT((P(7)+P(9)**2)/(P(7)+P(8)))*UI
      B7=  DSQRT((P(8)-0.999999900)/(P(7)+P(8)))*UE
      B0=B7/SIGMA**2
      BB= P(13)*P(4)*V2
      BBA=2*AE *U2
      B9=  P(13)*(P(4)*UE+ 0.0 )*DSQRT((P(8)-0.9999999)/(P(7)+P(8)))
      B9A=2*AE*B0
      B0=P(7)/(P(7)+P(8))
      B1=P(8)/(P(7)+P(8))
      X3=-XI*X/(2*P(13))**2*B7*2.D0*AE
      X4=-XI*X/(2*P(13))**2*B6*P(9)**2*AI
      X5=(X/(2*P(13)))**2*AE*(P(4)-1.D0)/(P(7)+P(8))
      X6=(X/(2*P(13)))**2*AI*(P(7)+P(9)**2)/(P(7)+P(8))*P(9)**2
      DAI=P(9)**4*P(2)**2
      NIN=N/2+1
      NIP=NIN-2
      DO 1  I=1,NIN
      DO 1 J=1,NIN
```

```
C  ACC_4 :RELATIVE TO FIRST INTEGRAL OF COEFFICIENT OF 4 TH DERIVATIVE.
C  CCEX(K+1.  :RELATIVE TO FIRST INTEGRAL OF (1+AE*X)**K FOR EXTERNAL
C  SCIN(K+1.  :RELATIVE TO SECOND INTEGRAL OF (1+AI*X)**K FOR INTERNAL
      ACC4(I,J)=XB*(CCEX(5,I,J)-P(9)**4*CCIN(5,I,J))
      ASC4(I,J)=XB*(SCEX(5,I,J)-P(9)**4*SCIN(5,I,J))
      ASS4(I,J)=XB*(SSEX(5,I,J)-P(9)**4*SSIN(5,I,J))
      ACC3(I,J)=A*X4*(AE*CCEX(4,I,J)-P(9)**4*AI*CCIN(4,I,J))
      ASC3(I,J)=A*X4*(AE*SCEX(4,I,J)-P(9)**4*AI*SCIN(4,I,J))
      ASS3(I,J)=A*X4*(AE*SSEX(4,I,J)-P(9)**4*AI*SSIN(4,I,J))
      ACC2(I,J)=12*(B*(AE**2*CCEX(3,I,J)-DAI*CCIN(3,I,J)))+12*CCRL(3,I,J)
     1-B2*CCEXP(2,I,J)+B3*CCEX(1,I,J)+B4*CCEXP(3,I,J)+B5*CCINP(3,I,J)
     1+X3*CCEX(4,I,J)+X4*CCIN(2,I,J)
      ASC2(I,J)=12*X9*(AE**2*SCEX(3,I,J)-DAI*SCIN(3,I,J)))+12*SCRL(3,I,J)
     1-B2*SCEXP(2,I,J)+B3*SCEX(1,I,J)+B4*SCEXP(3,I,J)+B5*SCINP(3,I,J)
     1+X3*SCEX(4,I,J)+X4*SCIN(2,I,J)
      ASS2(I,J)=12*(B*(AE**2*SSEX(3,I,J)-DAI*SSIN(3,I,J)))+12*SSRL(3,I,J)
     1-B2*SSEXP(2,I,J)+B3*SSEX(1,I,J)+B4*SSEXP(3,I,J)+B5*SSINP(3,I,J)
     1+X3*SSEX(4,I,J)+X4*SSIN(2,I,J)
      ACC1(I,J)=XI*(*(BA*CCIN(1,I,J)+B0*CCRL(3,I,J)))+BB*CCEX(2,I,J)+(XI*
     1X*B7-B4)*CCEX(3,I,J)-B5*CCIN(3,I,J)+X5*CCEX(4,I,J)+X6*CCIN(4,I,J)
     1+B8A*CCRL(2,I,J)
      ASC1(I,J)=XI*(*(BA*SCIN(1,I,J)+B0*SCRL(3,I,J)))+BB*SCEX(2,I,J)+(XI*
     1X*B7-B4)*SCEX(3,I,J)-B5*SCIN(3,I,J)+X5*SCEX(4,I,J)+X6*SCIN(4,I,J)
     1+B8A*SCRL(2,I,J)
      ASS1(I,J)=XI*X*(BA*SSIN(1,I,J)+B0*SSRL(3,I,J))+BB*SSEX(2,I,J)+(XI*
     1X*B7-B4)*SSEX(3,I,J)-B5*SSIN(3,I,J)+X5*SSEX(4,I,J)+X6*SSIN(4,I,J)
     1+B8A*SSRL(2,I,J)
      ACC0(I,J)=XI*(*B9*CCEX(2,I,J)-X*X*(B1*CCEX(3,I,J)+B0*CCIN(3,I,J))
     1           +B9A*XI*X*CCRL(2,I,J)
      ASC0(I,J)=XI*(*B9*SCEX(2,I,J)-X*X*(B1*SCEX(3,I,J)+B0*SCIN(3,I,J))
     1           +B9A*XI*X*SCRL(2,I,J)
1     ASS0(I,J)=XI*X*B9*SSEX(2,I,J)-X*X*(B1*SSEX(3,I,J)+B0*SSIN(3,I,J))
     1           +B9A*XI*X*SSRL(2,I,J)
      A(5,1)=ACC0(1,1)
      DO 9 IP=2,NIP
      A(2+2*IP,1)=ACC0(IP,1)
9     A(3+2*IP,1)=ASC0(IP,1)
      DO 10 IN=2,NIN
      PIN=(IN-1)*3.14159265358979300
      A(5,2*IN-2)=ACC0(1,IN)-PIN*ASC1(IN,1)-PIN**2*ACC2(1,IN)
     1                      +PIN**3*ASC3(IN,1)+PIN**4*ACC4(1,IN)
      A(5,2*IN-1)=ASC0(IN,1)+PIN*ACC1(1,IN)-PIN**2*ASC2(IN,1)
     1                      -PIN**3*ACC3(1,IN)+PIN**4*ASC4(IN,1)
      DO 10 IP=2,NIP
      A(2+2*IP,2*IN-2)=ACC0(IP,IN)-PIN*ASC1(IN,IP)-PIN**2*ACC2(IP,IN)
     1                            +PIN**3*ASC3(IN,IP)+PIN**4*ACC4(IP,IN)
      A(3+2*IP,2*IN-2)=ASC0(IP,IN)-PIN*ASS1(IP,IN)-PIN**2*ASC2(IP,IN)
     1                            +PIN**3*ASS3(IP,IN)+PIN**4*ASC4(IP,IN)
      A(2+2*IP,2*IN-1)=ASC0(IN,IP)+PIN*ACC1(IP,IN)-PIN**2*ASC2(IN,IP)
     1                            -PIN**3*ACC3(IP,IN)+PIN**4*ASC4(IN,IP)
      A(3+2*IP,2*IN-1)=ASS0(IP,IN)+PIN*ASC1(IP,IN)-PIN**2*ASS2(IP,IN)
     1                            -PIN**3*ASC3(IP,IN)+PIN**4*ASS4(IP,IN)
10    CONTINUE
      NIN=N/2
      A(1,1)=1
      A(2,1)=0
      IF(IBC.EQ.0) GO TO 20
C  CLAMPED-FREE CONDITIONS
      E=P(9)**2*P(10)**2
      EFF  =P(11)**2/(P(11)**2+(1-P(9)*P(10)*(1+AI)/(1+AE))**2/4)
      BA=EFF*(*B7*((1+AE)**2-(E*(1+AI)**2)*WE
```

```
      BR=CHI*((1+EPS  *(P(8)-1))/(P(7)+P(8))*SE  +RO*(1+AI)**2*P(10)**2)
      BC=EPS  *((1+AE)**2-       S*(1+AI)**2)*V2*WF -CHI*GAMMA*((2-P(8))*
     1SE +P(7)*(1+AI)**2*P(10)**2)
      BD=-CHI*(EPS  *R7*(SE +       S*(1+AI)**2*WF)+R6)
      XE=((1+AE)**4-(1+AI)**4*E**2)/(1-E**2)*(1+XI*X*NIF)
      A(3,1)=0
      A(4,1)=RA*XI*X + BR*X**2
      DO 11 IN=1,NIN
      A(1,2*IN)=1
      A(1,2*IN+1)=0
      A(2,2*IN)=0
      A(2,2*IN+1)=IN*PI
      A(3,2*IN)=IN**2*(-1)**IN*PI**2
      A(3,2*IN+1)=0
      A(4,2*IN)=A(4,1)*(-1)**IN
11    A(4,2*IN+1)=(-1)**IN*(IN*PI*(BC+BD*XI*X)-(IN*PI)**3*XE)
      GO TO 21
C  CLAMPED-CLAMPED CONDITIONS
20    A(4,1)=0
      A(3,1)=1
      DO 19 IN=1,NIN
      A(1,2*IN)=1
      A(1,2*IN+1)=0
      A(2,2*IN)=0
      A(2,2*IN+1)=IN*PI
      A(3,2*IN)=(-1)**IN
      A(3,2*IN+1)=0
      A(4,2*IN)=0
19    A(4,2*IN+1)=P(*IN*(-1)**IN
C  SUBSTRACT 1RST COL TO EVERY EVEN COL: 3RD TO 000. ORDER REDUCED BY 2
C  CHECK CARD LMNT=3.END IN DET*16 .
21    DO 13 I=1,N
      DO 12 J=2,NIN
      A(I,2*J)=(A(I,2*J)-A(I,1))/PI**4
12    A(I,2*J+1)=(A(I,2*J+1)-J*A(I,3))/PI**4
13    A(I,3)=(A(I,2) -A(I,1))/PI**4
      RETURN
      END
```

```
      GO TO 100
56    XP3=PAR(IP3)
      XP2=PAR(IP2)
      IF(EPS.LT.0.) XP1=PAR(3-IP2)
      PAR(IP2)=P2
      DP=DP2
      DO 5 NPAR2=1,NP2
      IF((IP2-1)*(IP2-2)*(IP2-3)*(IP2-5)*(IP2-13)*(IP2-14).EQ.0)GOTO 58
      IF((IPR-1)*(IPR-2)*(IPR-3)*(IPR-5)*(IPR-13)*(IPR-14))61,57,61
57    IF((IPR-1)*(IPR-2)) 60,59,60
58    IF((IP2-1)*(IP2-2).NE.0) GO TO 57
      IF(EPS.GT.0.) GO TO 59
      PAR(13)=-EPS*PAR(IP2)/XP2
      PAR(3-IP2)=XP1*PAR(IP2)/XP2
59    CALL COEFIL(PAR(1),PAR(2),N)
      IF(IPR.EQ.2) GO TO (60,61),IP2
60    IF(DABS(PAR(13)).LT.DM) GOTO 61
      SIGMA=1+0.65*PAR(14)*PAR(5)*PAR(3)
      PAR(10)=(PAR(1)+0.65*PAR(13)*PAR(5)*PAR(3))/SIGMA
      CALL RLCOEF(PAR(1),PAR(19),N)
61    CALL AXROOT(OMEG,OMP2,P3,DP3P2,PAR(IP2),DP2,DUI,SL,DM,I,IM,N,KEY)
      IPR=0
      IF(IABS(I)-IM)  4,96,96
4     IF(EPS.LT.0) WRITE(6,18) PARAM(3-IP2),PAR(3-IP2),PARAM(13),PAR(13)
      WRITE(6,14) PARAM(IP2),PAR(IP2),PARAM(IP3),P3(3),OMEG(3),SL,DUI,I
18    FORMAT(1H ,A8,F8.5,1X,1H,            A8,F8.5)
14    FORMAT(1H ,A8,F9.5,9X,               A8,F9.5, 9X,'OMEGA =',1PD12.5,'
     1',D9.2, 9X,'TAN=',D8.1, 3X,'DU/DIM=',D8.1,'    I=',I2/)
96    IF(I.GE.IM  *NPAR2) GO TO 99
      IF((PAR(17).LT.0.00) .OR. (PAR(18).LT.0.00)) GOTO 99
      IF( DABS(DP2/DP2MIN).GE.0.999D0) GO TO 5
      IF((DP2*DP2MIN.GE.-DP2MIN**2/3.00).OR.(NPAR2.LE.2)) GO TO 99
C  ATTEMPT AT POINT ON UPPER BRANCH.
      OMEG(2)=3*OMEG(1)-2*OMEG(3)
      OMEG(1)=OMEG(2)+(OMEG(2)-OMEG(3))/20.
      SL=-2.00*SL
      DUI=-DUI/2.00
      DP2=0
      P3(1)=P3(3)+4*DP3P2
5     PAR(IP2)=PAR(IP2)+DP2
99    PAR(IP2)=XP2
      PAR(IP3)=XP3
      IPR=IP2
      IF(EPS.GT.0.) GO TO 100
      PAR(13)=EPS
      PAR(3-IP2)=XP1
100   PAR(IP1)=PAR(IP1)+DP1
      STOP
      END
```

```
      SUBROUTINE LAGRAN(A,X1,X0,U,P,DM,KM,L,M,N,K,KEY)
      DIMENSION A(N,N),L(N),M(N)
      COMPLEX*16 A,X0,X1,X2,Y1,Y0,Y,X,DET
      REAL*8 U,P,DM,RX,DX
      K=0
4     CALL MATRIX(A,X0,U,P,N)
      Y0=DET(A,L,M,N)
      Z0=CDABS(Y0)
      IF(IABS(KEY).NE.1) GO TO 1
      WRITE(6,10)P,U,X0,Y0,X1
1     K=K+1
      CALL MATRIX(A,X1,U,P,N)
      Y1=DET(A,L,M,N)
      IF(K-1) 81,82,8
81    K=-K
      Z0=10*Z0
      IF(CDABS(Y1) .GT.10.* Z1) GO TO 3
82    X=(X0+X1)/2
      Y=(Y1+Y0)/2
8     X2=((X *Y0*Y1*(Y1-Y0)+X0*Y1*Y *(Y -Y1)+X1*Y *Y0*(Y0-Y ))/(Y -Y0)/
     1(Y0-Y1)/(Y1-Y )+(X1*Y0-X0*Y1)/(Y0-Y1)+(X1*Y-X*Y1)/(Y-Y1))/3.
      YR0=Y0
      YR1=Y1
      W=YR0*YR1-(Y0-YR0)*(Y1-YR1)
      Z1=CDABS(Y1)
      IF(W.LT.Z0*Z1/K**2) Z0=10.*Z0
      IF(( Z1*(1-1.3/K)  .GT. Z0).OR.(K.GE.KM)) GO TO 3
      IF(IABS(KEY).NE.1) GO TO 5
      WRITE(6,10) P,U,X0,Y0,X1,Y1,X2
10    FORMAT(' P2=',1PD10.3,' P3=',D11.4,2(' X=',2D9.2,' Y=',2D8.1),' X=
     1',D11.4,D9.2)
C  DEFINE ACCURACY ACCORDING TO DISTANCE FROM REAL AXIS
5     Y2=(0.0,-1.0)*X2
      DX=0.05*(ABS(Y2)+DM*5)
      IF( CDABS(X2-X1).LT.DX) GO TO 7
      RX=X2
      IF(RX+DM) 6,6,7
6     Z0=X1-X0
      X0=X2-RX
      X1=X0-(0.00,1.00)*RX
      K=-K-2
      GO TO 4
7     X=X1
      Y=Y1
      IF(Z).GT.Z0) GOTO 71
      X=X0
      X0=X1
      Y=Y0
      Y0=Y1
71    X1=X2
      IF(DABS(RX).LT.DM) X1=X1-RX
      Z0=Z1
      GO TO 1
```

```
3       WRITE(6,11) K,KM,P,U,X0,Y0,X1,Y1,X2
11      FORMAT('0-LAGRAN- INTERRUPTED BECAUSE OF DIVERGENCE OF FREQUENCY A
     1FTER K=',I2,' ITERATIONS IE'K<KMAX=',I2,'  ,LAST ITERATION TRACEBA
     1CK : '/' P2=',1P010.3,' P3=',011.4,2(' X=',2D9.2,' Y=',2D8.1),' X=
     1',011.4,D9.2)
        K=KM
2       X1=X2
        RETURN
        END
```

```
      SUBROUTINE AXROOT(OM,DOM,V,DV,P,DP,DVDIM,SL,DDMAX,I,IMAX,N,KEY)
      DIMENSION A(20,20),L(20),M(20),OM(3),V(3)
      COMPLEX*16 GI,OM,OM0,OM1,OM2,OM3,OME,A
      REAL*8 V,P,DP,U0,U3,X1,X2,X0,Y0,Y1,Y2,DV,DDMAX,SL,DVDIM,DOM
      GI=(0.D0,1.D0)
      INIT=1
      DV2=V(2)
      IF(KEY.LT.0) GO TO 10
      KEY=KEY-2
      I=0
      INIT=0
      V(3)=0
      OM(3)=0
C     CALCULATION OF FREQUENCIES AT INITIAL VELOCITIES
10    DO 1 K=1,2
      OM1=OM(3-K)
      IF((K-1)*INIT.LE.0) GO TO 11
      Y2=-GI*OM2
      V(2)=V(1)-DVDIM*Y2
      X2=OM2
      OM(2)= X2-Y2/(SL+DDMAX)
      IF( X2 .LT.DDMAX ) OM(2)=DDMAX*GI
      OM1=(OM1+9*OM(2))/10.
11    U3=V(K)
      OM2=OM(K)
      CALL LAGRAN(A,OM2,OM1,U3,P,DDMAX,IMAX,L,M,N,J,KEY)
      IF(J-IMAX) 1,100,100
1     OM(K)=OM2
      IF(I.EQ. -IMAX) J=IMAX
      Y1=-GI*OM(1)
      Y2=-GI*OM(2)
      IF(INIT+ DABS(I-1+Y2/Y1).GT. 0.05) GO TO 12
C     SPECIAL PROCEDURE FOR TOO CLOSE INITAL VALUES OF FREQUENCIES.
      V(2)=2*V(2)-V(1)
      V(1)=2*V(1)-U3
      U0=U3
      OM0=OM2
      I=-1
      GO TO 10
12    IF(I.EQ.-1) GO TO 5
      OM0=(OM(1)+OM(2))/2.
      U0=(V(1)+V(2))/2.
5     I=0
      IF(Y1**2.LT.Y2**2) I=1
      U1=V(1+I)
      U2=V(2-I)
      OM1=OM(1+I)
      OM2=OM(2-I)
C     ITERATIONS IN VELOCITY
      DO 2 I=1,IMAX
      Y0=-GI*OM0
      Y1=-GI*OM1
      Y2=-GI*OM2
```

```
      U3=((U0*Y1*Y2*(Y2-Y1)+U1*Y2*Y0*(Y0-Y2)+U2*Y0*Y1*(Y1-Y0))/(Y0-Y1)/
     1(Y1-Y2)/(Y2-Y0)+(U2*Y1-U1*Y2)/(Y1-Y2)+(U2*Y0-U0*Y2)/(Y0-Y2))/3.
      IF((Y1*Y2.GT. 0.00).AND.((1-2/I)*DABS(Y2) .GT. DABS(Y1))) GO TO 99
      X0=OM0
      X1=OM1
      X2=OM2
      DU= (ABS(U2-U1)+DABS(U1-U0))/2
      NDU=DABS((U3-U2)/DU)*(1-0.3)/1
C     CHECK TOO SLOW CONVERGENCE IF ERROR ON U3>30% OR OUTSIDE SPECIFIC
      IF((DABS(1-U3/U2).GT.0.3 .OR. NDU.GE.1) .AND. Y1*Y2.GT.0.) GOTO 99
      OME=((X0*Y1*Y2*(Y2-Y1)+X1*Y2*Y0*(Y0-Y2)+X2*Y0*Y1*(Y1-Y0))/(Y0-Y1)/
     1(Y1-Y2)/(Y2-Y0)+(X2*Y1-X1*Y2)/(Y1-Y2)+(X2*Y0-X0*Y2)/(Y0-Y2))/3.
      OM3=OME+G1*Y2/10.00
      IF(DABS(1-U3/U2)+DABS(Y2) .LT. DDMAX) GO TO 3
      CALL LAGRAN(A,OME,OM3,U3,P,DDMAX,IMAX,L,M,N,K,KEY)
      OM3=OME
      IF(K-IMAX) 25,100,100
25    Y3=-G1*OM3
      IF(DABS(1-U3/U2)+ ABS(Y3) .LT. DDMAX) GO TO 3
      IF((1-1/I)*Y2**2.GT.Y0**2) GO TO 24
      U0=U1
      OM0=OM1
      U1=U2
      OM1=OM2
      GO TO 26
24    U0=U2
      OM0=OM2
26    U2=U3
2     OM2=OM3
      I=IMAX
99    S =(Y2-Y1)/(U2-U1)
      IF( X2.GE.DDMAX ) S =(Y1-Y2)/(X1-X2)
      WRITE(6,102) I,U3,P,S
102   FORMAT('0-AXROOT- INTERRUPTED BECAUSE TOO SLOW CONVERGENCE AFTER I
     1=',I2,' ITERATIONS AT  U3=',1PD10.3,' . P=',D10.3,' . TAN=',E9.1/)
      I=IMAX*(1-2*INIT) + 1-INIT
      GO TO 999
C     STORAGE OF CRITICAL CHARACTERISTICS (VELOCITY,FREQUENCY&SLOPES)
3     V(3)=V(3) + (1-INIT)*(U3-DV)
      OM(3)=OM(3) + (1-INIT)*(OM3-DOM)
      NDV2=1
      IF(ABS(DV2).GT.1.5E-6)  GO TO 4
      IF(ABS(DV2).LT.0.5E-6) V(1)=U3-1.E-6
      IF(DABS(DV).GT.DDMAX) GOTO 4
      NDV2=0
      DV=U3-V(3)
      DOM=OM3-OM(3)
4     V(2)=NDV2*INIT*(U3-V(1)+DV2)
      V(1)=U3+2*(U3-V(3))-DV + V(2)
      OM(1)=OM3+2*(OM3-OM(3))-DOM
      OM(2)=OM(1)*(1+G1*DDMAX)
      DV=(U3-V(3))*(NIT
      V(3)=U3
      OM(3)=OM3
      DVDUM=(U2-U1)/(Y2-Y1)
      SL=1.DA
      IF(X2.GT.DDMAX) SL=(Y1-Y2)/(X1-X2)
      IF(J.EQ.IMAX) GO TO 104
      RETURN
100   WRITE(6,101) U3,P
101   FORMAT(' -AXROOT- INTERRUPTED BECAUSE OF DIVERGENCE OF FREQUENCY I
```

```
     IN -LAGRAN-  AT  U3=',1PD10.3,'  AND  P =',D10.3/)
      I=IMAX+1 - IN
999   IF(INIT.EQ.1) GO TO 103
      SL=1.000
      RETURN
103   P=P-DP
      DVOLM=DVOLM*0.75
104   DP=DP/2
      DV=DV/2
      V(2)=V(2)/4
      V(1)=V(3) + DV +V(2) /2
      DDM=DDM/2
      DM(1)=DM(3) + DDM
      DM(2)=DM(3)*0.99 + DDM*1.1
1000  RETURN
      END
```

```
      SUBROUTINE IMROOT(OM,DOM,V,DV,P,DP,DVDY,DOMAX,I,IMAX,N,KEY)
C
C     THIS SUBROUTINE HAS SAME INPUT REQUIREMENTS AS  AXROOT.
C                 EXEPT NO SLOPE.
C
      IMPLICIT REAL*8(A-H,O-Z)
      DIMENSION A(20,20),L(20),M(20),OM(3),V(3)
      INIT=1
      IF(KEY.LT.0) GO TO 10
      KEY=KEY-2
      I=0
      INIT=0
      V(3)=0
      OM(3)=0
10    OM2=OM(2)
      OM1=OM(1)
C     CALCULATION OF IMAGINARY FREQUENCY AT INITIAL VELOCITY FOR MINIMUM
      U3=V(1)
      CALL MINIM1(A,OM1,OM2,U3   ,P,DOMAX,IMAX,L,M,N,J,KEY)
      IF(J-IMAX) 1,100,100
1     OM(1)=OM2
      Y0=A(1,1)
      IF(INIT.EQ.0) GOTO 11
      V(2)=     Y0*DVDY +V(1)
11    DO 12 I=1,IMAX
      U1=U3
      U2=V(2)
C     CALCULATION OF VELOCITY FOR WHICH THE PRVIOUSLY FOUND FREQUENCY IS
      CALL VELSEC(A, U1,U2,OM2  ,P,DOMAX,IMAX,L,M,N,J,KEY)
      V(2)=U2
      OM3=OM2+10 *DOMAX
      U3=U2
C     CALCULATE THE NEW FREQUENCY FOR THE MINIMUM AT NEW VELOCITY.
      CALL MINIM1(A,OM2,OM3,U3   ,P,DOMAX,IMAX,L,M,N,J,KEY)
      IF(J-IMAX) 2,100,100
2     Y1=A(1,1)
      DVDY=(V(2)-V(1))/(Y1-Y0)
      U3   =A(1,1)*DVDY +V(2)
      IF((DABS(U3-U2).LT.DOMAX) .OR. (DABS(1-U2/U3).LT. DOMAX)) GOTO 3
12    OM2=OM3
C     STORAGE OF CRITICAL CHARACTERISTICS (VELOCITY,FREQUENCY&SLOPES)
3     V(3)=V(3) + (1-INIT)*(U3-DV)
      OM(3)=OM(3) + (1-INIT)*(OM3-DOM)
      IF(DABS(DV).LT.DOMAX) DV=U3-V(3)
      IF(DABS(DOM).LT.DOMAX) DOM=OM3-OM(3)
      V(1)=U3+2*(U3-V(3))-DV
      OM(1)=OM3+2*(OM3-OM(3))-DOM
      OM(2)=OM(1)*(1+10*DOMAX)
      DV=(U3-V(3))*INIT
      DOM=(OM3-OM(3))*INIT
```

```
      V(3)=U3
      DM(3)=DM3
      IF(J.EQ.IMAX) GO TO 104
      RETURN
100   WRITE(6,101) U3,P
101   FORMAT(' -AXRIOT- INTERRUPTED BECAUSE OF DIVERGENCE OF FREQUENCY I
     1N -LAGRAN-  AT  U3=',1PD10.3,'  AND  P=',D10.3/)
      I=IMAX+1 - INIT
999   IF(INIT.EQ.1) GO TO 103
      SL=1.D00
      RETURN
103   P=P-DP
      DVDY =DVDY *0.75
104   DP=DP/2
      DV=DV/2
      V(1)=V(3) + DV/2+(V(1)-V(3))/4
      DDM=DDM/2
      DM(1)=DM(3) + DDM
      DM(2)=DM(3)*0.99 + DDM*1.1
1000  RETURN
      END
      SUBROUTINE MINIM1(A,P0,P1,U,P,DM,KM,L,M,N,K,KEY)
      IMPLICIT REAL*8 (A-H,O-Z)
      DIMENSION A(N,N),L(N),M(N)
      DX=(P1-P0)/10
      X0=P0-DX
      CALL MATRIX(A,X0,U,P,N)
      Y0=DET(A,L,M,N)
      X1=P0+DX
      CALL MATRIX(A,X1,U,P,N)
      Y1=DET(A,L,M,N)
      YP0=(Y1-Y0)/(X1-X0)
      IF(IABS(KEY).NE.1) GO TO 1
      WRITE(6,10)P,U,X0,Y0,X1,Y1,YP0,P0,P1
1     DO 8  K=1,KM
      DX=(P1-P0)/10
      X0=P1-DX
      CALL MATRIX(A,X0,U,P,N)
      Y0=DET(A,L,M,N)
      X1=P1+DX
      CALL MATRIX(A,X1,U,P,N)
      Y1=DET(A,L,M,N)
      YP1=(Y1-Y0)/(X1-X0)
      P2=(YP1*P0-YP0*P1)/(YP1-YP0)
      IF(YP0*YP1*(1-1.D/K).GT.YP0**2) GO TO 3
      IF(DABS(P2-P1).LT.10.D0*DM .OR. DABS(1-P1/P2).LT.DM) GOTO 2
      IF(IABS(KEY).NE.1) GO TO 5
      WRITE(6,10) P,U,X0,Y0,X1,Y1,YP1,P1,P2
10    FORMAT(' P2=',1PD10.3,' P3=',D11.4,2(' DM=',D11.4,' DET=',D8.1),'
     1 SL1=',D8.1,' DM1=',D11.4,' DM2=',D11.4)
5     IF(DABS(YP1/YP0).GT.1.D0) GO TO 8
      P0=P1
      YP0=YP1
8     P1=P2
3     WRITE(6,11)
11    FORMAT('0-MINIM- INTERRUPTED BECAUSE OF DIVERGENCE OF SLOPE')
      K=KM
2     P1=P2
      CALL MATRIX(A,P2,U,P,N)
      Y2=DET(A,L,M,N)
      A(1,1)=Y2
```

```
      IF(IABS(KEY).NE.1) GO TO 9
      WRITE(6,12) U,P1,Y2
12    FORMAT(' MINIMUM DET:  P3=',1PD11.4,' DM=',D11.4,' DET=',D9.2)
9     RETURN
      END
      SUBROUTINE VELSEC(A,U0,U1,X,P,DM,KM,L,M,N,K,KEY)
      IMPLICIT REAL*8 (A-H,O-Z)
      DIMENSION A(N,N),L(N),M(N)
      K=0
4     CALL MATRIX(A,X,U0,P,N)
      Y0=DET(A,L,M,N)
1     K=K+1
      CALL MATRIX(A,X,U1,P,N)
      Y1=DET(A,L,M,N)
      IF(K-1) 81,82,8
81    K=-K
82    U=(U0+U1)/2
      Y=(Y1+Y0)/2
8     U2=((U *Y0*Y1*(Y1-Y0)+U0*Y1*Y *(Y -Y1)+U1*Y *Y0*(Y0-Y )/(Y -Y0)/
     1(Y0-Y1)/(Y1-Y )+(U1*Y0-U0*Y1)/(Y0-Y1)+(U1*Y-U*Y1))/(Y-Y1))/3.
      IF(( DABS(U2-U1).LT.DM).OR. (DABS(1 -U1/U2).LT.DM))GOTO 2
      IF(IABS(KEY).NE.1) GO TO 5
      WRITE(6,10) P,X,U0,Y0,U1,Y1,U2
10    FORMAT(' P2=',1PD10.3,' DM=',D11.4,2(' P3=',D11.4,' DET=', D8.1),'
     1=P3=',D11.4)
5     IF(Y0*Y1*(1-1/K).GT.Y0**2) GO TO 3
      U=U1
      Y=Y1
      IF(DABS(Y1/Y0).GT.1.) GOTO 71
      U=U0
      U0=U1
      Y=Y0
      Y0=Y1
71    U1=U2
      IF(K.LT.KM) GO TO 1
3     WRITE(6,11)
11    FORMAT('0-VELSEC- INTERRUPTED BECAUSE OF DIVERGENCE OF VELOCITY')
      K=KM
2     U1=U2
      IF(IABS(KEY).NE.1) GO TO 9
      WRITE(6,12) X,U1
12    FORMAT(' ROOT:          DM=',1PD11.4,' P3=',D11.4)
9     RETURN
      END
```